Dipl.-Ing. Michael Weißl, BSc.

Cellulose xanthate for advanced cellulose (nano)materials

DISSERTATION

zur Erlangung des akademischen Grades

Doktor der technischen Wissenschaften

eingereicht an der

Technischen Universität Graz

Betreuer

Assoc. Prof. Mag. Dr. Stefan Spirk

Institut für Papier, Faser und Zellstofftechnik

Graz, Mai 2018

Eidesstattliche Erklärung

Ich erkläre an Eides statt, dass ich die vorliegende Arbeit selbstständig verfasst, andere als die angegebenen Quellen/Hilfsmittel nicht benutzt, und die den benutzten Quellen wörtlich und inhaltlich entnommenen Stellen als solche kenntlich gemacht habe. Das in TUGRAZonline hochgeladene Textdokument ist mit der vorliegenden Dissertation identisch.

Graz, _____ _____

Datum Unterschrift

„Hazardous journey, small wages, bitter cold, long months of complete darkness, constant dangers, safe return doubtful. Honour and recognition in case of success! “

Ernest Shackleton (Antarctic Explorer), 1914

Danksagung

Eine Danksagung hat meist ein weinendes und ein lachendes Auge denn Danksagung bedeutet, dass etwas zu Ende geht und etwas Neues beginnt.

In diesem Fall enden drei Jahre, 36 Monate beziehungsweise 156 Wochen voller Freud und Leid, verbunden mit zahlreichen wissenschaftlichen Hochs aber auch vielen lehrreichen Tiefs. Es war eine lustige, prägende Zeit die mich Fachlich, vor allem aber auch Menschlich weiterentwickelte. Das Fachliche ist, wie es so üblich ist, auf den nächsten paar Seiten ausführlich beschrieben und diskutiert. Aber gerade das Menschliche ist das, was wirklich wertvoll ist und wofür ich mich noch einmal bei allen bedanken möchte.

Mathias, Werner, Carina, Feri, David, Mani, Wolfi und Kathi die Zeit mit euch in der Arbeitsgruppe und die zahlreichen lustigen Stunden während und insbesondere auch außerhalb der Arbeit machen die Zeit als Dissertant unvergessen.

Jana, Anne, Mike und Stefan bei euch möchte ich mich eure Arbeit im Rahmen der Bachelorlabore bedanken. Euer Engagement und die vielen Stunden in denen ihr Viskose gesponnen und gegossen habt, haben viele interessante Ergebnisse geliefert und mir bei meiner Arbeit sehr weitergeholfen.

Ein besonderer Dank gilt natürlich meinem Betreuer Assoc. Prof. Mag. Dr. Stefan Spirk. Durch deine offene Art der Betreuung war es mir möglich, meine eigenen Ideen in die Arbeit einzubringen und viele wertvolle Erfahrungen zu sammeln. Auch für die Möglichkeit an so vielen Konferenzen und internationalen Veranstaltungen teilzunehmen, möchte ich mich noch einmal besonders bedanken.

Des Weiteren möchte ich noch unserem Institutsvorstand Univ.-Prof. Dipl.-Ing. Dr.techn. Wolfgang Bauer und dem gesamten Team vom Institut für Papier-, Zellstoff-, und Fasertechnik für die herzliche Aufnahme am Institut und für seine immerwährende Unterstützung danken.

Danke auch an Dr. Armin Zankel und Prof. Harald Plank vom Institut für Elektronenmikroskopie für ihre immerwährende Unterstützung und ihre hervorragenden Aufnahmen meiner zahlreichen Proben.

Dr. Thomas Rath und Prof. Gregor Trimmel möchte ich für die Bereitstellung der Metall-Xanthogenate und ihre großzügige Unterstützung bei diversen Messungen und zugehörigen Diskussionen über die erhaltenen Daten herzlich danken.

Danke auch an Dr. Brigitte Bitschnau (XRD) vom Institut für physikalische Chemie und Prof. Helmar Wiltsche (ICP-OES) vom Institut für Analytische Chemie und Lebensmittelanalytik für ihre Unterstützung.

Meinen Eltern und meiner Familie möchte ich noch einmal für die großzügige finanzielle aber auch mentale Unterstützung während des gesamten Studiums danken. Danke, dass ihr immer zur Stelle seid.

Zu guter Letzt liebe Meli, möchte ich mich ganz besonders bei dir bedanken. Danke dass du mich die letzten Jahre immer motiviert, unterstützt und wieder aufgebaut hast, wenn ich an allem gezweifelt habe.

Danke euch allen!

Abstract

The Viscose process is still the most important technology in the production of wood based regenerated cellulose fibers. Although the process is in the focus of science and under industrial use since more than 100 years, there are still some unanswered questions and numerous options for new fields of application.

The major goal of this thesis was the development of out of the box applications for cellulose xanthate, leaving the initial area of fiber and film processing for textiles and non-wovens behind. An increasing social and economic pressure forces the utilization of green and renewable polymers instead of synthetic ones. The possibility of a water-based processing and the stability against diverse additives, makes cellulose xanthate a promising candidate and alternative material to olefin-based polymers.

Although the knowledge in the handling of Viscose and the equipment for the lab scale processing were quite limited in the early beginning of this thesis. Within the past years a strong progress in both, the knowledge and the equipment were achieved and interesting experiments and results could be generated.

The obtained results are summarized in two main chapters. In the first one, the development of know how in a laboratory scale processing of fibers and films, the processing of metal sulfide/ Viscose core-shell structured composite fibers and the employment of Viscose membranes in bio refinery processes are described. In the second chapter, the development of a thin film processing based on cellulose xanthate, the expansion of this system to a photoactive multilayer composite of metal sulfide and cellulose and the spin coating of cellulose xanthate/ cellulose carbamate blend films are explained.

During the last years, huge response and a very positive feedback from scientific and industrial community on the published or orally presented results was gained and many ideas for further projects occurred. This shows that there is still a lot of interest in the potential of cellulose xanthate itself and especially for new and out of the box applications in diverse areas.

Zusammenfassung

Obwohl der Viskoseprozess schon mehr als hundert Jahre im Fokus von Wissenschaft und Forschung steht, gilt er mit einer Produktionsmenge von mehr als drei Millionen Tonnen Faser pro Jahr, immer noch als der wichtigste Prozess in der Herstellung von Cellulose Regeneratfasern. Trotz seiner langen Historie gibt es noch immer einige ungeklärte Fragen im Prozessablauf und viel Spielraum für die Entwicklung und Modifikation von Materialen aus Viskose.

Ziel dieser Arbeit war es Anwendungsmöglichkeiten für Cellulose Xanthogenat abseits der klassischen Faser- und Filmherstellung zu finden. Die treibende Kraft dafür ist der steigende soziale aber auch ökonomische Druck, synthetische Polymere durch erneuerbare und umweltfreundliche Materialen zu ersetzen. Die Möglichkeit der wasserbasierten Prozessierung sowie die hohe Toleranz bzw. Stabilität gegenüber Prozessadditiven zur Modifikation diverser Eigenschaften machen Viskose daher zu einer vielversprechenden Alternative.

Im Rahmen der Dissertation wurde zahlreiche Versuche durchgeführt und dabei interessante Daten und Resultate erhalten, welche im Rahmen dieser Arbeit in zwei Kapitel zusammengefasst sind.

Der erste Teil beschreibt die Entwicklung von Methoden und Equipment für Faser- und Filmherstellung sowie deren Anwendung zur Herstellung von Metallsulfid/ Viskose Kompositfasern oder Membrane für Bioraffiniere Anwendungen. Der zweite Teil fast die Herstellung von Cellulose Dünnschichtfilmen auf Viskosebasis zusammen und erläutert die Entwicklung von Mehrschichtsystemen aus Viskose und $CuInS_2$ sowie von Cellulose Mischfilmen basierend auf dieser Methode. Die Cellulose Dünnschichtfilmefilme wurden darauffolgen im Bezug auf verschiedenste Eigenschaften wie Quellung und Trocknung oder deren Wechselwirkung mit Proteinen untersucht.

Durch die im Rahmen dieser Arbeit publizierten Beiträge und den zahlreich geführten Diskussionen wurden viele positive Rückmeldung aus Wissenschaft und Wirtschaft erhalten und weitere Ideen entwickelt, was das ungebrochene Interesse an Cellulose Xanthogenat selbst und auch an alternativen Einsatzmöglichkeiten zeigt.

Table of content

Aim of the thesis

The scope of this work is on the development of new materials from Viscose based cellulosic products in new areas and the utilization of Viscose as source for the production of cellulose thin films for high-end technologies.

So far, the Viscose technology is mostly employed to produce fibers for textile and non-woven products. The flexibility and the broad variety of modifications during and after the processing itself provides materials which became an integral part of humankind's life. For instance, the fibers can be incorporated in the production of standard and high value clothing or utilized in technical textiles after adjusting them to special properties like flame resistance for example. Another important area for fibers made from the Viscose process is the non-woven market. Many day care products like wipes, diapers or sanitary pads consist at least partly of Viscose fibers. As the Viscose process itself is well investigated and extensively described in literature so far, the focus was on the development of new materials utilizing the process itself, or materials derived from the Viscose process namely, cellulose fibers or films. To achieve this, the development of a small laboratory scale fiber spinning unit, simulating the most important parts of the Viscose process was necessary. The experience we made thereby is meanwhile an integral part of student lab courses. To reach a broader majority of students and teaching staff, the lab course experiments were described in detail and will be submitted as Laboratory experiment to the Journal of Chemical Education (2019). With increasing performance and reliability in the fiber spinning, we could focus more on the material development, as on the Viscose process itself. Through the addition of metal salts into the spinning bath, we were able to produce core shell structured (nano-)composites consisting of an inorganic shell and a cellulose core. This composite material processing was patented at the Austrian patent office in 2018 (A50790/2018) and later on submitted to Lenzinger Berichte (2019). Another interesting work is the film casting of cellulose membranes made from Viscose solution. The produced membranes were employed in the separation of lignosulfonates as shown in the Solvent Extraction and Ion Exchange Journal (2019).

Beside the material development, a second major objective of the thesis was the application of Viscose solutions in the processing of cellulose thin films. Cellulose thin films have a well-defined structure and a very smooth surface morphology. Both properties allow the utilization of such thin films to study fundamental cellulose reactions or their employment as model substrates for the development of high-end materials. After presenting a straight forward and

easy to go method for a water-based spin coating of cellulose thin films from Viscose solutions in Cellulose (2018), we could show how to form multilayered nano-structures of cellulose and metal sulfides in Carbohydrate Polymers (2019). In another project, *all*-cellulose thin films were spin coated, based on cellulose carbamate and Viscose, the summarized results were submitted to Cellulose (2019).

List of Papers described in the context of this thesis:

#1) Michael Weißl, Gregor Kraft, Josef Innerlohinger and Stefan Spirk; Spinning of Fibers from Wood – A Lab Experiment to Introduce Students in Viscose Fiber Manufacturing and Analysis; Journal of Chemical Education; 2019; submitted

#2a) Michael Weißl, Mike Pelzman, Armin Zankel, Brigitte Bitschnau, Helmar Wiltsche and Stefan Spirk; Processing of metal sulfide/ cellulose composite fibers in core-shell configuration; Lenzinger Berichte; 2019; submitted

#2b) Stefan Spirk, Gregor Trimmel, Michael Weißl, David Pfeifer, Mathias Hobisch, Bruno Alonso; In situ Synthese von Metallsulfidpartikeln auf/in Fasern und Filmen im Zuge des Viskoseverfahrens; A50790/2018

#3) Marlene Kienberger, Paul Demmelmayer, Michael Weißl, Armin Zankl and Stefan Spirk; Biobased support layers for the fractionation and selective extraction of lignosulfonates; Solvent Extraction and Ion Exchange Journal, 2019, accepted

#4) Michael Weißl, Katrin Niegelhell, David Reishofer, Armin Zankel, Josef Innerlohinger and Stefan Spirk; Homogeneous cellulose thin films by regeneration of cellulose xanthate: properties and characterization; Cellulose; 2018; 25; 711-721

#5) Michael Weißl, Thomas Rath, Jürgen Sattelkow, Harald Plank, Samuel Eyley, Wim Thielemans, Gregor Trimmel and Stefan Spirk; Multi-layered nanoscale cellulose/$CuInS_2$ sandwich type thin films; Carbohydrate Polymers; 2019; 203; 219-227

#6) Michael Weißl, Mathias Andreas Hobisch, Leena Sisko Johansson, Kay Hettrich, Eero Kontturi, Bert Volkert and Stefan Spirk; Cellulose carbamate derived cellulose thin films – Preparation, characterization and blending with cellulose xanthate; Cellulose; 2019, submitted

State of the art

Cellulose is the most abundant biopolymer on earth and occupies a major role in humankind's history in the form of wood and other plant materials. [1] In 1838, Anselme Payen, a French chemist, described a substance remaining after treating plants with acidic solutions and ammonia. [2] After subsequent extraction of the remaining products, he could determine a molecular formula of $C_6H_{10}O_5$ for the residue by elemental analysis. Later, he introduced the name *Cellulose* for the observed structure. The utilization of cellulose as raw material for industrial synthesis started around 150 years ago, with the reaction of cellulose and nitric acid to form cellulose nitrate. The developed modification process was further the initiation for the production of wood-based cellulose fibers and other cellulosic materials. [3, 4]

Today, cellulose is estimated to be an almost inexhaustible source of raw material with an annual production of around 1.5×10^{12} tons and large capital investments in numerous scientific projects to aim at developing green, biocompatible and renewable materials. [5] In this context, wood pulp is the most important cellulose source with a production of more than 300 million tons per year. Most of the pulp is employed in the production of paper and board and only around 2% of the cellulose material is subjected to the processing of man-made cellulose fibers, films and other materials like cellulose ethers and esters used as coatings, laminates, pharmaceuticals, food additives and cosmetics. [1] Besides this, latest research allows the employment of cellulose in more sophisticated applications like protein immobilization, composite formation or the separation of enantiomers. [6-9]

Cellulose structure

Cellulose consists of long chain repeating units of glucose and it is exactly the combination of carbohydrate chemistry and macromolecular effects which can be claimed responsible for all the interesting and manifold properties of this fascinating biopolymer. The influence of chain length, intermolecular interactions and cross-linking reactions strongly affect the physical properties of cellulose and explain the different behavior compared to low molecular mass carbohydrates. The regular distribution of functional groups along the polymer chain allows for manifold modifications and chemical reactions along the biopolymer. [1] It was Hermann Staudinger who discovered, that cellulose is not a random agglomeration of glucose molecules, but rather a long-chained glucose repeating unit, with covalent linkage of the single glucose molecules. In more detail, Staudinger proposed that cellulose consist of β-D-glucopyranose

rings, covalently bonded through an acetal linkage between the OH groups on the C4 and C1 carbon of the pyranose ring (β1-4 linked polymer). [10] Beside the OH group involved in the linkage of the single pyranose rings, there are three more OH groups available on every anhydroglucose unit (AGU). The available OH groups are placed on the C2, C3 and C6 carbon atom. On the C2 and C3 secondary alcohols are present while on the C6 a primary alcohol is located in a trans position relative to the secondary hydroxyl groups (Figure 1). To reach the preferred bonding angle of the acetal linkage, a 180° in plane rotation of every second AGU is necessary. [1] But this 180° rotation causes a bit of confusion and leads to some discussion about the definition of the smallest repeating unit in the cellulose chain. Long time cellobiose, the disaccharide of two AGU was claimed as repeating unit in cellulose, but meanwhile the AGU itself has been proposed as repeating unit, as this is in accordance to the nomenclature rules of the International Union of Pure and Applied Chemistry (IUPAC) avoiding confusion. [11]

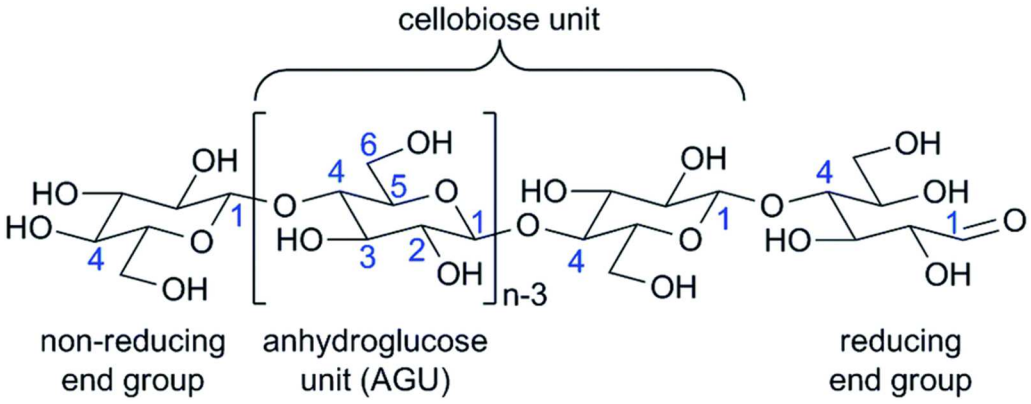

Figure 1 Illustration of AGU and cellobiose unit arranged in a cellulose polymer chain [12]

The number of AGU units connected to a polymer chain is expressed with the degree of polymerization (DP) and varies between the different cellulose sources. The determination of the DP can be done via various methods like light scattering, size exclusion chromatography or viscosity measurements. [13] Wood pulp has an average DP from 300 up to 1700, strongly depending on the type of wood. The DP of fibrous plant materials like cotton could raise up to 10000. Similar or even higher DP values were determined in cellulose from bacterial origin. As in every polymer, the cellulose chain has a first and a last repeating unit, which are termed non-reducing end (original C4 OH group) and reducing end, a C1 OH group in equilibrium with its aldehyde form. Besides the high chemical flexibility and reactivity, the hydroxy groups form strong intramolecular and intermolecular interactions. While intramolecular interactions (mostly O3H-O5 and O2H-O6 additionally in cellulose I) influence the polymer chain stability

and stiffness, intermolecular interactions strongly affect the crystallinity and supramolecular structure.[14, 15]

Polymorphism and crystalline structures of cellulose

The polymorphism of cellulose is a frequently occurring issue in literature and so far, the structures of cellulose I_α, I_β, cellulose II and cellulose III_I, III_{II} are explored in detail and accepted in the scientific community. [16-19] Another polymorph structure, cellulose IV_I and IV_{II} was under frequent discussion and considered as polymorph for a long time. But during the past years, scientific evidence refuting the existence of cellulose IV_I and IV_{II} as own polymorph structure was collected. This data confirms that the structure of cellulose IV is not an own polymorph but originates from a disordered cellulose I structure. [20]

Cellulose I is the naturally occurring cellulose polymorph and develops in the biosynthesis of cellulose in plants, algae and fungi. Although it is the natural polymorph, it is not the most stable form of cellulose from the thermodynamic point of few. In principle, cellulose I_α and I_β show an equal conformation of the heavy atoms and the polymer chains are all orientated in the same (parallel) direction. Slight differences in the orientation of the hydrogen bonding lead to different packing in either a triclinic or monoclinic unit cell containing either one or two cellulose chains. [21] If the Iα or the Iβ form is dominating depends on the cellulose source, Iα is preferably synthesized in simple organisms like algae or bacteria, whereas Iβ is dominant in plants. [12, 22]

Cellulose II is the other important polymorph. Cellulose II is the thermodynamically most favored form and crystallographically consist of a monoclinic unit cell with two antiparallel polymer chains. [1, 5]. Concerning the intermolecular hydrogen bonds, an O6H-O3 bridge is found in celluloseI, while in cellulose II the chains are intermolecularly linked by an O6H-O2 interaction. Figure 2 explains the intramolecular and intermolecular hydrogen bonds within cellulose I and cellulose II. [12]

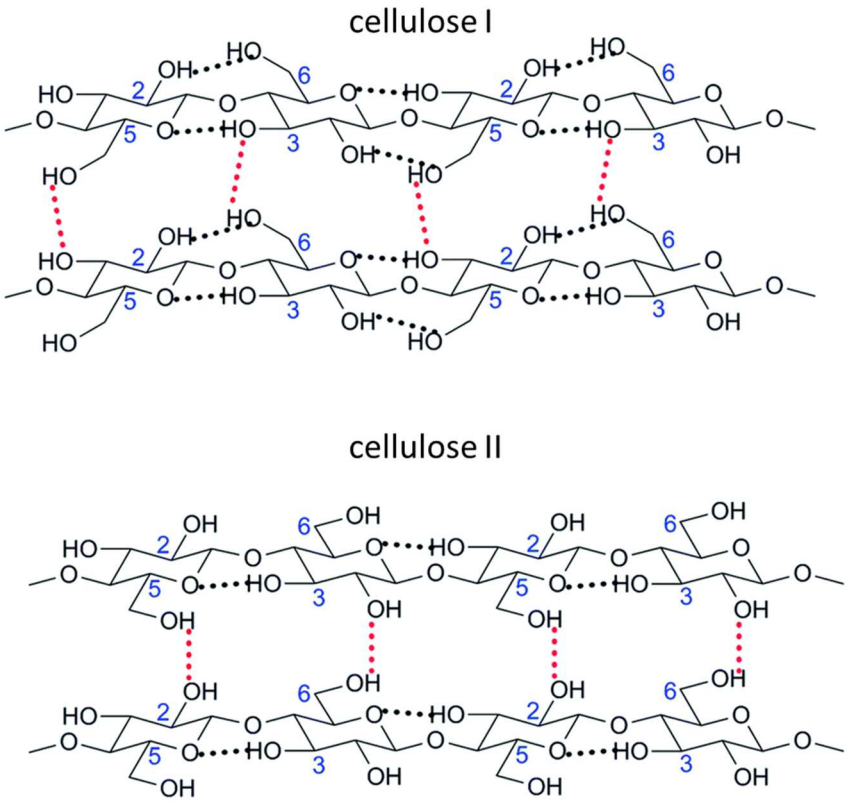

Figure 2 Explanation of intramolecular and intermolecular hydrogen bond interactions in cellulose I and cellulose II [12]

Cellulose III_I / III_{II} are obtained by either treating cellulose I or II in liquid ammonia and subsequent evaporation of the excessive ammonia. Both forms, cellulose III_I and III_{II} can be transferred back in their initial orientation as shown in Figure 3. [23-25]

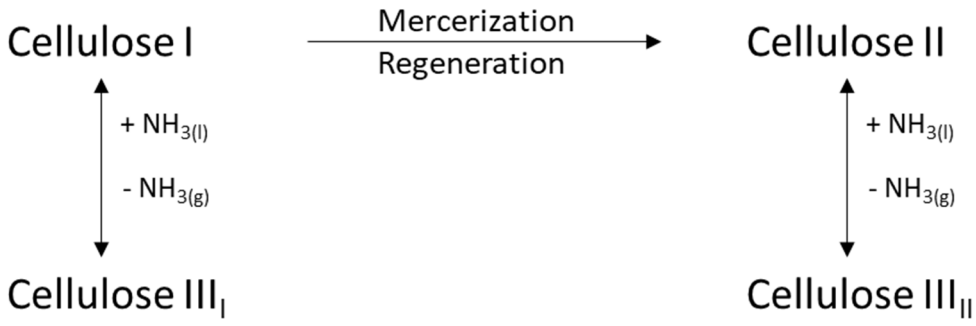

Figure 3 Cellulose polymorphism and it is possible conversions in between the different polymorphs

Development of morphological structures in plant fibers

Different pathways for the processing of cellulose are well described in literature so far. Among these pathways, the growth of cellulose via synthesis in plant cells is the most important process for the employment of cellulose as industrial raw material. Beside the formation in plant cells, certain bacteria, algae and fungi possess the ability to produce cellulose biomass. [5, 26]. As

alternative to the biosynthetic pathways in plants, algae and bacteria, the *in vitro* production of cellulose through enzymatic catalysis got in the focus of science in the past decades. [27]

Due to its importance, the growth of cellulose in plant cells and the fibrillary structures developing thereby is described in this chapter in more detail. Contrary to the majority of polysaccharides involved in plant matrixes, cellulose is not synthesized within the cell in the Golgi apparatus. Instead cellulose is directly built in the cellulose synthase complex (CSC), a very large complex directly bound to the plasma membrane of the cells. The CSC can be described as a six lobed rosette structure with a diameter up to 40nm, whereby each single CSC is assumed to synthesize up to 36 (6x6) cellulose chains. [28] But it is still under discussion how many cellulose chains are really extruded simultaneously, the most prominent numbers are 36 (6x6) or 24 (4x6; 6x4). The extruded single cellulose chains form the so called micro fibrils with a typical length of a few micrometers and a diameter of few nanometer. Later on, the micro fibrils align to macro fibrils with a length in the mm scale and a diameter in the micron region. [29] Those cellulose fibrils consist of areas with a highly ordered cellulose structures, so called crystalline regions or cellulose nanocrystals and are partly interrupted by small dislocations, where the highly ordered structure and the alignment of the cellulose chains is disturbed. [30] Within plane direction, the cellulose chains are attached by hydrogen bonding (Figure 2), in the out of the plane direction van der Waals forces are responsible for the interaction of the chains. Due to this high inter- and intramolecular interactions the crystalline areas are inaccessible for water at ambient pressure. [15, 31] It is noteworthy that the size of the single cellulose crystals strongly depends on the cellulose source. [32]

Beside different cell wall structures, the lumen and the middle lamella are integral parts of plant materials as shown in Figure 4.

The lumen acts as a capillary and contributes to the water uptake in plants. The cell wall consists of three sub parts, namely the primary wall, the secondary wall and the middle lamella. All parts are built up by cellulose fibrils and depending on their purpose, contain varying amounts of hemicellulose and lignin, the other two major constituents in plants. [5, 15] The secondary cell wall is by far the thickest layer and therefore responsible for the stability and mechanical properties of plant fibers. An important parameter for the stability is the fibrillar angle, describing the orientation of the helically wound fibers to the fiber axis itself. [33]

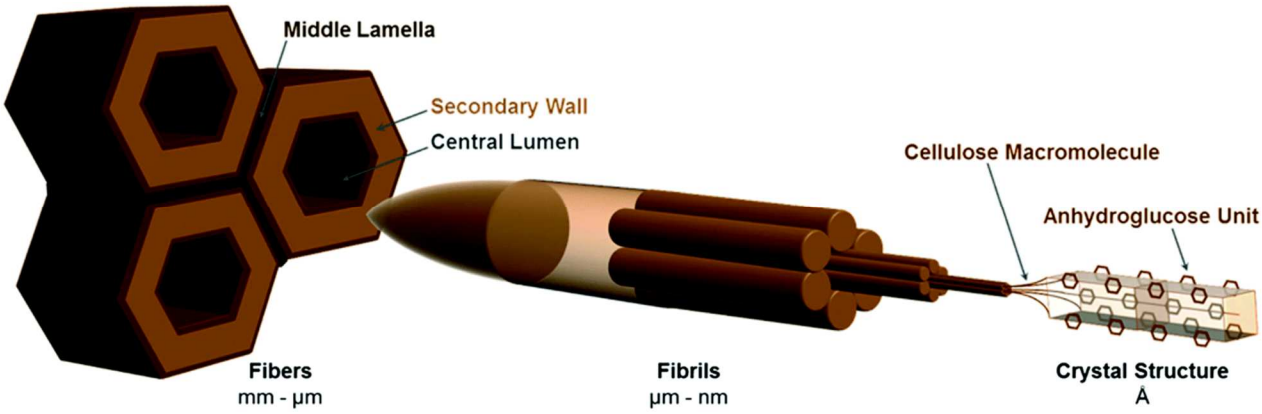

Figure 4 Development of the morphological structure, starting with single cellulose chains built in the cellulose synthase complex (CSC) [12]

Composition of wood based cellulose raw materials

Wood consists of the three main fractions cellulose, lignin and hemicellulose and contains minor amounts of proteins, resins and waxes.

Lignin is a nonlinear macromolecule, that consists of aromatic monomer units called phenylpropanoids. The lignin structures vary from plant to plant, and still are not fully resolved due to their high degree of complexity. The role of lignin in plant materials can be described as glue or cement-like, connecting the cellulose and hemicellulose polysaccharides together through covalent linkages and thereby enhance the rigidity of wood. A second important role of lignin is the control of the water uptake and water transport in plants. Due to its structure, lignin is much less hydrophilic compared to cellulose and hence prevent water from entering cell wall structures. [34] A side effect of the aromatic structure is the brownish coloring. Hence, it is necessary to remove lignin for the processing of whitish pulps and paper products. [22]

In contrast to the high-mass and linear homopolymer cellulose, hemicelluloses are low molecular mass heteropolymers consisting of many different monosaccharide molecules such as glucose, mannose and xylol just to mention a few representatives. With an amount of up to 35% of total mass, they contribute to the robustness of plant materials. The exact ratio of the single sugars present in hemicellulose depends on the source material. [15] Table 1 provides an overview of the composition of different plant materials.

Table 1 Overview of the major components in different plant materials [5]

Source	Cellulose [%]	Hemicellulose [%]	Lignin [%]	Extractives [%]
Cotton	95	2	1	0.4
Flax (retted)	71	21	2	6
Jute	71	14	13	2
Hemp	70	22	6	2
Corn cobs	45	35	15	5
Hardwood	43–47	25–35	16–24	2–8
Softwood	40–44	25–29	25–31	1–5
Bagasse	40	30	20	10
Coir	32–43	10–20	43–49	4

Important cellulose derivatives

With three hydroxy groups per AGU, cellulose has a huge potential for chemical modification and derivatization to functional products. Due to the strong intramolecular interactions and the difficulties in dissolving cellulose, most of the functionalization reactions are done in heterogeneous reactions. In this heterogeneous state, the expansibility of the hydroxy groups is limited and strongly depends on their role in the supramolecular structure. The secondary hydroxy group on the C3 carbon is strongly linked to neighboring pyranose rings within the cellulose chain and therefore hardly accessible for any reactions. The other secondary group on the C2 is due to its neighboring acetal group the most reactive one from the chemical point of view but sterically shielded. The primary hydroxy group at the C6 carbon, is due to it is exposed out of the plane position the most accessible functional group and plays an import role in the derivatization of cellulose. A further factor influencing the reactivity is the crystallinity of the material. Crystalline regions are inaccessible for reactants and reactions only occur on the surface of the crystallites. Thus, pretreatments like mechanical grinding, chemical induced widening of the pore and interfibrillar interstices or disrupting the fibrillary aggregation are frequently applied tools to enhance the accessibility of hydroxy groups for cellulose bulk modification. One very common method to reach higher accessibility of the cellulose network in the regenerate fiber processing is the swelling of cellulose in alkaline solvents like sodium hydroxide solutions, often called mercerization. [31]

An important parameter in the derivatization of cellulose is the degree of substitution (DS), a value describing how many of the hydroxy groups per AGU are substituted. In other words, the DS value is a number between 0 and 3 expressing the success of the derivatization reactions. In reality, the DS is most of the time below 2, because of the described difficulties in the accessibility of all hydroxy groups. The determination of the DS is possible by elemental analysis, spectroscopic methods (UV/VIS, IR, NMR) or colloid titration for example but strongly depends on the present substitute [13, 35]

Oxidation, esterification and etherification are just a few examples among the manifold derivatization reactions developed during the last decades. The products gained through these reactions became an essential part in nowadays life. It is almost impossible summarizing all the reactions described so far, thus just the most important reactions and products are shortly described in this section. [36, 37]

Oxidation

The presence of carbonyl and carboxyl groups on cellulose chains is essential for many technical and biomedical applications of cellulose. A usual method for the controlled substitution with carbonyl groups along the cellulose molecule is the treatment with sodium periodate. The periodate causes an oxidation of the secondary hydroxy groups at the C2 and C3 carbon and leads to the formation of aldehyde functions. A drawback of the periodate oxidation is the partial cleavage of the C2-C3 bond in the pyranose rings, which significantly influences the structure and the alignment of the cellulose chains in the supramolecular structure. [38-41]

TEMPO mediated oxidation is the method of choice for oxidizing the primary hydroxyl group on the C6 carbon and to thereby create carboxyl groups along the cellulose chains. In contrast to the periodate oxidation, the TEMPO mediated oxidation does not affect the pyranose structures. [42, 43] Figure 5 summarizes the possible oxidation pathways for cellulose.

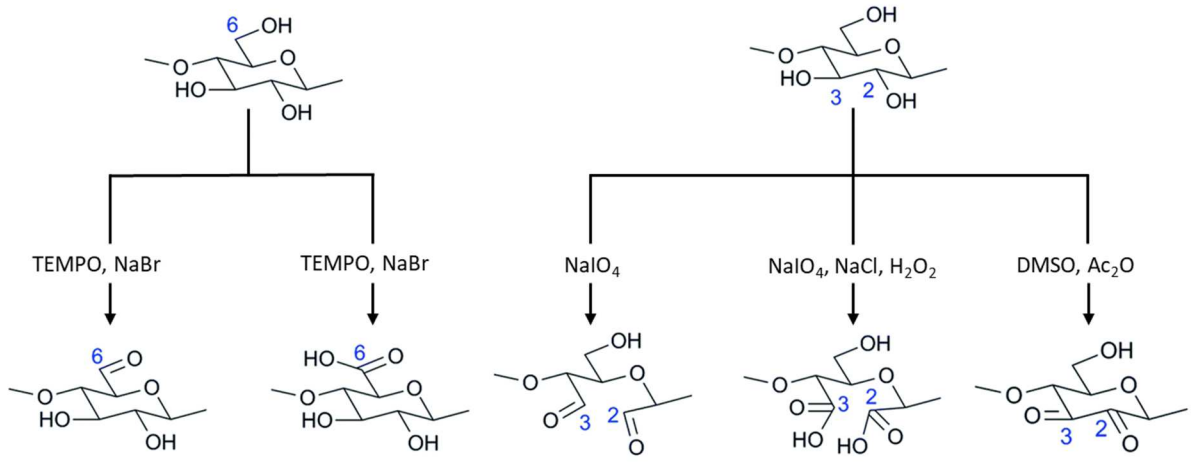

Figure 5 Selective oxidation reactions with corresponding oxidation chemicals for the hydroxy groups at C2, C3 and C6 position [12]

Etherification

Carboxymethylcellulose (CMC) is the most prominent representative among the group of cellulose ethers. Before the alkylation of the hydroxy groups can take place, a pre-activation of the cellulose in sodium hydroxide solution has to be performed. After successful activation of cellulose to alkali cellulose, the carboxymethyl groups are introduced via subsequent addition of chloroacetic acid (Figure 6), whereby a DS of almost 3.0 can be reached but is by far not necessary for industrial applications. [44, 45] CMC is employed in coatings, in the preparation of paintings and dyes, as thickener and binder in various chemical processes or in the immobilization of biomolecules.

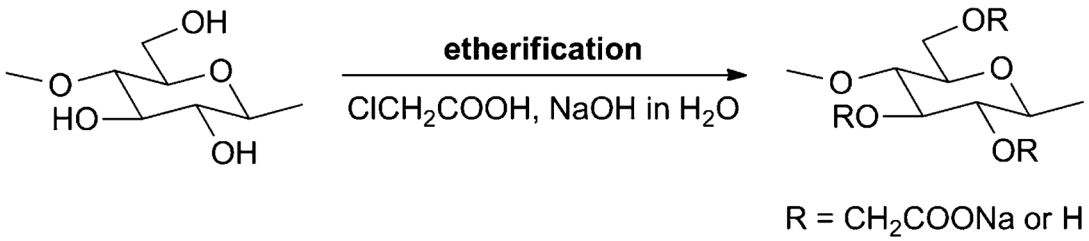

Figure 6 Synthesis of carboxymethyl cellulose

Ethyl and methyl cellulose are further important members in the family of cellulose ethers, their syntheses are comparable to the preparation of CMC. After a pretreatment in an alkaline solution, the methyl or ethyl halogens are added and the corresponding ethers are formed. Methyl ethers are utilized in the production of textiles or cellulose films, ethyl ethers are utilized in the pharmaceutical industry.

The silylation of cellulose to form silyl ethers is a useful tool for the processing of supramolecular cellulose structures like (ultra-) thin films or 3D network. One way for a successful preparation of silyl cellulose is the reaction of hexamethyldisilazane (HMDS) with cellulose in liquid ammonia. The reaction enables a full substitution of all hydroxy groups and leads to the formation of 2,3,6-tri-O-trimethylsilyl cellulose (TMSC). After dissolving and formation of the desired supramolecular structures, the silyl groups can either be partly or fully removed by simple desilylation in acidic atmosphere, with regenerated cellulose staying behind. [38, 46, 47]

Esterification

The most important cellulose ester for industrial belongings is cellulose acetate (CA). CA is produced within a reaction of cellulose in a mixture of acetic acid and acetic acid anhydride under sulfuric acid catalysis in a hundred-thousand-ton scale per year. (Figure 7) In the primary reaction, a full substitution of the hydroxy groups to the tri-acetyl cellulose occurs. Later on, the tri-acetyl cellulose is partly hydrolyzed until the desired DS is adjusted. Large parts of the cellulose acetate are subjected to fiber spinning and membrane casting, where the CA is dissolved in acetone and spun to cellulose fibers or membranes in a wet spinning process. [48]

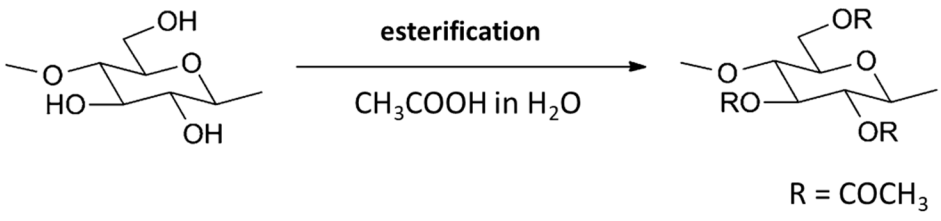

Figure 7 Synthesis of cellulose acetate

Cellulose sulfates show excellent rheological and film forming properties and can be synthesized via many different ways. The utilization of sulfuric acid, chlorosulfuric acid or sulfur trioxide are just a few examples therefore. [13] Due to their excellent film forming properties cellulose sulfates are used as coating material in biomedical engineering or as microcarriers for the transportation of drugs or proteins.[49] Among cellulose sulfonates, cellulose tosylate is the most important representative due to its promising application in the processing of cellulose based polymeric materials. Cellulose sulfonates are formed via simple esterification of cellulose sulfonic acid chlorides or anhydrides. [50]

Cellulose nitrate (CN) is a further prominent cellulose ester, formed by the reaction of hydroxyl groups with nitric acid in the presence of sulfuric, phosphoric or acetic acid. Nitrocellulose is well known for its employment in the photo and film production and its explosive character, utilized in the formation of gunpowder and fireworks. Today's most important applications are the formulation of coatings or dyes and the utilization of cellulose nitrate membranes in the blotting of DNA (Southern blot) and Proteins (Western blot). [31, 38, 51] Table 2 presents an overview of the most important cellulose derivatives in industrial terms.

Table 2 Industrially important cellulose derivatives, their annual production volume and major application areas [12]

Cellulose derivative	Production (t/a)	Application
Cellulose xanthate	3200000	Fibers and membranes
Cellulose acetate	900000	Coatings and membranes
Cellulose nitrate	200000	Membranes and explosives
Carboxymethyl cellulose	300000	Coatings, paints, adhesives and pharmaceuticals
Methyl cellulose	150000	Films, textiles, food and tobacco industry
Hydroxyethyl cellulose	50000	Paints, coatings, films and cosmetics
Ethyl cellulose	4000	Pharmaceutical industry

Dissolution of cellulose

The amphiphilic character, the high crystallinity caused by strong intra- and intermolecular interactions, the supramolecular structure and the high degree of polymerization are major reasons for the high stability of cellulose towards many solvents. The search for suitable cellulose solvents was one of the major issues in a broad variety of academic or industrially driven research projects. Suitable solvent systems are crucial for the shaping, the characterization and homogenous phase reactions of cellulose. In other words, only with a well performing cellulose solvent, scientific or technically important issues can be solved. The determination of key values like DS or DP, the monitoring of modification and derivatization reactions, or high value and large-scale processes like the shaping of cellulose to films and fibers, require suitable solvents. [52-54]

With increasing scientific efforts applied on issues like dissolving, derivatization, characterization and shaping of cellulose, a broad variety of cellulose solvent systems was developed during the last 150 years. To overview the numerous solvent systems, a classification based on the principal solvent mechanism seems to be a sufficient way to explain the world of solvent systems. In a first step, the solvent systems can be divided in derivatizing and non-derivatizing solvents. Within the non-derivatizing solvents, a further difference is made between solvents based on aqueous media and non-aqueous media. Figure 8 should give an overview of different categories for cellulose solvents and the most prominent representatives of each group. [36]

Although a large diversity on cellulose solvents is well described in literature, most of the systems are limited to a certain purpose. It is the toxicity of the solvents, their high costs, the limitation in the scale-up, the low cellulose dissolution capacity or unsolved questions in environmental and recycling issues, which make most of the described systems incapable for technical applications. A solvent suitable for the employment in large-scale cellulose processes should be environmentally harmless (or at least quantitatively recyclable in a closed process loops), cheap, easy to handle and capable to dissolve large amounts of cellulose. Among the most promising solvents, fulfilling a majority of the requirements, the processing and dissolving of cellulose xanthate and the direct dissolution in N-methylmorpholine-N-oxide (NMMO) are the systems with commercial success so far. [52]

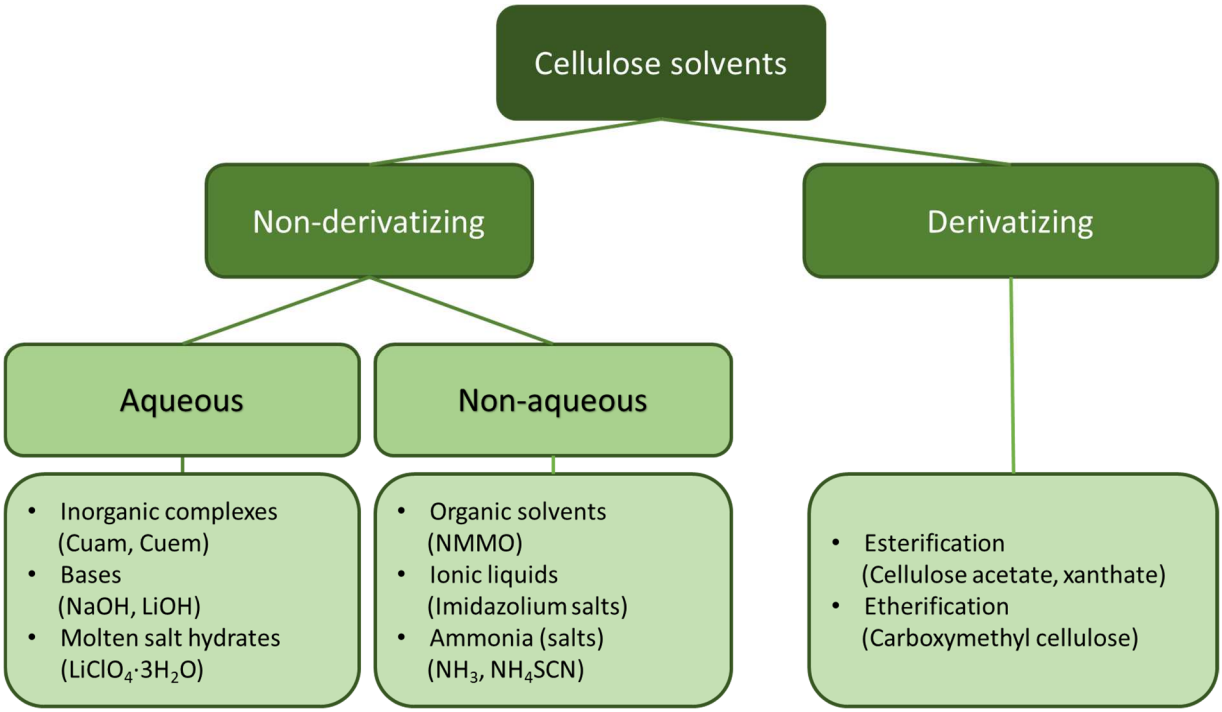

Figure 8 Classification of cellulose solvents and important examples of solvents

Aqueous non-derivatizing solvents

Employing inorganic salts and complexes for the dissolution of cellulose was a frequently investigated issue since the early days of cellulose processing. The most prominent representatives of non-derivatizing aqueous solvents are copper-based complexes like cuam (cuprammonium hydroxide) and cuen (cupriethylenediamine hydroxide). Both were frequently used for the processing of cellulose fibers and high quality membranes in the past decades. [55] The cuprammonium process is described in more detail in the following chapter, as the technology represents a milestone in the history of man-made cellulose production. [56]

Later on, another group of transition metal complexes based on nickel got in the focus of interest. With complexes like $Ni(tren)(OH)_2$ [tren = tris(2-aminoethyl) amine] up to 10% cellulose can be completely dissolved and subsequent esterification and etherification reactions in a homogenous reaction system can be performed. The major advantage of a homogenous reaction system is the high accessibility of the hydroxy groups, which are no longer blocked and shielded in the supramolecular structures. [57, 58]

Beside the well-known swelling of cellulose in sodium hydroxide solutions, called mercerization, it is less known that high concentrations of sodium or lithium hydroxide (10%) are also capable to fully dissolve cellulose at low temperatures. The disadvantage in these solvents is the rather low DP of 200 required to completely dissolve cellulose. [59] A further development in the use of LiOH and NaOH bases for cellulose dissolution is the addition of

urea and thiourea. The presence of urea leads to an accelerated cellulose dissolution, but introduces instability and temperature sensitivity to the system. The low dissolution temperature of around -10°C is considered as a further drawback. [60, 61]

Molten salt hydrates and mixtures thereof are further representatives of aqueous non-derivatizing solvents. These molten salts got into the focus of interest due to their ability to dissolve cellulose with high DP values up to 1500. Lithium perchlorate trihydrate ($LiClO_4 \cdot 3H_2O$) as pure substance and in mixture with magnesium perchlorate hydrate ($Mg(ClO_4)_2 \cdot H_2O$) is reported to dissolve high amounts of cellulose within a few minutes, yielding transparent solutions. Subsequent modification reactions or the regeneration of cellulose II from the molten salt solutions is possible. The limitation in these kind of solvents systems is to handle the process and the high process temperatures needed. [62]

Non-aqueous solvents

The diversity in non-aqueous non-derivatizing solvents is broad and ranges from one component systems up to complex mixtures of three and more components. The most famous system is the one component solvent N-methylmorpholine-N-oxide (NMMO), building the foundation of the so called Lyocell process. Interestingly, NMMO is considered as non-aqueous solvent although it has to be in its monohydrate state to successfully dissolve cellulose. The dissolution of cellulose in NMMO is based on pure physical phenomena, allowing the dissolution of large amounts of cellulose within short time periods. Beside its suitability for large scale applications, NMMO is also a proper solvent for manifold derivatization reactions or analytical purposes. [52]

In addition to the family of N-oxides of tertiary amides, N-alkylpyridinium based solvents, as N-ethylpyridinium are worth mentioning as important one-component systems. The major drawbacks of these solvent systems are the elevated temperature necessary to bring them in liquid state and their autocatalytic degradation tendency. [52]

For the two component systems, N,N-dimethylacetamide/lithium chloride (DMA/LiCl) and dimethylsulfoxide / tetrabutylammonium fluoride trihydrate (DMSO/TBAF) are those to be mentioned. DMA/LiCl is a well-known solvent system frequently applied in analytical processes. The major advantages of this system are the negligible polymer degradation even in the high DP range and the formation of transparent solutions. [63]

DMSO/TBAF is considered as rather new and powerful solvent system for the dissolution of high DP celluloses up to 650 in rather short time frames of around 15 minutes and without any

necessary pretreatment. Interesting is that among all tetrabutylammonium salts only the fluorine salt is capable to dissolve cellulose. [64]

Ionic liquids are the latest generation of powerful and ecofriendly systems, for the dissolution of high amounts of cellulose and subsequent formation of regenerated fibers and films. Characteristic for Ionic liquids is their low melting point below 100°C. Important representatives of this group are imidazolium-based liquids like 1-allyl-3-methylimidazolium chloride (AmimCl) or 1-ethyl-3-methylimidazolium acetate (EmimAc). They are able to dissolve up to 30% cellulose with DP values of 650 within 30 minutes. [65, 66] Whereby it is noteworthy that Rosenau showed that imidazolium cations react at the C2 with cellulose in its reducing form or any other present aldehydes and hence act as derivatizer for cellulose. [67]

Later on, pyridinium-based ionic liquids got in the focus of science and concentrations up to 37% dissolved cellulose have been reported. In addition to imidazolium and pyridinium based ionic liquids a group of cholinium-based systems was described as non-toxic, cheap, biodegradable and widely available alternative. [68, 69]

Meanwhile a large diversity in available cationic and anionic compounds for ionic liquid systems does exist. Figure 9 summarizes the most important anions and cations described so far.

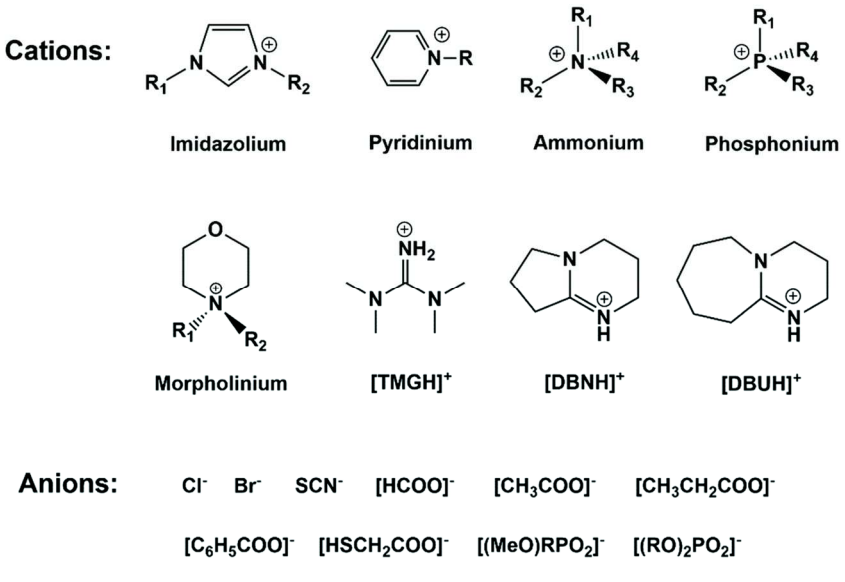

Figure 9 Important cations and anions molecules in ionic liquids. The abbreviations used for the explanation of the cations and anions in the figure are explained here: $[TMGH]^+$ = 1,1,3,3,-tetramethylguanidin; $[DBNH]^+$ = 1,5-diazabicyclo[4.3.0]non-5-enium; $[DBUH]^+$ = 1,8-diazabicyclo[5.4.0]undec-7-ene; $[SCN]^-$ = Thiocyanate; $[HCOO]^-$ = Formiate; $[CH_3COO]^-$ = Acetate; $[CH_3CH_2COO]^-$ = Propionate; $[C_6H_5COO]^-$ = Benzoate; $[HSCH_2COO]^-$ = Sulfanylacetate; $[(MeO)RPO_2]^-$ = Methylphosphonate; $[(RO)_2PO_2]^-$ = Dialkyphosphonate [54]

Derivatizing solvents

In contrast to non-derivatizing solvents, exploiting only physical phenomena, this class of solvents utilizes the accessible hydroxy groups to modify cellulose in a way that it becomes soluble. The main concept behind this class of systems is the formation of a hydrolytically instable, but soluble cellulose derivative through chemical modification.

The economically most successful derivatization reaction is the formation of cellulose xanthate (CX), starting from activated cellulose by simple addition of carbon disulfide (CS_2). [70] The CX is dissolved in sodium hydroxide and subsequently regenerated to cellulose fibers and films in the Viscose process. The Viscose technology is still the most important process for the production of regenerated cellulose fibers, although the technology is already in use for more than 100 years. More details on the fiber processing based on CX are discussed in the next chapter. [71]

In addition to the CX, a very similar process based on the formation of cellulose carbamate was frequently discussed in recent years. Cellulose carbamate is, like CX, formed in a reaction of cellulose with urea and counts as green and sustainable alternative to toxic chemicals used in the Viscose processing. The dissolution of cellulose carbamate and the further processing to fibers is similar to the Viscose technology and even mixtures of both derivatives can be processed. [72, 73]

Further important reactions in the processing of soluble cellulose materials are based on esterification reactions with carboxylic acids and anhydrides. Among these reactions the formation of soluble cellulose acetate and cellulose trifluoroacetate are worth mentioning. The later one is an important intermediated in the production of long chained or mixed cellulose ester with high DS. The formation of cellulose acetate, cellulose nitrate or trimethylsilyl cellulose and their employment in the processing of supramolecular structures was already described in the previous section. [74]

In addition to systems employing protic solvents, routes for the processing and subsequent dissolution of cellulose derivatives are described in literature too. One example is the dissolution of cellulose in dimethylformamide / dinitrogentetraoxide (DMF/N_2O_4) under the formation of cellulose nitrite. [75]

Regenerated cellulose

In former times, people relied on naturally occurring plant fibers like cotton, hemp or jute. With the identification of cellulose as structural compound in wood and the ongoing progress in the development of solvent systems in the 19th century, the foundation for the shaping of man-made cellulose products was laid. The shaping of dissolved cellulose into fibers and films was not a process planned in detail before, it happened more by coincidence and involved visionary scientists recognizing the potential behind the observed phenomena and reactions. [48]

In 1855, George Audemars from Switzerland described that fibers can be produced by simple air drawing from nitrocellulose that was dissolved in alcohol. This patent is counted as the beginning of man-made cellulose fiber production, but it took many more years, until Chardonnet could convince investors to open the first artificial silk production in 1892. [76]

Shortly after the first factory for artificial silk started, new companies with alternative processes followed. The second technology ready for commercialization was the cupro technology in 1899 by Glanzstoff. The fiber processing is thereby based on the discoveries of Mathias Eduard Schweizer, who observed the dissolution of cellulose in copper salts in ammonia. [76] Another process developed almost simultaneously is the Viscose technology, employing water soluble cellulose xanthate (explained in more detail in part I). [48]

During the 20th century, a huge progress in the demand and in the production of man-made cellulose fibers occurred. Especially the Viscose process with its outstanding fiber qualities conquered the markets. In recent decades, a change in human's attitude to more sustainable and environmentally friendly products in combination with decreasing fossil resources, led to the development of new cellulose fiber processing technologies. [77]

The first fully commercial technology in a serious of green and sustainable process developments was the Lyocell technology. The Lyocell process exploits NMMO as solvent for cellulose and is described as key technology in the sustainable production of cellulose materials, delivering a chance to decrease the dependence on fossil, cotton or environmentally hazardous based process technologies. [78]

The Carbacell and the Ioncell technology are two further processes based on latest developments in cellulose solvent systems, but are so far not commercialized in large scale. Both technologies offer a green and environmentally harmless fiber processing technology due to their closed process loops and the exploited chemistry. [77, 79, 80]

Cupro fibers

Since the early beginning of the commercial cupro fiber spinning by Glanzstoff in 1899, the technology had to compete with other upcoming processes like the Viscose technology. This permanent pressure and the ongoing competition lead to a fast development in both technologies and the invention of many important improvements and process upgrades. [48]

As traditional cellulose source, cotton linters (short fibers from cottonseeds) are utilized for the processing of cupro fibers. Experiments employing other raw materials like wood pulp, caused problems in the dope preparation and led to worse fiber qualities. As pretreatment, the cotton linters are purified in a sodium hydroxide solution, bleached and finally dehydrated to 50% water content. [48]

The cuprammonium complex is formed by dissolving copper hydroxide in ammonia under the development of a deep blue solution. The deep blue color originates from the cupric tetra amine hydroxide (CTH) complex, which is unstable. Fast decomposition to copper oxide occurs, if the solution is not protected from light and heat. The pretreated cotton linters are finally added to the solvent and dissolution is initiated by a complex formation between CTH and cellulose under the release of ammonia. The free ammonia reacts again with excessive copper hydroxide to CTH and subsequently to a complex with cellulose until a cellulose concentration of 10 to 12% is reached, and excessive copper hydroxide and ammonia are exhausted. The final concentration for copper and ammonia are in the range of 3 to 5% and 6 to 8%, respectively. For the complex formation, a preferred coordination of CTH to the hydroxy groups at C2 and C3 carbon is assumed. Before the solution is subjected to fiber spinning, filtration and degassing are required. [76]

Fiber spinning in the cuprammonium technology is done via a continuous wet spinning process (Figure 10), where the nozzle is in direct contact with the coagulation bath. The fundamental concept in the development of modern spinning equipment for cupro fibers is the separation of the three main steps in fiber formation, namely stretching (deformation of the complex), coagulation (solidification of the fibers) and regeneration. By successful separation of the single fiber formation reactions in independent steps, the fiber quality increased distinctly. As coagulation bath, water or water/acetone mixtures are typically employed. In the first step, the cellulose CTH complex decomposes due to hydrolysis and large parts of the cooper and almost 80% of the ammonia are removed, giving a structure called blue yarn. In the second step, the coagulation of the cellulose chains is forced by free hydroxy groups and in the last step, the remaining cooper and ammonium is removed.

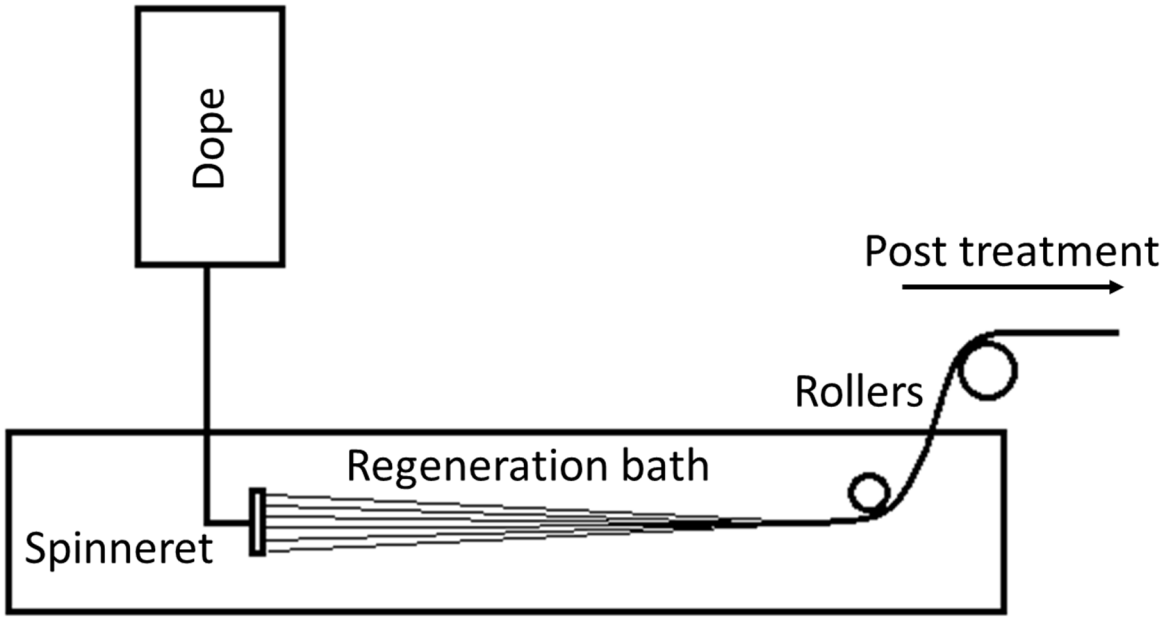

Figure 10 Flow scheme for the illustration of a wet spinning process with the nozzle directly in contact with the spinning bath

A major issue in this technology is the recycling and recovery of the used chemicals. For the copper, a recovery rate higher than 99% is reported. This high recovery rate could be achieved via a very complex and expensive process chain. The major parts of ammonia are recovered by ion exchange and distillation under reduced pressure, but the recovery rate is lower than that of copper. [48, 76]

Cupro fibers have a characteristic circular shape and a very smooth surface morphology. The development of core-shell structures is almost restrained and only a very thin shell with a higher porosity than the condensed fiber core is observed. The smooth and compact fiber structure is responsible for the pleasant and comfortable impression caused by cupro fibers, comparable to the properties of silk. The wet to dry ratio is reported to be 0.7, the tensile strength is a bit higher and the elongation a bit lower compared to Viscose based fibers.

Although the cupro fibers have some advantages compared to other regenerated cellulose fibers, the process could not match up with the fast development of the Viscose technology. Already in the 1930's, when man-made cellulose fiber production had its first great boost, Viscose fibers conquered the markets, mostly due to its simpler and more economic processing technology. Cupro fibers and membranes were produced for special applications and are still available, although the production capacity is far behind other technologies. Therefore, it plays only a minor role in the global fiber production.

Lyocell fibers

Although N-methylmorpholine-N-oxide (NMMO) was already described as cellulose solvent in the 1940's, intense research for its utilization in commercial cellulose processing started only in the 1980's. The research for the development of a scalable process was driven by many companies and scientific organizations in the US and Europe. After enterprise takeovers and a successful patent application, the Austrian Lenzing AG with its Tencel technology is the only commercial fiber producer employing NMMO as solvent. Meanwhile, the initial challenges such as solvent stabilization, recycling or the high fibrillation tendency of Lyocell fibers have been overcome and the annual production capacity is in the range of several hundred-thousand-tons with single plants able to produce one hundred thousand tons per year. [78, 81]

As starting material in the Lyocell process, high quality pulp with a DP from 400 up to 1000 can be employed without any further treatment. After passing a shredder, the pulp is subjected into a NMMO/water mixture (76-78 wt.% NMMO) with additional minor amounts of solvent stabilizer and degradation inhibitor. The mixture is heated to 70 – 90°C while the slurry is vigorously stirred and a swelling of the cellulose fibers is initiated. [48, 78]

The next step in the process chain is the complete dissolution of the cellulose. Therefore, the slurry is heated further under vacuum to remove water until NMMO is in its monohydrate form (13.3 wt.% water). The monohydrate allows for full cellulose dissolution (Figure 11). Cellulose concentrations in the Lyocell process are usually between 10 and 18%, whereby the high viscosity of the resulting spinning dope limits solubility. The pressure necessary for transportation and filtration of the dope is up to 180 bar. As NMMO is rather unstable and readily undergoes exothermic degradation reactions, causing the development of volatile amines and water vapor concomitant with a fast increase in pressure, special bursting discs are fixed along the whole process loop. After filtration, the dope is extruded into several single channels for fiber spinning. [78, 81]

Each channel ends up in spinning nozzles with several thousand single holes, through which the spinning solution is converted to fibers. Before the fibers enter the coagulation bath, they pass an air gap where the fibers are conditioned, oriented and stretched. The coagulation bath itself consists of diluted NMMO solution. [48]

A washing step in hot water finalizes the spinning and stretching process, and removes residual solvent from the fiber tow. The contaminated washing solution is further treated in the solvent recovery system to avoid any loss of the expensive NMMO. Possible post treatments in the

Lyocell process are bleaching (if required) and soft finish to enable further processing to yarn. [81]

Solvent recovery in the Lyocell process consists of two major steps, an ion exchange and the evaporation of excessive water. Ion exchange is done in the diluted solvent to remove cationic and anionic impurities, which would cause solvent instability and a decrease in fiber quality. Before reusing the purified solvent system, the water content is reduced to a level suitable for the uptake of new pulp. The total solvent recovery in commercial plants is reported with 99% and more. [48, 81, 82]

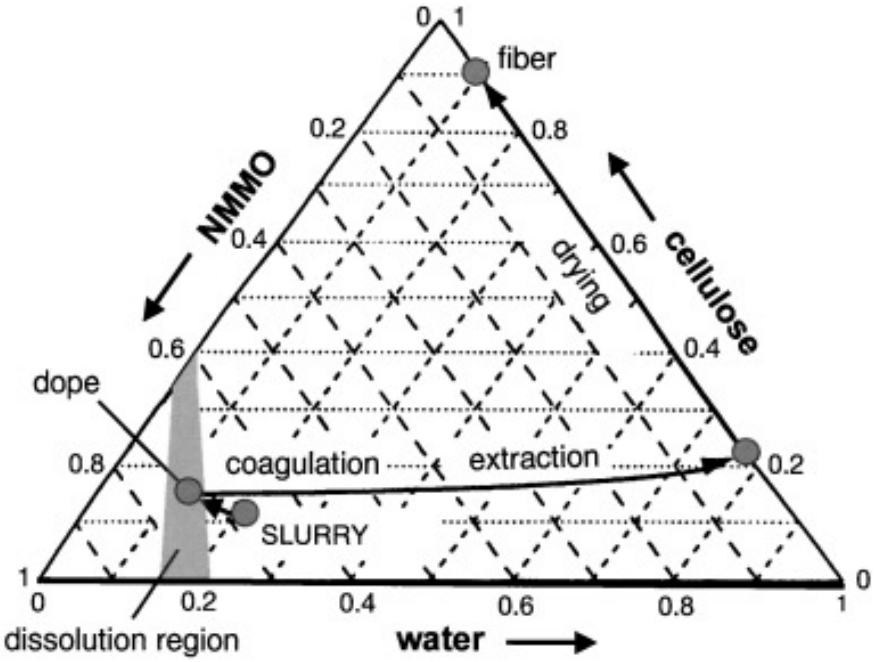

Figure 11 Phase triangle of the NMMO / water / cellulose system for the dissolution and processing of cellulose in the Lyocell process [48]

Lyocell fibers possess a roundish structure with a dense cellulose network and only small pores with a volume in the range of 10 to 100 nm. The crystallinity and the overall orientation are much higher compared to Viscose or carbamate based fibers. Mechanical properties and the wet to dry ratio exceed those of comparable Viscose fibers by far, enabling better textile properties and a broad spectrum for application. [78]

One property of Lyocell fibers noteworthy to mention is their high fibrillation tendency. The fibrillation behavior can be used as advantage in special applications but in the general textile fabrication, a high fibrillation tendency is undesired. To overcome this drawback, different cross-linking mechanisms employing triazine or other molecules have been developed to inhibit fibrillation on the fiber surface. [48]

As the Lyocell technology was protected with numerous patents, only the Lenzing AG utilizes the process in a commercial manner so far. However, the demand for Lyocell products is increasing, the markets develop rapidly and the production capacities are extended in large scale.

Ioncell fibers

In the early terms of the intense research activities on cellulose dissolution, the majority of ionic liquid systems were based on imidazolium salts. Within a short period, it could be shown that ionic liquids offer a well controllable, very simple and safe possibility for the production of cellulose fibers with process parameters comparable to the Lyocell technology. However, the imidazolium based liquids and their mostly halogenic anions caused severe degradation of the cellulose, especially at elevated temperatures. [83, 84]

In 2014, researchers from Aalto and Helsinki university published new ionic liquid systems with high spinning stability and competitive fiber properties. The new ionic liquid 1,5-diazabicyclo[4.3.0]non-5-enium acetate [DBNH][OAc] exploits a super base in combination with an acid ion pair. The process for the fiber spinning based on this solvent system was termed Ioncell F technology and the obtained fibers are called Ioncell F fibers. [77]

[DBNH][OAc] has, compared to NMMO, the advantage of a lower melting point and a much lower viscosity leading to faster cellulose dissolution. For example, a 13% cellulose solution is prepared in less than 60 minutes at 80°C. Concurrent with the accelerated dissolution, the mild conditions protect the cellulose and the solvent from severe degradation reactions, save thermal energy and increase economic efficiency. [85]

The fiber spinning itself is performed via a dry jet wet spinning, where the fiber formation proceeds in two major steps. A first solution state draw in an air gap and subsequent desolvation and structure formation in a coagulation bath. The solution state draw is enabled by the high viscosity of the spinning dope and within the longitudinal increased draw in the air gap, the dissolved molecules are stretched and become orientated along the fiber axes. In the second step, the desolvation in the coagulation bath and subsequent structure formation is initialized. The precipitation of the cellulose molecules in the spinning bath is, like in all the other regenerate fiber processes, diffusion controlled. Figure 12 illustrates the principle of dry wet spinning as applied in Ioncell and Lyocell technology. [86]

Due to the higher cellulose content in Ioncell spinning dopes, the mechanical properties of these fibers even exceed those of comparable Lyocell fibers as reported by Sixta. [77] In terms of

crystallinity, the Ioncell fibers do not show as high crystallinities as Lyocell fibers, however the overall fiber orientation is higher in the Ioncell fibers. [87]

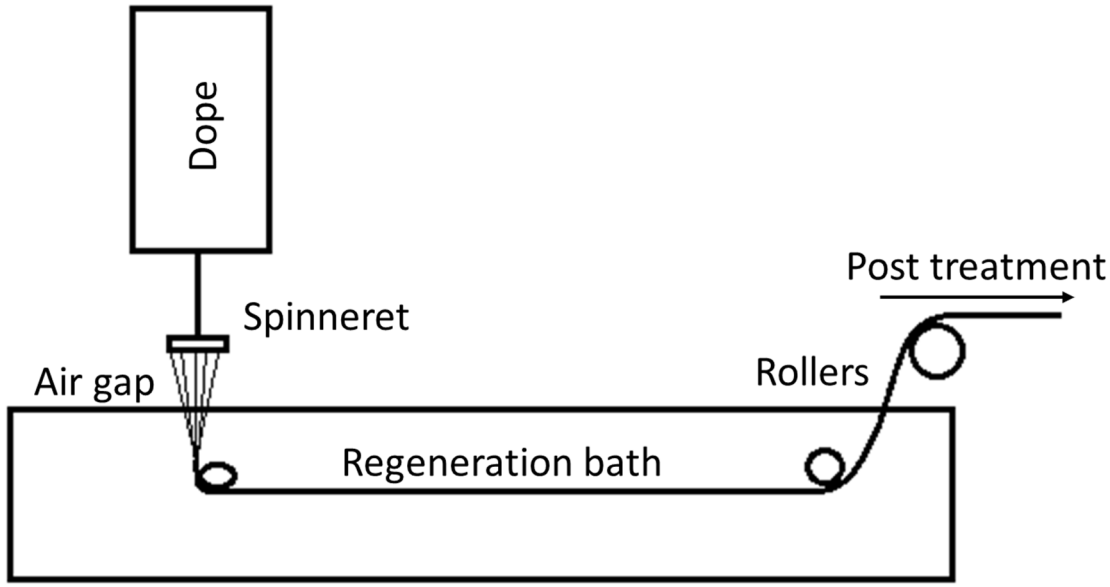

Figure 12 Flow scheme for the illustration of a dry-jet wet spinning process with the spinning nozzle above the spinning bath

The wet to dry tenacity ratio, describing the performance loss in wet state, is reported between 0.6 and 1.0 for Ioncell fibers. These values are higher as those reported for Viscose fibers (around 0.5) and similar to Lyocell fibers. The cross sectional shape of the fibers is roundish to oval and quite similar to fibers obtained from the Lyocell technology. [85]

The real breakthrough is connected to a successful recycling and recovery of the solvent. However, as the water has to be removed almost completely from the recovered ionic liquids and only partly in NMMO, this brings a cost advantage for the Lyocell process, which could only be overcompensated with better fiber properties, cheaper pulp materials or higher cellulose contents in the dope. Thereby, especially the low viscosity of the ionic liquids is a major advantage, as it enables higher cellulose contents and processing at lower temperatures, making the process more efficient. In addition, the lack of stabilizers as employed in the Lyocell fiber processing could also contribute to a better overall efficiency. [77]

Right now, the Ioncell technology is not fully commercialized but straight focused plans for the installation of a pilot plant in 2019/2020 and a further upscale to industrial scale by 2025 exist and a consortium of project partners strongly supporting this project has already formed.

Carbacell fibers

The ability to dissolve cellulose carbamate in weak bases and subsequent precipitation in acidic solutions was already explored in the 1930's. But it took 50 years longer until the results were rediscovered and a technology for the semi-commercial spinning of cellulose fibers was developed and published under the name Carbacell. The main objective of the Carbacell technology is to offer a possibility for the spinning of high quality cellulose fibers under the reuse of existing Viscose plants. The use of urea instead of carbon disulfide for the derivatization reaction raises the chance for a green and sustainable fiber production avoiding severe environmental hazards. [79]

The single processing steps in the Carbacell technology are similar to those in the Viscose processing. Both technologies start with an alkaline pretreatment of the pulp source to activate the cellulose for subsequent derivatization. After the alkaline treatment, the excessive base is removed by pressing the pulp, shredding and a pre-ripening to adjust the DP conclude the pulp treatment. The derivatization reaction in the carbamate process is performed in inert organic solvents or directly in liquid urea. [88]

In the beginning the decomposition of urea to biuret, triuret or higher homologues occurs and those react with the activated cellulose. The reaction conditions are important and severely influence the quality of the resulting carbamate and finally the fibers. Usually, the formation of cellulose carbamate with a nitrogen content of 2.5 to 4.5% (DS 0.3 to 0.6) is pursued, the DP of the cellulose is adjusted to 250 to 400 depending on the desired fiber properties. The dissolution of the carbamate is performed in 5% sodium hydroxide solutions and cellulose concentrations up to 10% can be achieved. A major advantage of the Carbacell technology vs the Viscose process is the increased storage stability of the carbamate. Carbamate is reported to be stable over months and could be subjected to spinning without any problems after long storage periods. The long storage stability allows for more flexibility in the process and a distribution of centrally produced carbamate to local spinning plants is possible. [79, 88]

After successful pulp dissolution, the spinning dope is filtered and degassed. A post-ripening step as required in the Viscose process is not necessary in the Carbacell process. The spinning of the dope to regenerate fibers is almost equal to the spinning of Viscose fibers. The possibility to utilize equipment of commercial Viscose lines for the processing of carbamate based fibers was shown several times. [79, 88]

The regeneration bath for the Carbacell process consists of sulfuric acids and sodium sulfate in concentrations comparable to the Viscose technology, but without heavy metal ions (e.g. $ZnSO_4$). After spinning of the fibers, the regeneration to cellulose takes place within a few seconds by deposition in a subsequent sodium hydroxide bath (> 1%) at elevated temperatures. The ammonia created thereby, could be recovered and reused. Figure 13 compares the process chains for the production of man-made cellulose fibers in the Viscose and the Carbacell technology. [79]

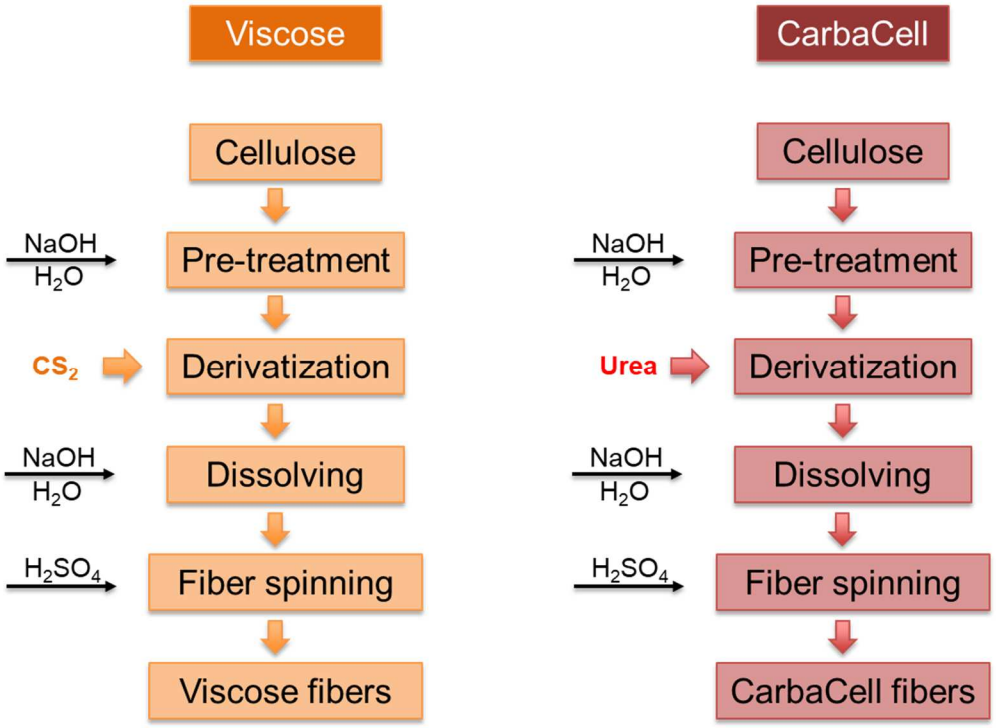

Figure 13 Comparison of the major process steps in Viscose and Carbacell technology

The fibers obtained in the Carbacell technology have a round to oval cross section and a dense morphological structure, comparable to fibers from the Lyocell process, but different to Viscose based fibers. Further, the Carbacell fibers show a well-defined and regular distributed pore size distribution in the range of 10 to 100 nm, depending on the process conditions. [79]

Concerning mechanical and physical parameters, fibers obtained in the Carbacell process are comparable to Viscose fibers and there is no severe difference in tenacity, wet to dry tenacity ratio or water retention value. The Carbacell technology provides fibers with properties comparable to high quality Viscose fibers but avoids toxic and environmentally harmful sulfur components for the derivatization or the use of heavy metal ions in the coagulation bath.

Part I

The Viscose process: Basic reactions, lab scale operation and advanced Materials

Content

#1) Michael Weißl, Gregor Kraft, Josef Innerlohinger and Stefan Spirk; Spinning of Fibers from Wood – A Lab Experiment to Introduce Students in Viscose Fiber Manufacturing and Analysis; Journal of Chemical Education; 2019; submitted

#2a) Michael Weißl, Mike Pelzman, Armin Zankel, Brigitte Bitschnau, Helmar Wiltsche and Stefan Spirk; Processing of metal sulfide/ cellulose composite fibers in core-shell configuration; Lenzinger Berichte; 2019; submitted

#2b) Stefan Spirk, Gregor Trimmel, Michael Weißl, David Pfeifer, Mathias Hobisch, Bruno Alonso; In situ Synthese von Metallsulfidpartikeln auf/in Fasern und Filmen im Zuge des Viskoseverfahrens; A50790/2018

#3) Marlene Kienberger, Paul Demmelmayer, Michael Weißl, Armin Zankl and Stefan Spirk; Biobased support layers for the fractionation and selective extraction of lignosulfonates; Solvent Extraction and Ion Exchange Journal, 2019, accepted

The success story of Viscose silk was initiated by Cross, Bewan and Beadlein in 1892. Rapidly it conquered the markets and replaced silks made from nitrocellulose and cuprammonium. [48, 70] In detail, Cross, Bewan and Beadlein explored the reaction of alkali cellulose and carbon disulfide to cellulose xanthate. They realized that the produced cellulose xanthate is very well soluble in a diluted sodium hydroxide solution and can be converted after a processing step to cellulose fibers or films by exposure to an acidic bath (Figure 14). Nowadays, this process is the most important process to manufacture man made wood based fibers with production volumes of several million tons per year. [89, 90] Although the basic principle is still the same as in the end of the 19th century, much progress has been made in the preparation of the alkali cellulose, the removal of undesired impurities, and the procedures to obtain spinning dopes suitable for the production of high quality fibers. [91-93] Besides progress in the fiber/film manufacturing, also the processes to recycle the used chemicals and to remove them from air have been improved significantly. [94] For instance, air pollution by the largest Viscose manufacturer in Europe, Lenzing AG, is at an extremely low level, which is a prerequisite considering that the plant site is located close to residential areas. [95] Nethertheless, the huge demand on easy flammable and harmful CS_2 for the xanthation and the release of toxic HS_2 gases during the production are considered as major drawbacks of the Viscose technology. Since the demand for fibers is steadily growing, and since cotton plantation is more or less on the limit of potential land use, the only way to close the gap is to focus on wood-based fibers. The Viscose process is certainly a part of the solution to this problem. [89]

The formation of alkali cellulose is the first step in the manufacturing of Viscose fibers. The main reactant is sodium hydroxide to give the sodium salt of cellulose. In industry, standard dissolving pulp is mixed with 18-20 wt.% NaOH to form a ca. 5 wt.% suspension. This suspension is exposed to a temperature between 25 and 55 °C for some hours. At this stage, the low molecular weight fraction of cellulose as well as the hemicelluloses dissolve and are removed by pressing the alkali cellulose. After pressing, the alkali cellulose contains 7-8 wt.% bound and ca 9 % adsorbed NaOH. Then the alkali cellulose is subjected to pre-ripening, i.e. storage at 30-55°C for a period between 10 and 30 hours under defined humidity control. During the pre-ripening a wealth of reactions take place, hydrogen bonds of the crystalline parts of the pulp are broken up and depolymerization of the cellulose macromolecules occurs. The average DP decrease from the range 850-600 to 500-350.

The next step in Viscose synthesis is xanthation. In this step, the alkali cellulose is converted to the sodium cellulose xanthate. In industry, this exothermic reaction is done in huge cylinders

where the CS_2 is reacted in vaporous state (either injected as gas or vaporized in vessel; reaction time ca 100 minutes, temperature needs to be kept between 25-30°C by cooling). In industry, cellulose xanthate with a gamma value of around 50 (DS 0.5) is usually manufactured for fiber spinning, which means that in average just 1 out of two AGU is substituted with xanthates. In fact, a wealth of reactions proceeds at this step, which can be classified into primary, secondary and side reactions. Therefore 30 up to 50 wt.% of CS_2 related to cellulose are needed in industrial scale to accomplish the reaction to the desired product. After the xanthation has been finished, the cellulose xanthate is diluted with NaOH, a usual ratio is 1:4 (1 part alkali cellulose, 4 parts NaOH) to form the so called Viscose. Then the Viscose (before xanthate) is transferred to a tank, where the ripening takes place for a period of 18-30 hours at a temperature smaller than 18°C. It is important to know that the thermodynamically most stable position for the xanthate is the C6 position; therefore any rearrangements, i.e. trans-xanthation reactions (either inter- or intramolecular) lead to preferred substitution at C6. In addition, also a partial cleavage of the xanthate groups occurs whereas hydrolysis is ca. 20 times faster at position C2 and C3 compared to C6, thereby also contributing to a final cellulose xanthate spinning dope where the xanthate groups are preferentially located at C6. [96]

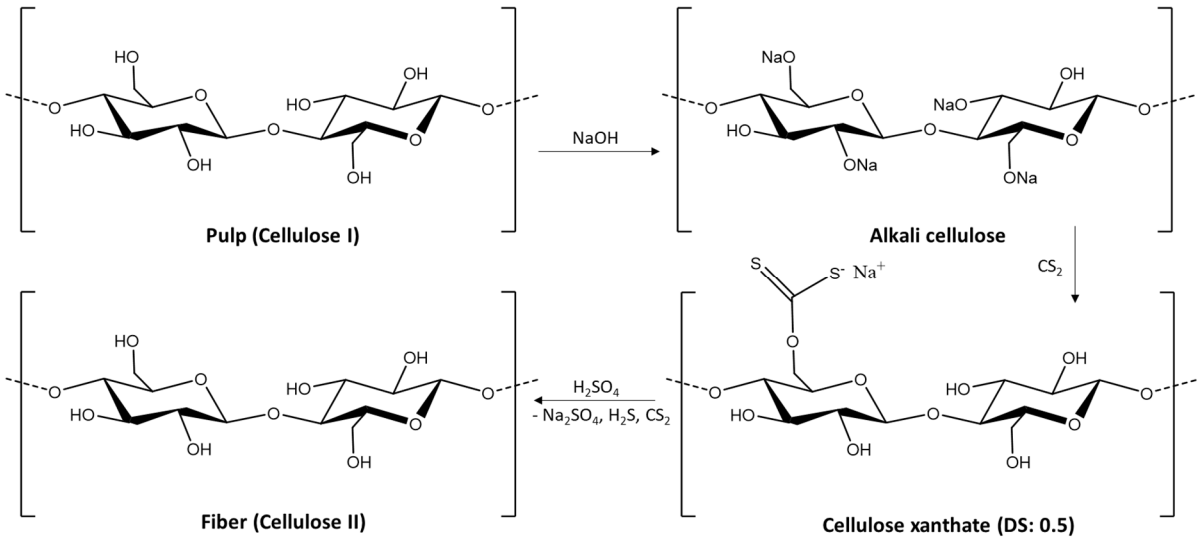

Figure 14 Simplified description of the main steps in the Viscose process, starting with the synthesis of alkali cellulose from a cellulose source, the followed xanthation and the final regeneration back to cellulose

Prior to fiber spinning, air bubbles and other solids in the cellulose xanthate solution must be removed since they would lead to a rupture of the fiber during spinning. Therefore, degassing and filtration of the xanthate solution is performed. Afterwards, the solution is pumped through a spinneret which is made of chemically inert alloys. The spinneret can consist of up to several thousands of nozzles with hole diameters between 40 to 200 microns. After passing the nozzle, the xanthate solution is injected into a temperature controlled regeneration bath. The

regeneration bath contains sulfuric acid (usually 5-15 wt.%), and additives such as $ZnSO_4$ and Na_2SO_4. Two processes, namely conversion to cellulose and coagulation, take place. Coagulation leads to a core-shell structure, which means that the outer parts of the injected xanthate solution solidifies, while the inner part is still in a liquid state. In addition, osmosis comes into play by to the removal of water due to presence of sodium sulfate. Subsequently, conversion to cellulose is induced by the sulfuric acid. The faster the regeneration, the thinner the shell and the worse the fiber quality is. Therefore, zinc sulfate is added in industry which forms a more stable xanthate, thereby slowing down regeneration speed. As a consequence, a thicker shell is formed during coagulation, the fiber can be stretched to a larger extent, and the mechanical properties improve. The fibers are collected on rollers, and washed several times with hot water. Afterwards they are subjected to post treatment, which usually involves surface modification using fatty alcohols to facilitate further processing. After drying the final fibers are obtained. [48, 96]

Lab scale fiber processing

Paper #1 summarizes the developments in laboratory scale fiber and film processing for scientific and teaching objectives, made during the last years. It is addressed to the Journal of Chemical Education, and was used in teaching and for the shaping of Viscose in laboratory courses. The paper provides a short historic overview, describes the main reactions in detail and suggests laboratory scale experiments for educational and scientific purpose in the Viscose process.

Figure 15 shows a laboratory scale equipment developed for a suitable and reproducible Viscose fiber spinning, either with self-made or provided Viscose. Spinning dopes with a concentration of 3-5 wt.% cellulose can be subjected into a regeneration bath by employing simple continuous flow pumps and spinning nozzles made from brass or tantalum alloys. For the fiber uptake, some simple roller systems consisting of PP and driven by KPG stirrers can be employed. To remove remaining sulfuric acid washing the fibers in water at elevated temperatures (80°C), is sufficient.

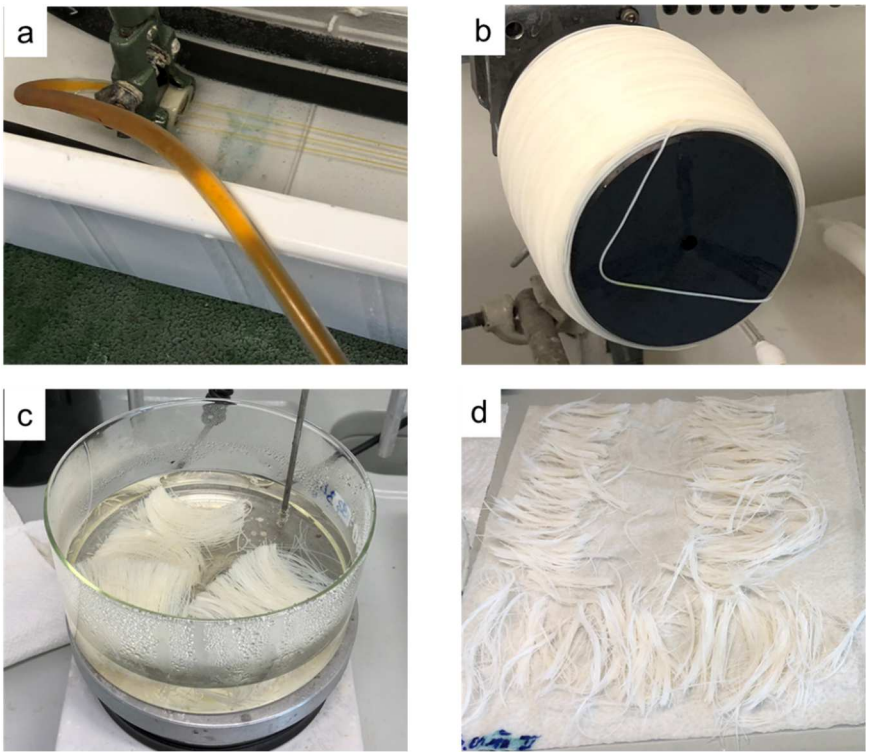

Figure 15 Laboratory scale Viscose fiber spinning for student courses and material development a) Injection of Viscose through a self-made spinneret b) Viscose fibers collected on a roller c) Washing of the fibers d) Drying of fibers

The fibers obtained by this simplified lab scale process possess a diameter in the range of 50 to 150 µm, strongly depending on the cellulose concentration of the dope and the draw ratio. The fiber surface structure is considering the used spinning nozzles regular and smooth. Fiber cross sections are comparable to industrially produced fibers. Figure 16 illustrates the progress during the regeneration of cellulose xanthate to cellulose II. In addition, spectra of cellulose I and alkali cellulose are presented to explain the ongoing reactions during the Viscose process.

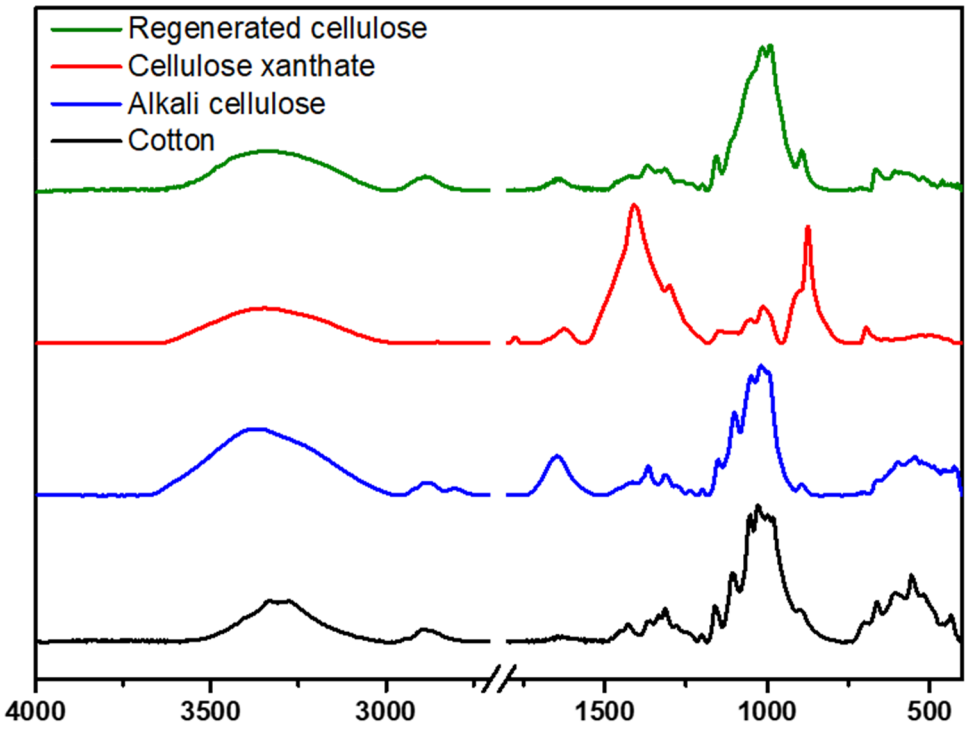

Figure 16 ATR-IR spectra of the different modifications and derivatives of cellulose, which appear during the steps of the Viscose process. Starting with cotton (cellulose I), via alkali cellulose and cellulose xanthate to regenerated cellulose (cellulose II)

The source material (pure cellulose from cotton) exhibits an IR spectrum that is characteristic for cellulose I with broad bands from 3600 to 3100 cm^{-1}(ν_{OH}) and from 3000 to 2850 cm^{-1} (C-H stretching vibrations), a series of small weak bands in the region of 1430 to 1150 cm^{-1} (C-O-H bending at 1430 cm^{-1}, C-H deformation at 1372 cm^{-1}, OH in plane deformation at 1330 and at 1200 cm^{-1}), strong and overlapping bands from 1160 to 950 cm^{-1} (asym. C-O-C vibration at 1155 cm^{-1}, sym. C-O vibration at 1060 cm^{-1} and C-O stretching at 1035 cm^{-1}) and a small band at 899 cm^{-1} (C-O-C valence vibration). [97] The alkali cellulose spectrum differs significantly from the cotton bands. The broad band at 3600 – 3000 cm^{-1} in the alkali cellulose spectrum is shifted from 3500 cm^{-1} to 3650 cm^{-1} and the form changed to a single band. The increased intensity at 1640 cm^{-1} indicates the presence of additional OH stretching and deformation vibrations caused by remaining water stored in the alkali cellulose.

In the case of CX, the interpretation of the IR spectra is not that straightforward. Significant amounts of primary and secondary reaction products can be identified. These products can be identified as CS_2 ($\nu_{C=S}$ at 1520 cm^{-1}), sodium sulfide (1420, 920 cm^{-1}) and sodium trithiocarbonate (1670, 1427, 925 and 885 cm^{-1}). [90, 98] The remaining bands at 1452 and 1382 cm^{-1} as well as a weak band at 2725 cm^{-1} can be assigned to NaOH, which is present from the dissolution of CX. Since NaOH is highly hygroscopic, the water peak at 1640 cm^{-1} is

pronounced as well. The C-S and C=S vibrations for the CX have been reported in the region around 900 cm^{-1} and between 1050-1250 cm^{-1} and interfere with these products as well as with vibrations at the pyranose ring, which also show absorption bands in this range. [99] Therefore, an unambiguous assignment is not possible. After regeneration and extensive washing of the spun fibers, again a cellulose spectrum is obtained which refers to cellulose II.

Core-shell structured metal sulfide/ Viscose composite fibers

Beside the traditional employment of Viscose fibers in textile and non-woven applications, the development of cellulose fiber based composite materials for technical textiles and other applications is a profitable and promising business. Blending spinning dopes, coagulation baths or post treatment solutions with organic and inorganic substances offer manifold composite processing routes. [100]

One example for the successful employment of Viscose based composite fibers are flame retardant textiles. For the production of flame-resistant fibers, different organic or inorganic compounds are either mixed into the spinning dope or fixed on the fiber surface in post treatment processes. Sodium tripolyphosphate, boric acid, ammonium chloride salts or phosphoric acid are just a few examples utilized as flame retardants. [101]

The incorporation of inorganic nanoparticles offers an additional way to equip Viscose fibers with properties enabling the application in new areas. Fe_2O_3 nanoparticle fixed on the porous fiber surface show excellent magnetic or UV absorption behavior, which is important in sun protecting textiles for example. [102-104] Metal sulfides are another class of interesting and promising inorganic particles with unique properties. They are frequently used as solid lubricants in heavy industries, mining or bearings (CuS), as friction stabilizer in all types of breaks (SnS), as photoactive material in solar cell and electrodes (CuS), as catalytic material (Ag_2S) in the degradation of organic pollutants or in the hydrogen production and of course as antibacterial (CuS, Ag_2S).[105-110]

In paper #2 the described fiber spinning equipment was employed for the preparation of core-shell nanocomposite fibers with an inorganic metal sulfide shell and a flexible cellulose fiber core. This enables the combination of the promising metal sulfide properties with a highly flexible, lightweight and renewable fiber as carrier material.

The mechanism and which species in detail are responsible for the generation of the metal sulfide is challenging to reveal. However, there are various plausible ways how the sulfides are formed during the processing step. For instance, thiocarbonates (i.e. dithio- and

trithiocarbonates) that are either present already in the CX or are formed during the spinning process can provide sulfur species for sulfide formation under formation of COS and CS_2, respectively. Thiolates may provide sulfur by elimination of H_2S in acidic medium to give the corresponding sulfide as well. Also cellulose sodium xanthate itself is capable to act as sulfur source by exchange of the sodium by the metal ion as soon as the spinning dope comes into contact with the spinning bath. The formed metal-xanthate complex may decompose as in other cases to the metal sulfides and organic leaving groups, here cellulose. Independent of the mechanism, the formation of the metal sulfides is diffusion controlled since the sulfides are only present on the fiber surface.

Figure 17 illustrates SEM cross section images of the core shell structured fibers after the final processing, the shell type form of the metal sulfide particles around the Viscose fiber core is clearly visible. With an increasing precursor salt concentration in the regeneration bath, the shell becomes more intense. The particle size of the metal sulfides ranges from the nanometer size to aggregates with a few microns.

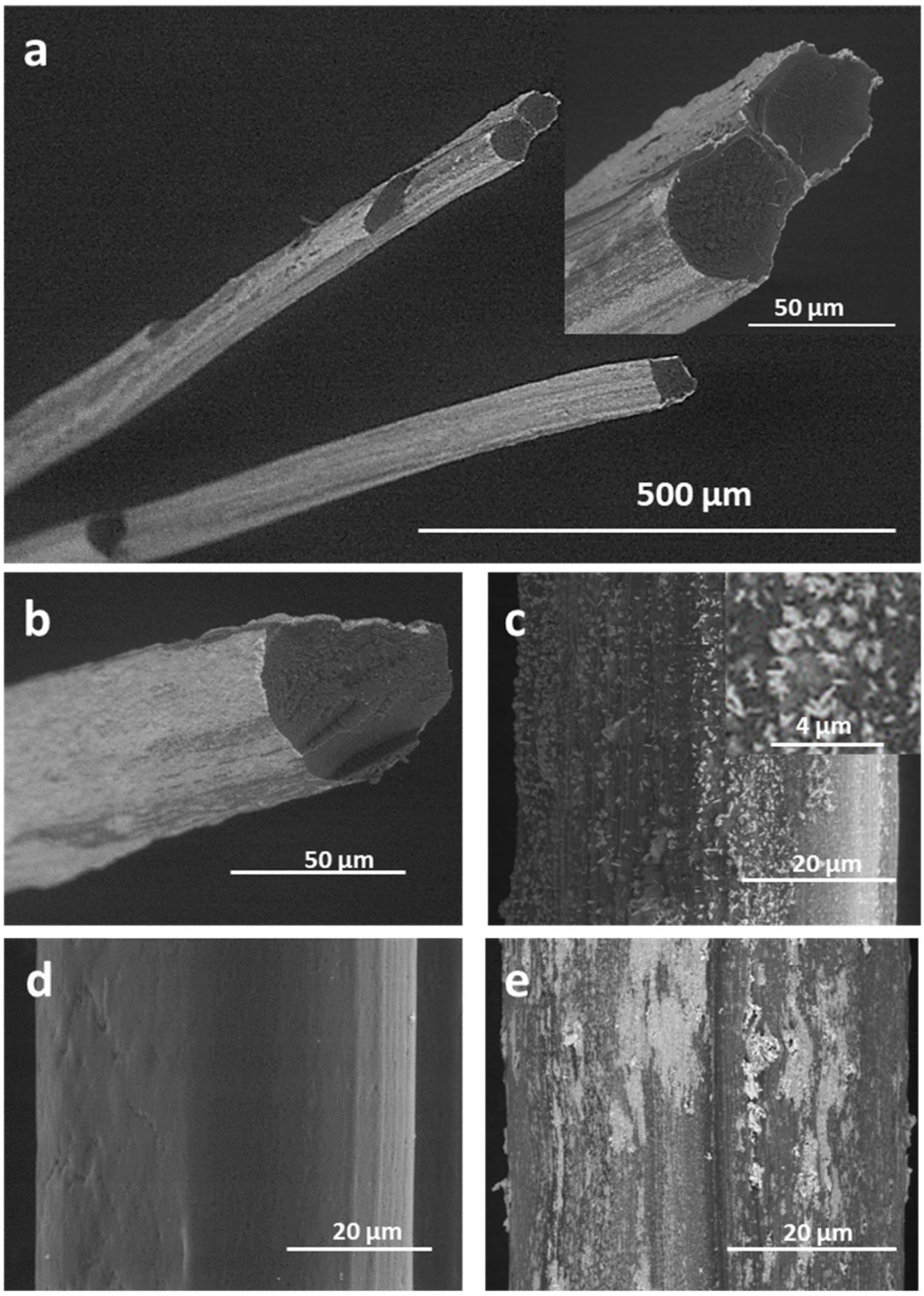

Figure 17 SEM surface and cross section images of a) Overview image of CuS coated fiber (104 mM) with an insert showing the core-shell structure b) CuS coated fiber (56 mM) with full coverage and any CuS particles in the fiber core, c) CuS coated fiber (26 mM $CuCl_2$) with an insert showing the morphology of the CuS particles d) uncoated reference fiber e) SnS/$SnSO_4$ coated fiber (15 mM $SnCl_2$)

As XRD diffraction patterns in Figure 18 indicate, the developed CuS and Ag_2S particles occur in a phase pure form. The phase purity was quite unexpected considering the numerous phases existing for both metal sulfide types and can be seen as advantage compared to other metal sulfide synthesis routes. For SnS, the phenomenon of phase pure particles could not be observed

in the XRD investigations, instead a mixture of two different SnS phases (10% SnS cubic and 66% SnS orthorhombic) and 25% of $SnSO_4$ was identified.

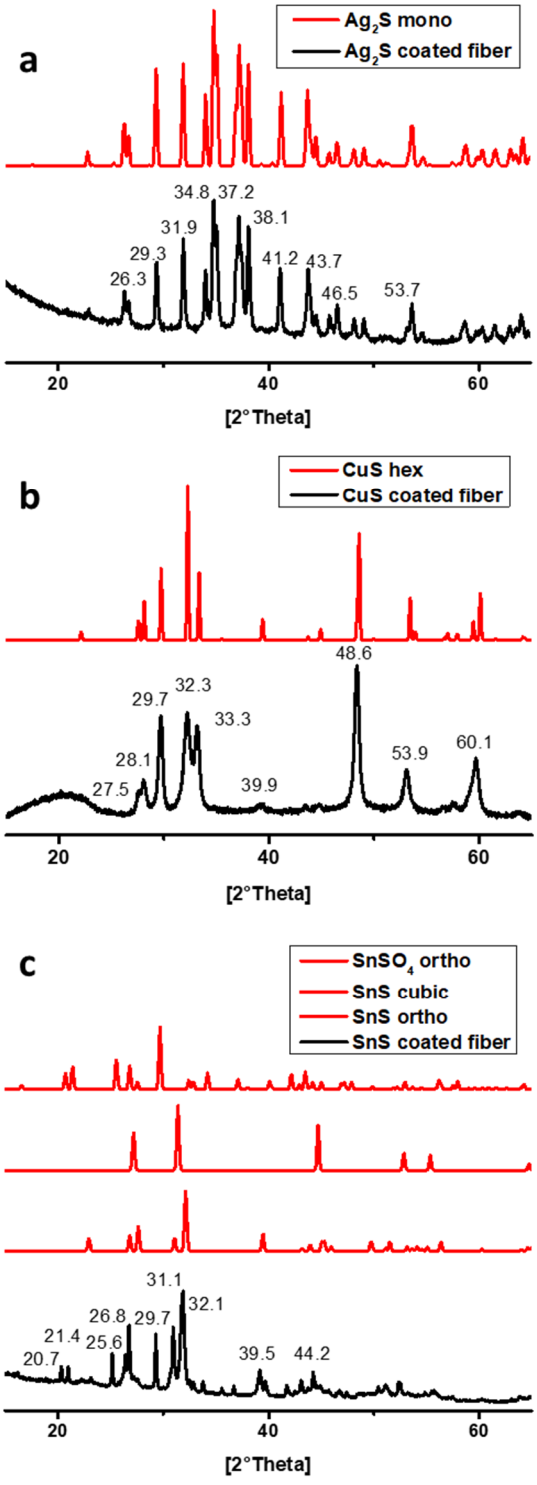

Figure 18 X-ray diffraction patterns of a) CuS coated fiber and CuS (hexagonal, 32106-ICSD) reference pattern b) Ag_2S coated fiber and Ag_2S (monoclinic, 44507-ICSD) reference pattern c) SnS/$SnSO_4$ coated fiber and reference patterns of SnS (orthorhombic, 106028-ICSD; cubic, 651015-ICSD) and $SnSO_4$ (orthorhombic, 245904-ICSD)

To obtain a more quantitative information about the metal load of the fibers, ICP-OES was employed. Table 3 summarizes the amount of metal, present on the Viscose fiber material. As already assumed by the SEM images, the increase of $CuCl_2$ from 26mM up to 104 mM leads to a significantly higher load of Cu on the fibers. In addition, it could be shown that already the presence of small amounts of silver (16 mM) and tin (15 mM) cations causes a remarkable metal sulfide formation on the fiber surface, although these low concentrations were not able to form a continuous shell around the fiber.

Table 3 Influence of metal salt concentration (mmol/L) in the spinning bath on the amount of deposited metal on the fiber (mmol metal/g fiber). LOQ: limit of quantification.

	Ag [mmol/g]	Cu [mmol/g]	Sn [mmol/g]
No salt added	< LOQ	< LOQ	< LOQ
$CuCl_2$ (26 mM)	< LOQ	0.47±0.01	< LOQ
$CuCl_2$ (52 mM)	< LOQ	0.55±0.02	< LOQ
$CuCl_2$ (104 mM)	< LOQ	1.05±0.05	< LOQ
$AgNO_3$ (16 mM)	0.64±0.01	< LOQ	< LOQ
$SnCl_2$ (15 mM)	< LOQ	< LOQ	0.23±0.02

In the future steps the influence of the metal sulfide formation on the fiber properties and the formation of the metal sulfide particles itself have to be studied in detail.

Viscose membranes for reactive lignosulfonate extraction

In addition to the regenerated cellulose fiber production, most of the processes are suitable for the shaping of cellulose films and membranes too. Often, it is only necessary to change the extrusion equipment to slit nozzles and slightly modify the process conditions. One important and well-known regenerated cellulose film manufactured in large scale is Cellophane®. Cellophane is obtained by utilizing the Viscose technology and extruding the spinning dope through broad slit within a wet spinning process. Its equivalent from the cuprammonium processing is called Cuprophan, but is much less known due to the lower commercial success of this technology. In addition, the lyocell process with its blow film technology offers a green and sustainable possibility for the cellulose film processing. [100]

Traditional applications for transparent cellulose films are packaging of goods, nutrition, cosmetic or medical products and their employment as filters and membranes in diverse separation processes. After cellulose films were replaced by synthetic polymers in packaging and separation applications meanwhile the situation has changed. Renewable materials are now again in the focus of packaging, composite and membrane processing. [100]

The formation of cellulose film composites offers a way to improve the mechanical properties and the resistance of the films against environmental conditions as high humidity. [111] A modification with inorganic and organic molecules on the surface or in the matrix enables special applications. Just to mention a few examples, films with outstanding fluorescent and luminescent behavior have been processed via incorporation of fluorescence dyes in never dried regenerated films. [112] Copper nanoparticles incorporated in the cuprammonium process caused efficient antibacterial behavior of the cellulose films. By treating cellulose films in a solution of $CdCl_2$ and Na_2S, CdS nanoparticles could be fixed tightly on the film surface. The CdS particles in combination with the cellulose matrix lead to a flexible photocatalytic composite with effective H_2 evolution under visible light irradiation. [113]

In the field of membrane science and development, regenerated cellulose based materials are employed in micro-, ultra-, and nanofiltration, in gas separation and reverse osmosis. The range of separation problems thereby is manifold and waste water purification, medical dialysis or natural gas fractionation are just a few examples. The main arguments for the utilization of cellulose membranes are the well-defined and easily controllable pore structure, the high hydrophilicity and their biocompatibility. [114]

In paper #3 the processing of cellulose membranes from Viscose solution and their subsequent employment in the liquid phase separation of a lignosulfonate (LS) feedstock is described.

For a long time, LS was considered as technically useless waste stream of chemical pulping, but in the past years a tremendous increase in the upcycling and recovering of LS for versatile applications like energy storage or carbon fiber processing has emerged. For the utilization of LS in these high value applications, is to ensure high purity of the recycled stream to avoid performance or value losses. [115] A challenge in the LS purification is the diverse composition of the spent liquor and the varying quality of the feed stock (source material, season and production site). As LS are soluble over the whole pH range, mass transfer unit operations (drying, distillation, extraction) can be performed for successful separation. [116]

Reactive extraction enables a high selectivity and avoids the formation of emulsions if applied in combination with membrane separation. Membrane technology is rather flexible in terms of membrane type (bulk, emulsion, supported liquid) and reactive extractant. N-trioctylamine (TOA), a well described extractant, was employed, suitable for LS separation and combinable with many different types of membranes (Figure 19). [117]

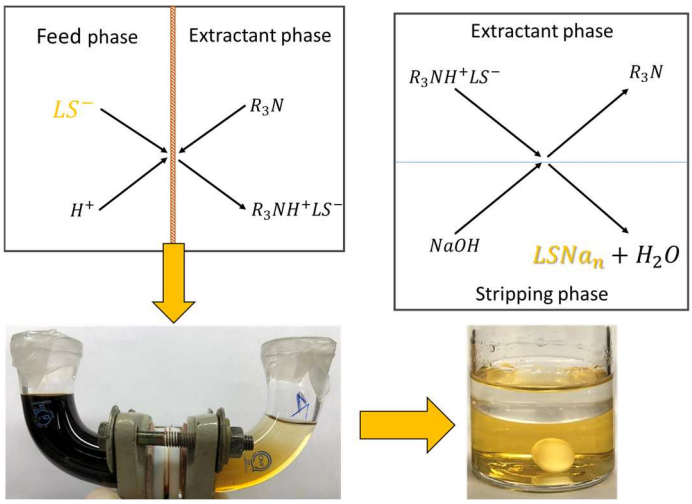

Figure 19 Reactive solvent extraction and fractionation of lingo sulfonates through Viscose based cellulose membranes

However, there is only limited literature about the combination of bio-based membranes and TOA. To the best of our knowledge, there is no literature describing LS separation with TOA as extractant and cellulose as membrane material.

A simple film casting of an industrially produced cellulose xanthate solution in PTFE shapes has been used to prepare cellulose membranes with diameters of 8 cm. After drying, the solid films were regenerated to cellulose by immersion in sulfuric acid and subsequently washed water and drying in a sheet former as shown in Figure 20. As post treatment, vapor phase hydrophobization with hexamethyldisilazane (HMDS) [118] or trifluoroacetic acid anhydride (TFAA) was performed according to slightly modified literature reports. [119]

The post treatment influenced the accessibility of the TOA into the membrane and hence the extraction efficiency was increased. The hydrophobicity of the membranes was strongly enhanced with ongoing exposure time and after 20 hours of exposure the water contact angle raised from 48° to 99° for the HMDS treated membranes. For TFAA treated membranes, 3 hours were sufficient to raise the water contact angle to 78°

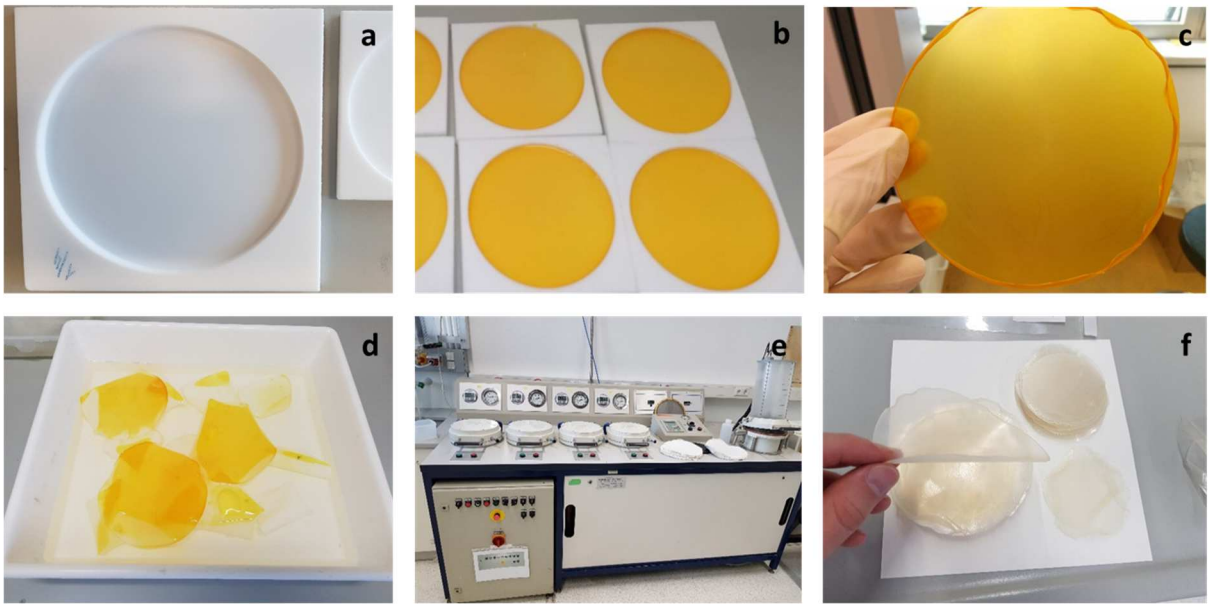

Figure 20 Laboratory scale cellulose membrane film casting a) Forms b) Filled with CX c) CX film after drying d) Regeneration to cellulose e) Drying on the sheet former f) final cellulose membranes

Prior to LS extraction experiments, DLS was employed to determine the range of molecular fractions of the feed stocks and the extracts (Table 4). Extraction experiments were performed with untreated, HMDS and TFAA treated membranes. The utilized model feed solutions possesses a very narrow molecular weight distribution, therefore any fractionation was not observed in these experiments, i.e. the hydrodynamic radii of the LS molecules in the model feed was similar to those in the extractant.

For the technical feeds, two fractions with a particle size of 160 to 360 nm and 950 to 4000 nm respectively, were employed. After extraction, only the phase with the smaller LS fragments was identified. The absence of the larger particles (>1000 nm, by DLS) in the extractant indicates a complete discrimination of the larger particles by the cellulose membrane.

The overall mass transfer was expected to be similar for hydrophobized and non-treated membranes, as the hydrophobization should just shift the contact point between the feed and extractant phase and indeed, the detected LS concentrations were in the same range for all experiments.

Table 4 Hydrodynamic diameter of LS fractions in the feed and the stripping phase determined by dynamic light scattering

Solution	Membrane	Particle size range I [nm]	Particle size range II [nm]
Technical feed (SAPPI)		160 - 360	950 - 4000
	cellulose	190 - 880	-
	HMDS, 20h	300 - 800	-
	TFAA + Ac_2O 3h	240 - 800	-
Model feed (Ca-LS)		180 - 420	-
	cellulose	200 - 650	-
	HMDS	170 - 360	-
	TFAA + Ac_2O 3h	280 - 540	-

In a further experiment the monosaccharide concentration of technical feeds before and after extraction were determined, to ensure that only LS passed the membrane. Monosaccharides were not detected in the stripping phase, whereas their concentration in the feed phase remained constant.

To summarize, cellulose membranes are capable for reactive extraction of LS with TOA as carrier. No emulsion or crud formation was observed during the experiments and DLS measurements demonstrated that a selective extraction with a simultaneous fractionation can be performed.

Part II

Cellulose based thin films: Film processing, characterization and utilization

Content

#4) Michael Weißl, Katrin Niegelhell, David Reishofer, Armin Zankel, Josef Innerlohinger and Stefan Spirk; Homogeneous cellulose thin films by regeneration of cellulose xanthate: properties and characterization; Cellulose; 2018; 25; 711-721

#5) Michael Weißl, Thomas Rath, Jürgen Sattelkow, Harald Plank, Samuel Eyley, Wim Thielemans, Gregor Trimmel and Stefan Spirk; Multi-layered nanoscale cellulose/$CuInS_2$ sandwich type thin films; Carbohydrate Polymers; 2019; 203; 219-227

#6) Michael Weißl, Mathias Andreas Hobisch, Leena Sisko Johansson, Kay Hettrich, Eero Kontturi, Bert Volkert and Stefan Spirk; Cellulose carbamate derived cellulose thin films – Preparation, characterization and blending with cellulose xanthate; Cellulose; 2019, submitted

Model systems and model compounds offer the possibility to study physical phenomena or chemical reactions in a well-defined and easy to control surrounding. However, the highly complex supramolecular cellulose structure and the unconventional physical and chemical behavior induced thereby, strongly decreases possible routes for the processing of cellulose model systems. [120]

For cellulose, systems based on thin and ultra-thin films are suitable materials to study reactions as well as various modification and processing methods. Water uptake, swelling and drying behavior or adsorption and interaction studies with different molecules are examples for important studies done with cellulose thin films in the recent years. Surface modification reactions, multilayer architectures and composite fabrication have been performed to define possible routes for a utilization of cellulose in high-end materials. [120]

For the processing of thin and ultrathin model surfaces two methods, namely spin coating and Langmuir–Blodgett (LB) deposition have been described as manufacturing methods. While spin coating is a fast and straightforward method LB deposition provides more precise adjustability of the film thickness. [121]

The processing of cellulose thin films comprises three main approaches which are either i) the employment of cellulose suspensions, ii) the dissolution of cellulose or iii) the use of soluble cellulose derivatives which can be converted back to the cellulose in a subsequent step after the film formation. The utilization of cellulose suspensions avoids organic solvents, but the obtained films have usually a high surface roughness due to the (nano-)fibrous or particulate nature of the used cellulose materials. Dissolving cellulose in proper solvents (e.g. DMA/LiCl or ionic liquids) requires tedious dissolution and purification procedures to remove both solvent and salt residues. [122] A smart method overcoming these problems is to use trimethylsilyl cellulose (TMSC), introduced by Klemm in 1993 and optimized by Kontturi. [123] TMSC is an acid labile and organosoluble cellulose derivative and can be converted back to cellulose by simple acidic vapor treatment. A disadvantage of TMSC is the rather high price, the limited accessibility and the use of organic solvents. Hence, an aqueous cellulose solution applicable in the formation of cellulose thin films would be desirable. [124]

Processing of CX based cellulose thin films

As CX is a widely available, cheap and water-soluble cellulose derivative, overcoming most of the mentioned drawbacks we became interested in its suitability for thin film formation (Figure 21). In Paper #4 a simple and easily scalable method for the processing of CX based cellulose thin film is described. As starting material an industrial CX stock solution was diluted to cellulose concentrations between 0.75 wt.% and 4 wt.%, filtered and subjected to spin coating. After spin coating, homogenous CX layers remained on the carrier substrates, which were further placed in HCl acidic atmosphere to induce the regeneration of CX to cellulose. After gas phase regeneration, NaCl crystals covered the whole film surface, which were easily removed a rinsing step with water. After rinsing and subsequent drying, cellulose films with a well-defined morphology were obtained (Figure 22a).

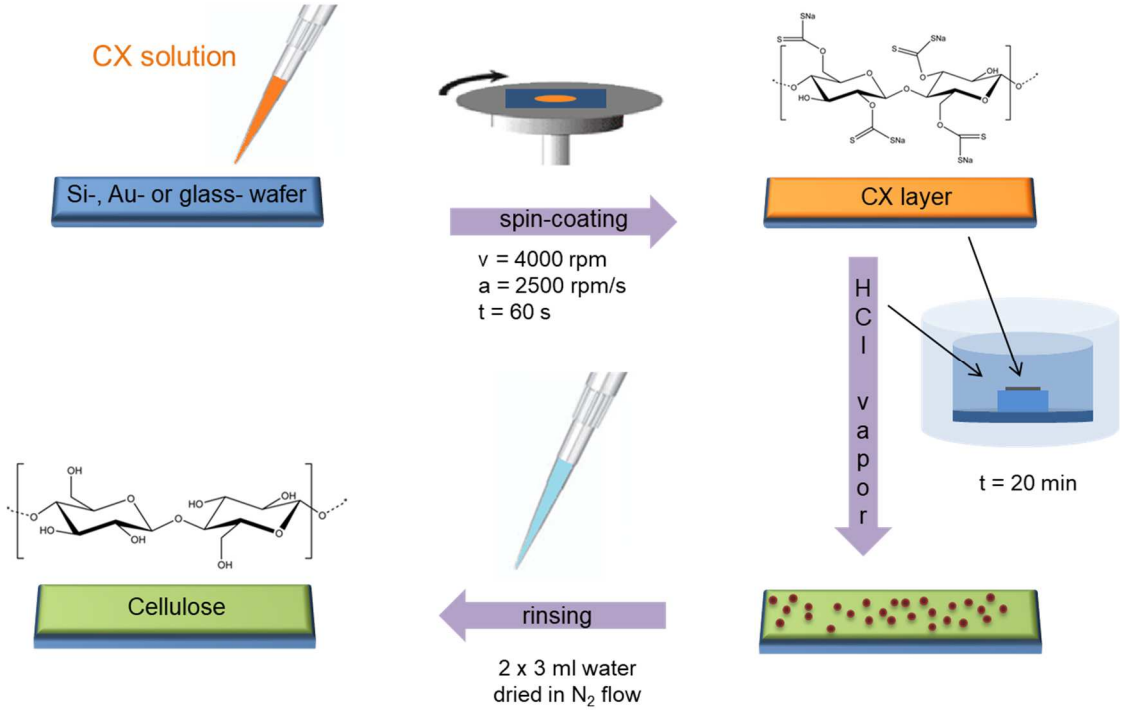

Figure 21 Schematic description of the CX based cellulose thin film processing, starting with the spin coating of CX solution subsequent HCl treatment of the obtained CX layers and final washing with water to remove the salts from the cellulose thin films

The full conversion of CX to pure cellulose was successfully shown by employing ATR-IR spectroscopy and XPS. Both methods confirmed that the remaining layers consist of cellulose and in addition, it could be shown that neither the processing nor the further heat treatment has an impact on the cellulose layers. The layer thickness of the different CX concentrations and its development in the single processing steps was monitored by profilometry. (Figure 22b)

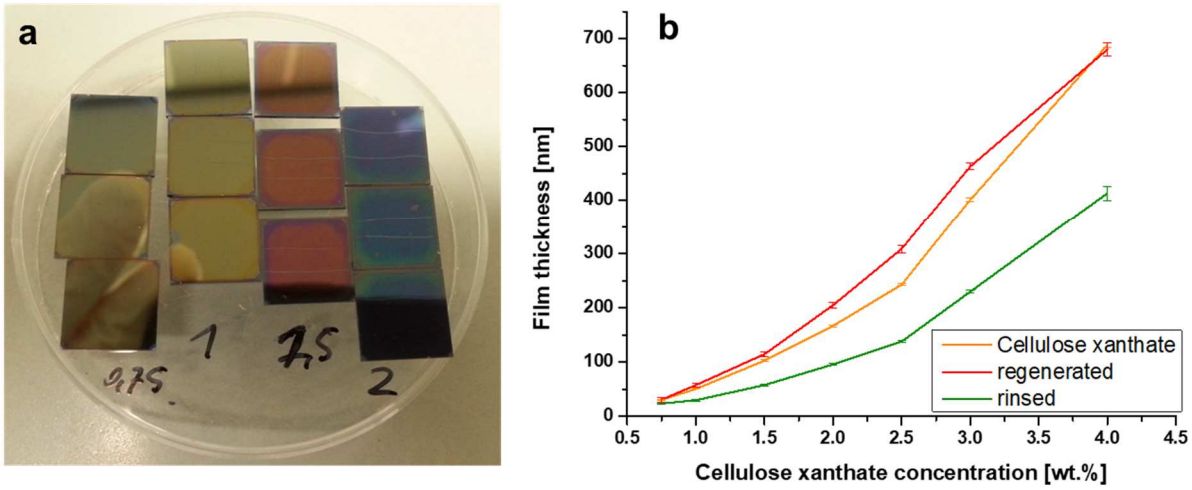

Figure 22 a) CX based cellulose thin films spin coated with varying CX concentration after the final processing b) Development of the layer thickness during processing determined by profilometry

For the CX layers, a continuous increase in layer thickness from 30 nm up to 680 nm was observed when increasing the CX concentration from 0.75 to 4.0 wt.%. HCl vapor treatment caused slightly increased thicknesses, but the roughness of the film surfaces strongly increased. The drastic change in the surface morphology is related to the previously described formation of NaCl on the film surface. After rinsing the regenerated films with water, the layer thickness decreased by around one third of the initially determined values. This strong reduction can be explained by the removal of sodium salts from the cellulose matrix and the change in the molecular structure from bulky CX to a cellulose.

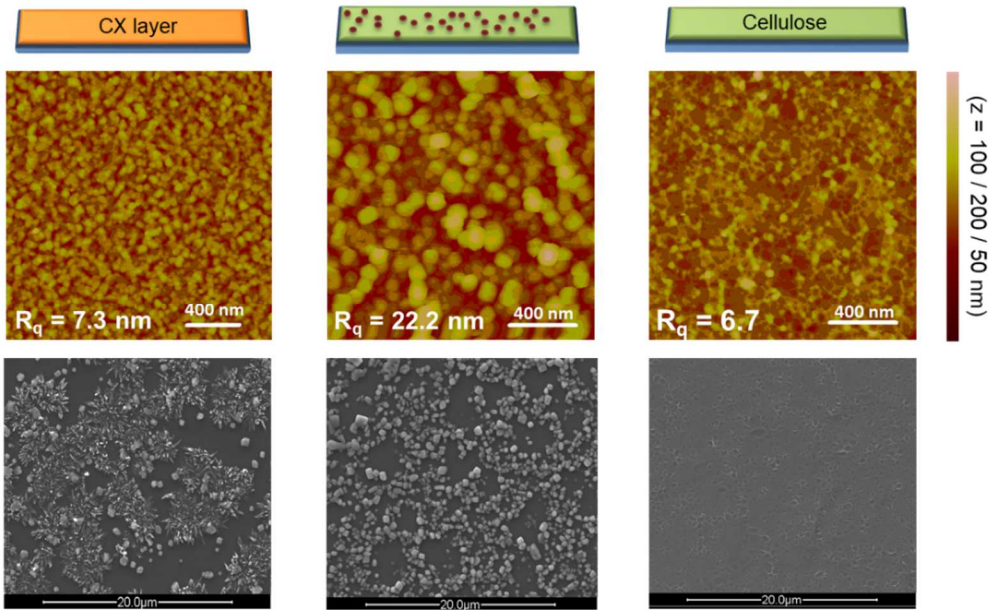

Figure 23 2x2 µm² AFM topography images (upper raw) and SEM images (lower raw) of CX based cellulose thin films after different process steps: spin coating (left), HCl vapor treatment (middle) and rinsing with water (right)

The surface morphology of the films and especially the influence of the ongoing formation and vanishing of crystallites structures during thin film processing was explored by AFM and SEM-EDX (Figure 23). For the CX layers rather smooth surfaces with an RMS roughness in the low nm range were observed. SEM-EDX images confirmed that small needle shaped sodium hydroxide crystals are present. After HCl vapor treatment the RMS roughness increased up to 30 nm, caused by large and spherical NaCl crystals present on the film surface. After the final film treatment, the morphology of the remaining cellulose layers could be described as regular and well defined. The only remaining irregularities in the film structures are small holes in the size of the previous removed sodium chloride crystals.

Further the interaction of the Viscose based thin films with two proteins namely bovine serum albumin (BSA) and fibrinogen (FIB) was explored by surface plasmon resonance. Comparable to cellulose thin films made from other precursors, only small amounts of BSA (0.2 mg/m²) could be adsorbed on the film surface while the adsorption of FIB was significantly higher (1.1 mg/m²) at the cellulose films after regeneration and washing.[125, 126] After additional heat treatment, the adsorption of both proteins decreased to around 50% of the previously adsorbed amounts.

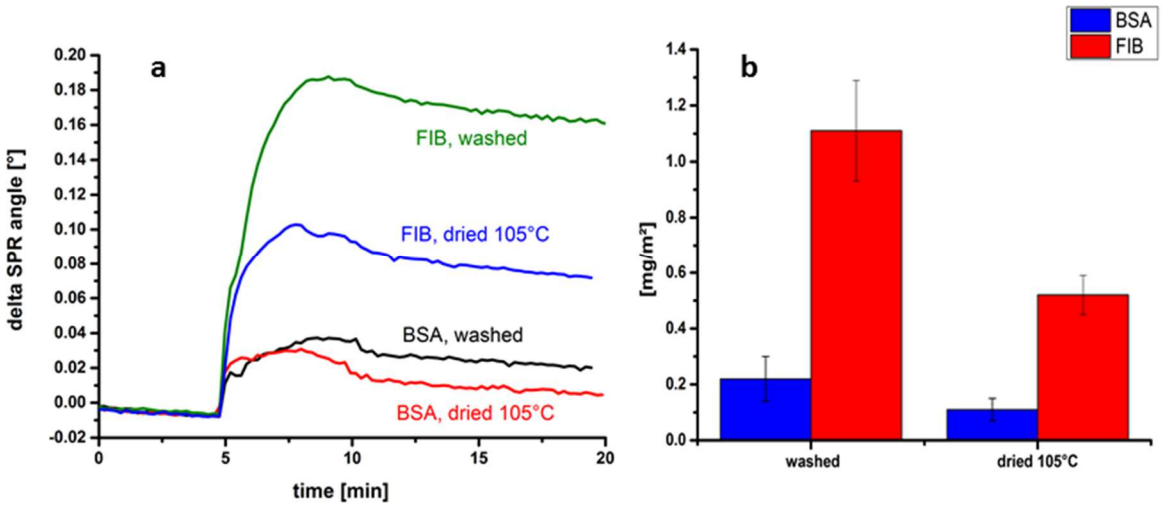

Figure 24 SPR sensogram (670 nm) recorded during the adsorption of FIB and BSA on washed and heat treated films (a, prepared from 1 wt.% CX solutions). (b) the amount of protein adsorbed on differently treated films, calculated through the change in the SPR angle via the de Feijter equation.

Overall, we could demonstrate that CX is a suitable precursor for cellulose thin films. CX allows to avoid organic solvents while the cellulose layer displayed properties comparable to those of other precursor materials.

Multi-layered nanoscale cellulose/$CuInS_2$ sandwich type thin films

In Paper #5 the method for the processing of CX based cellulose thin films was utilized for the manufacturing of a photoactive optoelectronic composite system. The composite is based on a multilayer architecture of alternating cellulose and metal sulfide thin layers. Cellulose was employed as bottom-, intermediate- and top layer, the metal sulfide layers built the photoactive material embedded in cellulose.

Because of their narrow bandgap, metal sulfides like the used $CuInS_2$ are interesting materials for optoelectronics. One way to introduce such metal sulfides in composite systems is via spin coating of organosoluble metal xanthate (MX) precursors and subsequent reaction to metal sulfides through a thermal treatment. Thereby, the metal xanthate precursor degrades following the Chugaev mechanism (intramolecular elimination reaction where the hydrogen from the β-carbon of the alkyl is removed by the sulfur) and volatile side products (small chained alkyl, carbonyl sulfide, and carbon disulfide) arise and evaporate from the metal sulfide matrix during the heat treatment (Figure 25a). [106, 107, 127, 128]

Figure 25b illustrates the processing of the multilayer architecture by altering spin coating of CX and CuInX followed by subsequent chemical (CX) or thermal (CuInX) regeneration. Since HCl degrades the $CuInS_2$ layers a different regeneration agent has to be employed and trifluoroacetic acid vapors appear to be a suitable alternative. Optoelectronic characterization and cross sectioning of the multilayered composites followed the layer by layer preparation.

The full conversion of xanthate precursors to cellulose and $CuInS_2$ was monitored by ATR-IR spectroscopy and XPS. Both methods proved that only the desired materials stayed behind and side products generated in the course of the reactions are completely removed from the matrix.

The thickness of the single cellulose layers was between 150 and 160 nm, those of the $CuInS_2$ was around 50 nm for the standard concentration (32 mg/mL) and 90 nm with doubled CuInX precursor concentration (64 mg/mL). Such a setup led to an overall thickness of 500 to 550 nm for a five layered composite.

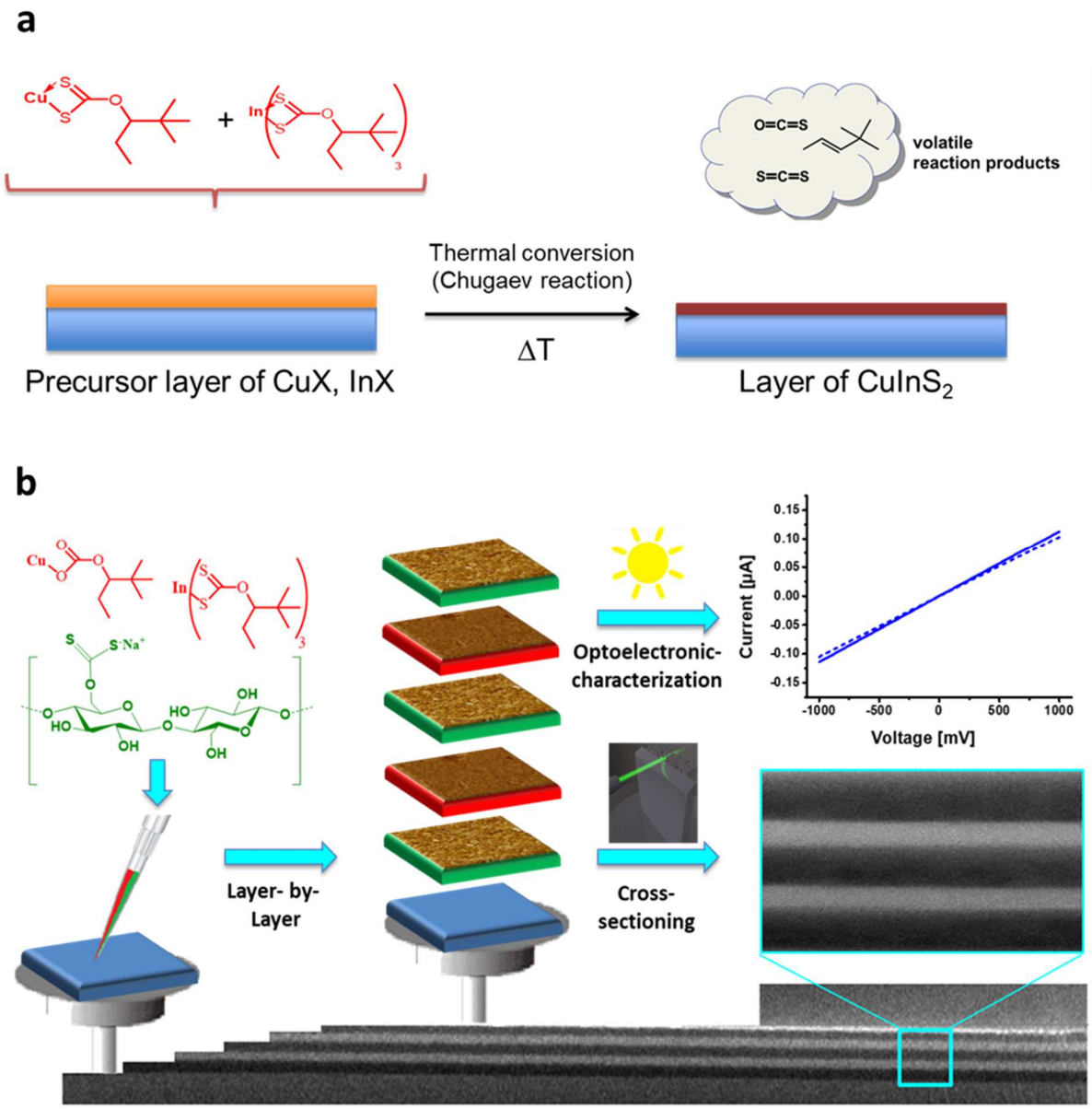

Figure 25 a) Explanation of the Chagaev reaction employed in the formation of metal sulfides from metal xanthate precursors [129] b) Schematic description of the processing of nanoscale cellulose/$CuInS_2$ sandwich type thin films explaining the different processing of the single layers and the subsequent characterization

The surface morphology was checked after each step in the multilayer fabrication by AFM. The AFM images showed that each layer shows a smooth surface without irregularities and that the layer structure is hardly influenced by the layer underneath.

Although profilometry and AFM images suggested a closed layer-by-layer structure free of any defects in the interface regions, cross section images were necessary for a final proof. However, as the multilayer consist of two very different materials namely organic cellulose and inorganic metal sulfides, the preparation of such cross-section images could not be performed with usual mechanical cutting or focused ion beam technologies. Instead, it was necessary to perform ion beam slope cutting with subsequent SEM imaging, to cut the sample and record cross sections

of them. In the ion beam slope cut technique, the sample is fixed on a metal plate and exposed to a perpendicular ion beam. The metal plate protects the hidden part of the sample and simultaneously the edge of the plate leads to a sharp cut along the sample.

Figure 26 presents the cross-section images and visualizes that the single layers have a high degree of conformity, are clearly separated from surrounding layers and that the system is homogeneous on large areas. The red arrows in the Figure mark the $CuInS_2$ layers (bright grey), which are surrounded by the cellulose layers (dark grey). The thick layer bellow and above represent the silicon wafer and the gold top layer sputtered on the sample before measuring. The layer thickness determined in the cross sectioning are well comparable to the data obtained with profilometry.

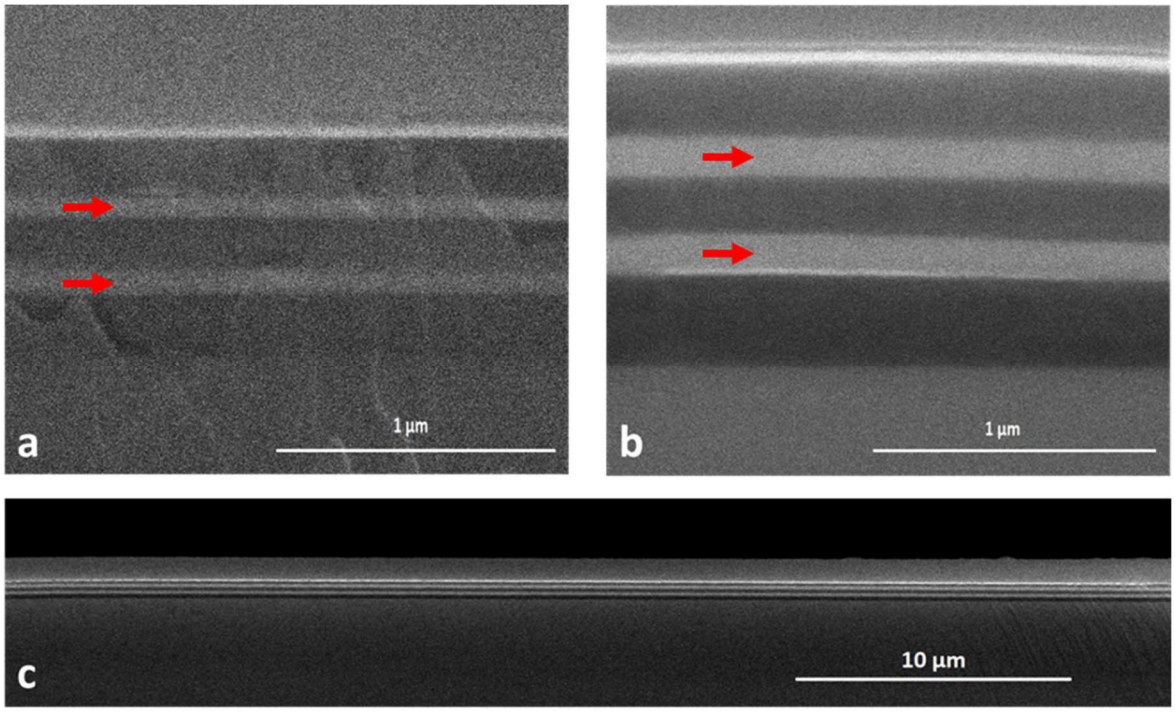

Figure 26 SEM images of cross sections of a five layered system, spin coated with 32.2 mg mL^{-1} CuInX (a) and 64.4 mg mL^{-1} CuInX (b, c). The layer sequence in all images is (from bottom to top): silicon-cellulose-CIS-cellulose-CIS-cellulose-metal stripe and the red arrows highlight the $CuInS_2$ layers in the composites

For the optoelectronic characterization, the absorption in the visible (VIS) range of the electromagnetic spectrum and current/voltage curves after different steps of processing and varying conditions were recorded. $CuInS_2$ absorbs in the VIS region (bandgap of 1.5 eV), whereas thin cellulose layers are almost transparent. Figure 27a shows the absorption behavior of the multilayer system with an increasing number of layers. With the presence of the first $CuInS_2$ layer the absorption is strongly increasing, whereas the subsequent deposition of another cellulose layer causes no further increase. Introducing a second metal sulfide layer almost doubles the absorption as expected.

Current/voltage curves are presented in Figure 27b and describe a linear characteristic due to the Ohmic nature of the contacts to the metal sulfide layers. Further, it is clearly visible that the $CuInS_2$ layers are conductive and exhibit photoconductivity upon illumination with a standard solar spectrum (AM 1.5 G spectrum at 100 mW cm^{-2}). Interestingly, the deposition of cellulose layers on top of the conductive layers caused a decrease in conductivity and the induced photocurrents.

Although several experiments were performed, the decrease in conductivity could neither be fully explained. The most reasonable explanation is a swelling of the cellulose layers during rinsing with water and a thereby induced formation of cracks in the metal sulfide layers.

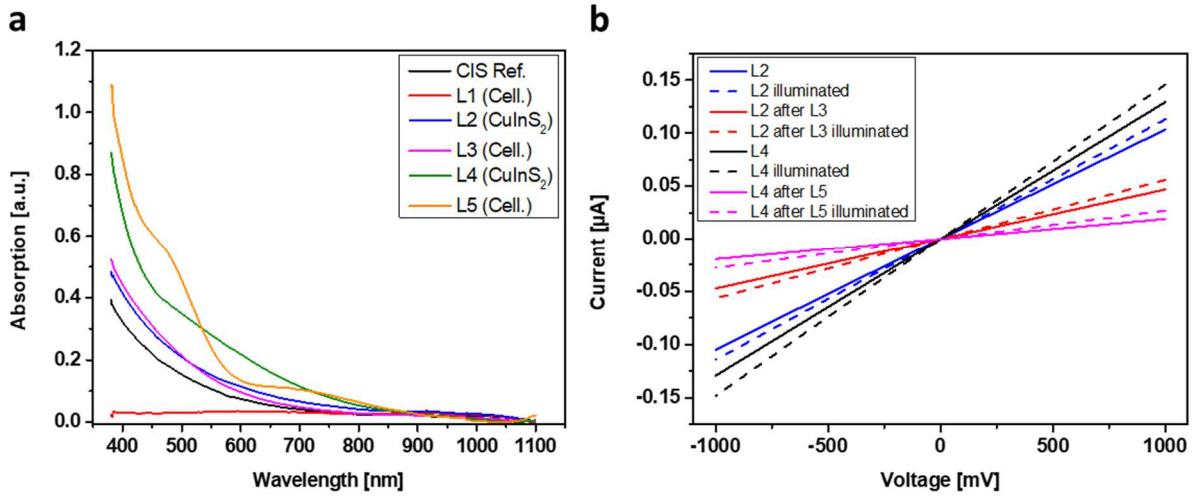

Figure 27 a) VIS absorption spectra of a cellulose $CuInS_2$ multilayer device with an increasing number of layers in the system b) Current/voltage characteristics of the $CuInS_2$ layers after every layer spin coated on the system

The spin coating of the 5 layered composites successfully demonstrates the feasibility for the large scale application of cellulose thin films and coatings in fields like printable, flexible or photoactive electronics.

Cellulose carbamate derived thin films and blending with Viscose for *all*-cellulose films

In Paper #6 we utilized once more the excellent film formation properties of CX to develop an all cellulose composite system of CX and cellulose carbamate (CC). CC is well known as promising, sustainable cellulose derivative. As both derivatives, CC and CX are soluble in diluted sodium hydroxide solutions, a partial substitution of CX with CC in the Viscose process is a frequently discussed issue. A reduction of the CX content in the spinning dope would reduce the necessary amount of CS_2 in the process and increase the sustainability of the overall Viscose process chain.

Before exploring the effect of varying CC concentrations on the cellulose thin film formation, the intrinsic suitability of CC for thin film processing and a characterization of the obtained films has to be examined. Therefore, CC was dissolved in sodium hydroxide solutions at -10°C, filtered and subjected to spin coating. After the spin coating of CC films, the development of a thick crystalline layer on the film surface was observed. Through simple rinsing with water this crystalline layer was removed and, the remaining layers consist of pure cellulose as proven by ATR-IR spectroscopy and XPS. The regeneration of CC to cellulose is initiated by spin coating of CC solutions without any further treatment and to the best of our knowledge the initiation of a reaction by spin coating is not described in literature so far.

Figure 28a summarizes the ATR-IR spectra of the CC source material, the thin films after spin coating, rinsing with water and HCl vapor treatment. For the CC powder, bands assigned to the carbamate groups are present. After spin coating, the spectrum is dominated by an intense CO band, which finally was assigned to sodium carbonate.

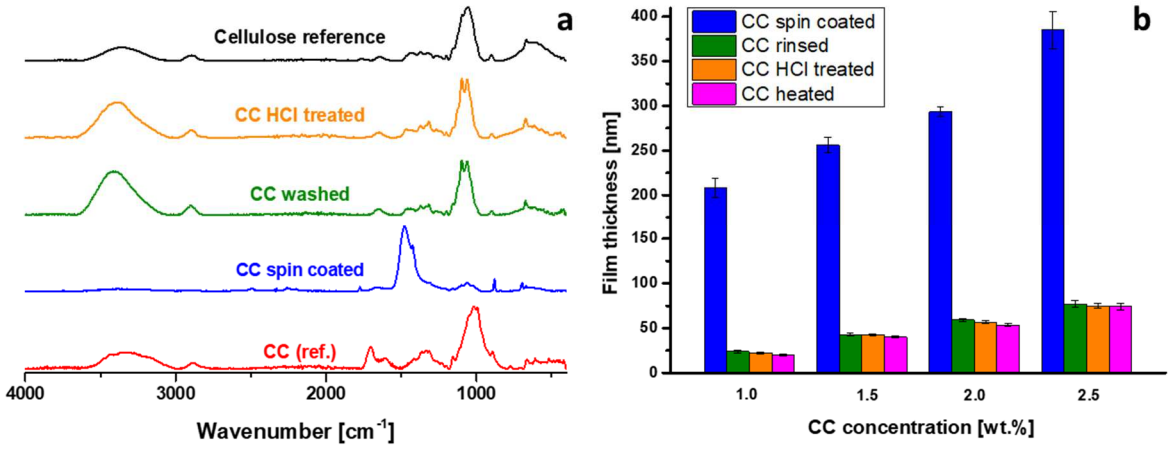

Figure 28 a) ATR-IR spectra of the CC source (ref.) and the CC during the processing to cellulose thin films. b) Film thickness of CC thin films during processing of different CC concentrations determined by profilometry

Sodium carbonate forms as a side product during spin coating concomitant with the regeneration of the CC of cellulose via an addition elimination mechanism as illustrated in Figure 29. After removing the degradation products by simple rinsing, a cellulose spectrum is obtained.

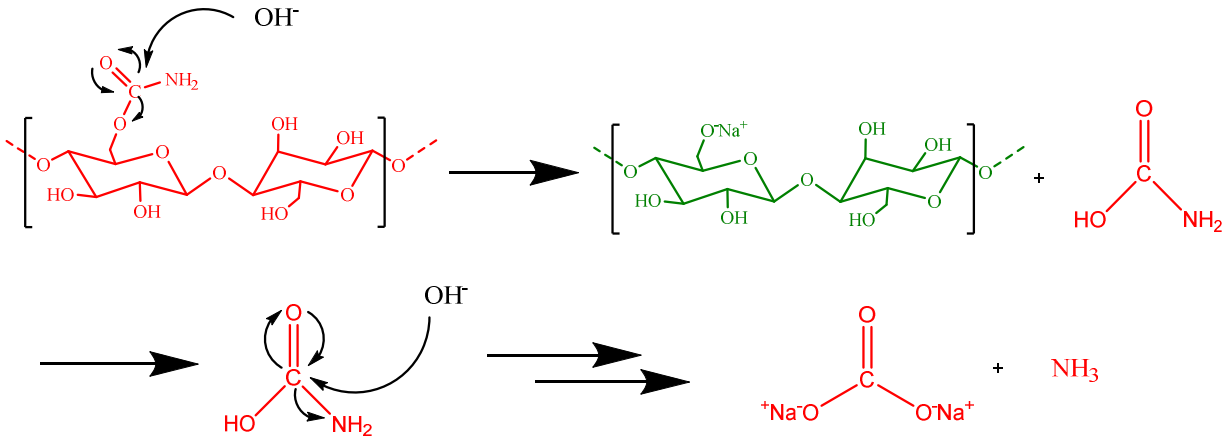

Figure 29 Cellulose carbamate decomposition induced by the increasing basicity of the system during ongoing spin coating with cellulose and sodium carbonate as remaining products

The layer thickness decreases after removing the crystalline top layer from the film surface. The thickness of the remaining cellulose layers depends on the CC concentration and ranges from 20 nm (1 wt.%) to 80 nm (2.5 wt.%, Figure 28b). Additional acidic vapor treatment or subsequent heat treatment did not cause significant changes in structure and layer thickness.

AFM images demonstrate the formation of larger cellulose aggregates on the film surfaces, as compared to other sources like TMSC or CX. However, this aggregation tendency explains the slightly increased surface roughness.

After the successful preparation of CC based thin films, solutions of CC and CX in different ratios (1:0, 3:1, 1:1, 1:3, 0:1) were utilized for the cellulose blend film formation. Regeneration of CX to cellulose was performed in an HCl atmosphere, followed by a rinsing step. The final *all*-cellulose blends, are employed to explore the mutual influence of CC and CX on the film formation and the resulting film properties.

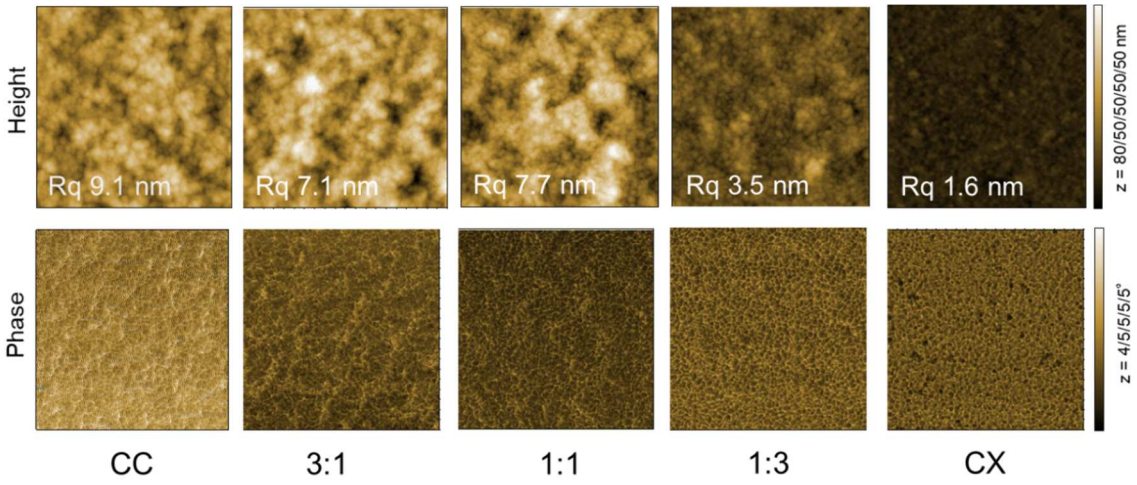

Figure 30 2x2 µm² AFM height (upper row) and phase (lower row) images of 2% CC, blend (3:1, 1:1, 1:3) and 2% CX films after HCl vapor treatment and rinsing

The AFM images of the blend films (Figure 30) display a homogenous surface structure with a slightly increasing surface roughness at higher CC concentrations. The film thickness was around 50 nm for all blend films and only slightly higher for the films spin coated from pure CX and CC and used as reference material. The static water contact angels showed a reverse behavior in comparison to the surface roughness and decreased from 37° to 24° at the highest CC concentration.

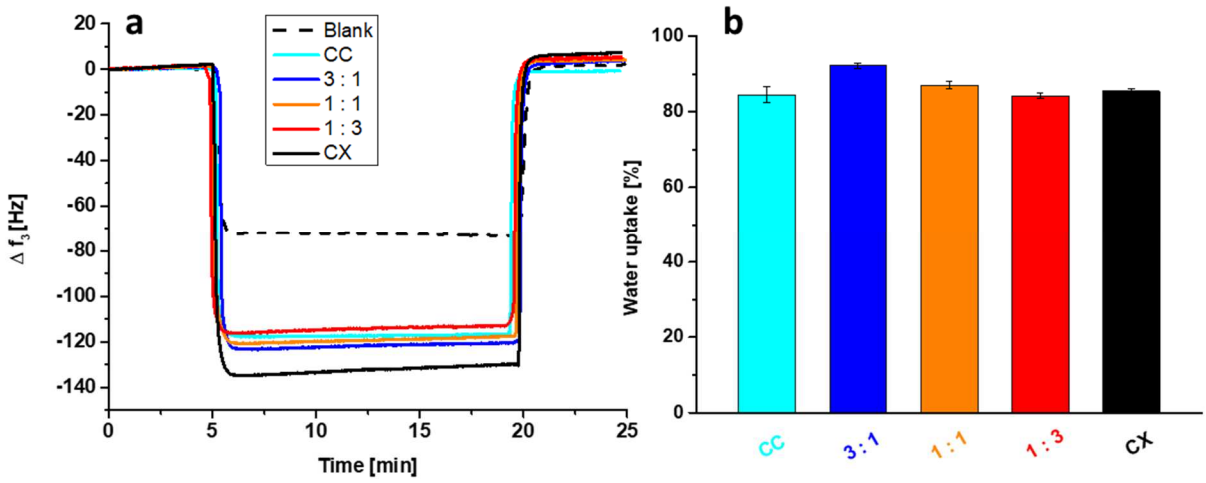

Figure 31 a) QCM-D monitored frequency shifts (Δf3) of 2% CX, 2% CC and blend (1:3, 1:1, 3:1) films in a H_2O/D_2O exchange experiment after regeneration. b) Water uptake of the reference materials (film made from pure CC and C) and the blend films during the H_2O/D_2O exchange experiment

Further, the water uptake and swelling behavior of the films made from different blend ratios and the pure CX and CC respectively, was investigated by employing QCM-D. The H_2O/D_2O exchange induces Δf_3 frequency shifts for a bare substrate and the blend films (Figure 31a). The blank displayed a shift of around 70 Hz whereas the cellulose coated wafers had a much higher shift of 120 Hz. Only one sample, the pure CX film deviated from the average 120 Hz shift, due to a slightly thicker cellulose layer. Based on the measured frequency shifts during H_2O/D_2O exchange, the overall water uptake was determined. Figure 31b illustrates that the blend ratio and respectively the proportion of CX and CC in the *all*-cellulose films shows no severe influence on the water uptake.

In conclusion, this contribution showed that CC is a suitable material for the spin coating of cellulose thin films. Regeneration of CC to cellulose proceeds via an addition elimination reaction during spin-coating. Blending of CC with CX leads to smooth *all*-cellulose model systems, providing valuable information on the mutual influence of CC on CX and vice versa.

Conclusion and Outlook

This thesis describes various investigations with the main idea to explore alternative applications of cellulose xanthate. The summarized results emerge from very different fields of science like fiber spinning, composite formation, membrane casting or thin film processing and demonstrate the huge potential of cellulose xanthate. The development of a laboratory scale fiber spinning unit and a simple process for the formation of cellulose films and membranes was performed and allowed to explore new materials and alternative applications for Viscose based products. Further the spinning unit is meanwhile an integral part in the education of students and give insights into fiber spinning for the next generation of chemists, process engineers and biorefinery engineers to understand the principles and importance of wood based fiber production. The core shell coated metal sulfide composite fibers spun with the laboratory scale spinning unit demonstrate a promising field of Viscose fibers in technical applications like car breaks or bearings. The technology is ready to be scaled up and there is serious interest from industrial partners in further developing the technology. The membranes from CX utilized in lignosulfonate separation are an interesting alternative to olefin-based membranes as they overcome some of their drawbacks.

For the cellulose thin films made from cellulose xanthate the situation was a bit easier, as profound knowledge on the processing of thin films itself and suitable equipment has already been developed. Nethertheless, with cellulose xanthate a new precursor for cellulose thin films could successfully be implemented. CX displays some important advantages in comparison to previously used materials as it is cheap, widely available, and easy to process. In addition, it enables a water based film processing avoiding any organic solvents. The spin coating of multilayered thin film composites based on cellulose and CuInS demonstrates a potential large-scale application for CX based cellulose films in flexible electronics. Further, cellulose thin films are often discussed as model systems to investigate diverse reactions and interactions and hence the processing of CX/ CC based blend films brings along a new model system for studying cellulose interfaces and all cellulose composites.

As the discussion about the results is still ongoing, continuously new ideas arise and work on this topic will continue. So far, the most interesting ongoing studies are the utilization of CX based thin films for adsorption and cellulose swelling studies as well as an up-scale experiment for the metal sulfide coated fibers, done by colleagues and my successors.

Literature

1. Klemm, D., et al., *Cellulose: Fascinating Biopolymer and Sustainable Raw Material.* Angewandte Chemie International Edition, 2005, **44**, p. 3358
2. Payen, A., *Mémoire sur la composition du tissu propre des plantes et du ligneux.* Comptes rendus de l'Académie des sciences, 1838, **7**, p. 1052
3. Fisher, C.H., *Anselm Payen Pioneer in Natural Polymers and Industrial Chemistry*. 1989, Springer, Dordrecht (Netherlands), p. 47
4. Balser, K., et al., *Ullmann's Encyclopedia of Industrial Chemistry*. 1986, VCH, Weinheim, 419
5. Klemm, D., et al., *Polysaccharides II: Polysaccharides from Eukaryotes*. 2002, WileyVCH, Weinheim, p. 290
6. Martínez, A.J., et al., *Immobilized biomolecules on plasma functionalized cellophane. I. Covalently attached α-chymotrypsin.* Journal of Biomaterials Science, 2000, **11**, p. 415
7. Erdtmann, M., et al., *Photochemical immobilization of heparin, dermatan sulphate, dextran sulphate and endothelial cell surface heparan sulphate onto cellulose membranes for the preparation of athrombogenic and antithrombogenic polymers.* Biomaterials, 1994, **15**, p. 1043
8. Felix, G., *Regioselectively modified polysaccharide derivatives as chiral stationary phases in high-performance liquid chromatography.* Journal of Chromatography A, 2001, **906**, p. 171
9. Linder, Å., et al., *Mechanism of Assembly of Xylan onto Cellulose Surfaces.* Langmuir, 2003, **19**, p. 5072
10. Staudinger, H., *Über Polymerisation.* Berichte der deutschen chemischen Gesellschaft 1920, **53**, p. 1073
11. French, A.D., *Glucose, not cellobiose, is the repeating unit of cellulose and why that is important.* Cellulose, 2017, **24**, p. 4605
12. Credou, J., et al., *Cellulose: from biocompatible to bioactive material.* Journal of Materials Chemistry B, 2014, **2**, p. 4767
13. Klemm, D., et al., *Comprehensive Cellulose Chemistry. Volume 1. Fundamentals and Analytical Methods*. 1998, Wiley, Weinheim, 8677
14. Röhrling, J., et al., *Determination of carbonyl functions in cellulosic substrates.* Lenzinger Berichte, 2002, **81**, p. 89
15. Kalia, S., et al., *Cellulose Fibers: Bio- and Nano-Polymer Composites: Green Chemistry and Technology*. 2011, Springer, Heidelberg
16. Marchessault, R.H., et al., *X-Ray Structure of Polysaccharides.* Advances in Carbohydrate Chemistry, 1967, **22**, p. 421
17. Walton, A.G., et al., *Nucleation and Crystallization of Polymers and Biopolymers.* Croatica Chemica Acta, 1973, **42**, p. 363
18. VanderHart, D.L., et al., *Studies of microstructure in native celluloses using solid-state carbon-13 NMR.* Macromolecules, 1984, **17**, p. 1465
19. Sugiyama, J., et al., *Combined infrared and electron diffraction study of the polymorphism of native celluloses.* Macromolecules, 1991, **24**, p. 2461
20. Wada, M., et al., *Polymorphism of Cellulose I Family: Reinvestigation of Cellulose IVI.* Biomacromolecules, 2004, **5**, p. 1385
21. Horii, F., et al., *CP/MAS carbon-13 NMR spectra of the crystalline components of native celluloses.* Macromolecules, 1987, **20**, p. 2117
22. Kontturi, E.J., *Surface chemistry of cellulose: from natural fibres to model surfaces*, in *Doctoral thesis*. 2005, Technische Universiteit Eindhoven.

23. Zugenmaier, P., *Conformation and packing of various crystalline cellulose fibers.* Progress in Polymer Science, 2001, **26**, p. 1341
24. Heß, K., et al., *Zur Kenntnis der Hochtemperatur-Modifikation der Cellulose.* Zeitschrift für Physikalische Chemie, 1941, **49B**, p. 235
25. Gardiner, E.S., et al., *Packing analysis of carbohydrates and polysaccharides. The crystal structures of celluloses IV_I and IV_{II}.* Canadian Journal of Chemistry, 1985, **63**, p. 173
26. Kondo, T., et al., *"Nematic Ordered Cellulose": A Concept of Glucan Chain Association.* Biomacromolecules, 2001, **2**, p. 1324
27. Nobles, D.R., et al., *Cellulose in Cyanobacteria. Origin of Vascular Plant Cellulose Synthase?* Plant Physiology, 2001, **127**, p. 529
28. Wightman, R., et al., *Trafficking of the Plant Cellulose Synthase Complex.* Plant Physiology, 2010, **153**, p. 427
29. Zimmermann, T., et al., *Cellulose Fibrils for Polymer Reinforcement.* Advanced Engineering Materials, 2004, **6**, p. 754
30. Niinivaara, E., et al., *Mimicking the Humidity Response of the Plant Cell Wall by Using Two-Dimensional Systems: The Critical Role of Amorphous and Crystalline Polysaccharides.* Langmuir, 2016, **32**, p. 2032
31. Roy, D., et al., *Cellulose modification by polymer grafting: a review*. Chemical Society Reviews, 2009, **38**, p. 2046
32. Jonoobi, M., et al., *Different preparation methods and properties of nanostructured cellulose from various natural resources and residues: a review.* Cellulose, 2015, **22**, p. 935
33. Deprez, T., et al., *Cellulose: structure and properties, derivatives and industrial uses*. 2010, Nova Science Publishers, New York, 528
34. Chabannes, M., et al., *In situ analysis of lignins in transgenic tobacco reveals a differential impact of individual transformations on the spatial patterns of lignin deposition at the cellular and subcellular levels.* The Plant Journal, 2001, **28**, p. 271
35. Malmström, E., et al., *Controlled grafting of cellulose fibres–an outlook beyond paper and cardboard.* Polymer Chemistry, 2012, **3**, p. 1702
36. Heinze, T., et al., *Unconventional methods in cellulose functionalization.* Progress in Polymer Science, 2001, **26**, p. 1689
37. Credou, J., et al., *A one-step and biocompatible cellulose functionalization for covalent antibody immobilization on immunoassay membranes.* Journal of Materials Chemistry B, 2013, **1**, p. 3277
38. Klemm, D., et al., *Comprehensive Cellulose Chemistry Volume 2 Functionalization of cellulose* 1998, Wiley-VCH, Weinheim
39. Varma, A.J., et al., *Oxidation of cellulose under controlled conditions.* Polymer Degradation and Stability, 2002, **77**, p. 25
40. Kim, U.-J., et al., *Periodate Oxidation of Crystalline Cellulose.* Biomacromolecules, 2000, **1**, p. 488
41. Siller, M., et al., *Effects of periodate oxidation on cellulose polymorphs.* Cellulose, 2015, **22**, p. 2245
42. Orelma, H., et al., *Generic Method for Attaching Biomolecules via Avidin–Biotin Complexes Immobilized on Films of Regenerated and Nanofibrillar Cellulose.* Biomacromolecules, 2012, **13**, p. 2802
43. Benhamou, K., et al., *Control of size and viscoelastic properties of nanofibrillated cellulose from palm tree by varying the TEMPO-mediated oxidation time.* Carbohydrate Polymers, 2014, **99**, p. 74
44. Mann, G., et al., *Cellulose ethers with a block-like distribution of the substituents by structure-selective derivatization of cellulose.* Polymer, 1998, **39**, p. 3155

45. Heinze, T., et al., *Unconventional Cellulose Esters: Synthesis, Characterization and Structure–Property Relations.* Cellulose, 2003, **10**, p. 283
46. Petzold, K., et al., *Silylation of Cellulose and Starch – Selectivity, Structure Analysis, and Subsequent Reactions.* Cellulose, 2003, **10**, p. 251
47. Mormann, W., et al., *Silylation of Cellulose with Hexamethyldisilazane in Liquid Ammonia First Examples of Completely Trimethylsilylated Cellulose.* Macromolecules, 1999, **32**, p. 1706
48. Woodings, C., *Regenerated Cellulose Fibres*. 2001, Woodhead Publishing, Cambridge, 352
49. Wu, Q.-X., et al., *Sodium cellulose sulfate: A promising biomaterial used for microcarriers' designing.* Frontiers of Chemical Science and Engineering, 2019, **13**, p. 46
50. Schmidt, S., et al., *Synthesis of soluble cellulose tosylates in an eco-friendly medium.* Green Chemistry, 2014, **16**, p. 1941
51. Bass, J.J., et al., *An overview of technical considerations for Western blotting applications to physiological research.* Scandinavian journal of medicine & science in sports, 2017, **27**, p. 4
52. Heinze, T., et al., *Solvents applied in the field of cellulose chemistry: a mini review.* Polímeros, 2005, **15**, p. 84
53. Liebert, T.F., *Cellulose Solvents – Remarkable History, Bright Future*. 2010, Oxford University Press, Oxford, p. 3
54. Zhang, J., et al., *Application of ionic liquids for dissolving cellulose and fabricating cellulose-based materials: state of the art and future trends.* Materials Chemistry Frontiers, 2017, **1**, p. 1273
55. Lina, Z., et al., *Blend membranes of cellulose cuoxam/casein.* Journal of Membrane Science, 1995, **103**, p. 65
56. Schweizer, E., *Das kupferoxyd-ammoniak, ein auflösungsmittel für die pflanzenfaser*. Journal für praktische Chemie, 1857, **72**, p. 109
57. Burger, J., et al., *Coordination equilibria in transition metal based cellulose solvents.* Macromolecular Symposia, 1995, **99**, p. 113
58. Heinze, T., et al., *Carboxymethylation of cellulose in unconventional media*. Cellulose, 1999, **6**, p. 153
59. Isogai, A., et al., *Dissolution of Cellulose in Aqueous NaOH Solutions.* Cellulose, 1998, **5**, p. 309
60. Cai, J., et al., *Hydrogen-Bond-Induced Inclusion Complex in Aqueous Cellulose/LiOH/Urea Solution at Low Temperature.* ChemPhysChem, 2007, **8**, p. 1572
61. Liu, S., et al., *Effects of polymer concentration and coagulation temperature on the properties of regenerated cellulose films prepared from LiOH/urea solution.* Cellulose, 2009, **16**, p. 189
62. Fischer, S., et al., *The behaviour of cellulose in hydrated melts of the composition LiXċn H_2O ($X=I^-$, NO_3^-, CH_3COO^-, ClO_4^-).* Cellulose, 1999, **6**, p. 213
63. Striegel, A., *Theory and applications of DMAC/LICL in the analysis of polysaccharides.* Carbohydrate Polymers, 1997, **34**, p. 267
64. Heinze, T., et al., *Effective preparation of cellulose derivatives in a new simple cellulose solvent.* Macromolecular Chemistry and Physics, 2000, **201**, p. 627
65. Zhang, H., et al., *1-Allyl-3-methylimidazolium Chloride Room Temperature Ionic Liquid: A New and Powerful Nonderivatizing Solvent for Cellulose.* Macromolecules, 2005, **38**, p. 8272
66. Wu, J., et al., *Homogeneous Acetylation of Cellulose in a New Ionic Liquid.* Biomacromolecules, 2004, **5**, p. 266

67. Ebner, G., et al., *Side reaction of cellulose with common 1-alkyl-3-methylimidazolium-based ionic liquids*. 2008, 7322
68. Heinze, T., et al., *Ionic Liquids as Reaction Medium in Cellulose Functionalization.* Macromolecular Bioscience, 2005, **5**, p. 520
69. Liu, Q.-P., et al., *Ionic liquids from renewable biomaterials: synthesis, characterization and application in the pretreatment of biomass.* Green Chemistry, 2012, **14**, p. 304
70. Cross, C.F., et al., *Patent 8700*. 1892: Great Britain.
71. Polyuto, A.A., et al., *Study of the Possibility of Processing Cotton Cellulose in Bulk for Fabrication of Viscose Fibre.* Fibre Chemistry, 2000, **32**, p. 353
72. Jacobson, R.A., *Carbamic Esters from Urea.* Journal of the American Chemical Society, 1938, **60**, p. 1742
73. Willberg-Keyriläinen, P., et al., *Production of cellulose carbamate using urea-based deep eutectic solvents.* Cellulose, 2018, **25**, p. 195
74. Hasegawa, M., et al., *Dissolving states of cellulose and chitosan in trifluoroacetic acid.* Journal of Applied Polymer Science, 1992, **45**, p. 1857
75. Vigo, T.L., et al., *Reaction of cellulose with chlorodimethylformiminium chloride and subsequent reaction with halide ions.* Journal of Polymer Science 1972, **10**, p. 397
76. Lewin, M., *Handbook of Fiber Chemistry*. 2006, CRC Press, Boca Raton, 1056
77. Sixta, H., et al., *Ioncell-F: A High-strength regenerated cellulose fibre.* Nordic Pulp & Paper Research Journal, 2015, **30**, p. 43
78. Fink, H.P., et al., *Structure formation of regenerated cellulose materials from NMMO-solutions.* Progress in Polymer Science, 2001, **26**, p. 1473
79. Fink, H.-P., et al., *Progress in cellulose shaping: 20 years industrial case studies at Fraunhofer IAP*. Cellulose, 2014, **21**, p. 31
80. Schleicher, H., et al., *Vergleich verschiedener Wege der CS_2-freien Herstellung von cellulosischen Chemiefasern.* Lenzinger Berichte, 1994, **74**, p. 5
81. Perepelkin, K.E., *Lyocell fibres based on direct dissolution of cellulose in N-methylmorpholine N-oxide: Development and prospects.* Fibre Chemistry, 2007, **39**, p. 163
82. Rosenau, T., et al., *The chemistry of side reactions and byproduct formation in the system NMMO/cellulose (Lyocell process).* Progress in Polymer Science, 2001, **26**, p. 1763
83. Zhang, Z., et al., *An unexpected reaction between 5-hydroxymethylfurfural and imidazolium-based ionic liquids at high temperatures.* Molecules 2011, **16**, p. 8463
84. Laus, G., et al., *Ionic liquids: current developments, potential and drawbacks for industrial applications.* Lenzinger Berichte, 2005, **84**, p. 71
85. Hummel, M., et al., *Ionic Liquids for the Production of Man-Made Cellulosic Fibers: Opportunities and Challenges*. 2016, Springer International Publishing, Cham, p. 133
86. Mortimer, S.A., et al., *The influence of air-gap conditions on the structure formation of lyocell fibers.* Journal of Applied Polymer Science, 1996, **60**, p. 1747
87. Gindl, W., et al., *Anisotropy of the modulus of elasticity in regenerated cellulose fibres related to molecular orientation.* Polymer, 2008, **49**, p. 792
88. Ganster, J., et al., *The structure of man-made cellulosic fibres*. 2009, Woodhead Publishing, p. 201
89. Hämmerle, F.M., *The cellulose gap.* Lenzinger Berichte, 2011, **89**, p. 12
90. Wilkes, A.G., *The viscose process*. 2001, Woodhead Publishing, p. 37
91. He, L., et al., *A Real-Time Technique for Monitoring Cellulose Dissolution during the Xanthation Process.* Industrial & Engineering Chemistry Research, 2016, **55**, p. 10823
92. Klare, H., *100 Jahre Celluloseregeneratfaserstoffe – Geschichte und Perspektiven.* Acta Polymerica, 1985, **36**, p. 347

93. Wöss, K., et al., *Rapid determination of γ-value and xanthate group distribution on viscose by liquid-state 1H NMR spectroscopy.* Carbohydrate Polymers, 2016, **141**, p. 184
94. You-xin, L., et al., *Cost-benefit analysis of the recovery of carbon disulfide in the manufacturing of viscose rayon.* Scandinavian Journal of Work, Environment & Health, 1985, **11**, p. 60
95. Shen, L., et al., *Life cycle assessment of man-made cellulose fibers.* Lenzinger Berichte 2010, **88**, p. 1
96. Götze, K., *Chemiefasern nach dem Viskoseverfahren*. 1951, Springer Verlag, Heidelberg, Germany
97. Široký, J., et al., *Attenuated total reflectance Fourier-transform Infrared spectroscopy analysis of crystallinity changes in lyocell following continuous treatment with sodium hydroxide.* Cellulose, 2010, **17**, p. 103
98. Fink, H., et al., *Reifebestimmung und Ultrafiltration von Viscose.* Angewandte Chemie, 1934, **47**, p. 602
99. Ogura, K., et al., *Studies on the derivatives of sodium cellulose xanthate. Part I. Infrared absorption spectra and characteristic frequencies of C-S and C=S groups in sodium cellulose xanthate and its stable derivatives.* Journal of Polymer Science, 1968, **6**, p. 63
100. Wang, S., et al., *Recent advances in regenerated cellulose materials.* Progress in Polymer Science, 2016, **53**, p. 169
101. Bychkova, E.V., et al., *Fire-Resistant Viscose Rayon Fiber Materials.* Fibre Chemistry, 2016, **48**, p. 217
102. Araki, J., et al., *A preliminary study for fiber spinning of mixed solutions of polyrotaxane and cellulose in a dimethylacetamide/lithium chloride (DMAc/LiCl) solvent system.* Polymer, 2006, **47**, p. 8241
103. Liu, S., et al., *Structure and Properties of Cellulose/Fe_2O_3 Nanocomposite Fibers Spun via an Effective Pathway.* The Journal of Physical Chemistry C, 2008, **112**, p. 4538
104. Hribernik, S., et al., *Synthesis of magnetic iron oxide particles: Development of an in situ coating procedure for fibrous materials.* Colloids and Surfaces A: Physicochemical and Engineering Aspects, 2012, **400**, p. 58
105. Breitwieser, D., et al., *In situ preparation of silver nanocomposites on cellulosic fibers – Microwave vs. conventional heating.* Carbohydrate Polymers, 2013, **94**, p. 677
106. Fradler, C., et al., *Flexible polymer/copper indium sulfide hybrid solar cells and modules based on the metal xanthate route and low temperature annealing.* Solar Energy Materials and Solar Cells, 2014, **124**, p. 117
107. Reishofer, D., et al., *Biobased Cellulosic–$CuInS_2$ Nanocomposites for Optoelectronic Applications.* ACS Sustainable Chemistry & Engineering, 2017, **5**, p. 3115
108. Rath, T., et al., *Solution-processed small molecule/copper indium sulfide hybrid solar cells.* Solar Energy Materials and Solar Cells, 2013, **114**, p. 38
109. Yu, W., et al., *Ag_2S Quantum Dots as an Infrared Excited Photocatalyst for Hydrogen Production.* ACS Applied Energy Materials, 2019, **2**, p. 2751
110. Koteeswara Reddy, N., et al., *Review on Tin (II) Sulfide (SnS) Material: Synthesis, Properties, and Applications.* Critical Reviews in Solid State and Materials Sciences, 2015, **40**, p. 359
111. Yang, Q., et al., *Facile fabrication of transparent cellulose films with high water repellency and gas barrier properties.* Cellulose, 2012, **19**, p. 1913
112. Shi, X., et al., *A Facile Construction of Supramolecular Complex from Polyaniline and Cellulose in Aqueous System.* Macromolecules, 2011, **44**, p. 4565
113. Ke, D., et al., *CdS/Regenerated Cellulose Nanocomposite Films for Highly Efficient Photocatalytic H_2 Production under Visible Light Irradiation.* The Journal of Physical Chemistry C, 2009, **113**, p. 16021

114. Mohamed, M.A., et al., *Feasibility of recycled newspaper as cellulose source for regenerated cellulose membrane fabrication.* Journal of Applied Polymer Science, 2015, **132**
115. Ortner, A., et al., *Laccase modified lignosulfonates as novel binder in pigment based paper coating formulations.* Reactive and Functional Polymers, 2018, **123**, p. 20
116. Aro, T., et al., *Production and Application of Lignosulfonates and Sulfonated Lignin.* ChemSusChem, 2017, **10**, p. 1861
117. Chakrabarty, K., et al., *Separation of lignosulfonate from its aqueous solution using emulsion liquid membrane.* Journal of Membrane Science, 2010, **360**, p. 34
118. Chinga-Carrasco, G., et al., *Bleached and unbleached MFC nanobarriers: properties and hydrophobisation with hexamethyldisilazane.* Journal of Nanoparticle Research, 2012, **14**, p. 1280
119. Rodionova, G., et al., *Gas-phase esterification of microfibrillated cellulose (MFC) films.* Cellulose, 2013, **20**, p. 1167
120. Kontturi, E., et al., *Cellulose—model films and the fundamental approach.* Chemical Society Reviews, 2006, **35**, p. 1287
121. Kontturi, E., et al., *Novel method for preparing cellulose model surfaces by spin coating.* Polymer, 2003, **44**, p. 3621
122. Kargl, R., et al., *Cellulose thin films from ionic liquid solutions.* Nordic Pulp & Paper Research Journal, 2015, **30**, p. 6
123. Schaub, M., et al., *Ultrathin films of cellulose on silicon wafers.* Advanced Materials, 1993, **5**, p. 919
124. Wolfberger, A., et al., *Photoregeneration of Trimethylsilyl Cellulose as a Tool for Microstructuring Ultrathin Cellulose Supports.* Molecules, 2014, **19**, p. 16266
125. Mohan, T., et al., *Interaction of Tissue Engineering Substrates with Serum Proteins and Its Influence on Human Primary Endothelial Cells.* Biomacromolecules, 2017, **18**, p. 413
126. Mohan, T., et al., *Triggering Protein Adsorption on Tailored Cationic Cellulose Surfaces.* Biomacromolecules, 2014, **15**, p. 3931
127. Rath, T., et al., *Direct extreme UV-lithographic conversion of metal xanthates into nanostructured metal sulfide layers for hybrid photovoltaics.* Journal of Materials Chemistry A, 2013, **1**, p. 11135
128. Reishofer, D., et al., *On the formation of Bi_2S_3-cellulose nanocomposite films from bismuth xanthates and trimethylsilyl-cellulose.* Carbohydrate Polymers, 2017, **164**, p. 294
129. Rath, T., et al., *A Direct Route Towards Polymer/Copper Indium Sulfide Nanocomposite Solar Cells.* Advanced Energy Materials, 2011, **1**, p. 1046

List of figures

List of tables

Curriculum Vitae

Personal information

DI Michael Weißl, BSc.

Mariatrosterstraße 94/4
A – 8043 Graz

+43664/73516525
michael.weissl@tugraz.at

Date of birth: 18.11.1991 (Vöcklabruck)
Nationality: Austria

Education

since 09/2016 — **Doctoral thesis**
Institute of Paper, Pulp and Fibre Technology, TU Graz
Focus on: Biomaterials, surfaces modification and characterization, Cellulose processing and functionalization, Composite engineering
PhD topic: Viscose process revisited - from process optimization to new materials
Supervisor: Assoc.Prof. Mag. Dr. Stefan Spirk, Univ.Prof. DI Dr. Wolfgang Bauer

10/2014 - 08/2016 — **Master studies - Technical Chemistry** - *Graduation with excellent success*
Institute of Chemistry and Technology of Materials, TU Graz
Focus on: (Bio-)polymers, Polymer synthesis and processing, Surface and bulk characterization of polymeric materials
Master thesis: In-situ synthesis of metal-sulfide coated fibers in the course of the Viscose process
Supervisor: Assoc.Prof. Mag. Dr. Stefan Spirk, Univ.Prof. DI Dr. Franz Stelzer

10/2011 - 09/2014 — **Bachelor studies - Chemistry**
TU Graz (NAWI Graz)
Bachelor thesis in the field of analytical chemistry

09/2002 - 06/2010 — **Secondary school** - *Graduation with excellent success*
BRG Schloss Wagrain Vöcklabruck

09/1998 - 07/2002 — **Primary school**
Volksschule Schörfling am Attersee

Work experience

since 09/2016	**Graz University of Technology** Scientific co-worker at Institute of Paper, Pulp and Fiber Technology (full time since 02/2018, part time before)
07/2016 – 01/2018	**Hairdreams GmbH** Project manager R&D (part time 20 h/week)
12/2015 - 06/2016	**Graz University of Technology** Project Assistant at Institute for Chemistry and Technology of Materials
2012 – 2015	**Lenzing AG** 4 times, a 6 week lasting industrial placement in R&D and analytical laboratories
02/2011 - 06/2011	**Lenzing AG** 5 months industrial placement in analytical and process control laboratory
07/2010 - 01/2011	**Military service** training to paramedic

Scientific output

7	Peer reviewed publication as Author (2+3 under review) and Co-Author (2)
1	Invention report at TU Graz, ongoing patent process
10	Talks at international Conferences
3	Poster presentations at international Conferences
2	Awards for scientific presentations on international conferences

Soft skills

Foreign languages	Fluent English (spoken and written)
EDP knowledge	Advanced knowledge in MS-Office and Origin
Driving license	Car (B)

Additional Information

Since 08/2010	Volunteer paramedic at the Austrian Red Cross
	Interested in traveling, out-door sports and reading

DI Michael Weißl

Scientific Output

List of paper as author and co-author

7) M. Weißl, G. Kraft, J. Innerlohinger and S. Spirk, Spinning of Fibers from Wood – A Lab Experiment to Introduce Students in Viscose Fiber Manufacturing and Analysis, Journal of Chemical Education, 2019, submitted
6) Michael Weißl, Mike Pelzman, Armin Zankel, Brigitte Bitschnau, Helmar Wiltsche and Stefan Spirk; Processing of metal sulfide/ cellulose composite fibers in core-shell configuration; Lenzinger Berichte; 2019; submitted
5) M. Weißl, M. Andreas Hobisch, L. S. Johansson, K. Hettrich, E. Kontturi, B. Volkert and S. Spirk, Cellulose carbamate derived cellulose thin films – Preparation, characterization and blending with cellulose xanthate, Cellulose, 2019, submitted
4) M. Kienberger, P. Demmelmayer, M. Weißl, A. Zankl and S. Spirk, Biobased support layers for the fractionation and selective extraction of lignosulfonates, Solvent Extraction and Ion Exchange Journal, 2019, accepted
3) M. Weißl, T. Rath, J. Sattelkow, H. Plank, S. Eyley, W. Thielemans, G. Trimmel and S. Spirk, Multi-layered nanoscale cellulose/CuInS2 sandwich type thin films, Carbohydrate Polymers, 2019, 203, 219-227
2) W. Schlemmer,K. Niegelhell, M. Hobisch, M. Süssenbacher, K. Zajki-Zechmeister, M. Weissl, D. Reishofer, H. Plank andS. Spirk, Deposition of Cellulose-Based Thin Films on Flexible Substrates, Materials, 2018, 11, 2433-2436
1) M. Weißl, K. Niegelhell, D. Reishofer, A. Zankel, J. Innerlohinger and S. Spirk, Homogeneous cellulose thin films by regeneration of cellulose xanthate: properties and characterization, Cellulose, 2018, 25, 711-721

Patents

1) S. Spirk, G. Trimmel, M. Weißl, D. Pfeifer, M. Hobisch, B. Alonso; In situ Synthese von Metallsulfidpartikeln auf/in Fasern und Filmen im Zuge des Viskoseverfahrens A50790/2018

Oral conference contributions

10) M. Weißl, M. Andreas Hobisch, L. S. Johansson, K. Hettrich, E. Kontturi, B. Volkert and S. Spirk, Aqueous processing of all cellulose blend thin films, ACS Spring Meeting, 2019, Orlando, USA
9) M. Weißl and S. Spirk, Cellulose xanthate for functional cellulose thin films, 1st CelCon, 2018, Graz, Austria
8) M. Weißl and S. Spirk, Nanocomposite thin films from cellulose – current state and challenges, Advanced Materials Day, 2018, Graz, Austria
7) M. Weißl, D. Reishofer, B. Alonso, E. Belamie, H. Amenitsch, A. Zankel, T. Rath, J. Innerlohinger, H. Plank, G. Trimmel and S. Spirk, Cellulose metal sulfide based nanocomposite thin films, 3rd EPNOE Junior, 2018, Maribor, Slovenia
6) M. Weißl, D. Reishofer, B. Alonso, E. Belamie, H. Amenitsch, A. Zankel, T. Rath, J. Innerlohinger, H. Plank, G. Trimmel and S. Spirk, Cellulose metal sulfide based nanocomposite thin films, 18th ECCM, 2018, Athen, Greece
5) M. Weißl, K. Niegelhell, D. Reishofer, A. Zankel and S. Spirk, Cellulose xanthate as an aqueous source to generate functional cellulose thin films, DocDays TU Graz, 2018, Graz, Austria
4) M. Weißl, K. Niegelhell, D. Reishofer, A. Zankel and S. Spirk, Cellulose xanthate as an aqueous source to generate functional cellulose thin films, ACS Spring Meeting, 2018, New Orleans, USA
3) M. Weißl, K. Niegelhell, D. Reishofer, A. Zankel and S. Spirk, Viscose based cellulose thin films, a new model system for studying cellulose surface interactions, 22nd Austrian Carbohydrate Workshop, 2018, Wien, Austria
2) M. Weißl, K. Niegelhell, D. Reishofer and S. Spirk, Viscose based cellulose thin films, a new model system for studying cellulose surface interactions, 25th ICM&T, 2017, Portoroz, Slovenia
1) M. Weißl, K. Niegelhell, D. Reishofer and S. Spirk, Viscose based cellulose thin films, a new model system for studying cellulose surface interactions, 5th EPNOE Conference, 2017, Jena, Germany

Poster presentations as author

3) M. Weißl, and S. Spirk, Diclofena-Viscose composite fibers with controllable release behavior, European Cellulose Materials PhD Students Conference, 2018, Bratislava, Slovakia
2) M. Weißl, M. Julin, and S. Spirk, Coating of cellulose fibres with inorganic nanoparticles in the course of the Viscose process, European Cellulose Materials PhD Students Conference, 2017, Leitring, Austria
1) M. Weißl, M. Julin, and S. Spirk, Modification of cellulose fibers with inorganic nanoparticles in the course of the Viscose process, 2nd International EPNOE Junior Scientists Meeting, 2016, Sophia-Antipolis, France

Appendix

Paper #1

Spinning of Fibers from Wood – A Lab Experiment to Introduce Students in Viscose Fiber Manufacturing and Analysis

Submitted to Journal of Chemical Education

For this paper, I was responsible for the development of the fiber spinning equipment, I conducted most of the experiments, interpreted the data and wrote a significant part of the manuscript.

Spinning of Fibers from Wood – A Lab Experiment to Introduce Students in Viscose Fiber Manufacturing and Analysis

Michael Weißl[†], Gregor Kraft[‡], Josef Innerlohinger[‡] and Stefan Spirk[†*]

[†]Graz University of Technology, Institute of Paper, Pulp and Fiber Technology, Inffeldgasse 23A 8010 Graz

[‡]Lenzing AG, Werkstrasse 2, 4860 Lenzing, Austria.

Correspondence:

Stefan Spirk

stefan.spirk@tugraz.at

+43 (316) 873 – 30763

Abstract

Despite being a rather old industrial process, the manufacturing of viscose fibers still accounts for the major fraction of all man-made cellulosic fibers. Here, we describe a set of experiments employing a simple setup to introduce students into the principles of cellulose fiber spinning according to the viscose process. This involves four main steps, namely alkali cellulose preparation from wood pulp, xanthation, fiber spinning and characterization of the fibers using optical microscopy and IR spectroscopy. The setup for fiber spinning is kept simplistic and allows for performing the experiments even without professional spinning equipment. The course is designed in a modular manner, so that depending on the skills and equipment of the labs, several steps can be omitted and therefore the duration of the course ranges from 5 days to half a day.

Keywords: Cellulose xanthate, wood based, fiber spinning, Viscose process, lab course

INTRODUCTION

Man-made wood based cellulose fibers are a promising alternative to cotton based fibers. Their production neither requires large agricultural areas, irrigation and extensive use of fertilizers or pesticides, nor do they contribute to the pollution of our environment due to their intrinsic biodegradability.[1, 2] The history of man-made wood-based fibers dates back to 1884, when Svan dissolved nitrocellulose and then injected this solution in a regeneration bath to produce cellulose fibers with a wonderful shining, the first artificial silk. In the years to come, a variety of other processes was introduced and commercialized, such as the cuprammonium rayon and - with large success - the viscose silk.[3] Soon after the discovery of viscose silk by Cross, Bewan and Beadlein in 1892, it conquered the markets and replaced artificial silks made from nitrocellulose and cuprammonium.[4, 5] In detail, Cross, Bewan and Beadlein explored the reaction of alkali cellulose and carbon disulfide to cellulose xanthate. They realized that the produced cellulose xanthate is very well soluble in a diluted sodium hydroxide solution and can be converted after a processing step to cellulose fibers or films by exposure to an acidic bath. Nowadays, this process is the most important process to manufacture man made wood based fibers with production volumes of several million tons per year.[1, 6]Although the basic principle is still the same as in the end of the 19th century, much progress has been made in the preparation of the alkali cellulose, the removal of undesired impurities, and the procedures to obtain spinning dopes suitable for the production of high quality fibers.[7-9] Besides progress in the fiber/film manufacturing, also the processes to recycle the used chemicals and to remove them from air have been improved significantly.[10, 11] For instance, air pollution by the largest viscose manufacturer in Europe, Lenzing AG, is at an extremely low level, which is a prerequisite considering that the plant site is located close to residential areas.[12] Since the demand for fibers is steadily growing, and since cotton plantation is more or less on the limit of potential land use, the only way to close the gap is to focus on wood based fibers.[13] The viscose process is certainly a part of the solution to this problem.

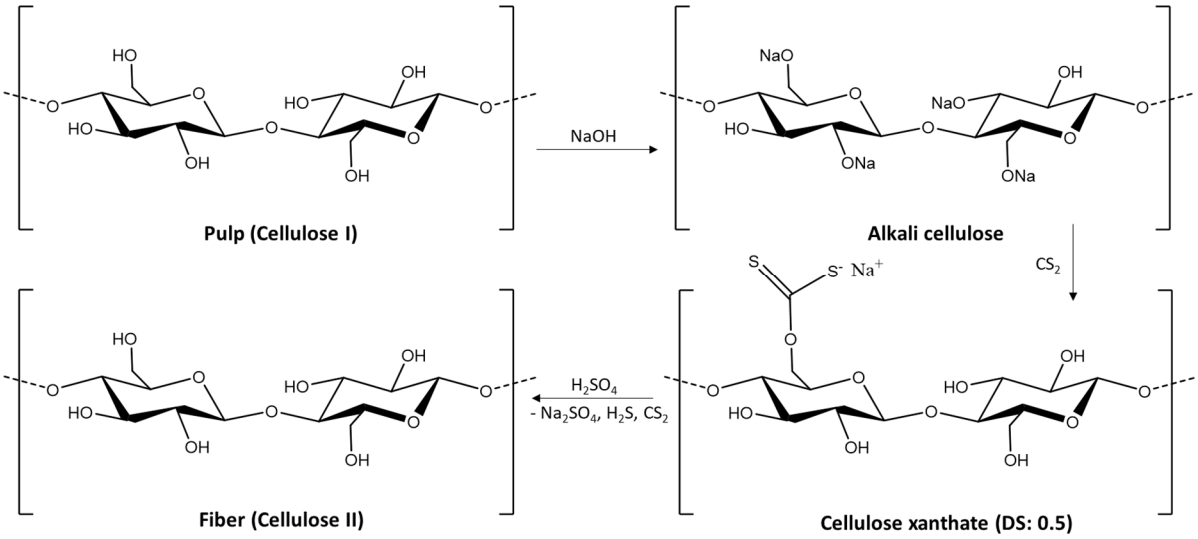

Scheme 1. Simplified description of the main steps in the viscose process, starting with the synthesis of alkali cellulose from a cellulose source, the followed xanthation and the final regeneration back to cellulose.

Pedagogical goals:

- Understanding challenges in cellulose processing and how to overcome these
- Acquiring practical knowledge in wood based fiber manufacturing
- Exploring the morphological properties of the spun wood based fibers
- Distinguishing between the supramolecular structure of viscose fibers and natural ones (e.g., cotton)

Evaluation: Examination whether the students can follow the whole process chain, starting from pulp, alkali cellulose, cellulose xanthate and regeneration to cellulose and how this refers to the working principle of fiber spinning.

Experimental overview:

The experimental parts necessary for the production of viscose fibers in a laboratory course in principle comprises the same steps that are necessary in large scale viscose fiber production. However, simplified equipment can be used and it is not necessary to perform all the steps in

the course giving flexibility while adjusting to the skills and opportunities in the used chemistry labs. The options range from half a day lab course, where the focus is only on the main part (the fiber spinning), to a four day lasting lab course, where all the important steps of wood-based fiber production are practiced. In the following, an overview of the single parts of 4 times 5 hours laboratory course on viscose fiber spinning will be given; detailed information of every step is available in the supporting information.

Alkali cellulose reaction: In this first part, the reaction of cellulose to alkali cellulose takes place. A native cellulose source (pulp, cotton, paper) is stirred in an 18 wt. % sodium hydroxide solution for two hours. After this, the excessive sodium hydroxide solution is removed from the cellulose by the pressing and the cellulose is aged overnight.[14, 15]

Xanthation: The aged alkali cellulose is stirred and carbon disulfide is added dropwise. After addition of the carbon disulfide, the xanthation takes place, and the white alkali cellulose fibers are converted to an orange, sticky pulp. The cellulose xanthate can then be dissolved in a 4 wt. % sodium hydroxide solution under constant stirring and cooling, resulting in the so called viscose solution. After the cellulose xanthate is completely dissolved, the viscose solution is subjected to aging before it can be used for fiber spinning.[14]

Fiber spinning: The aged cellulose xanthate is injected into a 10 wt. % sulfuric acid solution at 50°C. For the injection different experimental setups are used. The basic spinneret consists of a simple syringe with an injection needle, while a more sophisticated one employs a syringe pump with different spinning nozzles. The fibers are collected for example with a simple stirring bar when injected by hand, or by a rotating polypropylene cylinder operated by a laboratory stirrer, in the case a syringe pump is used.

Characterization: In the last part of the course, the changes in chemistry during the viscose process are observed by IR spectroscopy[16] and the effects of different injection needles, injection speeds and the way of injection (manual injection by hand, or controlled pressure by syringe pump) on fiber quality are studied.

Hazards:

Depending on the individual sub-steps of the laboratory experiment, attention has to be paid on potentially occurring risks. General the use of protective glasses, gloves and a lab coat is obligatory in all process steps and the safety data sheets of the used chemicals have to be studied.

In the alkali cellulose synthesis, the 18 wt. % sodium hydroxide solution has to be handled with care due to its high alkalinity. Especially, the xanthation has to be performed with care, because of dealing with carbon disulfide, a highly flammable and potential harmful compound. The use of a fume hood is obligatory and any type of operations should be performed using syringes.

For the regeneration of the cellulose xanthate, the spinning bath should also be placed in a fume hood, because during regeneration, traces of hydrogen sulfide gas are formed. H_2S is toxic and potentially harmful to environment and health. Additionally, the work with the 10 wt. % sulfuric acid requires attention. After the fibers have been washed, they can be handled and investigated without any safety equipment.

RESULTS AND DISCUSSION

We focus on our standard lab protocol where the students focus on the optical and microscopic observations in the fiber form and structure, when using needles with different diameters for the injection or when changing the injection speed of the syringe pump. From the microscopy images, the fiber diameter has to be calculated and the changes in diameter have to be explained. The second important part in the analytical section is to acquire IR spectra of all the cellulose derivatives appearing in the process and to explain the changes in structure and the ongoing chemical reactions using the infrared spectra.

However, if available, many other characterization techniques like tensile testing for the fibers or viscosimetric studies of the ripening of the cellulose xanthate solution are possible.

Determination of the cellulose content:

The determination of the cellulose content in the spinning dope is an easy way to characterize the dope without any further analytical instrument needed, as described in the supporting information. The absolute cellulose content could then be compared with the theoretical cellulose content based on the used amount of cellulose source. Normally the absolute and theoretical cellulose content fit quite well, in this case 3.5% were calculated and 3.6% were determined.[17]

Microscopy images and fiber diameter:

The fibers presented in Figure 1 exhibited large differences in terms of fiber diameter, fiber morphology and uniformity. The used spinning dope was the same in all the experiments and only a few variations such as the used injection mode (manually, continuous), the collection of the fibers (rotating fiber collector) and the diameter of the employed injection needles (450 µm, 800 µm) were explored. The manually injected fibers showed a relatively large variation in the fiber diameter and uniformity. The diameter itself with around 450 and 820 microns, respectively, was in the same range as the diameter of the used injection needles since no

additional force was applied for the collection of the fibers. The large variation in the diameters was caused by fluctuations of the caused injection pressure.

In contrast, the continuously injected and fibers collected under tension appeared quite uniform, and the variation in the diameters was much smaller. The diameters with around 60 µm for the thin needle and 250 µm for the thicker needle were significantly reduced, compared to the manual injection.

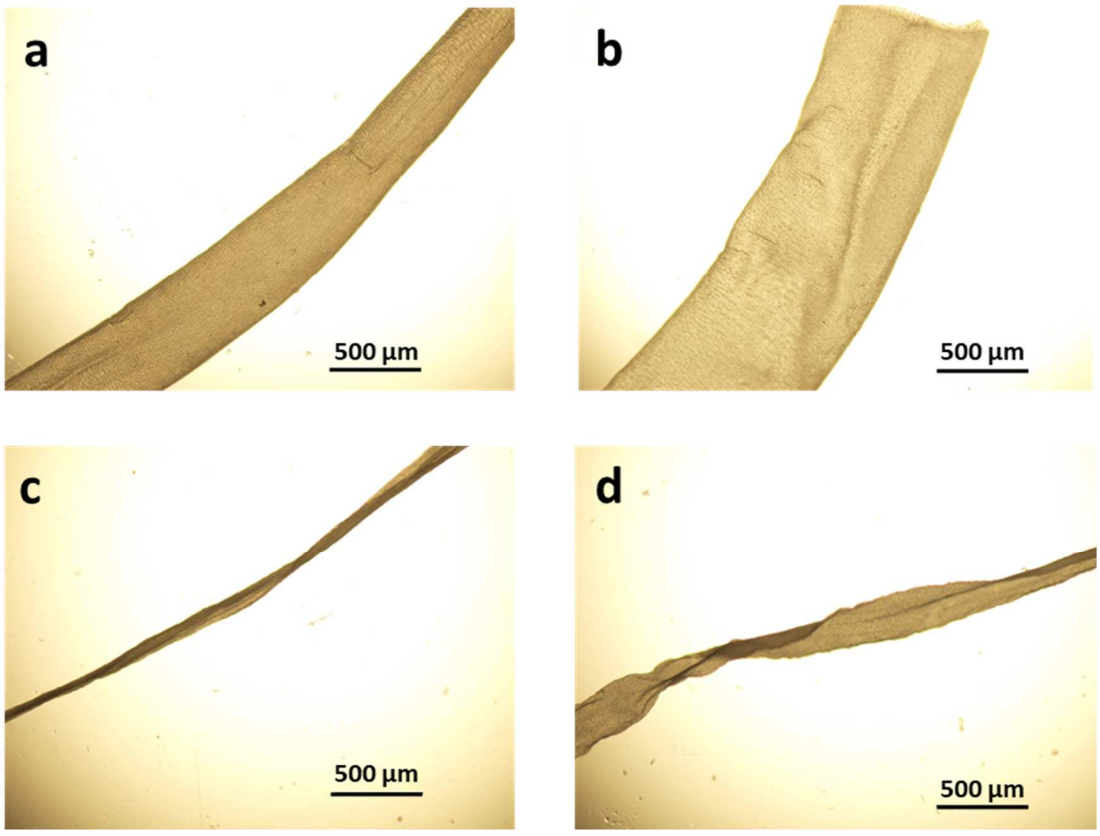

Figure 1. Fibers obtained either through manual injection of the viscose (a, b) or from continuous injection with help of the syringe pump (c, d). For the fiber spinning different injection needles with a diameter of 450 µm (a, c) and 800 µm (b, d) have been used.

ATR-IR spectra:

IR spectroscopy is a widely available and commonly used method to study the reactions of cellulose and its derivatives. The used starting material, highly purified cotton fibers, exhibit an

IR spectrum, characteristic for cellulose I with broad bands from 3600 to 3100 cm^{-1}(ν_{OH}) and from 3000 to 2850 cm^{-1} (C-H stretching vibrations), a series of small weak bands in the region of 1430 to 1150 cm^{-1} (C-O-H bending at 1430 cm^{-1}, C-H deformation at 1372 cm^{-1}, OH in plane deformation at 1330 and at 1200 cm^{-1}), strong and overlapping bands from 1160 to 950 cm^{-1} (asym. C-O-C vibration at 1155 cm^{-1}, sym. C-O vibration at 1060 cm^{-1} and C-O stretching at 1035 cm^{-1}) and a small band at 899 cm^{-1} (C-O-C valence vibration).[18] The alkali cellulose spectrum differs significantly from the cotton bands. The broad band at 3600 – 3000 cm^{-1} in the alkali cellulose spectrum is shifted from 3500 cm^{-1} to 3650 cm^{-1} and the form changed to a single band. The increased intensity at 1640 cm^{-1} indicates the presence of additional OH stretching and deformation vibrations caused by remaining water stored in the alkali cellulose.

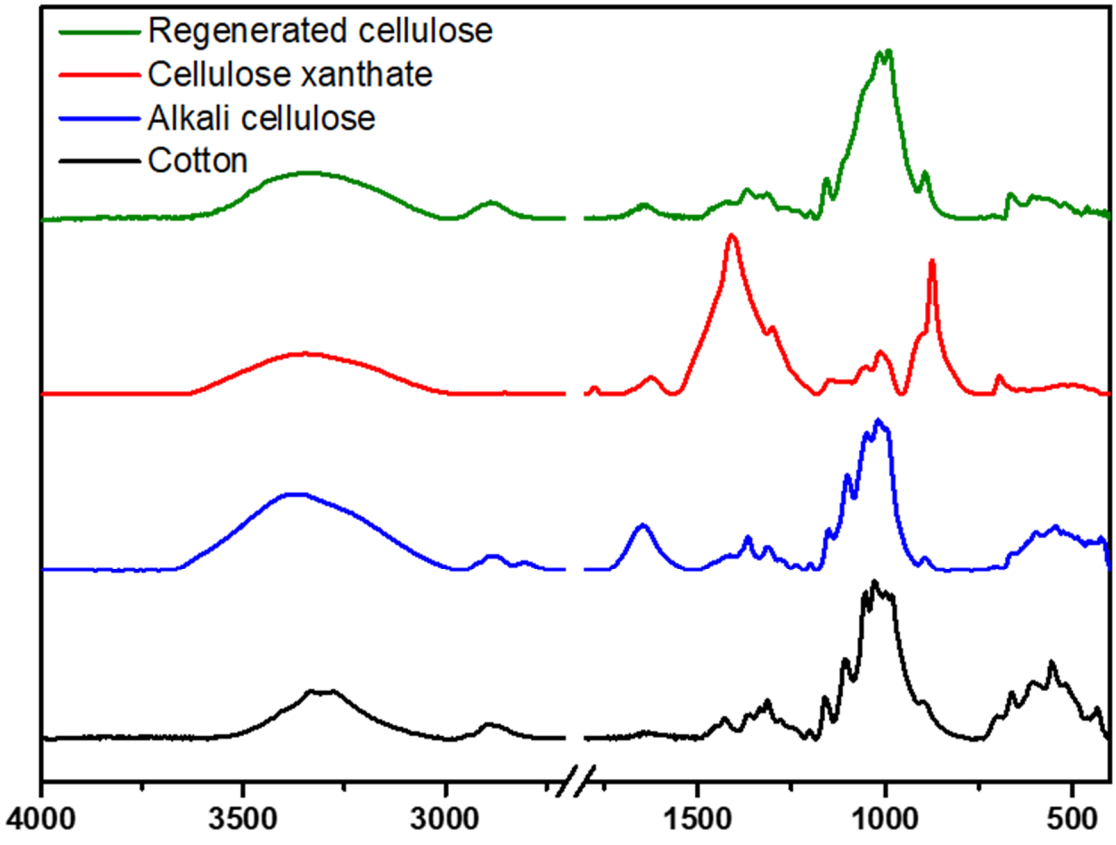

Figure 2. ATR-IR spectra of the different modifications and derivatives of Cellulose which appear during the steps of the viscose process. Starting with cotton (cellulose I), via alkali cellulose and cellulose xanthate to regenerated cellulose (cellulose II)

In the case of CX, the interpretation of the IR spectra is not that straightforward. Significant amounts of primary and secondary reaction products can be identified. These products can be identified as CS_2 ($\nu_{C=S}$ at 1520 cm^{-1}), sodium sulfide (1420, 920 cm^{-1}) and sodium trithiocarbonate (1670, 1427, 925 and 885 cm^{-1}).[6, 19] The remaining bands at 1452 and 1382 cm^{-1} as well as a weak band at 2725 cm^{-1} can be assigned to NaOH, which is present from the dissolution of CX. Since NaOH is highly hygroscopic, the water peak at 1640 cm^{-1} is pronounced as well. The C-S and C=S vibrations for the CX have been reported in the region around 900 cm^{-1} and between 1050-1250 cm^{-1} and interfere with these products as well as with vibrations at the pyranose ring, which also show absorption bands in this range.[20] Therefore, an unambiguous assignment is not possible. After regeneration and extensive washing of the spun fibers, again a cellulose spectrum is obtained which refers to as cellulose II.

CONCLUSIONS

The procedure for the synthesis of cellulose xanthate and the following spinning of regenerated cellulose fibers, described in this contribution is an easy to follow lab experiment, which does not require expensive materials or extraordinary characterization techniques. An additional benefit of this experiment is that it is not necessary to have extensive and specialized knowledge in the production of man-made fibers based on the Viscose process. The time necessary for the course is very flexible, depending on which steps are done with the students and which materials are prepared beforehand. A basic knowledge in organic chemistry and a laboratory equipped with the standard tools, safety precautions and a motivated teacher are required.

The students who participated in these lab courses at Graz University of Technology provided very good feedback. At the end of the course, they did not only see how to derivatize and dissolve cellulose but also how man-made cellulose fibers, a daily used product, were generated. Additional knowledge in organic chemistry, macromolecular science, renewable materials and analytical methods were taught during this lab exercise.

Supporting Information. The Supporting Information is available on the ACS Publications website at DOI: 10.1021/acs.jchemed. It contains laboratory handouts for the individual steps in the fiber spinning process (including theoretical background, schemes and photographs, Fig. S1-S5), instructor notes, examples for exam questions including key, ATR-IR spectra of cellulose I (starting material), alkali cellulose, cellulose xanthate and regenerated spun cellulose fibers (Fig: S6-S9) including assignment of the most important bands.

AUTHOR INFORMATION

Notes

The authors declare no competing financial interests.

Acknowledgements

Part of these activities received funding from the European Union's Horizon 2020 research and innovation programme under grant agreement No. 656760 (project BET-BioEnergyTrain).

Literature

(1) Hämmerle, F. M. The cellulose gap. *Lenz. Ber.* **2011,** *89*, 12-21.

(2) Smole, M. S.; Hribernik, S.; Kleinschek, K. S.; Kreže, T. Plant Fibres for Textile and Technical Applications. In *Advances in Agrophysical Research*, Grundas, S.; Stepniewski, A., Eds. InTech open: 2013; pp 369-398.

(3) Götze, K. *Chemiefasern nach dem Viskoseverfahren*. 3rd ed.; Springer Verlag: Heidelberg, Germany, 1967.

(4) Cross, C. F.; Bevan, E. J.; Beadle, C. Patent 8700. 8700, 1892.

(5) Woodings, C. 1 - A brief history of regenerated cellulosic fibres. In *Regenerated Cellulose Fibres*, Woodings, C., Ed. Woodhead Publishing: 2001; pp 1-21.

(6) Wilkes, A. G. 3 - The viscose process A2 - Woodings, Calvin. In *Regenerated Cellulose Fibres*, Woodhead Publishing: 2001; pp 37-61.

(7) Klare, H. 100 Jahre Celluloseregeneratfaserstoffe – Geschichte und Perspektiven. *Acta Polym.* **1985,** *36*, 347-352.

(8) He, L.; Hu, H.-C.; Chai, X.-S. A Real-Time Technique for Monitoring Cellulose Dissolution during the Xanthation Process. *Ind. Eng. Chem. Res.* **2016,** *55*, 10823-10828.

(9) Wöss, K.; Weber, H.; Grundnig, P.; Röder, T.; Weber, H. K. Rapid determination of γ-value and xanthate group distribution on viscose by liquid-state 1H NMR spectroscopy. *Carbohydr. Polym.* **2016,** *141*, 184-189.

(10) Liang, Y. X.; Qu, D. Z. Cost-benefit analysis of the recovery of carbon disulfide in the manufacturing of viscose rayon. *Scand. J. Work, Environment & Health* **1985**, 60-63.

(11) Renyou, Z.; Min, H.; Xiaojun, L.; Xueliang, W.; Yunqiao, J. CS2 recovery system for viscose staple fiber production CN104258684, 2015.

(12) Shen, L.; Patel, M. Life cycle assessment of man-made cellulose fibres *Lenz. Ber.* **2010,** *88*, 1 - 59.

(13) Hoeven, D. v. d. *Fibres of the future cotton and its limits*; Bio based press: www.biobasedpress.eu, 2016.

(14) Klemm, D., Philipp, B. , Heinze, T. , Heinze, U. and Wagenknecht, W. Appendix to Volume 2: Experimental Procedures for the Functionalization of Cellulose. In *Comprehensive Cellulose Chemistry Functionalization of Cellulose.*

(15) Mozdyniewicz, D. J.; Nieminen, K.; Sixta, H. Alkaline steeping of dissolving pulp. Part I: cellulose degradation kinetics. *Cellulose* **2013,** *20*, 1437-1451.

(16) Weißl, M.; Niegelhell, K.; Reishofer, D.; Zankel, A.; Innerlohinger, J.; Spirk, S. Homogeneous cellulose thin films by regeneration of cellulose xanthate: properties and characterization. *Cellulose* **2018,** *25*, 711-721.

(17) Klemm, D., Philipp, B. , Heinze, T. , Heinze, U. and Wagenknecht, W. In *Comprehensive Cellulose Chemistry Fundamentals and Analytical Methods.*

(18) Široký, J.; Blackburn, R. S.; Bechtold, T.; Taylor, J.; White, P. Attenuated total reflectance Fourier-transform Infrared spectroscopy analysis of crystallinity changes in lyocell following continuous treatment with sodium hydroxide. *Cellulose* **2010,** *17*, 103-115.

(19) Fink, H.; Stahn, R.; Matthes, A. Reifebestimmung und Ultrafiltration von Viscose. *Angew. Chem.* **1934,** *47*, 602-607.

(20) Ogura, K.; Sobue, H. Studies on the derivatives of sodium cellulose xanthate. Part I. Infrared absorption spectra and characteristic frequencies of C=S and C-S groups in sodium cellulose xanthate and its stable derivatives. *J. Polym Sci. Part B: Polym. Lett.* **1968,** *6*, 63-67.

Supporting Information

Spinning of Fibers from Wood – A Lab Experiment to Introduce Students in Viscose Fiber Manufacturing and Analysis

Michael Weißl[†], Gregor Kraft[‡], Josef Innerlohinger[‡] and Stefan Spirk[†]

[†]Graz University of Technology, Institute of Paper, Pulp and Fiber Technology, Inffeldgasse 23A 8010 Graz

[‡]Lenzing AG, Werkstrasse 2, 4860 Lenzing, Austria.

Correspondence:

Stefan Spirk

stefan.spirk@tugraz.at

+43 (316) 873 – 30763

Preamble and pedagogical discussion of the single sections

We performed the fiber spinning experiments in different master courses in our chemistry, biorefinery engineering and advanced materials science curricula. The group size was 2 to 4 students, depending on the course type and its aims. Cellulose xanthate was only prepared in the advanced courses and that course lasted for a period of one week with 5 hours daily lab work, including preparation of alkali cellulose, xanthation and fiber spinning. In the basic courses of fiber spinning, students did not synthesize the cellulose xanthate but used ready-made samples for fiber spinning. Here, the duration of the course was two days with 5 hours of daily lab work including characterization. In the light version of the lab course (2-3 hours), just fiber spinning is demonstrated and the characterization part is reduced to analyzing the IR spectra and judging microscopy images which both had been acquired beforehand.

Before start of the lab work, an examination was performed in order to see whether students understood the tasks of the lab work and whether the students were aware of the safety precautions required for the different experiments. We started this lab exercises in 2015 and in the meanwhile, ca 150 students did these experiments in the various courses. Feedback from the students has been very positive.

Laboratory Hand Out - Part 1: Alkali cellulose synthesis

Aims of the task

Understand processes during conversion of cellulose to alkali cellulose and to connect these to fiber spinning requirements

Theoretical background[1]

The formation of alkali cellulose is the first step in the manufacturing of viscose fibers. The main reactant is sodium hydroxide to give the sodium salt of cellulose. In industry, standard dissolving pulp is mixed with 18-20 wt.% NaOH to form a ca. 5 wt.% suspension. This suspension is exposed to a temperature between 25 and 55 °C for some hours. At this stage, the low molecular weight fraction of cellulose as well as the hemicelluloses dissolve and are removed by pressing the alkali cellulose. The removal of hemicellulose is essential for the resulting fiber quality since hemicellulose xanthate (which would be produced in the next step if they were not removed) are much more unstable than cellulose xanthate. This subsequently leads to formation of gels, thereby deteriorating the filterability of the obtained solutions. Further, hemicellulose incorporation into the cellulose fiber matrix during spinning leads to fiber with lower tenacity. After pressing, the alkali cellulose typically contains less than 3.5 wt.%. hemicelluloses, for speciality products even contents of below 1.6 wt.% are required. The pressing step also removes excess NaOH, which reacts with the CS_2 in the xanthation step. After pressing, the alkali cellulose contains 7-8 wt.% bound and ca 9 % adsorbed NaOH. Then the alkali cellulose is subjected to pre-ripening, i.e. storage at 30-55°C for a period between 10 and 30 hours under defined humidity control. During the pre-ripening a wealth of reactions take place, hydrogen bonds of the crystalline parts of the pulp are broken up and depolymerization

of the cellulose macromolecules occurs. The most important reactions are depicted in Scheme S1.

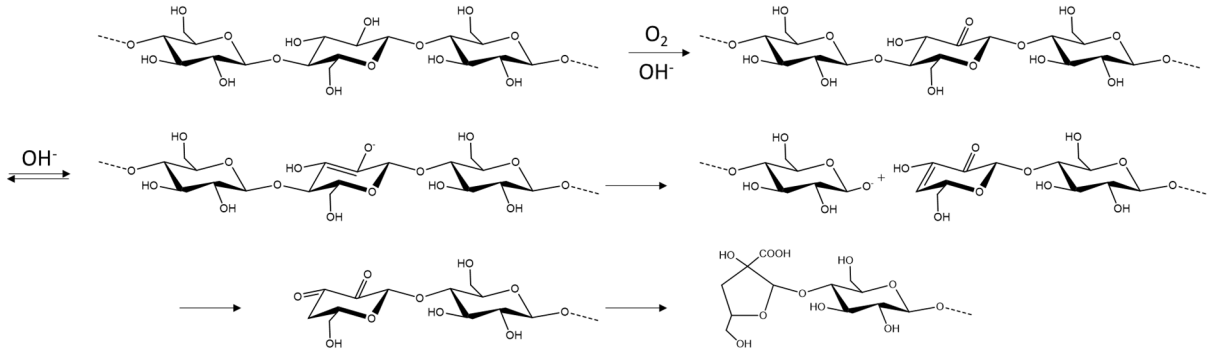

Scheme S1. Reactions during the processing of pulp to alkali cellulose

For fiber spinning, it is required to have a rather homogenous degree of polymerization (DP) for the material of interest. The average DP decrease from the range 850-600 to 500-350.

Materials needed:

Cellulose source (cotton, pulp)	7 g	No hazards
Sodium hydroxide	27 g	Harmful (strong base)
DI water	123 ml	No hazards
Laboratory stirrer	1	
1000 ml flask	1	

Protective gear (glasses, gloves, lab coat) for everybody

Before start:

Make sure that everything you need is organized and available.

Be sure, that the lab stirrer and the flask are safely installed.

Inform yourself how to deal with strong bases and what to do in case of an accident.

To consider for the laboratory report:

Save a gram of your cellulose source for the IR spectroscopy

Note the changes in the cellulose appearance during the reaction

Describe the differences in optical appearance between cellulose, wet alkali cellulose (after pressing) and dried alkali cellulose

Task:

Take 7 g of the cellulose (pulp is preferable, cotton is also possible), cut it into small pieces, and transfer it into the 500 ml flask. Dissolve 27 g sodium hydroxide in 123 ml DI water to

prepare an 18 wt.% NaOH solution. After the NaOH has been completely dissolved, add the solution to your flask. Mount the lab stirrer and the flask, before you start adding the pulp into the NaOH solution. After two hours of stirring, transfer the alkali cellulose on a kitchen paper and remove the excess sodium hydroxide solution by pressing the alkali cellulose with your hands. The pressed alkali cellulose is pulled apart into small pieces and dried overnight. Figure S1 depicts the process of the alkali cellulose synthesis as described above.

Figure S1. Illustration of alkali cellulose preparation. a: starting material-a cellulose source, b: stirring of the cotton fibers in 18% NaOH solution, c: alkali cellulose before pressing, d: alkali cellulose after pressing.

Laboratory Hand Out - Part 2: Xanthation

Aims of the task

Connect the processes happening during xanthation of alkali cellulose to fiber spinning parameters.

Understand importance of spinning dope preparation

Theoretical background[2-7]

The next step in viscose synthesis is xanthation. In this step, the alkali cellulose is converted to the sodium cellulose xanthate. In industry, this exothermic reaction is done in huge cylinders where the CS_2 is reacted in vaporous state (either injected as gas or vaporized in vessel; reaction time ca 100 minutes, temperature needs to be kept between 25-30°C by cooling). The degree of xanthation is expressed in industrial terms as the so called gamma number. The gamma number is related to the degree of substitution (DS) via equation (1):

$$\gamma = 100 * DS(X) \quad (1)$$

In industry, cellulose xanthate with a gamma value of around 50 is usually manufactured for fiber spinning, which means that in average just 1 out of two AGU is substituted with xanthates. Higher gamma numbers can be realized if subsequent additions of CS_2 are performed, in lab scale even full substitution (gamma 300) can be realized.

In fact, a wealth of reactions proceed at this step, which can be classified into primary, secondary and side reactions. Therefore 30 up to 50 wt.% of CS_2 related to cellulose are needed

in industrial scale to accomplish the reaction to the desired product. Primary reactions refer to those reactions where the desired cellulose xanthate is formed (eq 2-5).

$$CS_2 + \text{Cell-O}^-Na^+ \rightarrow \text{Cell-OCS}_2^-Na^+ \quad (2)$$

$$CS_2 + Na^+OH^- \rightarrow \text{HS-CSO}^-Na^+ \quad (3)$$

$$HCS_2O^-Na^+ + \text{Cell-OH} \rightarrow \text{Cell-OCS}_2^-Na^+ + H_2O \quad (4)$$

$$HCS_2O^-Na^+ + Na^+OH^- \rightarrow CS_2O^{2-} + 2\ Na^+ \quad (5)$$

The secondary reactions are those that occur with the formed products from the primary reactions such as the thiol and the dithiocarbonate. The latter for instance reacts with CS_2 to

form COS, which in turn reacts with NaOH to the carbonate under release of thiols, which then are further converted to the trithiocarbonate (eq 6-10).

$$CS_2 + CS_2O^{2-} \rightarrow COS + CS_3^{2-} \quad (6)$$

$$COS + 3\ OH^- \rightarrow CO_3^{2-} + SH^- + H_2O \quad (7)$$

$$CS_2 + SH^- \rightarrow CS_3H^- \quad (8)$$

$$CS_3H^- + OH^- \rightarrow CS_3^{2-} + H_2O \quad (9)$$

$$CS_2O^{2-} + 2\ OH^- \rightarrow 2\ SH^- + CO_3^{2} \quad (10)^-$$

In addition, the reaction of NaOH and CS_2 (side reactions) leads to a variety of different sulfur containing compounds such as sodium carbonate, sodium thiolate, sodium trithiocarbonate, hydrogen sulfide, and sodium sulfide. (eq 11-14)

$$CS_2 + 4\ NaOH \rightarrow Na_2CO_3 + 2\ NaHS + H_2O \quad (11)$$

$$2\ CS_2 + 4\ NaOH \rightarrow Na_2CO_3 + Na_2CS_3 + H_2S + H_2O \quad (12)$$

$$3\ CS_2 + 6\ NaOH \rightarrow 2\ Na_2CS_3 + Na_2CO_3 + 3\ H_2O \quad (13)$$

$$5\ CS_2 + 12\ NaOH \rightarrow Na_2S + 2\ Na2CO3 + 3\ Na_2CS_3 + 6\ H_2O \quad (14)$$

From these reactions, it is also obvious why the pressing step after alkali cellulose preparation is so important. Every mol of NaOH can consume CS_2 which is an economically important factor. After the xanthation has been finished, the cellulose xanthate is diluted with NaOH, a usual ratio is 1:4 (1 part alkali cellulose, 4 parts NaOH) to form the so called viscose. Then the viscose (before xanthate) is transferred to a tank, where the ripening takes place for a period of 18-30 hours at a temperature smaller than 18°C. The conditions for the ripening are crucial: cellulose xanthate decomposes at higher temperatures but also at the lower temperatures transxanthation reactions occur, which are, however, beneficial for fiber spinning. In order to obtain mechanically strong fibers, the macromolecules must be of similar size and in addition, they must be able to align with each other under flow conditions. This can be realized much

easier when the xanthate substitution pattern along the cellulose chain is homogeneous. Here, it is important to know that the thermodynamically most stable position for the xanthate is the C6 position; therefore any rearrangements, i.e. transxanthation reactions (either inter- or intramolecular) lead to preferred substitution at C6. In addition, also a partial cleavage of the xanthate groups occurs whereas hydrolysis is ca. times faster at position C2 and C3 compared to C6, thereby also contributing to a final cellulose xanthate spinning dope where the xanthate groups are preferentially located at C6. An overview is presented in Scheme S5.

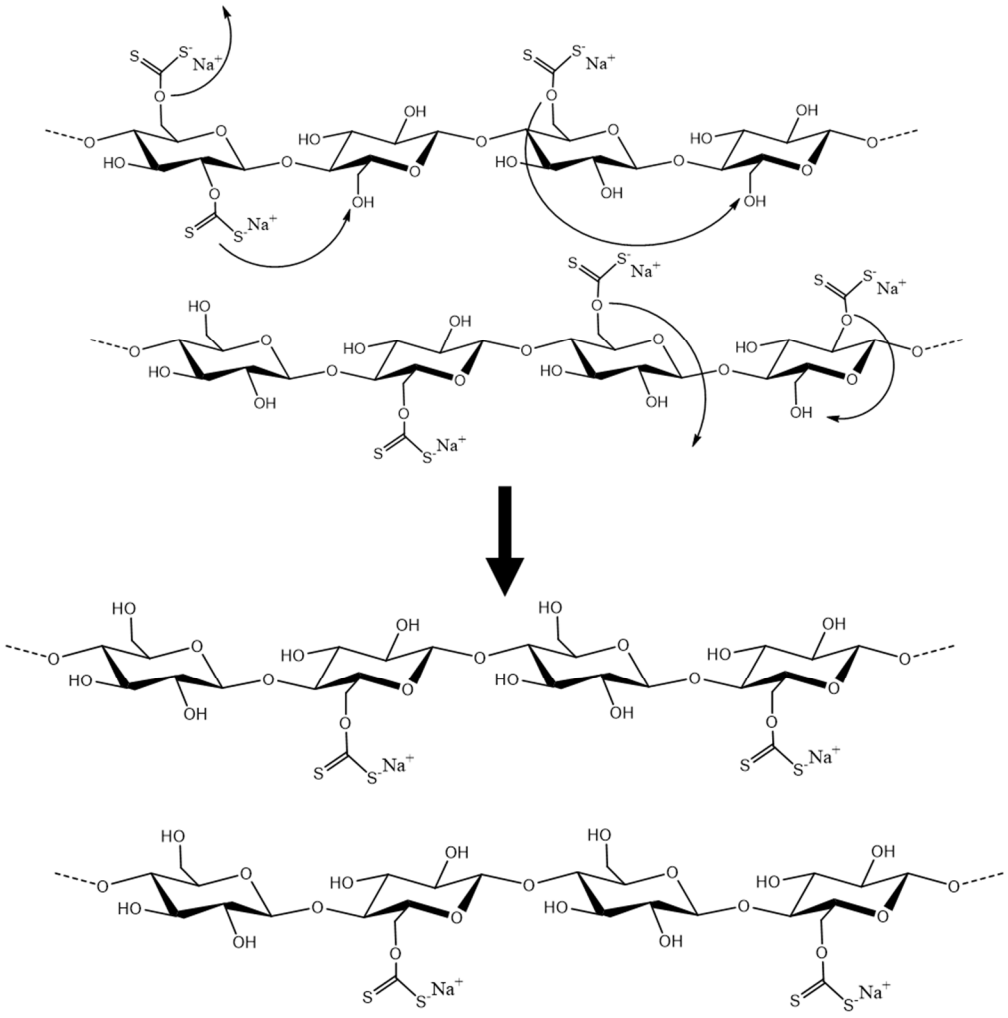

Scheme S2. Overview of cleavage and transxanthation reactions

Materials needed:

Alkali cellulose	4.5 g (dry mass cellulose)	Low hazards
Sodium hydroxide	4 g	Harmful (strong base)
DI water	100 ml	No hazards
Carbon disulfide	7.1 ml (9 g)	Harmful (toxic)
Water bath	1	
250 ml 3 neck flask	1	
Dropping funnel or septum	1	
Laboratory stirrer	1	
Reflux cooler	1	
Heating plate	1	

Protective gear (glasses, gloves, lab coat) for everybody

Before start:

Make sure that everything you need is organized and available.

Ensure yourself that your apparatus is mounted the right way.

Inform yourself about the correct handling and the dangers of CS_2 by reading the SDS accurately.

To consider for the laboratory report:

Save a bit of the remaining alkali cellulose for the IR spectroscopy

Observe and explain the ongoing reactions during xanthation.

Task:

Determine the weight of the overnight dried alkali cellulose to calculate the dry mass cellulose content of your alkali cellulose (15):

$$\frac{weight\ of\ cellulose}{weight\ of\ alkalicellulose}\ x\ 100 = cellulose\ content\ [\%] \qquad (15)$$

Transfer the amount of alkali cellulose, which equals 4.5 g pure cellulose into a 250 ml three-necked flask, add the stirrer and fix everything. Deposit a water bath below the flask and pre heat the alkali cellulose to 30 °C. Install a reflux condenser on one bottom of the flask and a dropping funnel on another one. (Figure S2a) After pre-heating the alkali cellulose, transfer CS_2 (2 g per gram of cellulose) into the drooping funnel using a syringe and start adding the CS_2 dropwise to the alkali cellulose under constant stirring. It should be mentioned here that for the lab scale synthesis a larger excess than in industrial production was used to accomplish for faster reaction. After addition is completed, continue stirring for three more hours. The starting material is finally converted into an orange sticky pulp (Figure S2b). This material is then dissolved in 100 ml of a 4% NaOH solution as shown in Figure S2c (25 ml per gram cellulose). After one more hour of continuous stirring and cooling in an ice bath, the cellulose xanthate is completely dissolved and the resulting product is ready, the so-called viscose solution. (Figure S2 d). The viscose solution is stored overnight at room temperature, to allow for ripening and therefore make it useable for the fiber spinning.

Figure S2. Overview on the xanthation of alkali cellulose. a: Preparation of the xanthation apparatus with the alkali cellulose deposited in the flask, b: Start of xanthation by adding CS_2 dropwise, c: Cellulose xanthate after 3 hours of stirring, d: Final viscose solution

Laboratory Hand Out - Part 3: Fiber spinning

Aims

Judging the influence of experimental parameters in viscose fiber spinning and connecting them to fiber quality and additive dosage.

Theoretical background[8]

Prior to fiber spinning, air bubbles and other solids in the cellulose xanthate solution must be removed since they would lead to a rupture of the fiber during spinning. Therefore, degassing and filtration of the xanthate solution is performed. Afterwards, the solution is pumped through a spinneret which is made of chemically inert alloys. The spinneret can consist of up to several thousands of nozzles with hole diameters between 40 to 200 microns. After passing the nozzle, the xanthate solution is injected into a temperature controlled regeneration bath. The regeneration bath contains sulfuric acid (usually 5-15 wt.%), and additives such as $ZnSO_4$ and Na_2SO_4. Two processes, namely conversion to cellulose and coagulation, take place. Coagulation leads to a core-shell structure, which means that the outer parts of the injected xanthate solution solidifies, while the inner part is still in a liquid state. In addition, osmosis comes into play by to the removal of water due to presence of sodium sulfate. Subsequently, conversion to cellulose is induced by the sulfuric acid. The faster the regeneration, the thinner the shell and the worse the fiber quality is. Therefore, zinc sulfate is added in industry which forms a more stable xanthate, thereby slowing down regeneration speed (Scheme S6). As a consequence a thicker shell is formed during coagulation, the fiber can be stretched to a larger extent, and the mechanical properties improve. The fibers are collected on rollers, and washed several times with hot water. Afterwards they are subjected to post treatment, which usually

involves surface modification using fatty alcohols to facilitate further processing. After drying the final fibers are obtained.

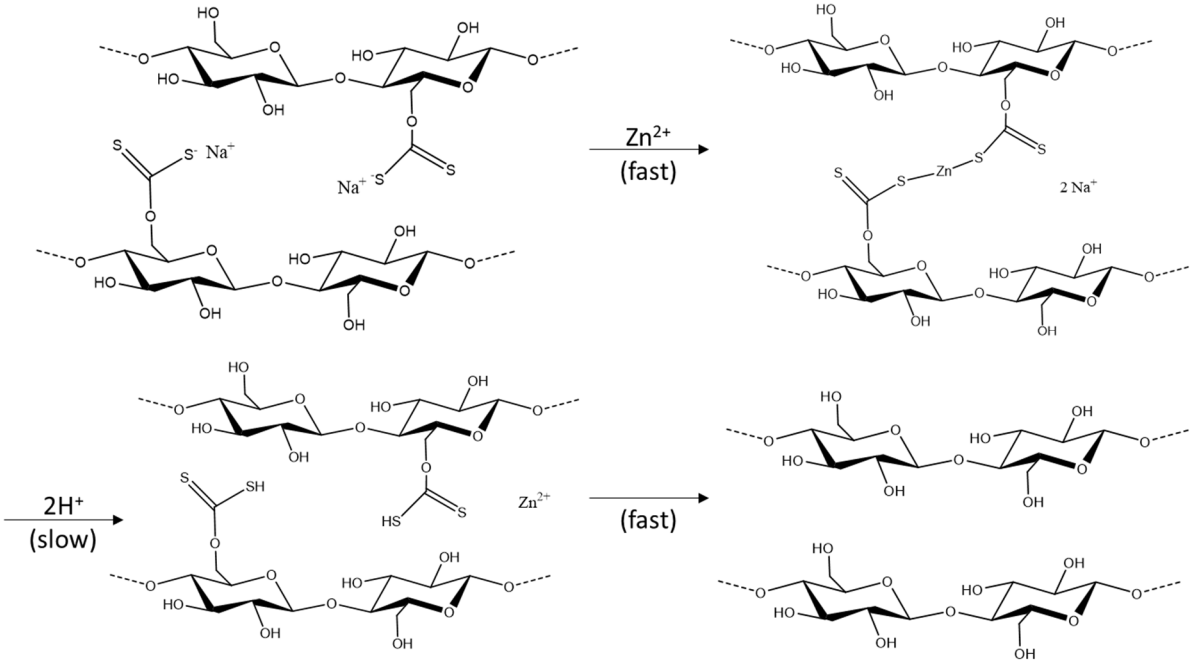

Scheme S3. Formation of zinc sulfate and subsequent regeneration to cellulose.

Materials needed:

Level 1:

Sulfuric acid	15 ml	Harmful (strong acid)
Crystallizing dish 115mm	2	
Magnetic stirrer	2	
Syringe	1	
Injection needles	2 / ∅	45µm / 70 µm
DI water	135 ml	

Protective gear (glasses, gloves, lab coat) for everybody

Level 2 (additional):

Syringe pump	1
Lab stirrer	1
Roller to collect the fiber	1
Sulfuric acid resistant plastic tube	1
Sulfuric acid	200 ml
DI water	1800 ml

Before start:

Make sure that everything you need is organized and available.

Inform yourself about the correct handling and the dangers of sulfuric acid solutions.

To consider for the laboratory report:

Determine the cellulose content in your viscose dope

Observe the ongoing reactions while the viscose solution is injected in the sulfuric acid solution

Describe the difference in the spun fibers before and after the washing step.

Tasks:

Determination of the cellulose content in the dope

The weight of a petri dish is determined before transferring a few ml (3-5) of viscose solution into the dish. The dish is slowly shaken, until the xanthate forms a thin film over the whole dish. The dish is placed in a drying oven at 60°C until the whole water is removed and a dry

solid xanthate film is obtained. This film is placed into sulfuric acid solution (10%) either with the dish or by peeling it off the dish.

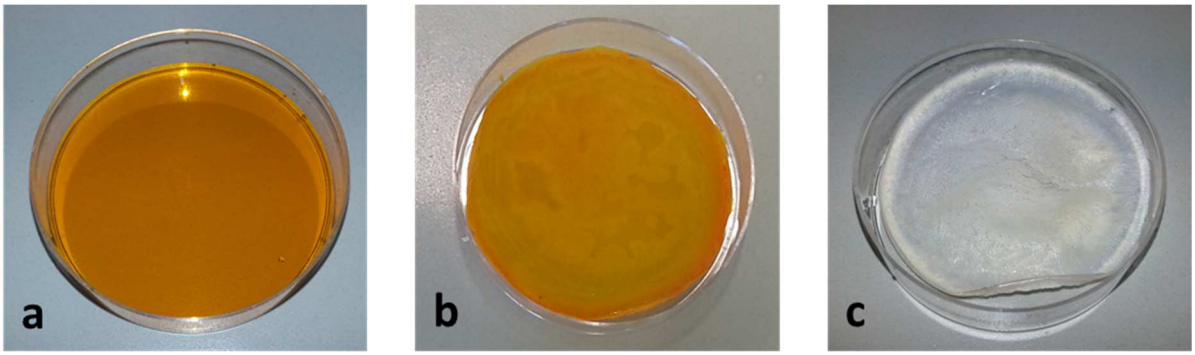

Figure S3 Involved steps in the determination of the cellulose content in the spinning dope. a: viscose solution transferred into a petri dish, b: the cellulose xanthate film after drying, c: the remaining cellulose film after regeneration in H_2SO_4 and washing of the film

The regenerated cellulose film is extensively washed with water and dried again at 60°C until its dry mass remains constant. The cellulose content is determined as followed (16):

$$Cellulose\ content\ [\%] = \frac{Dry\ mass\ (cellulose\ film)}{Dry\ mass\ (cellulose\ xanthate\ film)} * 100 \qquad (16)$$

Fiber spinning (Level 1)

150 ml 10 wt% sulfuric acid solution are deposited in a petri dish (diameter 115 mm, glass) and the solution is heated to 50°C to accelerate the regeneration of the cellulose xanthate. The spinning dope is transferred into a syringe and the syringe is equipped with an injection needle (45 / 70 µm in diameter). The needle is placed in the sulfuric acid bath and the cellulose xanthate

is injected. Fibers can be either collected after simple injection or by employing a slowly rotating stirring bar.

Regeneration is complete, when the color of the fiber changes from yellowish to white. Then, the fibers are immersed into a water bath for 15 minutes at elevated temperatures (T = 85°C). After washing has been completed, the fibers are dried at room temperature.

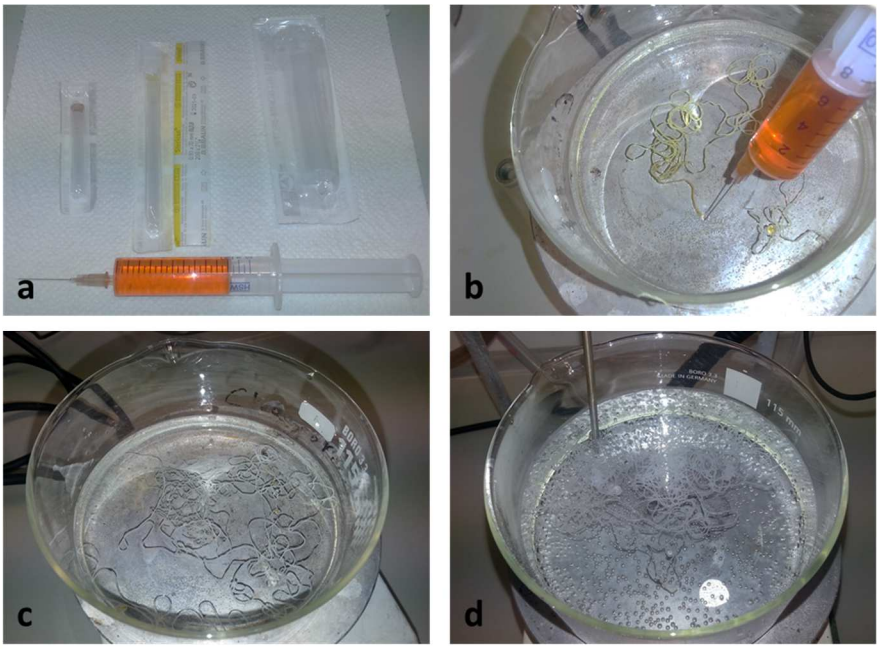

r

Figure S4. Different steps in the manual fiber spinning process. a: equipment, b: fiber spinning through manual injection, c: the fully regenerated fibers, d: fibers during washing in hot water.

Fiber spinning (Level 2)

2 liters 10 wt% sulfuric acid solution are placed in a sulfuric acid resistant plastic tube (30 x 35 cm), equipped with a membrane. The fiber collector is placed into the sulfuric acid solution, opposite to the membrane. A syringe (20 ml) is filled with the viscose spinning dope and inserted in the syringe pump. An injection needle is fixed onto the syringe and placed into the sulfuric acid bath through the membrane. The viscose is injected continuously into the sulfuric acid using the syringe pump and the developing cellulose monofilament is collected on the slowly rotating fiber roller. It is important, to adjust the injection speed in order to avoid breaking of the fiber. After injecting the spinning dope, the fibers are stirred in the sulfuric acid until the regeneration of the cellulose is completed. The fibers can then be cut from the fiber collector and immersed in hot water (T=85°C) for 15 minutes. Afterwards, the water is exchanged and the fibers are immersed again for 15 minutes at 85°C and finally dried at room temperature.

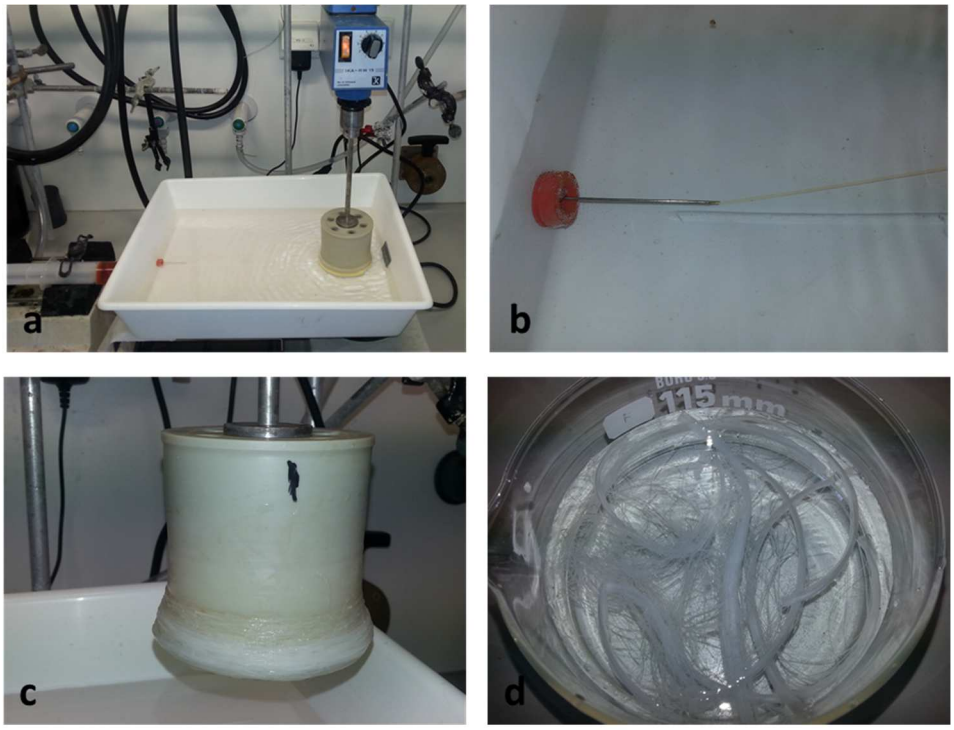

Figure S5. Different steps in the manual fiber spinning process. a: equipment, b: fiber spinning through continuous injection with a syringe pump, c: fully regenerated fibers on the fiber collector, d: fibers during washing in hot water

Laboratory Hand Out - Part 4: Characterization

Aims of the task

Correlate IR spectra of natural and man-made cellulose

Use IR spectroscopy to identify and assign intermediates in the viscose process

Evaluate fiber quality by optical microscopy and correlate it to the manufacturing process.

Theoretical background[4, 9, 10]

In nature, cellulose adopts a particular crystalline structure which is referred to as cellulose I. In this kinetically stabilized configuration, the reducing ends of cellulose are pointing at the same direction, which is called a parallel chain alignment. During the conversion to alkali cellulose the crystalline domains are partly destroyed and hydrogen bonds are broken up. After conversion to the xanthate and regeneration back to cellulose the thermodynamically stable form, so called cellulose II is obtained which is also partially crystalline. In this arrangement, the chains are aligned in an antiparallel manner i.e., the reducing ends of neighboring chains point at the opposite direction. As a consequence, the hydrogen bonding pattern is changing when going from cellulose I to alkali cellulose, cellulose xanthate and finally cellulose II. These differences in the arrangement of the chains can be tracked by simple analytical methods such as infrared spectroscopy. In IR spectroscopy, the vibrations of connected atoms can be detected via their absorption. A very prominent absorption band for cellulose is the OH stretching vibration, which appears in the range of 3200 to 3600 cm^{-1}. In this area, differences in the hydrogen bonding system between cellulose I and II can be visualized and assigned to different modes. The broad band at 3600 – 3000 cm^{-1} in the alkali cellulose spectrum is shifted from 3500 cm^{-1} to 3650 cm^{-1} and the form changed to a continuous band. The higher intensity at 1640 cm^{-1} indicates the presence of additional OH stretching and deformation vibrations caused by bound water in the alkali cellulose. In addition, other functional groups in the course of the

conversion can be tracked such as C-S and C=S vibrations in the xanthate and the various products described above. However, the IR analysis is not as straightforward as for the other sulfur containing products in the viscose process since there are many different compounds present in the solution.

The shape of fibers can influence their optical appearance such as shine but also their water uptake capability. Therefore, optical microscopy is an easy tool to observe differences in fiber appearance and to evaluate the influence of experimental variations. Parameters such as fiber diameter, transparency as well as homogeneity can be determined and compared on a qualitative way.

Materials needed:

Microscope slides

Tweezers

Optical microscope, equipped with a camera

IR spectrometer

Before start:

Inform yourself about the operating principle of the optical microscope and the IR spectrometer which are provided.

Task:

Investigate the form of the fibers spun with different needles and by different techniques (by hand, or semi-continuous with the syringe pump) and document the differences with the help of a microscope.

What is the difference in the optical appearance of the differently produced fibers and where do the difference originate from?

Calculate the diameter of the different fibers and explain why some are thicker/thinner than others.

Record IR spectra of the starting material (cotton), the stored alkali cellulose, a dried cellulose xanthate film and the regenerated fibers. Observe the difference in the spectra and try to assign the characteristic IR bands to the functional groups.

Explain the difference in the IR spectrum of the cellulose used as starting material and the cellulose obtained through the fiber spinning.

Examples for exam questions:

1) Name the main reactions in the Viscose process and complete the reaction scheme for the Viscose process

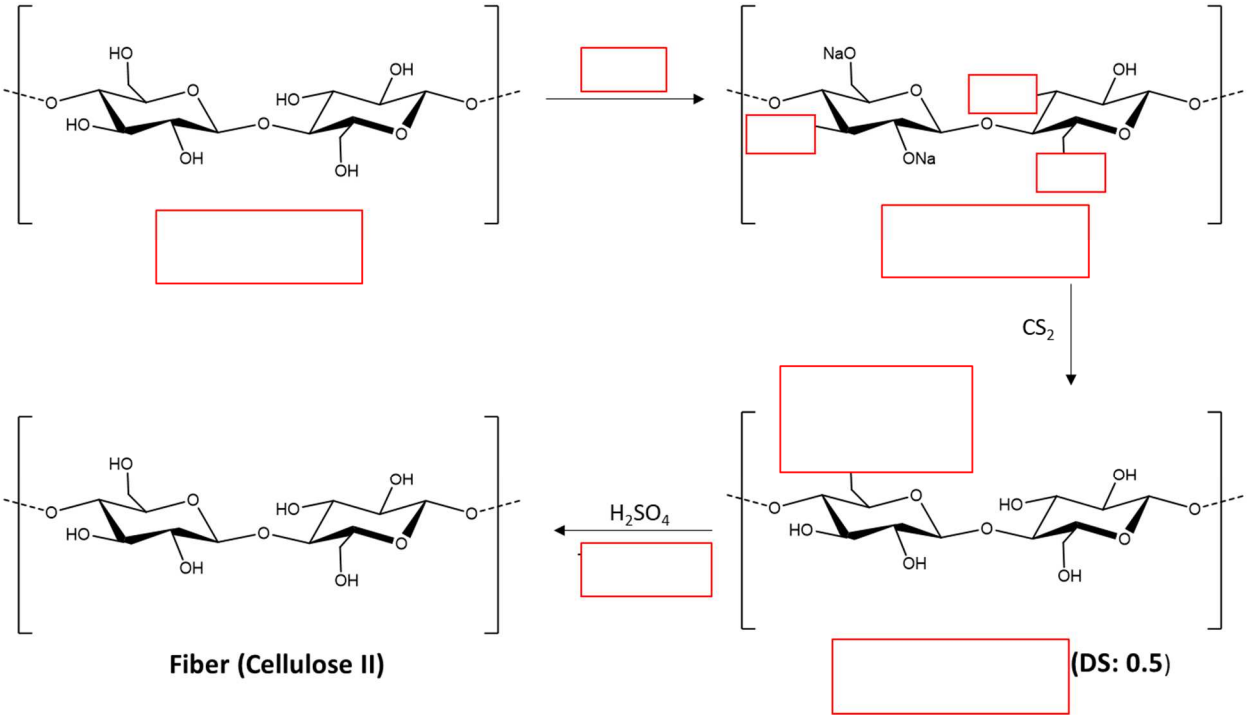

2) Explain shortly the preparation of alkali cellulose. Which reactions are going on during the synthesis and the ripening?

3) How does the alkali treatment affect the pulp fibers?

4) What is the gamma number?

5) What are primary and secondary reactions in the xanthation process, complete the reactions below and say if they are primary or secondary.

CS_2 + ____-O^-Na^+ → Cell-_____

$CS_2 + CS_2O^{2-} \rightarrow COS$ + _____

CS_2 + _____ → HS-CSO^-Na^+

6) Which chemical processes happen during the ripening of cellulose xanthate and how do they relate to its spinnability?

7) Highlight the typical concentration of sulfuric acid in the spinning bath

1-3% 5-15% 45-655

8) What are the two processes taking place in the regeneration bath? Explain in 4 sentences what is meant and how they affect the fiber quality

9) Describe in 2 sentences the role of Zn^{2+} cations in the fiber spinning

10) What is the difference between cellulose I and II? How can differences be detected?

Examples for exam questions – key:

1) Name the main reactions in the Viscose process and complete the reaction scheme for the Viscose process

Alkali cellulose synthesis, xanthation, regeneration, washing and post treatment of the fibers

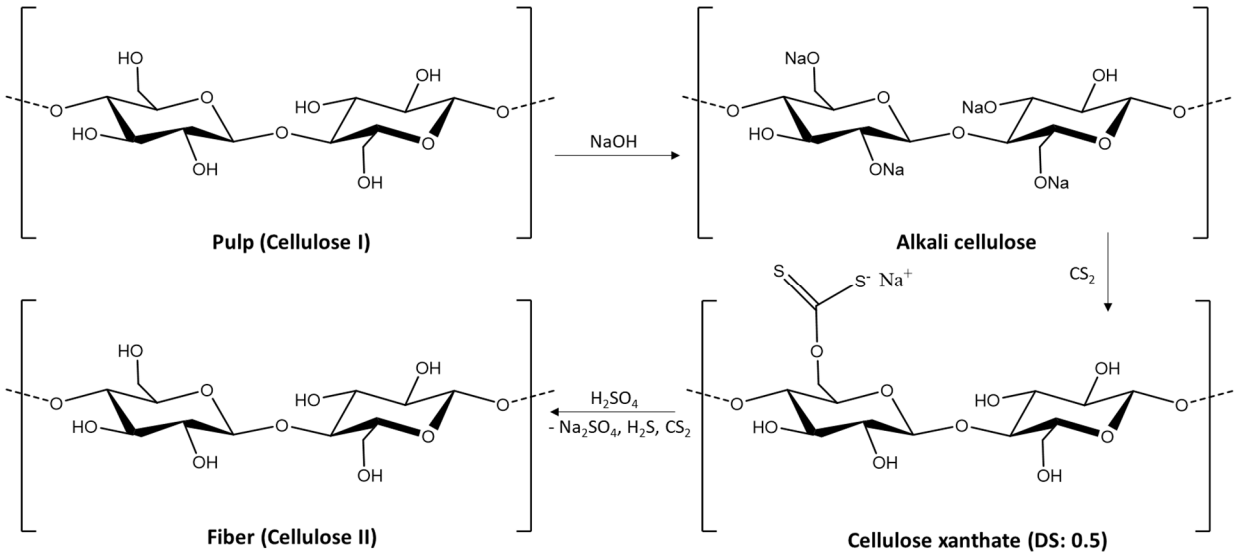

2) Explain shortly the preparation of alkali cellulose. Which reactions are going on during the synthesis and the ripening?

The main reactant that is used is sodium hydroxide, to formally form the sodium salt of cellulose, therefore pulp is mixed with 18-20 wt% NaOH to form a ca. 5 wt% suspension. During this reaction low molecular weight fractions of cellulose as well as the hemicelluloses are dissolved. During the ripening, a wealth of reactions take place, hydrogen bonds of the

crystalline parts of the pulp are broken up and depolymerization of the cellulose macromolecules occurs.

3) How does the alkali treatment effect the pulp fibers?

The degree of polymerization is narrowed and the average DP decrease from the range 850-600 to 500-350

4) What is the gamma number?

The degree of xanthation is expressed in industrial terms as the so called gamma number. The gamma number is related to the degree of substitution via equation (E1):

$$\gamma = 100 * DS(X)$$

5) What are primary and secondary reactions in the xanthation process, complete the reactions below and say if they are primary or secondary.

In fact, a wealth of reactions proceed at this step, which can be distinguished in primary, secondary and side reactions. Primary reactions refer to those reactions where the desired cellulose xanthate is formed. The secondary reactions are those that occur with the formed products from the primary reactions

$$CS_2 + \text{Cell-O}^-Na^+ \rightarrow \text{Cell-OCS}_2^-Na^+ \text{ primary}$$

$$CS_2 + CS_2O^{2-} \rightarrow COS + CS_3^{2-} \text{ secondary}$$

$$CS_2 + Na^+OH^- \rightarrow \text{HS-CSO}^-Na^+ \text{ primary}$$

6) Which chemical processes happen during the ripening of cellulose xanthate and how do they relate to its spinnability?

During ripening transxanthation reactions (either inter- or intramolecular) leads to preferred substitution at C6. In addition, also a partial cleavage of the xanthate groups occurs. Through this reactions, the xanthate substitution pattern along the cellulose chain gets homogenized

and the chains are able to align with each other in a flow, what gives the fundamental condition for strong fibers.

7) Highlight the typical concentration of sulfuric acid in the spinning bath

1-3% **5-15%** 45-65%

8) What are the two processes taking place in the regeneration bath? Explain in four sentences what is meant and how they affect the fiber quality

Conversion to cellulose and coagulation, take place. Coagulation leads to a core-shell structure, which means that the outer parts of the injected xanthate solution solidifies, while the inner part is still liquid. Conversion to cellulose is induced by the sulfuric acid. The faster the regeneration, the thinner the shell and the worse the fiber quality is.

9) Describe in 2 sentences the role of Zn^{2+} cations in the fiber spinning

Zinc sulfate is added to form a more stable xanthate, thereby slowing down regeneration speed. As a consequence a thicker shell can be formed during coagulation and the mechanical properties of the fibers increase.

10) What is the difference between cellulose I and II?

How can differences be detected?

Cellulose in nature adopts a particular crystalline structure which is referred to as cellulose I, which is kinetically stabilized. In this configuration, the reducing ends of cellulose are pointing at the same direction, which is called a parallel chain alignment. In the arrangement of cellulose II (the thermodynamically stable form), the chains are aligned in an antiparallel manner, i.e. the reducing ends of neighboring chains point at the opposite direction. These differences in the arrangement of the chains can be tracked by simple analytical methods such as infrared spectroscopy.

ATR-IR spectra with the most important bands being assigned:

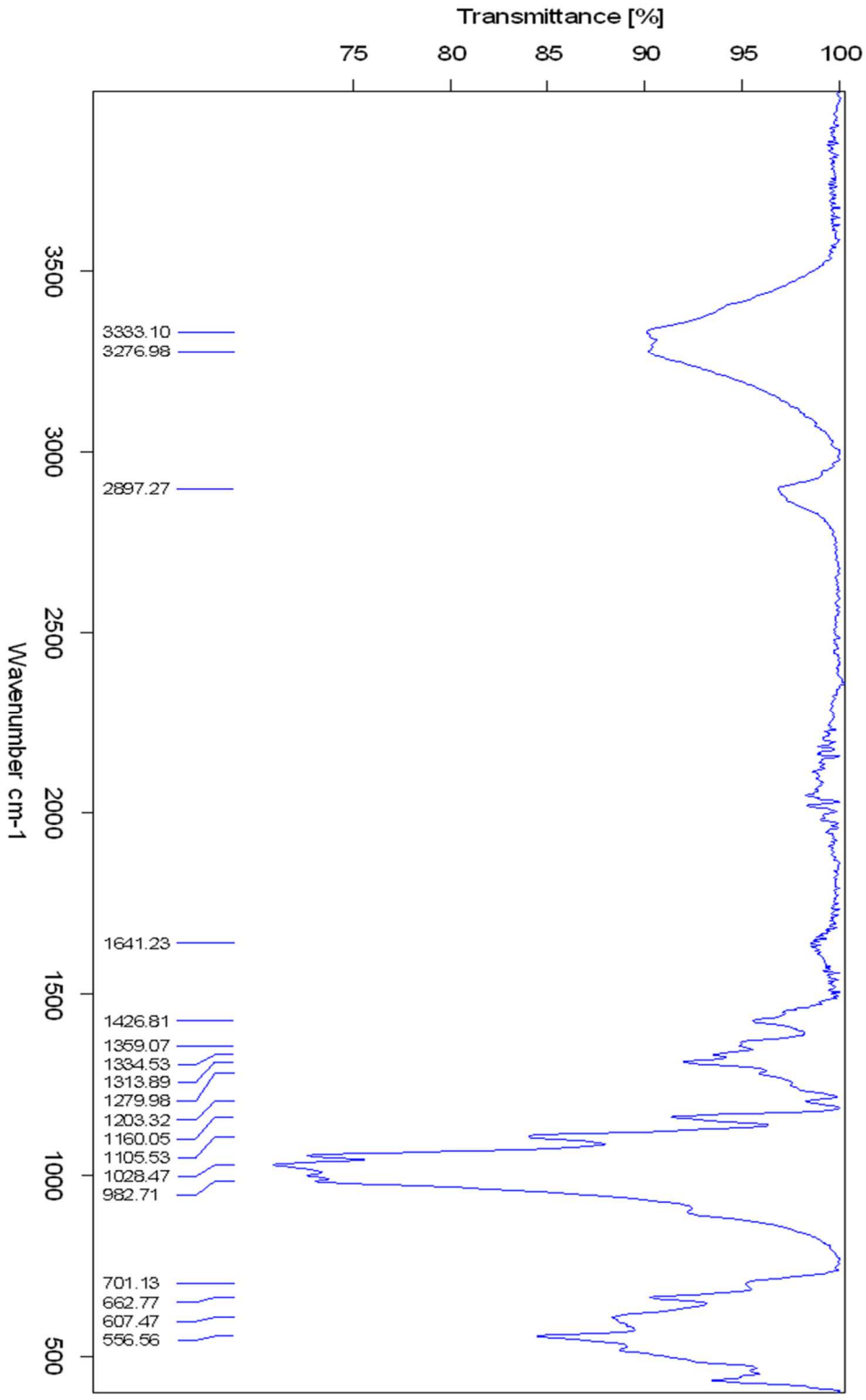

Figure S6. ATR-IR spectrum of the used cellulose source

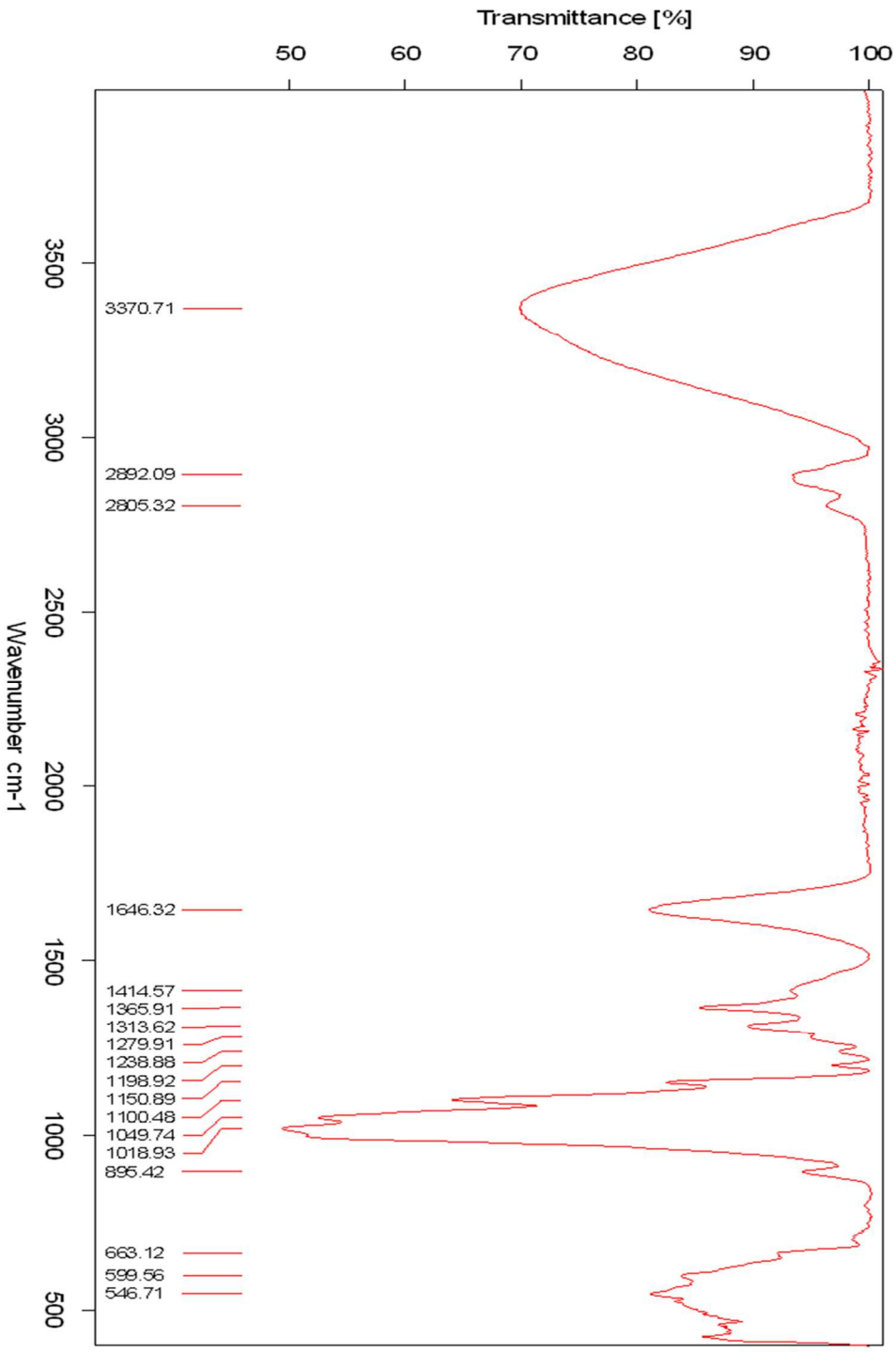

Figure S7. ATR-IR spectrum of the alkali cellulose

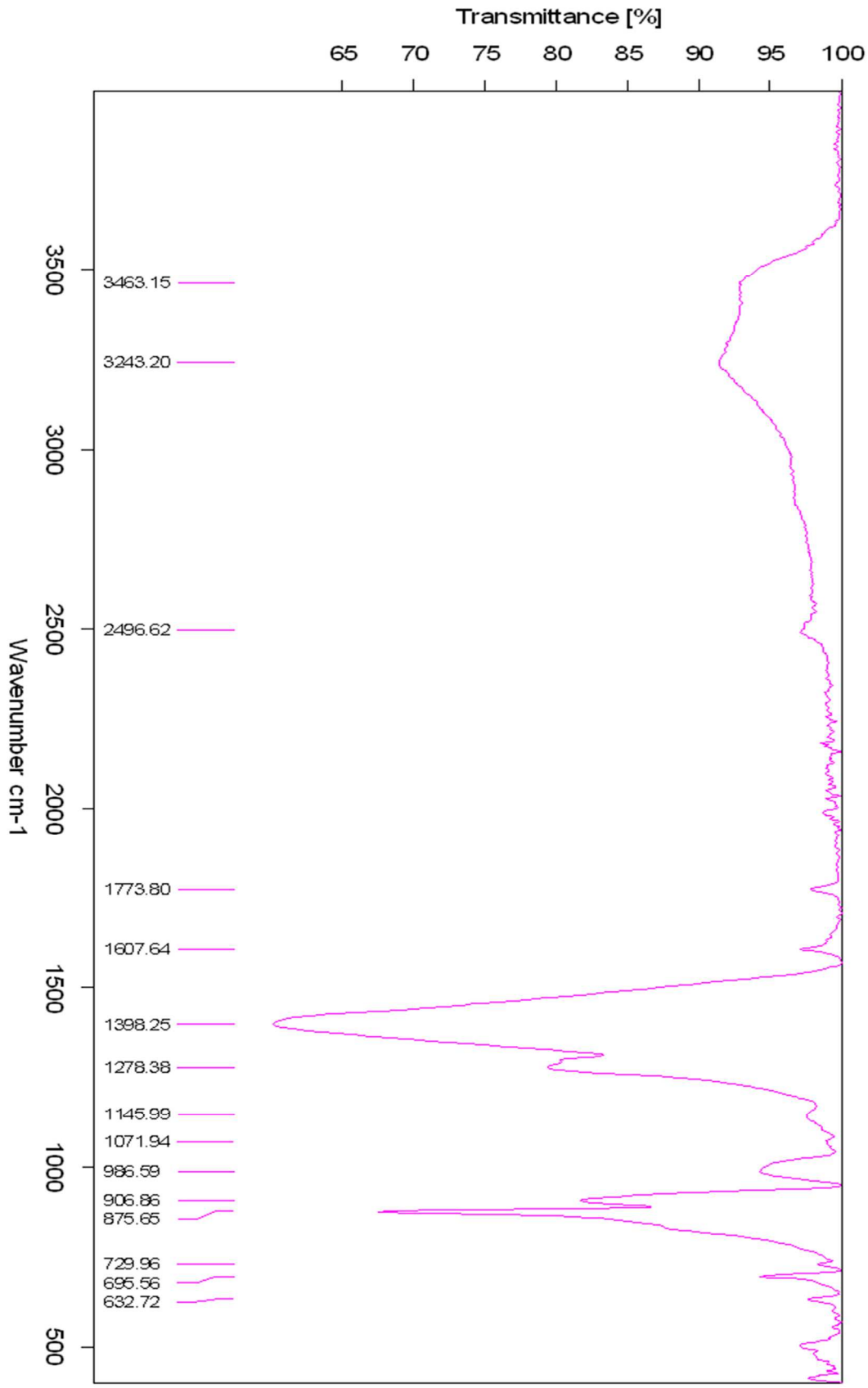

Figure S8. ATR-IR spectrum of the cellulose xanthate

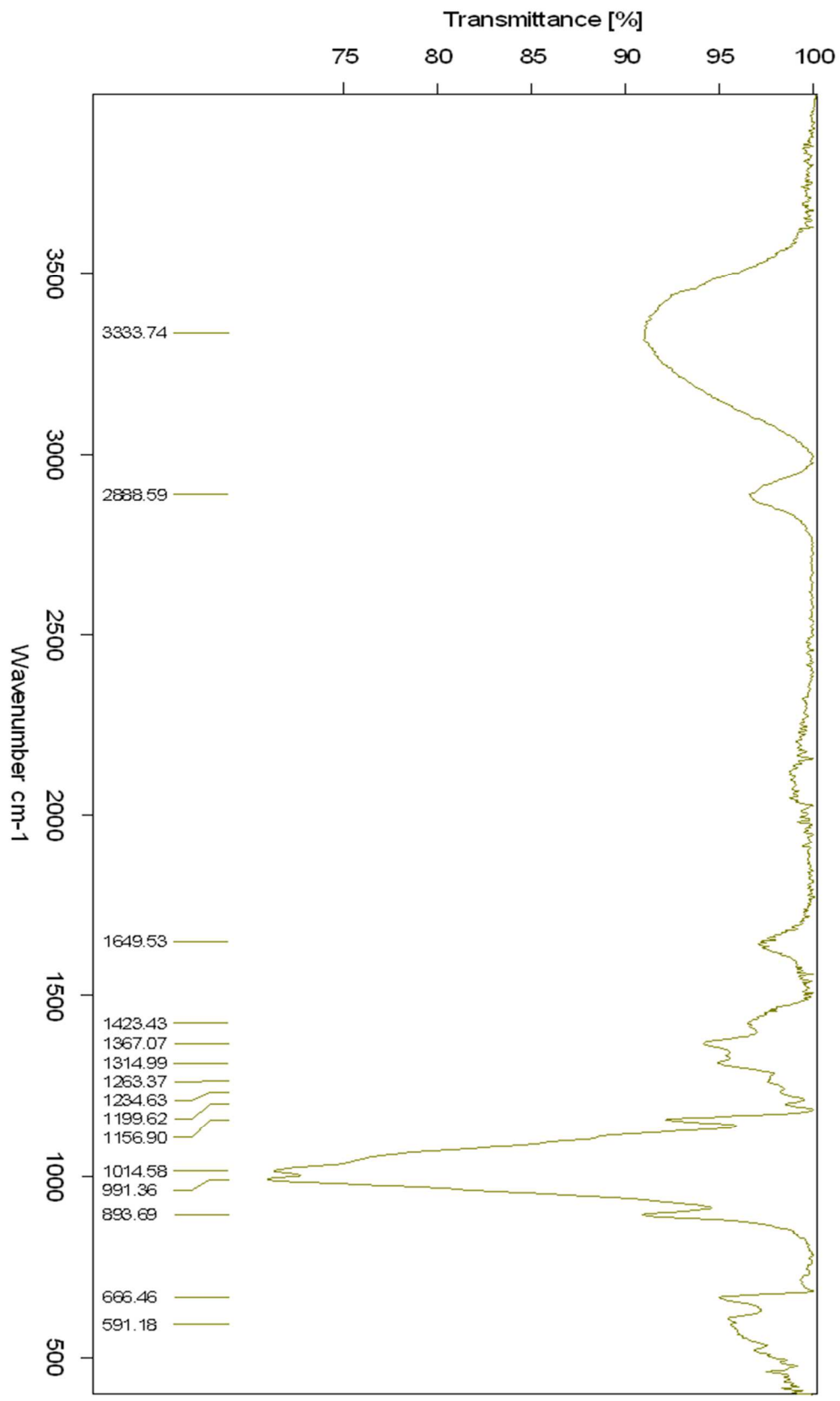

Figure S9. ATR-IR spectrum of the regenerated and washed cellulose fibers

References

(1) Sixta, H. *Handbook of Pulp*. Wiley: New York, 2008.

(2) Andrews, D. A.; Hurtubise, F. G.; Krassig, H. The Presence of Monothiocarbonate Substituents in Cellulose Xanthates. *Can. J. Chem.* **1960,** *38*, 1381-1394.

(3) Hovenkamp, S. G. Sodium dithiocarbonate as a by-product in xanthating reactions. A contribution to the chemistry of viscose. *J. Polym. Sci. C* **1963,** *2*, 341-355.

(4) Ogura, K.; Sobue, H. Studies on the derivatives of sodium cellulose xanthate. Part I. Infrared absorption spectra and characteristic frequencies of C-S and C=S groups in sodium cellulose xanthate and its stable derivatives. *J. Polym. Sci, Part B: Polym. Lett.* **1968,** *6*, 63-67.

(5) Dautzenberg, H.; Philipp, B. Über Bildungsweise und Verhalten des Natriumdithiocarbonats. *Z. Anorg. Allg. Chem.* **1970,** *375*, 113-123.

(6) Wöss, K.; Weber, H.; Grundnig, P.; Röder, T.; Weber, H. K. Rapid determination of γ-value and xanthate group distribution on viscose by liquid-state 1H NMR spectroscopy. *Carbohydr. Polym.* **2016,** *141*, 184-189.

(7) He, L.; Hu, H.-C.; Chai, X.-S. A Real-Time Technique for Monitoring Cellulose Dissolution during the Xanthation Process. *Ind. Eng. Chem. Res.* **2016,** *55*, 10823-10828.

(8) Woodings, C. *Regenerated Cellulose Fibres*. Woodhead Publishing: 2001.

(9) Klemm, D.; Heublein, B.; Fink, H.-P.; Bohn, A. Cellulose: Fascinating Biopolymer and Sustainable Raw Material. *Angew. Chem. Int. Ed.* **2005,** *44*, 3358–3393.

(10) Weißl, M.; Niegelhell, K.; Reishofer, D.; Zankel, A.; Innerlohinger, J.; Spirk, S. Homogeneous cellulose thin films by regeneration of cellulose xanthate: properties and characterization. *Cellulose* **2018,** *25*, 711-721.

Paper #2

Processing of metal sulfide/ cellulose composite fibers in core-shell configuration

Submitted to Lenzinger Berichte

For this paper, I conducted most of the experiments, interpreted the data and wrote a significant part of the manuscript.

Processing of metal sulfide/ cellulose nanocomposite fibers in *core-shell* configuration

Michael Weißl[1], Mike Pelzmann[1], Armin Zankel[2], Brigitte Bitschnau[3], Helmar Wiltsche[4], Gregor Trimmel[5], and Stefan Spirk[1]*

1) Institute of Paper, Pulp and Fiber Technology, Graz University of Technology, Inffeldgasse 23, A-8010 Graz, Austria

2) Institute for Electron Microscopy and Nanoanalysis, NAWI Graz, Graz University of Technology and Centre for Electron Microscopy Graz, Steyrergasse 17, A-8010 Graz, Austria

3) Institute of Physical and Theoretical Chemistry, Graz University of Technology, Stremayrgasse 9, A-8010 Graz, Austria

4) Institute of Analytical Chemistry and Food Chemistry, Graz University of Technology, Stremayrgasse 9, A-8010 Graz, Austria

5) Institute for Chemistry and Technology of Materials, Graz University of Technology, Stremayrgasse 9, A-8010 Graz, Austria

Correspondence:

Stefan Spirk

stefan.spirk@tugraz.at

+43 (316) 873 – 30763

Abstract

A proof of concept for a simple and straightforward processing of *core-shell* structured nanocomposite fibers, consisting of a metal sulfide shell and a viscose fiber core is described. The metal sulfide shell forms by the addition of the corresponding metal salt precursor into the sulfuric acid regeneration bath; any further reactants are not needed. A reaction of the dissolved metal cations (Ag, Cu, Sn) with sulfur sources present in the viscose spinning dope leads to the formation of (nano)crystalline metal sulfide particles (CuS, Ag_2S, SnS) on the viscose fibers. The metal loading on the fibers and the thickness of the formed shell depends on the type of precursor salt and concentration and can reach up to 10 wt% under the chosen conditions. The formation of metal sulfides exclusively takes place on the fiber surface and some metal sulfides (CuS and Ag_2S) unexpectedly come in phase pure configurations. The materials have been characterized by SEM (morphology), XRD (metal sulfide phase) and ICP-MS (amount of metal sulfide on fiber).

Keywords

Cellulose xanthate, viscose process, metal sulfide, fiber functionalization, core-shell structure, nanocomposite, hybrid material

Introduction

The basic idea behind the viscose process is to convert cellulose into a soluble derivative that can be processed and shaped into fibers or films. The conversion to a soluble precursor proceeds via the formation of alkali cellulose which is then reacted with CS_2 to give cellulose xanthate (CX). The properties of the resulting CX dope are adjusted by the ripening procedure which exploits reactivity differences of the hydroxyl groups leading to favored xanthate substitution at the C6 position in an industrial context.[1,2]

However, the reaction of the alkali cellulose and CS_2 is not straightforward. A wealth of other reaction products are formed as well, which comprise sulfur containing species such as sulfides, thiolates and thiocarbonates.[3-5] In the course of the spinning procedure into sulfuric acid, these species decompose to give, among others, H_2S, CS_2, and Na_2SO_4 while converting the CX to a cellulose fiber or film. The properties of the obtained cellulose fibers can be further tuned by either incorporating additional functionality into the CX dope or by post-treatment of the fibers.[6,7] Crosslinking, hydrophobization, amination or physicochemical deposition of functional molecules and inorganic particles are common routes to extend the application range of fibers.[8] Such fibers often carry inorganic nanoparticles with antibacterial (e.g., Ag, Cu), magnetic (e.g., Fe_2O_3) or self-cleaning properties (e.g., TiO_2) for instance.[7,9,10] One class of inorganic nanoparticles that has not been extensively investigated in this context are metal sulfides. Metal sulfides find applications in various fields. For instance, some metal sulfides (e.g. Bi_2S_3, $CuInS_2$) have a narrow band gap, i.e. they can generate a current when they are exposed to light.[11,12] This can be exploited in thin film solar cells and optoelectronics for instance.[13-15] As a consequence of the low HOMO-LUMO gap, metal sulfides are also employed in photocatalysis (e.g., Ag_2S for hydrogen production or degradation of organic pollutants).[16,17] Fluorescence is another feature of many metal sulfides (e.g. ZnS, CdS) that can be used in quantum dot based sensing applications.[18,19] Some sulfides (Li_2S, Na_2S) in turn are used as active electrode material in batteries and energy storage systems[20] while antibacterial

properties are provided by Ag_2S and CuS.[21] CuS and SnS are further used in lubricants and friction stabilizers, for instance in breaking systems in automotive industry. There, the metal sulfides provide high durability, prevent break fading and produce only a limited amount of rim dust. [22,23]

While for many nanoparticles it is rather simple to deposit them on cellulosic materials, for the metal sulfides the preparation is a challenge since most manufacturing methods require elevated temperatures (>200°C) to generate these.[24] However, most metal ions form binary as well as complex sulfides when they come in contact with sulfur containing anions (e.g. S^{2-}, CS_3^{2-}) in aqueous solution. The tendency to form sulfides is the more pronounced, the softer the character of the metal ion is according to the HSAB concept.[25] In general, metal sulfides decompose under strongly acidic conditions to the corresponding metal sulfate and SO_2.[26] The decomposition depends on the temperature and the type and molarity of the used acid. Further, the solubility of the metal sulfide under the chosen conditions determines whether the process proceeds fast or rather slow since decomposition is limited by mass transport into the acidic solution.[27]

Here, we aim at exploiting the sulfur containing side products in the viscose dope to serve as a sulfur source in the generation of metal sulfides in the presence of metal cations. For the proof of principle, we selected three metal ions of different softness according to the HSAB concept (Ag: soft, Cu: intermediate, Sn: hard) and study their influence on sulfide formation on the viscose fiber *in situ*.

Experimental Part

Materials and fiber processing

$CuCl_2$ and $SnCl_2$ were purchased from Aldrich, and $AgNO_3$ was obtained from Roth. Deionized water was obtained from an Elga PURELAB Prima (Bucks, United Kingdom) water treatment system. Lenzing AG (Lenzing, Austria) kindly provided a cellulose xanthate (CX) spinning dope with 10% cellulose content, 6% NaOH, a gamma number of 52 and a DP of 550, which was used as stock solution. The stock solution was diluted with water (1:2 w/w), vigorously shaken on a vortex and evaporated for at least 20 minutes in a desiccator before fiber spinning. The dope was injected into a 15% sulfuric acid (VWR chemicals, v/v) bath through two injection needles (diameter 450 µm) with a speed of 1.2 m/min and collected on a rotating polypropylene (PP) cylinder (v = 8 m/min) on the opposite direction of the regeneration bath. After injecting the viscose solution completely, the fibers were rotated in the acid bath for additional 15 minutes. After spinning, the fibers were cut from the PP role and washed two times in water for 15 minutes each. The fibers were dried overnight at room temperature under ambient conditions. The core-shell formation of a metal sulfide layer on a viscose fiber filament was realized by addition of metal salts ($CuCl_2$: 2.5, 5.0, 10 g/L spinning bath, $SnCl_2$: 5.0 g/L spinning bath, $AgNO_3$: 5.0 g/L spinning bath) into the regeneration bath and injecting the spinning dope as described (Table 1).

Table 1. Overview on type and amount of added metal salts to the spinning bath

Spinning bath additive	Concentration [g/L]	Concentration [mM]
$CuCl_2$	2.5	26
$CuCl_2$	5.0	52
$CuCl_2$	10.0	104
$AgNO_3$	5.0	16
$SnCl_2$	5.0	15

The setup is shown in Figure 1 at the example of $CuCl_2$ as spinning bath additive. Finally, the fibers are collected on a rotating PP cylinder.

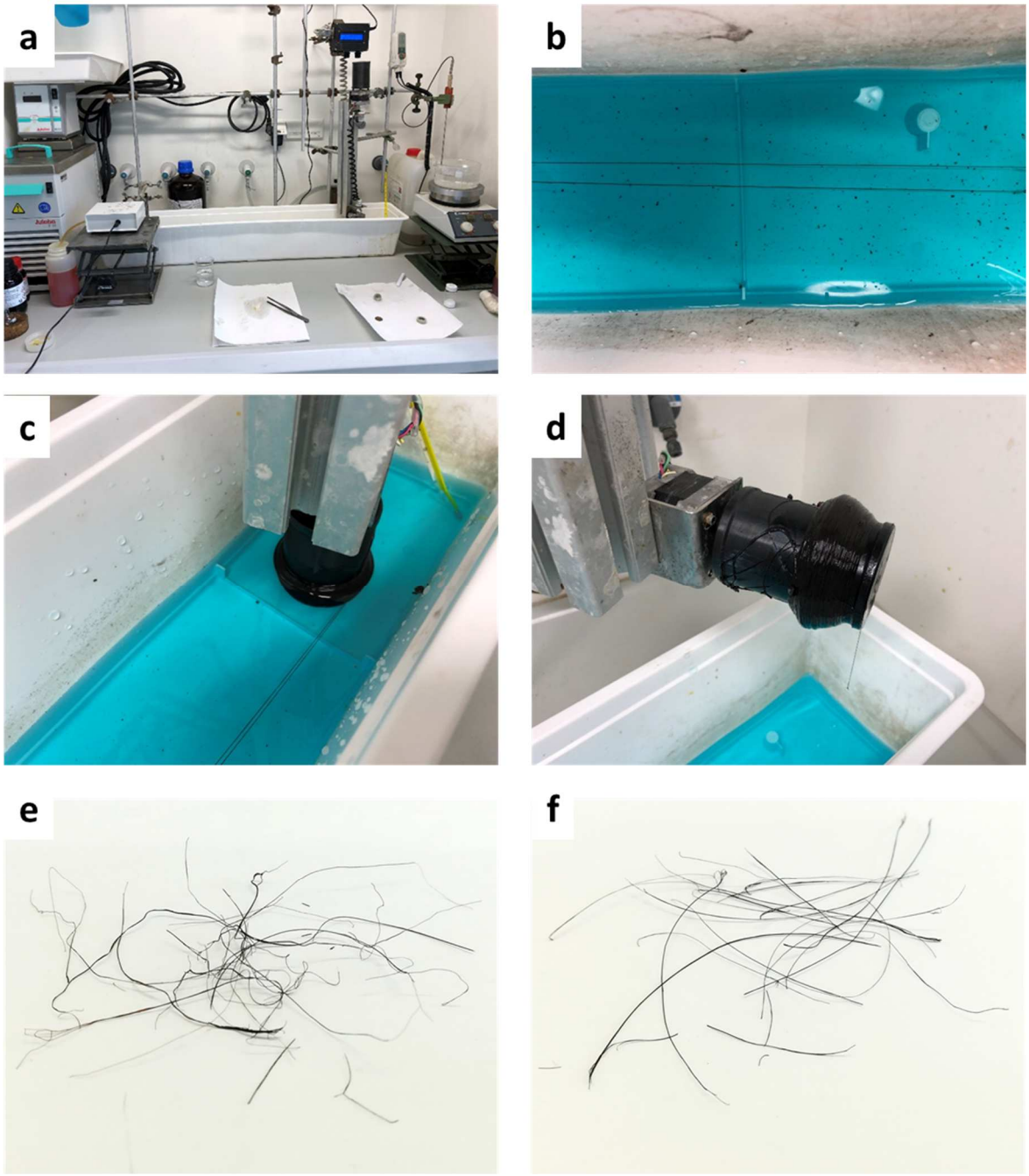

Figure 1. Manufacturing of CuS coated viscose fibers a) lab scale fiber spinning equipment b) development of a CuS layer on the regenerating fibers in the spinning bath (c=10 g/L), c) collecting the CuS fibers at the end of the spinning bath d) CuS coated fibers after removal from the spinning bath e/f) CuS coated fiber after washing and drying (26 and 104 mM $CuCl_2$).

Attenuated total reflection: infrared spectroscopy (ATR-IR)

The infrared spectra were recorded with an ALPHA FT-IR spectrometer (Bruker; Billerica, MA, U.S.A.). For the measurement, an attenuated total reflection (ATR) attachment was used with 64 scans at a resolution of 4 cm−1 and a scan range between 4000 and 400 cm^{-1}. The samples were prepared on Au-coated glass slides (SPR102-AU). The data were analyzed with OPUS 4.0 software.

Scanning electron microscopy (SEM)

The fibers were imaged in the low vacuum mode of the environmental scanning electron microscope ESEM Quanta 600 FEG equipped with a Schottky emitter (FEI, Eindhoven, The Netherlands). In this mode it is possible to investigate electrically non-conductive specimens at conventional electron energies without additional coating like carbon or gold. An acceleration of voltage of 7kV was applied to the primary electrons and water vapor was used as imaging gas

In order to get topographic contrast, the large field detector (LFD, dedicated SE detector of the low vacuum mode) was used for the detection of secondary electrons (SE). At each position synchronously, an image with backscattered electrons (BSE) was recorded in order to get material contrast (Z-contract; i.e. the higher the atomic number Z of the material the brighter the imaged region).

Inductively coupled plasma – optical emission spectroscopy (ICP-OES)

100 mg sample were dissolved in a mixture of 4 ml HNO_3 and 1 ml HCl under microwave assistance at 40 bar and 230°C (Multiwave 3000, Anton Paar; HF-Vials). After dissolution and restocking to a total volume of 50 ml quantification with ICP-OES (Spectro Ciros Vision EOP; 1350 W RF power; 0.6 L/min assist gas; 12 L/min cool gas; 0.83 L/min nebulizer gas, Crossflow nebulizer in Scott- spray chamber) was carried out. Calibration was done with 5-points between 0,04 und 4 mg/L with a Roth 28 elements standard; Sc was used as internal standard (1 mg/L).

X-ray powder diffraction (XRPD)

The samples were analyzed by powder X-ray diffraction using a Bruker D8 Advance diffractometer (Bragg Brentano geometry, CuKα radiation) with LynxEye Detector. Patterns were recorded with a step size of 0.02◦ in the 2θ-range 10◦to 100◦, 2s per step. Rietveld refinement was carried out using X'PertHighScorePlus (Panalytical).

Results and discussion

We used a simplified setup for the fiber spinning experiments, with a syringe pump operating at 1.2 m/min, spinning nozzles (diameter 450 µm), a regeneration bath (15% H_2SO_4) and a cylinder to collect the fibers. White cellulose fibers with an average diameter of 50 microns were obtained after washing them in hot water and subsequent drying.

The addition of metal salts ($CuCl_2$, $SnCl_2$, $AgNO_3$) to the regeneration bath led to strong coloration of the formed fibers directly after injection of the CX. The resulting fibers featured a brownish to black color, which can be associated to the respective metal sulfides (Figure 1 e,f). Extensive washing of the fibers even at elevated temperatures (60°C) did not lead to any leaching or decoloration of fibers, *i.e.* the metal sulfides irreversibly stick to the cellulose surface. The fiber diameter for all the samples was between 45 and 55 µm as determined by optical microscopy.

The amount of the deposited metals was determined using ICP-OES. Table 2 shows how the different metal concentrations influence the amount of metal sulfide on the surface. The increase in copper chloride concentration from 26 to 104 mmol/L in the spinning bath led only to a doubling of the deposited copper on the fiber surface (0.47 vs 1.05 mmol Cu/g fiber).

Table 2. Influence of metal salt concentration (mmol/L) in the spinning bath on the amount of deposited metal on the fiber (mmol metal/g fiber). LOQ: limit of quantification.

	Ag [mmol/g]	Cu [mmol/g]	Sn [mmol/g]
No salt added	< LOQ	< LOQ	< LOQ
$CuCl_2$ (26 mM)	< LOQ	0.47±0.01	< LOQ
$CuCl_2$ (52 mM)	< LOQ	0.55±0.02	< LOQ
$CuCl_2$ (104 mM)	< LOQ	1.05±0.05	< LOQ
$AgNO_3$ (16 mM)	0.64±0.01	< LOQ	< LOQ

$SnCl_2$ (15 mM)	< LOQ	< LOQ	0.23±0.02

The use of a softer metal ion according to the HSAB concept (i.e. Ag^+) led to a much higher deposition on the fiber (0.64 mmol/g) at much lower metal salt concentration in the spinning bath, while the use of a harder ion (i.e. Sn) deposition was lower (0.22 mmol/g at 16 mM $SnCl_2$ concentration in the spinning bath).

XRD was used to elucidate the type of material that was created on the surface. It also allows for distinguishing between different polymorphs of the same compound. This is important since copper and silver sulfide come in various polymorphs, if they are synthesized by non-specific procedures.[21,24,28-30] The XRD patterns confirmed that for silver and copper the corresponding sulfides have been exclusively formed (Figure 2). Additionally, they appear in a phase pure form (CuS: covellite, Ag_2S: acanthite) as the diffraction pattern perfectly matches those of the reported ones for these polymorphs. The XRD patterns also showed that that the crystals are smaller in the case of the CuS compared to the Ag_2S (ca 20 vs 35 nm). In the case of tin, XRD revealed that a mixture of different sulfur containing salts is present consisting of 66% orthorhombic and 10% cubic tin sulfide as well as 24% tin sulfate, the hydrolysis product of the sulfide.

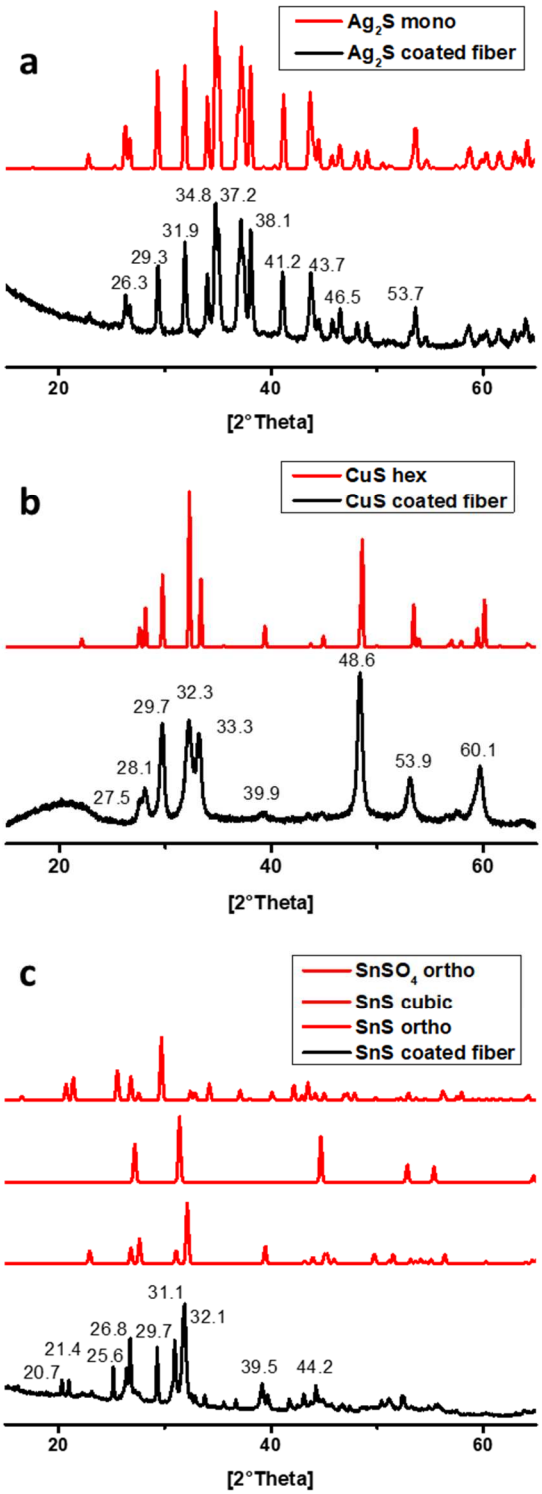

Figure 2. X-ray diffraction patterns of a) CuS coated fiber and CuS (hexagonal, 32106-ICSD) reference pattern b) Ag_2S coated fiber and Ag_2S (monoclinic, 44507-ICSD) reference pattern c) SnS/$SnSO_4$ coated fiber and reference patterns of SnS (orthorhombic, 106028-ICSD; cubic, 651015-ICSD) and $SnSO_4$ (orthorhombic, 245904-ICSD)

SEM provided morphological information about the crystalline structures developing on the fiber surface during the regeneration procedure. The amount of crystallites visible on the fiber surface depends on the amount of the metal salt concentration in the spinning bath. The thickness of the shell becomes thicker at the highest used $CuCl_2$ concentration. High concentrations of $CuCl_2$ (52 and 104 mM) in the spinning bath result in full coverage of the fibers (Figure 3ab). The lowest concentration of $CuCl_2$ (26 mM) in the regeneration bath does not lead to complete coverage of the fiber surface (Figure 3c). The morphology of the CuS particles is disk-like and comparable to literature reports on covellite (Fig. 3c).[28] The reference fibers spun in the absence of any metal cations possess a smooth and regular fiber surface with an obviously dense and closed structure (Figure 3d). The cross sectional analysis further confirms that the metals sulfides are only present at the surface of the fibers, forming a shell, while in the bulk of the fiber no CuS was detected. For $SnCl_2$ as additive, particles with different shapes are present in the fibers surface (Fig. 3e) which can be assigned to the different metal sulfide phases and the formed $SnSO_4$. The deposited materials do not form continuous layers on the fiber surface and inhomogeneous spots are present on the fiber.

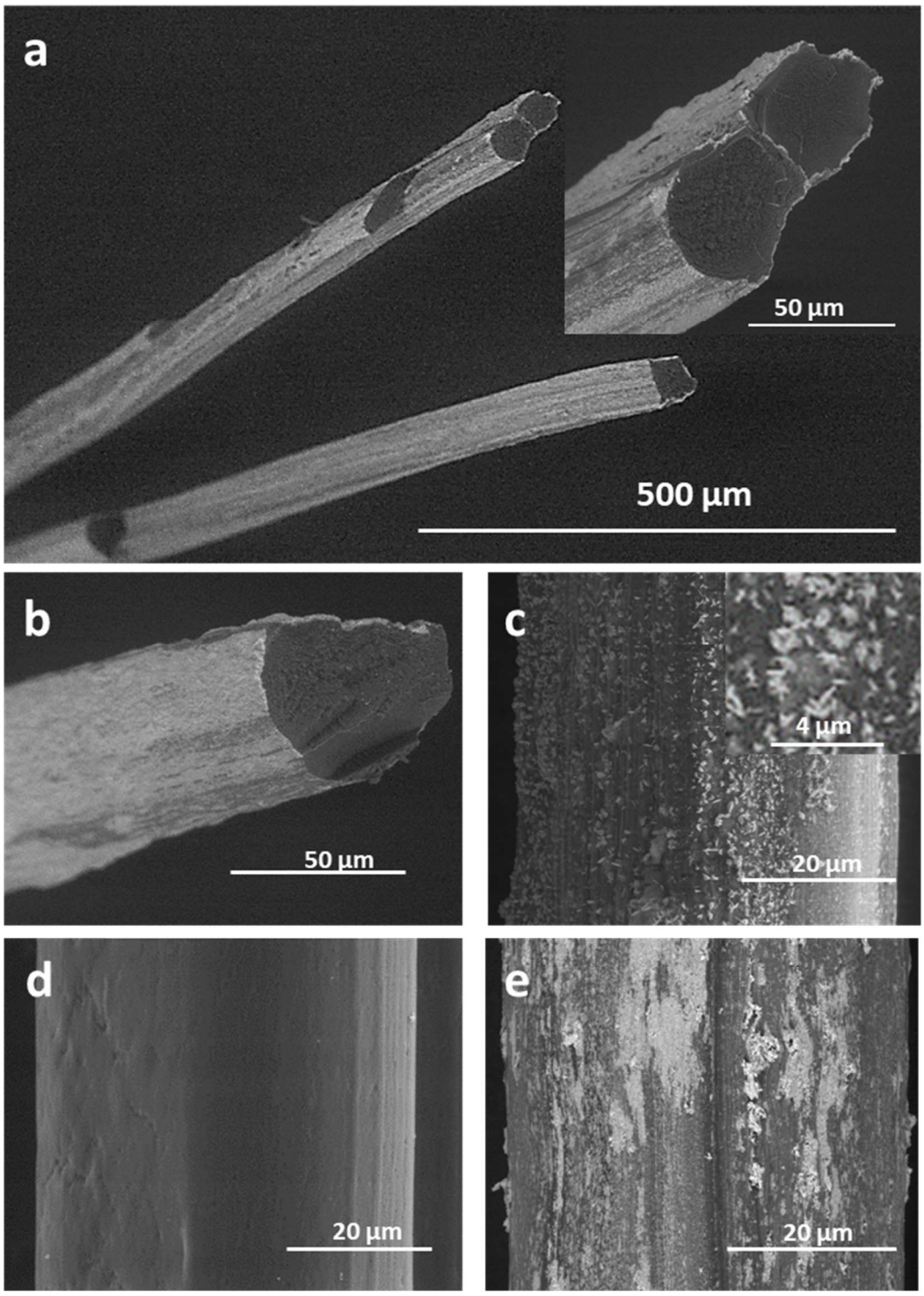

Figure 3. SEM surface and cross section images of a) Overview image of CuS coated fiber (104 mM) with an insert showing the core-shell structure b) CuS coated fiber (56 mM) with full coverage and any CuS particles in the fiber core, c) CuS coated fiber (26 mM $CuCl_2$) with an insert showing the morphology of the CuS particles d) uncoated reference fiber e) $SnS/SnSO_4$ coated fiber (15 mM $SnCl_2$)

The influence of the metal salts in the spinning bath on the regeneration process was investigated by ATR-IR spectroscopy. A comparison of the spectra of dry CX used as spinning dope, a spun fiber without metal salt additive in the spinning bath and one with $CuCl_2$ (104 mM) and $AgNO_3$ (15 mM, Figure 4). The spectrum of the dried CX is complex and consists of cellulose xanthate as well as of decomposition and side products present in the provided CX solution. As dominating side products, sodium sulfide (intensive bands at 1420 and 920 cm^{-1}), sodium trithiocarbonate (1670, 1427, 925 and 880 cm^{-1}) and sodium hydroxide with intense bands at 1452 cm^{-1} and 1380 cm^{-1} could be identified.[3-5] The series of intense bands between 1200 and 950 cm^{-1} can be assigned to the vibrations of the pyranose ring, overlapping with the C-S and C=S vibrations of the xanthate, reported in the same region.

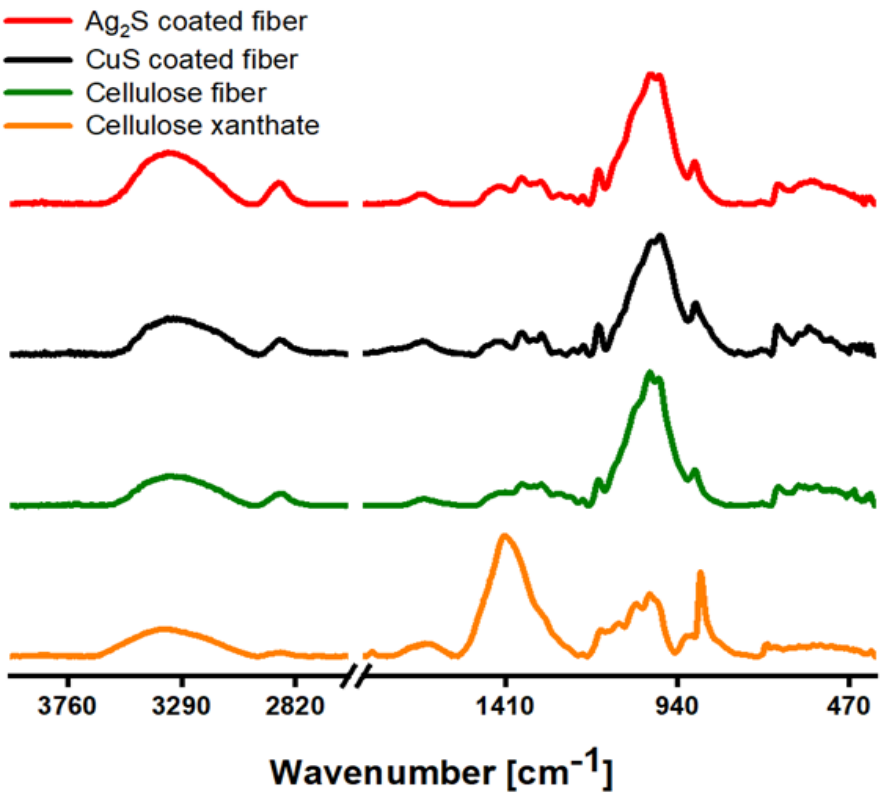

Figure 4. ATR-IR spectra of dried viscose (yellow), regenerated cellulose fiber as reference material (green), CuS (black) and Ag_2S (red) coated fibers after spinning and washing

After fiber spinning and processing, the uncoated cellulose reference fibers display bands at 3600 to 3000 cm^{-1} (OH vibration), at 2850 cm^{-1} (CH vibration), a series of less intense bands

from 1430 to 1180 cm^{-1} (C-O-H bending at 1430 cm^{-1}, C-H deformation at 1372 cm^{-1}, OH in plane deformation at 1330 and at 1200 cm^{-1}) and strong overlapping bands from 1150 to 950 cm^{-1} (C-O-C vibration at 1155 cm^{-1}, O vibration at 1060 cm^{-1} and C-O stretching at 1035 cm^{-1}) accompanied by a small band at 899 cm-1 (C-O-C vibration at 1155 cm^{-1}).[31] The bands described for the cellulose reference fibers are all related to cellulose II vibrations and hence confirm a full regeneration of the cellulose xanthate under the chosen conditions.[32] The presence of different metal cations in the spinning bath does not impact the regeneration of cellulose xanthate to cellulose. Since the metal sulfides are not absorbing in the investigated area of the spectrum, identical spectra compared to the cellulose reference are obtained.

The IR spectra confirm the presence of several sulfur containing species in the CX. A complication is the hydrolytic sensitivity of metal sulfides under acidic conditions that leads to the corresponding sulfates and SO_2. The tendency to hydrolyze increases with increasing hardness of the metal ion. This is observed in our case for Sn, which is considered hard according to the HSAB concept and which already shows significant amounts of tin sulfate on the surface of the fiber (24%, according to XRD). Further, the rate constants for the formation of the sulfides are in general higher for soft ions than for harder ones.[33] Also this behavior has been observed in our experiments, since even low amounts of silver in the spinning bath led to significant sulfide formation on the surface of the cellulose fibers, while comparable amounts of the harder tin yielded lower amounts.

The mechanism and which species in detail are responsible for the generation of the metal sulfide is challenging to reveal. However, there are various plausible ways how the sulfides are formed during the processing step (Scheme 1). For instance, thiocarbonates (i.e. dithio- and trithiocarbonates) that are either present already in the CX or are formed during the spinning process can provide sulfur species for sulfide formation under formation of COS and CS_2, respectively. Thiolates may provide sulfur by elimination of H_2S in acidic medium to give the

corresponding sulfide as well. Also cellulose sodium xanthate itself is capable to act as sulfur source by exchange of the sodium by the metal ion as soon as the spinning dope comes into contact with the spinning bath. The formed metal-xanthate complex may decompose as in other cases to the metal sulfides and organic leaving groups, here cellulose.[34] Independent of the mechanism, the formation of the metal sulfides is diffusion controlled since the sulfides are only present on the fiber surface. So far it is unclear why CuS and Ag_2S come phase pure when they are synthesized on the fibers. Particularly copper sulfides have a large variation of different phases, both copper and sulfur rich ones. Even for synthetic routes where mainly covellite is obtained usually other phases are present in minor amounts.[28] The same applies for Ag_2S, where often sulfur rich phases are observed (typical ratio Ag:S= 1.92), particularly when particle size reaches the nanometer regime.[30]

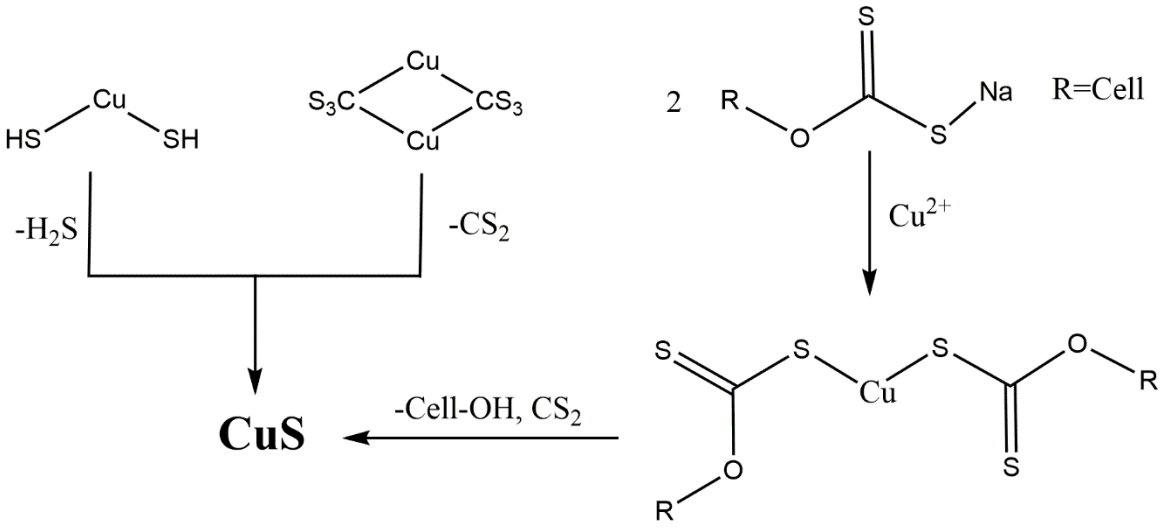

Scheme 1. Formation of metal sulfides based on a reaction of the added metal cations with thiols, trithiocarbonates present as by products in viscose, or the cellulose xanthates itself.

Conclusion

We presented a facile approach to produce metal sulfide decorated viscose fibers by addition of metal salts to the spinning bath. The amount of material on the fiber can be either tuned by the concentration as well as by the hard/softness of the metal ions. The procedure works best for soft ions since they feature higher affinity towards sulfide formation. Further, they show higher stability towards hydrolysis, the counter reaction that results in the formation of the corresponding sulfates and SO_2, respectively, under the conditions present in the spinning bath. The mechanism for metal sulfide formation remains unclear so far. However, there are different options which species may provide the sulfur for the sulfide formation, which include thiolates, thiocarbonates and the xanthates. An intriguing observation was that CuS and Ag_2S come in a phase pure form (covellite and acathite, respectively) which is an unexpected result given the wealth of known polymorphs for copper sulfide. This could be an advantage for future applications where particularly phase pure covellite could be used in optoelectronic applications. However, the fiber properties itself (tensile strength, water uptake etc.) are of course influenced by the metal sulfide layer. Further, we did not investigate in detail how the presence of the employed metal salts in the spinning bath influences coagulation and regeneration of the fibers; this will be done in scale up experiments.

We just presented a part of our work on metal sulfide decoration of cellulose fibers produced via the viscose route. We have evidence that the procedure works for a wide range of metal ions, whereas soft metals preferentially form sulfides on the fibers and survive the acidic conditions. Since metal sulfides have a large potential for various applications, such nanocomposites may serve as new interesting materials for advanced applications.[35]

Acknowledgements

Lenzing AG is gratefully acknowledged for providing viscose spinning dope. Dr. Josef Innerlohinger, Dr. Thomas Röder (both Lenzing AG) and Dr Ingo Berndt are gratefully thanked

for the fruitful discussion and their support. Chris Corner is acknowledged for inspiration during the writing of this paper.

References

(1) Götze, K. *Chemiefasern nach dem Viskoseverfahren*; 2nd ed.; Springer Verlag: Heidelberg, Germany, 1951.

(2) Wöss, K.; Weber, H.; Grundnig, P.; Röder, T.; Weber, H. K. Rapid determination of γ-value and xanthate group distribution on viscose by liquid-state 1H NMR spectroscopy. *Carbohydr. Polym.* **2016,** *141* (Supplement C), 184.

(3) Andrews, D. A.; Hurtubise, F. G.; Krassig, H. The Presence of Monothiocarbonate Substituents in Cellulose Xanthates. *Can. J. Chem.* **1960,** *38* (8), 1381.

(4) Dautzenberg, H.; Philipp, B. Über Bildungsweise und Verhalten des Natriumdithiocarbonats. *Z. Anorg. Allg. Chem.* **1970,** *375* (2), 113.

(5) Ogura, K.; Sobue, H. Studies on the derivatives of sodium cellulose xanthate. Part I. Infrared absorption spectra and characteristic frequencies of C-S and C=S groups in sodium cellulose xanthate and its stable derivatives. *J. Polym. Sci, Part B: Polym. Lett.* **1968,** *6* (1), 63.

(6) Weber, F.; Koller, G.; Schennach, R.; Bernt, I.; Eckhart, R. The surface charge of regenerated cellulose fibers. *Cellulose (Dordrecht, Neth.)* **2013,** *20* (6), 2719.

(7) Malucelli, G. Surface-Engineered Fire Protective Coatings for Fabrics through Sol-Gel and Layer-by-Layer Methods: An Overview. *Coatings* **2016,** *6* (3).

(8) Klemm, D.; Philip, B.; Heinze, T.; Heinze, U.; Wagenknecht, W. *Comprehensive Cellulose Chemistry, Volume 2: Derivatization of Cellulose*; Wiley, 1998.

(9) Breitwieser, D.; Moghaddam, M. M.; Spirk, S.; Baghbanzadeh, M.; Pivec, T.; Fasl, H.; Ribitsch, V.; Kappe, C. O. In situ preparation of silver nanocomposites on cellulosic fibers – Microwave vs. conventional heating. *Carbohydr. Polym.* **2013,** *94* (1), 677.

(10) Hribernik, S.; Sfiligoj-Smole, M.; Bele, M.; Gyergyek, S.; Jamnik, J.; Stana-Kleinschek, K. Synthesis of magnetic iron oxide particles: Development of an in situ coating procedure for fibrous materials. *Colloids Surf., A* **2012,** *400*, 58.

(11) Weißl, M.; Rath, T.; Sattelkow, J.; Plank, H.; Eyley, S.; Thielemans, W.; Trimmel, G.; Spirk, S. Multi-layered nanoscale cellulose/CuInS2 sandwich type thin films. *Carbohydr. Polym.* **2019,** *203*, 219.

(12) Reishofer, D.; Ehmann, H. M.; Amenitsch, H.; Gspan, C.; Fischer, R.; Plank, H.; Trimmel, G.; Spirk, S. On the formation of Bi2S3-cellulose nanocomposite films from bismuth xanthates and trimethylsilyl-cellulose. *Carbohydr. Polym.* **2017,** *164*, 294.

(13) Fradler, C.; Rath, T.; Dunst, S.; Letofsky-Papst, I.; Saf, R.; Kunert, B.; Hofer, F.; Resel, R.; Trimmel, G. Flexible polymer/copper indium sulfide hybrid solar cells and modules based on the metal xanthate route and low temperature annealing. *Sol. Energy Mater. Sol. Cells* **2014,** *124*, 117.

(14) Reishofer, D.; Rath, T.; Ehmann, H. M.; Gspan, C.; Dunst, S.; Amenitsch, H.; Plank, H.; Alonso, B.; Belamie, E.; Trimmel, G.et al. Biobased Cellulosic–CuInS2 Nanocomposites for Optoelectronic Applications. *ACS Sustain. Chem. Eng.* **2017,** *5*, 3115.

(15) Rath, T.; Kaltenhauser, V.; Haas, W.; Reichmann, A.; Hofer, F.; Trimmel, G. Solution-processed small molecule/copper indium sulfide hybrid solar cells. *Sol. Energy Mater. Sol. Cells* **2013,** *114*, 38.

(16) Shi, E.; Xu, Z.; Wang, W.; Xu, Y.; Zhang, Y.; Yang, X.; Liu, Q.; Zeng, T.; Song, S.; Jiang, Y.et al. Ag2S-doped core-shell nanostructures of Fe3O4@Ag3PO4 ultrathin film: major role of hole in rapid degradation of pollutants under visible light irradiation. *Chem. Eng. J. (Amsterdam, Neth.)* **2019,** *366*, 123.

(17) Yu, W.; Yin, J.; Li, Y.; Lai, B.; Jiang, T.; Li, Y.; Liu, H.; Liu, J.; Zhao, C.; Singh, S. C.et al. Ag2S Quantum Dots as an Infrared Excited Photocatalyst for Hydrogen Production. *ACS Appl. Energy Mater.* **2019,** *2* (4), 2751.
(18) Yang, J.; Wang, J.; Zhao, K.; Izuishi, T.; Li, Y.; Shen, Q.; Zhong, X. CdSeTe/CdS Type-I Core/Shell Quantum Dot Sensitized Solar Cells with Efficiency over 9%. *J. Phys. Chem. C* **2015,** *119* (52), 28800.
(19) Pons, T.; Pic, E.; Lequeux, N.; Cassette, E.; Bezdetnaya, L.; Guillemin, F.; Marchal, F.; Dubertret, B. Cadmium-Free CuInS2/ZnS Quantum Dots for Sentinel Lymph Node Imaging with Reduced Toxicity. *ACS Nano* **2010,** *4* (5), 2531.
(20) Manthiram, A.; Fu, Y.; Chung, S.-H.; Zu, C.; Su, Y.-S. Rechargeable Lithium–Sulfur Batteries. *Chem. Rev.* **2014,** *114* (23), 11751.
(21) Sadovnikov, S. I.; Gusev, A. I. Universal Approach to the Synthesis of Silver Sulfide in the Forms of Nanopowders, Quantum Dots, Core-Shell Nanoparticles, and Heteronanostructures. *European Journal of Inorganic Chemistry* **2016,** *2016* (31), 4944.
(22) Koteeswara Reddy, N.; Devika, M.; Gopal, E. S. R. Review on Tin (II) Sulfide (SnS) Material: Synthesis, Properties, and Applications. *Crit. Rev. Solid State Mater. Sci.* **2015,** *40* (6), 359.
(23) Österle, W.; Dmitriev, I. A. The Role of Solid Lubricants for Brake Friction Materials. *Lubricants* **2016,** *4* (1), 5.
(24) Gorai, S.; Ganguli, D.; Chaudhuri, S. Synthesis of Copper Sulfides of Varying Morphologies and Stoichiometries Controlled by Chelating and Nonchelating Solvents in a Solvothermal Process. *Crystal Growth & Design* **2005,** *5* (3), 875.
(25) Pearson, R. G. Hard and Soft Acids and Bases. *J. Am. Chem. Soc.* **1963,** *85* (22), 3533.
(26) Narasagoudar, R. A.; Johnson, J. W.; O'Keefe, T. J. The anodic dissolution of ZnS electrodes in sulfuric acid solutions. *Hydrometallurgy* **1982,** *9* (1), 37.
(27) Biswas, A. K.; Mohan, N. P. Kinetics of dissolution of copper(II) sulphide in aqueous sulphuric acid solutions. *Journal of Applied Chemistry and Biotechnology* **1971,** *21* (1), 15.
(28) Jiang, X.; Xie, Y.; Lu, J.; He, W.; Zhu, L.; Qian, Y. Preparation and phase transformation of nanocrystalline copper sulfides (Cu9S8, Cu7S4 and CuS) at low temperature. *Journal of Materials Chemistry* **2000,** *10* (9), 2193.
(29) Freymeyer, N. J.; Cunningham, P. D.; Jones, E. C.; Golden, B. J.; Wiltrout, A. M.; Plass, K. E. Influence of Solvent Reducing Ability on Copper Sulfide Crystal Phase. *Crystal Growth & Design* **2013,** *13* (9), 4059.
(30) Sadovnikov, S. I.; Gusev, A. I.; Rempel, A. A. Nonstoichiometry of nanocrystalline monoclinic silver sulfide. *Physical Chemistry Chemical Physics* **2015,** *17* (19), 12466.
(31) Weißl, M.; Niegelhell, K.; Reishofer, D.; Zankel, A.; Innerlohinger, J.; Spirk, S. Homogeneous cellulose thin films by regeneration of cellulose xanthate: properties and characterization. *Cellulose* **2018,** *25* (1), 711.
(32) Široký, J.; Blackburn, R. S.; Bechtold, T.; Taylor, J.; White, P. Attenuated total reflectance Fourier-transform Infrared spectroscopy analysis of crystallinity changes in lyocell following continuous treatment with sodium hydroxide. *Cellulose* **2010,** *17* (1), 103.
(33) Luther, G. W.; Rickard, D. T.; Theberge, S.; Olroyd, A. Determination of Metal (Bi)Sulfide Stability Constants of Mn2+, Fe2+, Co2+, Ni2+, Cu2+, and Zn2+ by Voltammetric Methods. *Environ. Sci. Technol.* **1996,** *30* (2), 671.

(34) Rath, T.; Edler, M.; Haas, W.; Fischereder, A.; Moscher, S.; Schenk, A.; Trattnig, R.; Sezen, M.; Mauthner, G.; Pein, A.et al. A Direct Route Towards Polymer/Copper Indium Sulfide Nanocomposite Solar Cells. *Adv. Energy Mat.* **2011,** *1* (6), 1046.
(35) Liu, Y.; Li, Y.; Kang, H.; Jin, T.; Jiao, L. Design, synthesis, and energy-related applications of metal sulfides. *Materials Horizons* **2016,** *3* (5), 402.

Paper #3

Biobased support layers for the fractionation and selective extraction of lignosulfonates

Accepted in Solvent Extraction and Ion Exchange Journal

For this paper, I prepared and modified the membranes and wrote parts of the manuscript.

Biobased support layers for the fractionation and selective extraction of lignosulfonates

Marlene Kienberger*[1], Paul Demmelmayer[1], Michael Weißl[2], Armin Zankl[3], Stefan Spirk[2]

[1]Institute of Chemical Engineering and Environmental Technology, Graz University of Technology, Inffeldgasse 25c, 8010 Graz

[2]Institute of Paper, Pulp and Fiber Technology, Graz University of Technology

[3]Institute for Electron Microscopy and Nanoanalysis, NAWI Graz, Graz University of Technology and Centre for Electron Microscopy Graz, Austria

Abstract

The paper presents an experimental study on the preparation and characterization of cellulose films and their use for reactive lignosulfonate extraction. The extraction of lignosulfonates leads to emulsion and crud formation when standard equipment is applied, by using cellulose films as support layer between the aqueous feed phase and the organic extractant phase, emulsion formation is prevented. The results showed that selective separation and a fractionation of the lignosulfonates can be realized with this novel approach simultaneously.

Keywords: lignosulfonates; reactive extraction; bio-based membranes; membrane technology; fractionation of lignosulfonates;

Table of content

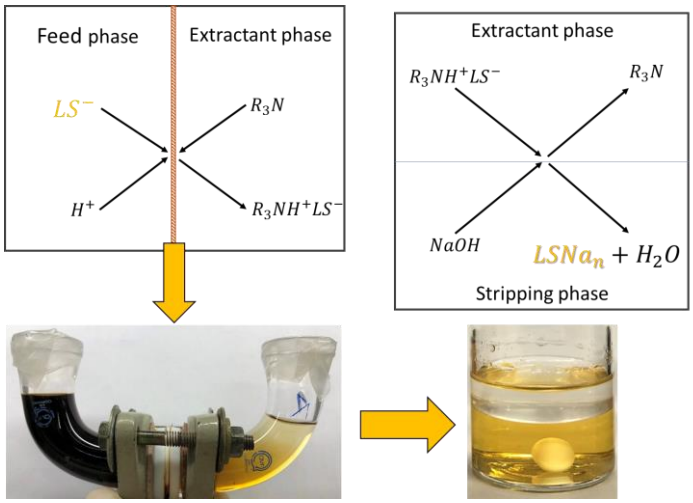

Introduction

Climate change requires a transition from today`s fossil based to a future biobased economy. As a direct consequence, the production of bulk chemicals derived from renewable resources must be promoted and further developed to be competitive in terms of price, availability and volume. In this context, the pulp- and paper industry takes an essential role in this transition process, as it offers constant supply of raw materials throughout the whole year at large quantities. The raw material wood consists of three main polymeric components (lignin, hemicellulose and cellulose) as well as low molecular compounds with extractives being the most abundant ones. One major route of separation of cellulose from the other components is the sulfite process, which yields, besides cellulose, lignosulfonates (LS). These LS have been commercialized already in the beginning of the 20th century with mainly low cost applications as dust controlling agents, flocculants or emulsion stabilizers. The past 15 years, however, showed a tremendous increase in upcycling the LS and many new applications in energy storage, fine-chemical production (e.g. vanillin) and carbon fibers have emerged. In many of these applications, the presence of impurities (e.g. carbohydrates, wood degradation products, extractives or process chemicals) may lead to performance loss of the LS. [1]

A major challenge in the purification of LS is the varying feedstock quality (i.e. summer vs winter, tree species, location) and alterations in the composition of the spent liquor. Further, LS are soluble over the

whole pH range, necessitating the use of mass transfer unit operations such as drying, distillation or extraction. The Howard process, the drying of spent liquor and the ultrafiltration of spent liquor are currently employed state of the art processes for the isolation of LS. These processes, however, do not selectively remove LS from the spent liquor. As a consequence, the obtained fractions contain hemicellulose and other wood degradation products. [2]

Technologies for the selective isolation of lignosulfonates from sulfite pulping need to provide a certain selectivity, need to be able to prevent emulsion and crud formation, and need to be applicable to a complex process stream. Reactive extraction allows for the selective extraction of LS from spent liquors. In addition, the formation of emulsions can be prevented when used in combination with membrane technology. Membrane technology offers rather high flexibility when it comes to the type of membrane (bulk, emulsion, supported liquid) as well as the reactive extractant. A very well-known extractant is *n*-trioctylamine (TOA) which has been described in combination with different membrane types and solvent carriers. [3]–[6] Fractionation of lignosulfonates was performed using long chained aliphatic amines [7] and also a comparsion between ultrafiltration and extraction was reported. Both approaches showed to be effective whereas ultrafiltration is considered the best performing technology so far. [8]

Most of the studies use model solutions and show that extraction and liquid membrane permeation can be applied for the LS isolation. [4] The studies use TOA as carrier, and in most cases dichloroethane resulted in the highest mass transfer. Despite their good performance in the extraction, the use of halogenated solvents in general will be limited in the near future by new legislation, particularly within the EU (e.g. REACH).

The surface properties are crucial for support layers used in extraction processes. [9] The support layer has two main functions First, mass transfer has to be ensured, and second, emulsion prevention is targeted. Low interfacial tension causes faster degradation of the liquid membrane by easier emulsion formation or washing out, but on the other side it increases the mass transfer by facilitating the contact

between the two phases. [10] In a previous work, a commercially available polyethylene sheet was used for this purpose and showed to be effective, in both, emulsion prevention and to facilitate the mass transfer. Both, hydrophilic and hydrophobic polyethylene sheets were used in that study. [11]

As can be seen from the applications, lignosulfonates are used as emulsifiers, which renders the use of conventional extraction equipment for their isolation difficult because it is accompanied by emulsion and crud formation. In a prior work, we demonstrated that emulsion formation can be effectively prevented by using supported liquid membrane permeation equipment [11] These results make liquid membrane permeation with supported membranes a potential future isolation technology for the treatment of complex process streams, such as process streams from wood pulping.

The present paper investigates the use of bio-based support layers made from cellulose for the use in lignosulfonate extraction. The first part of the paper summarizes the manufacturing and modification of the films as well as the characterization thereof. The second part summarizes the results gathered in a u-tube setup using the cellulose films as rigid surface between the aqueous feed phase and the organic extractant phase to prevent emulsion formation. The extraction experiments use TOA as reactive extractant diluted in 1-octanol.

Experimental details

Chemicals

For the film preparation, a cellulose xanthate (CX) stock solution consisting of 10 wt% cellulose, 6 wt% NaOH, having a gamma value of 52 and a degree of polymerization of 550, was used. The stock solution was provided by Lenzing AG (Lenzing, Austria) and used without any further treatment.

For the modification of the cellulose films, trifluoroacetic anhydride (TFAA; CAS 407-25-0) was purchased from Sigma-Aldrich in a purity of >99%, acetic anhydrid (CAS 108-24-7) was purchased in a purity of >99% from Roth and hexamethyldisilazan (HMDS; CAS 999-97-3) was purchased from Sigma-Aldrich in a quality of >99%. All chemicals were used as received.

The feed phase for the extraction experiments was Ca-lignosulfonates purchased from Sigma Aldrich (Ca-LS; CAS 8061-52-7) and spent liquor from sulfite cooking provided by the company SAPPI (SAPPI Gratkorn, Austria). The spent liquor had a pH value of 3.6, the lignosulfonate concentration was 88.0 g/L, the dry mass content was 12% and the ash content was 0.38%. The main carbohydrates in the used spent liquor are xylose and mannose, the concentration of xylose was 0.17 wt% which corresponds to a concentration of 0.2 g/L with respect to the dry mass. For mannose, the concentration was 2.24 wt% which corresponds to a concentration of 3 g/L with respect to the dry mass.

The feed phase was prepared by dissolving 100 g/L Ca-LS in deionized water and adjustment of the pH value to 3.6 was done with dilute H_2SO_4.

The stripping phase consisted of 0.3 mol/LNaOH, NaOH was purchased from Carl Roth in a purity of ≥ 32% (extra pure) (CAS 1310-73-2).

The extractant phase consisted of 20 wt% *n*-trioctylamine (TOA; CAS 1116-76-3 purchased from Sigma Aldrich with a purity of 98%, diluted in 1-octanol (CAS 111-87-5), purchased from Sigma Aldrich with a purity of >99%.

Preparation of the cellulose films

The CX stock solution was diluted with distilled H_2O in a ratio of 1:1 (w/w) for the film casting. After dilution and vigorous mixing, the CX was evaporated in a desiccator for 15 min at 25°C to avoid the formation of air bubbles during the film casting. 6.6 g of the diluted CX solution was then transferred in PTFE forms with a diameter of 8 cm and a depth of 8 mm. For drying, the forms were placed in a dryer without ventilation for 70 min at 80°C. To force the regeneration of CX to cellulose, the dried films were placed into a sulfuric acid bath (2 wt%). After 20 min exposure to the acidic bath, the films were fully regenerated. Afterwards, the films were subjected to extensive washing with deionized water and pure cellulose films were obtained which was confirmed by IR spectroscopy.

The wet films were stored in deionized water until drying them on a sheet former (Rapid Köthen RK-4A, Paper Testing Instruments GmBH, Austria).

Modification of the cellulose films

The modification of the cellulose films was performed in a 25 ml round flask, the respective chemical was transferred into the flask and the cellulose film was placed above the liquid phase covering the neck of the round flask. For the modification with TFAA a 1:1 mixture (v/v) with acetic anhydride was prepared. Table 1 summarizes the parameters during modification for the two modification reagents.

Table 1. Summary of parameter for the modification of the cellulose films.

chemical	Volume /ml	Pressure /mbar	Temperature /°C	Time /h
TFFA: acetic anhydrid	4	vacuum	50	1 and 3
HMDS	2	Ambient pressure	100	2 and 20

After the modification no further treatment was performed.

Characterization of the cellulose films

Attenuated total reflection – infrared spectroscopy (ATR-IR)

The infrared spectra were recorded on an ALPHA FT-IR spectrometer (Bruker; Billerica, MA, U.S.A.). For the measurements, an attenuated total reflection (ATR) element was used with 48 scans at a resolution of 4 cm^{-1} and a scan range between 4000 and 400 cm^{-1}. The data were analyzed with OPUS 7.5 software.

Contact angle (CA) and surface free energy determination (SFE)

For the calculation of the surface free energy (SFE) Milli-Q water (≥18 $M\Omega cm^{-1}$) and 1-octanol were employed as test liquids. The drop shape analysis was done in the sessile drop modus at 25 °C with a DSA100 system (Krüss GmbH, Hamburg, Germany) equipped with a T1E CCD video camera (25 fps). The dispense rate of the 2 µL droplets was adjusted to 166 µL/min and the time before the image was captured was set to 1 sec. Each sample was measured at least seven times. The contact angle calculations

(software: Advance) were performed with the Young-Laplace equation and the surface free energy calculation with the Owens-Wendt-Rabel & Kaelble method. [12]

SEM

The specimens were embedded in the resin Epofix from Struers (Germany) at room temperature for 8 h. After hardening, the specimens were cut with an ultramicrotome (Leica EM UC6, Leica Microsystems Vienna, Austria) using a histo-diamond-knife (Diatome Ltd., Biel, Switzerland). A 10 nm thick layer of carbon was coated onto the freshly produced cross sections using an EPA (Leybold Heraeus, Germany). The characterization of the specimen was performed with the high resolution scanning electron microscope Zeiss Sigma VP 300 (Oberkochen, Germany), equipped with a Schottky field emitter using the inlens detector for the detection of secondary electrons (InLens according to the databar of the micrographs). All images were acquired at an acceleration voltage of 3 kV at small working distances with magnifications according to the databar.

Thickness

A micron screw LDAL 03 (Lehmann AG, Switzerland) was employed for the determination of the cellulose film thickness. For each sample at least 4 cellulose films have been characterized, with 2-5 measurements over the area of the cellulose film, in total 15 data points for each cellulose film were measured.

Characterization of the feed and the stripping phase

Dynamic light scattering (DLS) for particle size determination

The feed and the stripping phase were dissolved to a concentration of 1-1.5 g/L in deionized water or in 0.3 M NaOH before the DLS measurements. The measurement was performed using an Anton Paar LitesizerTM 500 (Anton Paar, Austria), the evaluation of the particles size was done byAnton Paar Kalliope software. The measurements were carried out in PS cuvettes at 23°C using the side scattering mode at a wavelength of 658 nm.

UV-Vis spectroscopy

The lignosulfonate concentration in the feed phase and the stripping phase was measured at 280 nm with an UV-1800 Spectrophotometer (Shimadzu, Germany). In order to ensure constant measurement conditions, the samples were diluted in 0.3 M NaOH and measured at 20 °C using PP UV-cuvettes with 10 mm transmitting path length. For the evaluation of the lignosulfonate concentration, an extinction coefficient of $\varepsilon = 13.2\ l \cdot g^{-1} \cdot cm^{-1}$ was used in the spent liquor [13], and for the pure Ca-LS an extinction coefficient of $\varepsilon = 7.64\ l \cdot g^{-1} \cdot cm^{-1}$ was determined. The determination of the lignosulfonate concentration using UV-Vis Spectroscopy is state of the art, however, it is known, that different batches of lignosulfonates lead to different extinction coefficient and also the matrix of the spent liquor influences the value of the lignosulfonates. [14]

Sugar content

The sugar content was measured using high performance liquid chromatographie (HPLC) equipped with an AMINEX HPX 87C column and an IR-detector. Deionized water was used as solvent phase.

Experimental set-up for extraction experiments

The experiments were carried out in a u-tube set up made from DN10 glass tubes. Figure 1 shows the experimental set up for the extraction experiments.

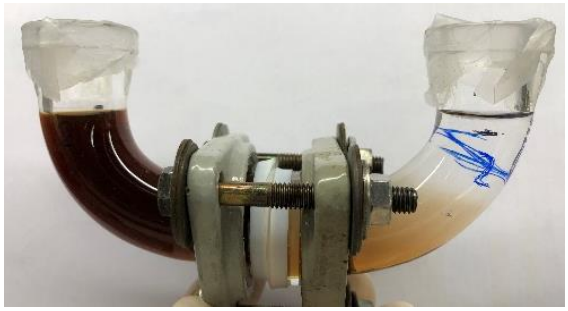

Figure 1. U-tube set-up for the extraction experiments. Left leg of the u-tube = feed phase; right leg of the u-tube extractant phase, at the bottom of the u-tube between the two PTFE sealings, the cellulose film with a mass transfer area of 2.27 cm^2 was placed.

The feed phase and the extractant phase were separated by a cellulose film and kept for 48 h. Afterwards, they were analyzed towards their LS content by photometry (feed phase) while the extractant phase was

back extracted using 0.3 M NaOH over a period of 48 hours followed by LS determination in the stripping phase using photometry

Results and Discussion

Preparation and characterization of the cellulose films

Cellulose films were manufactured using a simple casting process employing cellulose xanthate (CX), which is widely used for the manufacturing of viscose fibers and regenerated cellulose membranes. The CX solution was placed in a petri dish having a diameter of ca 8 cm, and after drying the CX films were converted to cellulose by exposure to an acidic bath of sulfuric acid. After drying, the films were modified using hexamethyldisilazane [15] and trifluoroacetic acid anhydride [16]. Figure 2 compares the infrared spectra of the dried CX films, the corresponding cellulose membrane and the membranes after gas phase modification.

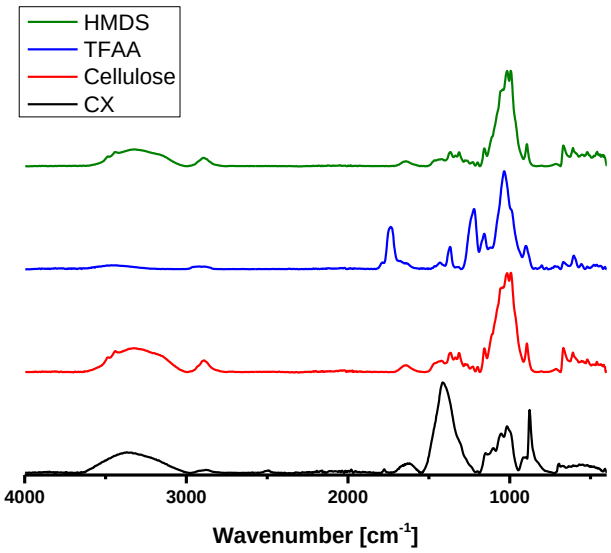

Figure 2. IR spectra for the untreated cellulose film (red), the cellulose xanthate CX (black) and after modification of the cellulose films with TFAA (blue) and HMDS (green)

The spectrum of the CX film is complex and shows besides bands for the CX,decomposition and side products present in the provided CX solution. As dominating side products, sodium sulfide (intensive bands at 1420 and 920 cm^{-1}), sodium trithiocarbonate (1670, 1427, 925 and 880 cm^{-1}) and sodium hydroxide with the intense bands at 1452 cm^{-1} and 1380 cm^{-1} could be identified. The series of intense

bands between 1200 and 950 cm^{-1} can be assigned to the vibrations of the pyranose ring, overlapping with the C-S and C=S vibrations of the xanthate reported in the same region. [17], [18] [21]

The cellulose membrane displays bands at 3600 to 3000 cm^{-1} (ν_{OH}), at 2850 cm^{-1} (ν_{CH}), a series of less intense bands from 1430 to 1180 cm^{-1} (C-O-H bending at 1430 cm^{-1}, C-H deformation at 1372 cm^{-1}, OH in plane deformation at 1330 and at 1200 cm^{-1}) and strong overlapping bands from 1150 to 950 cm^{-1} ($\nu_{C\text{-}O\text{-}C}$ at 1155 cm^{-1}, $\nu_{C\text{-}O}$ at 1060 cm^{-1} and C-O stretching at 1035 cm^{-1}) accompanied by a small band at 899 cm-1 ($\nu_{C\text{-}O\text{-}C}$). [19], [20] Gas phase modification with HMDS could not be confirmed via IR spectroscopy since there were not any bands identified that correspond to Si-C and Si-O-C vibrations (1250 and 850 cm^{-1}.) [21], [22]. Probably just the outermost layer was modified by the HMDS and therefore the amount of functional groups is below the detection limit of the employed IR spectrometer. In contrast, for the TFAA clear differences in the spectra were visible in the IR spectrum. Strong bands at 1740 cm^{-1} ($\nu_{C=O}$), and between 1250 and 1100 cm^{-1} ($\nu_{CF3;}$ $\nu_{F\text{-}CF2;}$ $\nu_{F\text{-}C\text{-}F;}$ $\nu_{C\text{-}C}$) clearly prove the covalent attachment of the TFAA onto the cellulose membrane via an ester bond. [23] Further the ν_{OH} bands nearly vanished, pointing at complete esterification with the TFAA within the penetration depth of the ATR IR spectrometer (ca 5 microns). Further evidence for the successful modification of the surface was provided by wettability determination of the membranes using water and 1-octanol. **Fehler! Verweisquelle konnte nicht gefunden werden.** summarizes the data for the surface properties in terms of contact angle and surface free energy (SFE) of the cellulose films. The contact angle measurements confirm the successful hydrophobization of the membranes via the gas phase, also for the HMDS treated cellulose films. A significant increase in the hydrophobicity of both materials (HMDS and TFAA treated) was observed, which is more pronounced the longer the exposure to the compounds had been. The highest increase in the water contact angle was determined for HMDS treated membranes, from 48° up to 99° after 20 hours exposure time. For the TFAA treated cellulose films, the water contact angle increased to 78° after 3 hours of exposure. The drastic increase in hydrophobicity of cellulose is also reflected in the surface free energy (polarity) of the respective material. The SFE decreases by ~50% for all modifications compared to the reference material.

Table 2. Wettability with water and 1-octanol and, surface free energy (γ) data, for the different materials.

sample	Water CA [°]	1-octanol CA [°]	γ [mN/m]	γ^D [mN/m]	γ^P [mN/m]
reference without modification	48 ± 3	37 ± 2	62 ± 5	1.3 ± 0.4	60.3±4.7
HMDS, 2h	83 ± 3	38 ± 1	24 ± 4	12.0±1.3	11.9±2.5
HMDS, 20h	99 ± 2	21 ± 2	29 ± 2	28.7±1.7	0.6±0.4
TFAA + Ac_2O 1h	63 ± 5	9 ± 2	38 ± 8	8.9±1.9	29.4±6.2
TFAA + Ac_2O 3h	79 ± 3	8 ± 2	28 ± 4	16.8±1.6	11.6±2.4

For further trials in LS separation, we selected the HMDS 20 h and TFAA +Ac2O 3h and the reference.

The thickness of the manufactured cellulose films was for the reference without modification 53.1 µm (σ = 5), the HMDS modified cellulose films had a thickness of 61.4 µm (σ = 7.9) and TFAA modified cellulose films lead to a thickness of 69.6 µm (σ = 6.8).

This data points at modification of the film not only on the surface but to some extent also in the bulk. For related cases, such as trimethylsilyl cellulose films for instance, the conversion of a fully substituted film to cellulose leads to film thickness reduction of 50-70% due to the formation of hydrogen bonds in cellulose. [24], [25] The disruption of the hydrogen bonded network may lead to higher porosity of the membranes, which should be beneficial for separation processes. However, the SEM cross-sectional analyses of the cellulose did not show a highly porous structure. It can be clearly seen that there is a bead like structure in the micro-scale. However, it has to be noted that the cross section of the films were done from dry specimen by embedding in epoxy resin followed by microtomy. However, cellulose films, even those that are hydrophobized may undergo swelling which may allow for mass transport throughout the membrane to some extent. Further characterization of the specific surface area and pore size distribution using N2 gas adsorption did not give any meaningful results (i.e. lowly porous

structures with SSA< 5m^2/g). Interestingly, cellulose films derived from the Lyocell process exhibit a similar structure than the films produced in the present work. [26]

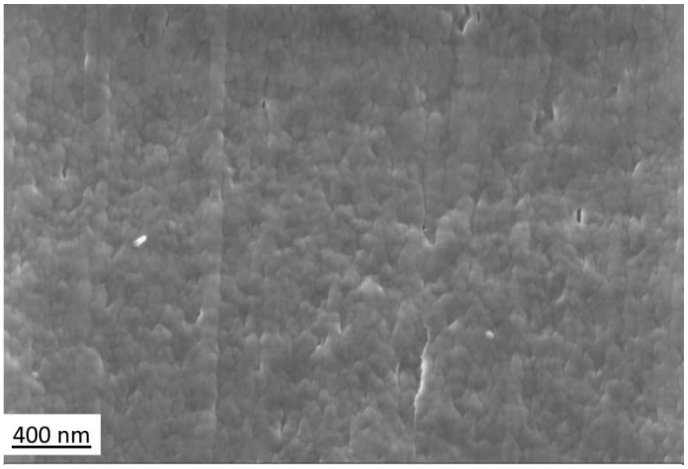

Figure 3. Representative SEM cross-sectionalimage of the unmodified cellulose film

Characterization of the feed- and stripping phase

Besides the concentration of LS, it is crucial to know the molecular weight distribution or the hydrodynamic diameter thereof in the feed and the stripping phase.

Table 3 summarizes the range of the molecular fractions, detected by DLS for all extraction experiments. For experiments performed with the model feed, the starting material already had a narrow molecular weight distribution, which was related to the manufacturing process of LS, i.e. ultrafiltration. The hydrodynamic diameter of the Ca-LS feed solution was between 180 and 420 nm. With this starting material clearly no fractionation could be observed, the determined hydrodynamic diameter in the stripping solution validates this assumption.

The DLS measurement of the technical feed phase showed two peaks, the particle size of the first fraction was in a range between 160 and 360 nm and the second fraction was in the range of 950 and 4000 nm. To verify the results measurements were repeated after a sedimentation time of 2 hours and still two peaks and hence two fractions were clearly seen. After the extraction experiment just one peak, the smaller fraction appears in the stripping phase. While the cellulose films completely discriminated

the larger fraction, the smaller fraction preferably passed the cellulose film and appeared in the extractant and later in the stripping phase.

Table 3. Hydrodynamic diameter of LS in the feed and the stripping phase.

		Particle size nm^{-1}	
Solution	**Sample**	**range**	**range**
Technical feed (SAPPI)		160 - 360	950 - 4000
	cellulose	190 - 880	-
	HMDS, 20h	300 - 800	-
	TFAA + Ac2O 3h	240 - 800	-
Modeled feed (Ca-LS)		180 - 420	-
	cellulose unterated	200 - 650	-
	HMDS	170 - 360	-
	TFAA + Ac2O 3h	280 - 540	-

Extraction experiments

Lignosulfonates act as emulsion stabilizers, the extraction thereof in conventional equipment is hence because of the formation of stable emulsions or in the case of the treatment of an aqueous process stream additionally of crud formation, not possible. The presented approach uses cellulose films as rigid surfaces to prevent crud – and emulsion formation, while the lignosulfonates are extracted.

Equation 1 and 2 summarize the proposed reaction mechanism for the lignosulfonate extraction and the back-extraction thereof using amines (R_3N). In literature two mechanisms, co and for counter transport, are described, while counter transport is achieved if chloride ions are present in the feed and the stripping phase, in the present case co-transport of lignosulfonates (LS^-) is predominant. [3], [7], [27]

$$LS^- + H^+ + \overline{R_3N} \leftrightarrow \overline{R_3NH^+LS^-} \qquad \text{Equation 1}$$

$$\overline{R_3NH^+LS^-} + NaOH \leftrightarrow \overline{R_3N} + LSNa_n + H_2O \qquad \text{Equation 2}$$

Emulsion- or crud formation depends on the pH-value, at low pH-values emulsion- or crud formation is more likely than at high pH values. [28] The extraction hence is the crucial process step, as the back-extraction is performed with NaOH at a pH of 13.

Figure 4 shows the crud formation in the direct two phase contact during phase equilibria measurements at two different pH values.

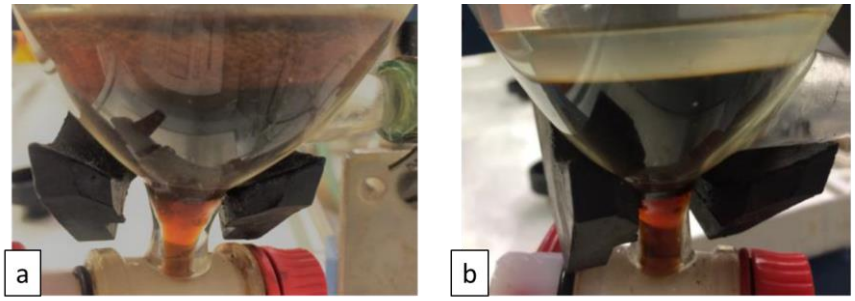

Figure 4. a) Emulsion /crud formation of xy at pH 3.6 b) Emulsion /crud formation of xy at pH 12

Table 4 summarizes the mass transfer results for the performed experiments. While the untreated cellulose films had a hydrophilic character, the modified cellulose films were hydrophobic, the cellulose wass hence either wetted with the aqueous or with the organic phase. None of the performed experiments led to emulsion or crud formation (see Figure 1a). For the mass transfer similar results for both, the hydrophilic and the hydrophobic cellulose films was assumed, as just the contact point between the feed and the extractant phase changed. Because of the small mass transfer area, the resulting concentrations in the stripping solution were lower. However, the measured lignosulfonate concentrations were in the same range for all experiments. The phase ratio of the aqueous feed and the organic extractant phase was 1:1 by volume, by transferring this approach to liquid membrane permeation this ratio can be drastically reduced and if stirring is applied too, higher mass transfer would be expected. [4]

Table 4. Results for the extraction experiments for the technical and the modeled feed and the different tested cellulose films. Data summarized are after 48 hours of extraction time. T = 25°C, ambient pressure, $c_{LS,initial}$ = 88.0 $g \cdot l^{-1}$

Solution	Sample	Phase	c_{LS} /g·l^{-1}
Technical feed (SAPPI)	cellulose untreated	Feed	84.6
		Stripping	1.19
	HMDS	Feed	84.6
		Stripping	1.22
	TFAA + Ac_2O 3h	Feed	80.5
		Stripping	1.37
Modeled feed (Ca-LS)	cellulose unterated	Feed	101.7
		Stripping	0.98
	HMDS	Feed	101.8
		Stripping	0.94
	TFAA + Ac_2O 3h	Feed	96.0
		Stripping	0.96

To ensure 100% back-extraction of the lignosulfonates a phase ration of 1:3 by volume (extractant phase:stripping phase) was used. [7]

Sugar extraction

For the experiment using the technical feed solution also the sugar concentration in both, the feed and the stripping phase was determined. As expected, the sugar concentration remained stable in the feed phase, and no sugars were detected in the stripping phase. In general, analysis of lignosulfonate containing streams is tricky, therefore, these findings were verified with an extraction experiment using a pure glucose feed stream, under the same conditions as for the other extraction experiments. The feed consisted of 10 g·/L glucose, but in the stripping phase glucose could not be detected by HPLC.

Conclusions

In order to use lignosulfonates as raw material for renewable based products, they need to have a defined quality, i.e. impurities such as hemicellulose or acids should not be present. Further, a narrow molecular weight distribution is preferred. The solubility of LS throughout the whole pH range and their ability to stabilize emulsions, makes extractive isolation challenging. However, extraction provides the

possibility to enhance the selectivity and even lignosulfonate fractionation is reported. We demonstrated that the used support layers made from cellulose are capable to prevent emulsion or crud formation. The support was further modified via the gas phase to characterize the influence of the surface properties on emulsion formation and on the mass transfer. Further, the results show that simultaneous selective lignosulfonate extraction and fractionation can be realized. The experiments were carried out in a u-tube setup with a mass transfer area of 2.27 cm^{-2}. The small membrane area led to small mass transfer, however, as conventional extraction cannot be applied for the isolation of lignosulfonates, the obtained results are very promising with respect to the requirements on lignosulfonate to serve as raw material for future applications and products.

Funding and disclosure

There are no financial conflicts of interest to disclose.

References

[1] A. Ortner, K. Hofer, W. Bauer, G. S. Nyanhongo, and G. M. Guebitz, "Laccase modified lignosulfonates as novel binder in pigment based paper coating formulations," *React. Funct. Polym.*, vol. 123, pp. 20–25, 2018.

[2] T. Aro and P. Fatehi, "Production and Application of Lignosulfonates and Sulfonated Lignin," *ChemSusChem*, vol. 10, pp. 1861–1877, 2017.

[3] K. Chakrabarty, K. V. Krishna, P. Saha, and A. K. Ghoshal, "Extraction and recovery of lignosulfonate from its aqueous solution using bulk liquid membrane," *J. Memb. Sci.*, vol. 330, no. 1, pp. 135–144, 2009.

[4] K. Chakrabarty, P. Saha, and A. K. Ghoshal, "Separation of lignosulfonate from its aqueous solution using emulsion liquid membrane," *J. Memb. Sci.*, vol. 360, no. 1, pp. 34–39, 2010.

[5] C. K. Xian, N. Othman, N. Harruddin, N. A. Nasruddin, and Z. Y. Ooi, "Extraction of lignosulfonate using TOA-kerosene-PVDF in supported liquid membrane process," *J. Teknol. (Sciences Eng.)*, vol. 67, no. 2, pp. 59–63, 2014.

[6] K. Chakrabarty, P. Saha, and A. K. Ghoshal, "Separation of lignosulfonate from its aqueous solution using supported liquid membrane," *J. Memb. Sci.*, vol. 340, no. 1, pp. 84–91, 2009.

[7] A. K. Kontturi and G. Sundholm, "The Extraction and Fractionation of Lignosulfonates with Long Chain Aliphatic Amines," *Acta Chem. Scand. A*, vol. 40, pp. 121–125, 1986.

[8] O. Ringena, B. Saake, and R. Lehnen, "Isolation and fractionation of lignosulfonates by amine extraction and ultrafiltration: A comparative study," *Holzforschung*, vol. 59, pp. 405–412, 2005.

[9] P. K. Parhi, "Supported liquid membrane principle and its practices: A short review," *J. Chem.*, vol. 2013, 2013.

[10] P. Dżygiel and P. P. Wieczorek, "Supported Liquid Membranes and Their Modifications: Definition, Classification, Theory, Stability, Application and Perspectives," in *Liquid Membranes*, V. Kislik, Ed. Amsterdam: Elsevier, 2010, pp. 73–140.

[11] M. Kienberger, M. Hackl, and M. Siebenhofer, "Emulsion Prevention with Supported Liquid Membrane Permeation," *Chem. Eng. Technol.*, vol. 41, no. 3, pp. 504–508, 2018.

[12] D. K. Owens and R. C. Wendt, "Estimation of the Surface Free Energy of Polymers," *J. Appl. Polym. Sci.*, vol. 13, pp. 1741–1747, 1969.

[13] A.-K. Kontturi, G. Sundholm, K. M. Nielsen, R. Zingales, I. Vikholm, F. Urso, J. Weidlein, and R. A. Zingaro, "The Extraction and Fractionation of Lignosulfonates with Long Chain Aliphatic Amines.," *Acta Chemica Scandinavica*, vol. 40a. pp. 121–125, 1986.

[14] I. Sumerskii, P. Korntner, G. Zinovyev, T. Rosenau, and A. Potthast, "Fast track for quantitative isolation of lignosulfonates from spent sulfite liquors," *RSC Adv.*, vol. 5, no. 112, pp. 92732–92742, 2015.

[15] G. Chinga-Carrasco, N. Kuznetsova, M. Garaeva, I. Leirset, G. Galiullina, A. Kostochko, and K. Syverud, "Bleached and unbleached MFC nanobarriers: Properties and hydrophobisation with hexamethyldisilazane," *J. Nanoparticle Res.*, vol. 14, no. 12, pp. 1–10, 2012.

[16] G. Rodionova, B. Hoff, M. Lenes, Ø. Eriksen, and Ø. Gregersen, "Gas-phase esterification of microfibrillated cellulose (MFC) films," *Cellulose*, vol. 20, no. 3, pp. 1167–1174, 2013.

[17] K. Ogura and H. Sobue, "Studies on the derivatives of sodium cellulose xanthan. Part I. Infrared absorption spectra and characteristic frequencies of C=S and C-S groups in sodium cellulose xanthane and its stable derivatives," *Polym. Lett.*, vol. 6, pp. 63–67, 1968.

[18] H. Dautzenberg and B. Philipp, "Über Bildungsweise und Verhalten des Natriumdicarbonats," *Zeitschrift für Anorg. und Allg. Chemie*, vol. 375, no. 2, pp. 113–208, 1970.

[19] J. Široký, R. S. Blackburn, T. Bechtold, J. Taylor, and P. White, "Attenuated total reflectance Fourier-transform Infrared spectroscopy analysis of crystallinity changes in lyocell following continuous treatment with sodium hydroxide," *Cellulose*, vol. 17, no. 1, pp. 103–115, 2010.

[20] M. Weißl, K. Niegelhell, D. Reishofer, A. Zankel, J. Innerlohinger, and S. Spirk, "Homogeneous cellulose thin films by regeneration of cellulose xanthate: properties and characterization," *Cellulose*, vol. 25, no. 1, pp. 711–721, 2018.

[21] H. M. A. Ehmann, O. Werzer, S. Pachmajer, T. Mohan, H. Amenitsch, R. Resel, A. Kornherr, K. Stana-Kleinschek, E. Kontturi, and S. Spirk, "Surface-Sensitive Approach to Interpreting Supramolecular Rearrangements in Cellulose by Synchrotron Grazing Incidence Small-Angle X-ray Scattering," *ACS Macro Lett.*, vol. 4, no. 7, pp. 713–716, Jul. 2015.

[22] T. Mohan, S. Spirk, R. Kargl, A. Doliška, A. Vesel, I. Salzmann, R. Resel, V. Ribitsch, and K. Stana-Kleinschek, "Exploring the rearrangement of amorphous cellulose model thin films upon heat treatment," *Soft Matter*, vol. 8, no. 38, pp. 9807–9815, 2012.

[23] R. L. Redington and K. C. Lin, "Infrared spectra of trifluoroacetic acid and trifluoroacetic anhydride," *Spectrochim. Acta Part A Mol. Spectrosc.*, vol. 27, no. 12, pp. 2445–2460, 1971.

[24] E. Kontturi and A. Lankinen, "Following the Kinetics of a Chemical Reaction in Ultrathin Supported Polymer Films by Reliable Mass Density Determination with X-ray Reflectivity," *J. Am. Chem. Soc.*, vol. 132, pp. 3678–3679, 2010.

[25] T. Mohan, S. Spirk, R. Kargl, A. Doliška, H. M. A. Ehmann, S. Köstler, V. Ribitsch, and K. Stana-Kleinschek, "Watching cellulose grow – Kinetic investigations on cellulose thin film formation at the gas–solid interface using a quartz crystal microbalance with dissipation (QCM-D," *Colloids Surfaces A*, vol. 400, pp. 67–72, 2012.

[26] H.-P. Fink, P. Weigel, and A. Bohn, "Supermolecular structure and orientation of blown cellulosic films," *J. Macromol. Sci. Part B*, vol. 38, no. 5–6, pp. 603–613, Sep. 1999.

[27] A.-K. Kontturi, K. Kontturi, P. Niinikoski, and G. Sundholm, "Extraction and fractionation of lignosulfonate by a supported liquid membrane," *Prog. Colloid Polym. Sci.*, vol. 88, pp. 90–95, 1992.

[28] A.-K. Kontturi and G. Sundholm, "Amine Extraction of Lignosulfonates," *Acta Chem. Scand. A*, vol. 40, pp. 121–125, 1986.

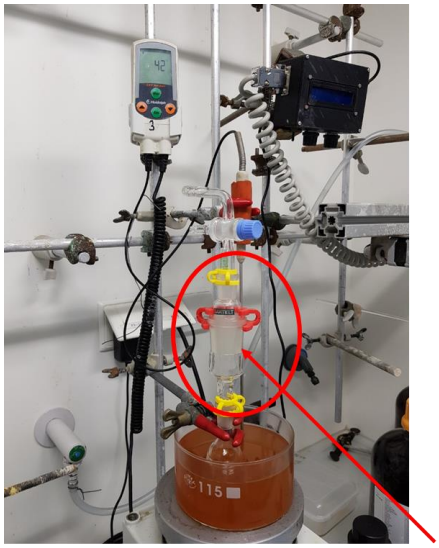

Figure 5. Experimental set-up for the modification of the cellulose films.

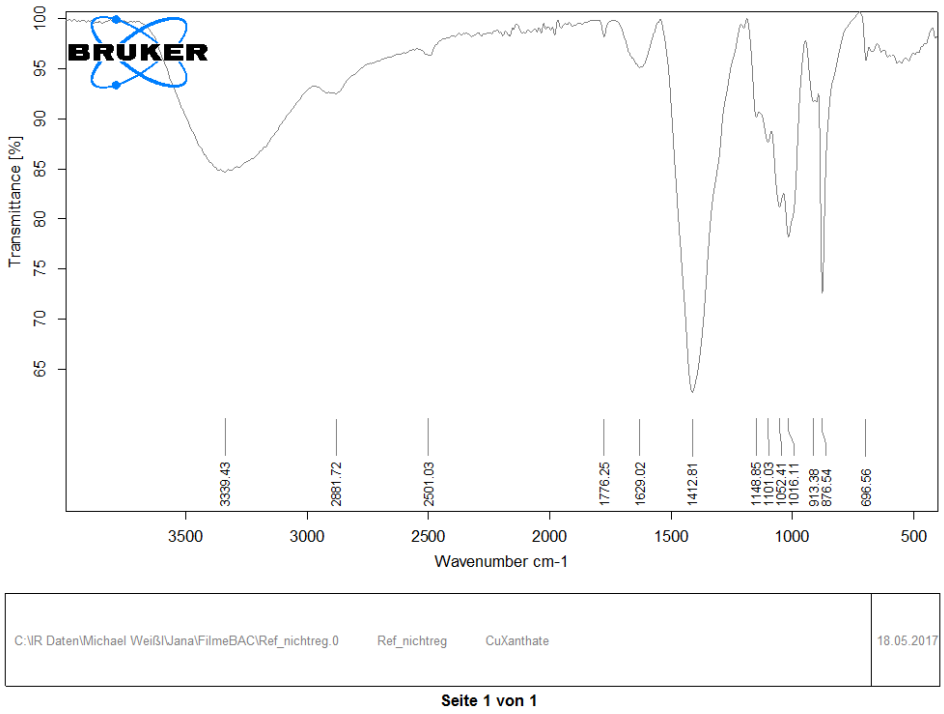

Figure 6. CX IR spectrum for CX

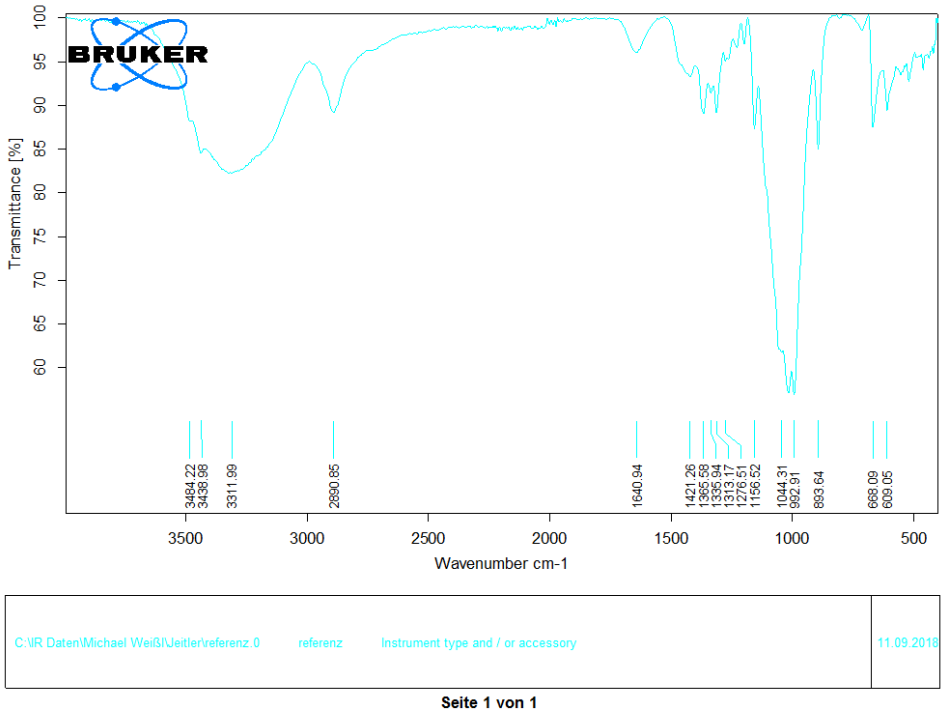

Figure 7. CX IR spectrum for the unmodified reference cellulose film

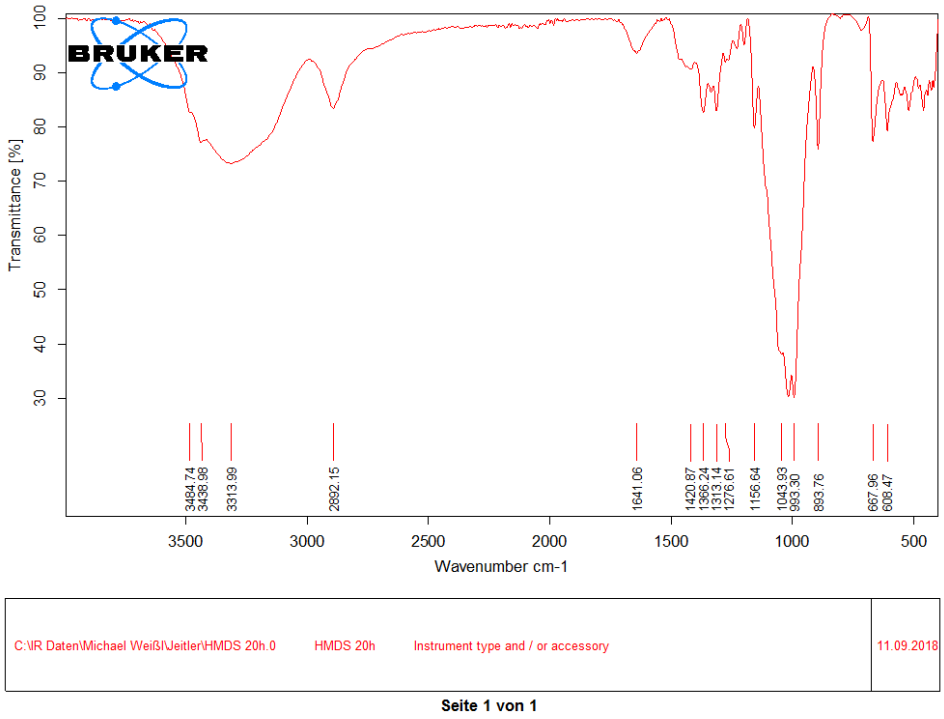

Figure 8. CX IR spectrum for the HMDS modified cellulose film

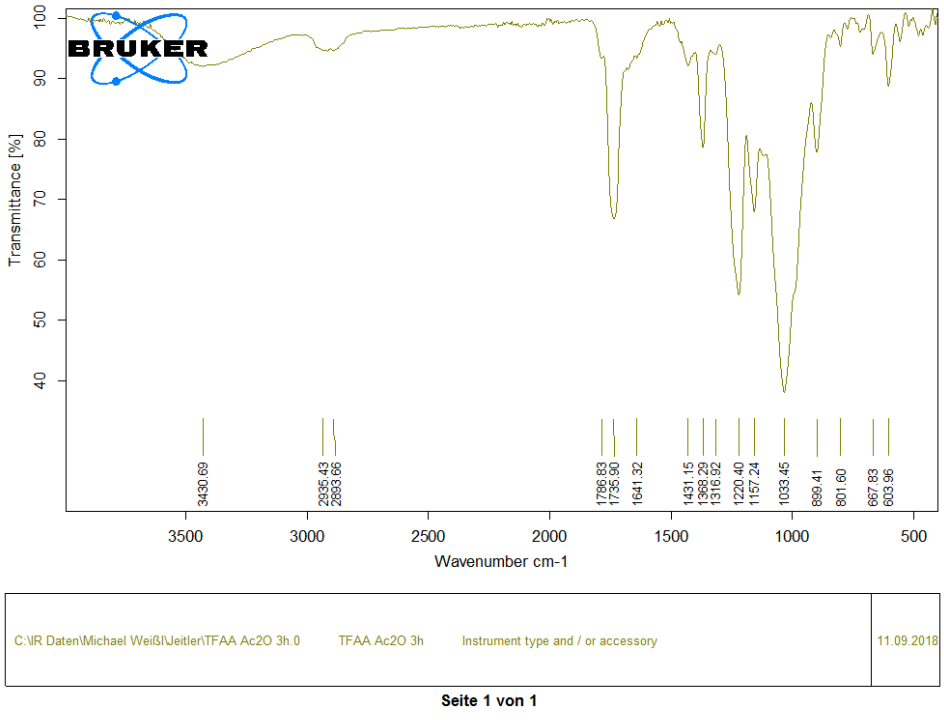

Figure 9. CX IR spectrum for the TFAA modified cellulose film

Paper #4

Homogeneous cellulose thin films by regeneration of cellulose xanthate: properties and characterization

Published in Cellulose

For this paper, I conducted most of the experiments, interpreted the data and wrote a significant part of the manuscript.

Cellulose (2018) 25:711–721
https://doi.org/10.1007/s10570-017-1576-3

ORIGINAL PAPER

Homogeneous cellulose thin films by regeneration of cellulose xanthate: properties and characterization

Michael Weißl · Katrin Niegelhell · David Reishofer · Armin Zankel · Josef Innerlohinger · Stefan Spirk

Received: 31 July 2017 / Accepted: 11 November 2017 / Published online: 15 November 2017

Abstract The preparation and characterization of cellulose thin films derived from cellulose xanthate is reported. The films are prepared by depositing alkaline aqueous solutions of cellulose xanthate onto silicon wafers, followed by a spin coating step. Depending on the xanthate concentration used for spin coating, films with 50 and 700 nm thickness are obtained. The cellulose xanthate is converted to cellulose by exposing the films to HCl vapors over a period of 20 min. The conversion is monitored by ATR-IR spectroscopy, which allows for tracking the rupture of C–S and C=S bonds during the regeneration process. The conversion is accompanied by a reduction of the film thickness of ca 40% due to the removal of the bulky xanthate group. The films feature a homogenous, but porous morphology as shown by atomic force microscopy. Further, the films were investigated towards their interaction with Bovine Serum Albumin (BSA) and fibrinogen by means of multi-parameter surface plasmon resonance spectroscopy. Similar as other cellulose thin films BSA adsorption is low while fibrinogen adsorbs to some extent at physiological pH (7.4).

Keywords Cellulose thin films · Xanthate · Vapor phase hydrolysis · Protein adsorption

Electronic supplementary material The online version of this article (https://doi.org/10.1007/s10570-017-1576-3) contains supplementary material, which is available to authorized users.

M. Weißl
Institute for Chemistry and Technology of Materials, Graz University of Technology, Stremayrgasse 9, 8020 Graz, Austria

M. Weißl · K. Niegelhell · D. Reishofer · S. Spirk (✉)
Institute for Paper, Pulp and Fibre Technology, Graz University of Technology, Inffeldgasse 23A, 8010 Graz, Austria
e-mail: stefan.spirk@tugraz.at

A. Zankel
Institute for Electron Microscopy and Nanoanalysis, NAWI Graz, Graz University of Technology and Centre for Electron Microscopy, Steyrergasse 17, 8010 Graz, Austria

J. Innerlohinger
Lenzing AG, Werkstrasse 2, 4860 Lenzing, Austria

Introduction

In recent years, cellulose thin films have attracted significant interest in both basic and applied research since they provide a confined two dimensional environment with defined morphology and chemistry (Kontturi et al. 2003, 2006, 2013). Therefore, they have been proposed as supports for biosensors, as matrix for catalysis as well as material for optoelectronic devices such as transistors and solar cells (Blomstedt et al. 2007; Filpponen et al. 2012;

Niegelhell et al. 2016; Orelma et al. 2011, 2012; Reishofer et al. 2017; Taajamaa et al. 2013; Wolfberger et al. 2015). Further, these films have been employed as models to investigate and to better understand interactions of water with cellulose, particularly in the context of cell wall structure and their relation to industrially applied drying processes (Ehmann et al. 2015; Niinivaara et al. 2015, 2016).

The strategies to prepare such films are based on three main approaches which comprise either (1) the use of cellulose suspensions, (2) the dissolution of cellulose or (3) the employment of cellulose derivatives which are converted back to cellulose after the film forming process (Kontturi et al. 2006). The advantage of using suspensions is to avoid the use of organic solvents but the obtained films are not completely flat due to the (nano)fibrous or particulate nature of the cellulosic starting materials. In contrast, the preparation of cellulose thin films derived from dissolved cellulose requires tedious dissolution procedures (e.g. DMA/LiCl or ionic liquids) (Kargl et al. 2015). Additionally, the solvent (and/or salt) needs to be removed from the films, which necessitates extensive washing procedures of the films. An elegant method to prepare cellulose thin films overcoming these problems has been introduced by Klemm in 1993 and further developed by Kontturi in the beginning of the century. (Kontturi et al. 2003; Schaub et al. 1993) The method employs an acid labile organosoluble cellulose derivative, trimethylsilyl cellulose (TMSC), which is converted to cellulose after processing by simple exposure to HCl vapors. Since the whole process runs via gas phase reaction and since only volatile side products are formed, washing steps are not necessary. In addition, the solubility of this cellulose derivative can be tuned by variation of the DS_{TMS} and therefore allows easy manufacturing, e.g. by spin coating, the most common thin film formation technique. The films obtained by this process are smooth and featureless with RMS roughnesses of down to 1.5 nm as determined by atomic force microscopy. However, although TMSC is a commercial cellulose derivative, whose production is in principle scalable, it is a rather expensive material. Although eco-solvents such as ethyl acetate have been proposed as solvents for TMSC, the use of an aqueous cellulose solution for film formation would be desirable (Wolfberger et al. 2014, 2015).

In this context, a widely used, water soluble cellulose derivative, which can be easily converted back to cellulose, is cellulose xanthate (CX). CX has been first prepared already in the end of the nineteenth century and was since then used as a soluble cellulose derivative for the production of regenerated fibers and films. In a typical fiber/film producing process, the xanthates are regenerated by immersion in an acidic bath which in addition contains some additives to improve fiber/film properties. Nowadays, the market for viscose based products is steadily increasing by ca 10% year whereas specialities become more and more attractive to manufactures (Götze 1951; Hämmerle 2011).

For all these reasons, we became interested whether cellulose xanthate can be employed for the formation of thin cellulose films having film thicknesses below 100 nm. Cellulose thin films from TMSC have shown potential for some applications but the use of CX as starting material may lead to new materials with interesting properties while being biobased and scalable to large quantities. The resulting films could then either be converted by simple immersion in an acidic bath to regenerate the cellulose or to expose them to an acidic atmosphere (e.g. HCl) similar to TMSC films. In the following, we report our approach to prepare such films starting from different concentrations of cellulose xanthate in aqueous alkaline solutions and their influence on film properties.

Experimental

Materials

A cellulose xanthate (CX) stock solution (10 wt%, gamma: 52, NaOH: 6%, degree of polymerization: 550) was provided by Lenzing AG (Lenzing, Austria) and used without any further treatment. CX solutions with 0.75, 1.0, 1.5, 2.0, 2.5, 3.0 and 4.0 wt% were prepared by adding de-ionized water from an Elga PURELAB Prima (Bucks, United Kingdom) water treatment system to the stock solutions. Afterwards, the solutions were vigorously mixed using a vortex shaker over a period of 30 s, followed by a filtration step. Sulfuric acid (95 wt%) and hydrochloric acid (37 wt%) were purchased from VWR Chemicals and hydrogen peroxide (30 wt%) from Sigma–Aldrich. Silicon wafers, glass slides (Roth), Au-coated glass

slides as substrate (SPR102-AU), Filter Chromafil Xtra PVDF-45/25 0.45 μm were used as obtained. BSA and fibrinogen were purchased from Sigma, Aldrich.

Cellulose thin film preparation

As substrates for the cellulose films, single side polished silicon wafers from Siegert Wafers (Aachen, Germany, wafer thickness: 675 ± 25 μm, 1 cm × 1 cm) and gold coated glass slides from BioNavis (Tampere, Finland, gold layer thickness: 50 nm, 1 cm × 2 cm) were used. The slides were cleaned by dipping them into piranha acid [H_2SO_4:-H_2O_2 = 3:1 (v/v)] for 30 min (10 min for gold slides) and intensely washed with MilliQ water afterwards.

For spin coating, 80 μl of viscose solution (per square centimeter substrate) were deposited onto the surfaces and subjected to spin coating (a = 2500 rpm s^{-1}, v = 4000 rpm, t = 60 s). Afterwards, the thin films were stored at room temperature overnight, followed by regeneration of the deposited CX layers in vaporous HCl atmosphere (created from concentrated hydrochloric acid). During the regeneration procedure, the HCl was deposited into a petri dish, and the substrates were positioned above the liquid HCl phase in another petri dish. A third petri dish was used as a lid to close the system. After 20 min exposure to the gaseous HCl atmosphere, regeneration of the cellulose xanthates to cellulose is accomplished as proven by ATR-IR spectroscopy. Afterwards, the films were rinsed twice with water (3 ml) followed by drying in a stream of dry nitrogen.

Optical microscopy

Light microscopy investigations were carried out on an Olympus BX60 fitted with an Olympus E-520 camera. Prior to investigating the samples, carrier substrates were fixed on a glass layer.

Profilometry

The layer thickness was determined with a Bruker DekTak XT surface profiler. The scan length was set to 1000 μm over the time duration of 3 s with the hills and valleys scanning profile. The diamond stylus had a radius of 12.5 μm and the employed force was 3 mg. The measured profile was then used to determine the thickness. Each layer thickness has been determined by averaging 6 measurements on three different slides.

Attenuated total reflection: infrared spectroscopy

The infrared spectra were recorded with an ALPHA FT-IR spectrometer (Bruker; Billerica, MA, U.S.A.). For the measurement, an attenuated total reflection (ATR) attachment was used with 64 scans at a resolution of 4 cm^{-1} and a scan range between 4000 and 400 cm^{-1}. The samples were prepared on Au-coated glass slides (SPR102-AU). The data were analyzed with OPUS 4.0 software.

Atomic force microscopy

The atomic force microscopy (AFM) images were recorded in tapping mode with a Veeco Multimode Quadrax MM AFM (Bruker; Billerica, MA, USA). For the measurements silicon cantilevers (NCH-VS1-W from NanoWorld AG, Neuchatel, Switzerland; Coating: none) with a resonance frequency of 297 kHz were used. All measurements were performed under ambient atmosphere and at room temperature. The image processing and the calculation of the root mean square roughness (calculated from 2 μm × 2 μm and 10 μm × 10 μm images) were done with the Nanoscope software (V7.30r1sr3; Veeco).

Contact angle and surface free energy determination

For the calculation of the surface free energy (SFE) Milli-Q water (≥ 18 MΩ cm^{-1}) and diiodomethane were employed as test liquids. The drop shape analysis was done in the sessile drop modus at 25 °C with a DSA100 system (Krüss GmbH, Hamburg, Germany) equipped with a T1E CCD video camera (25 fps). The dispense rate of the 3 μl droplets was adjusted to 166 μl/min and the time before the image was captured was set to 2 s. Each sample was measured at least three times. The contact angle (CA) calculations (software: DSA1 v 1.90) were performed with the Young–Laplace equation and the surface free energy calculation with the Owens–Wendt–Rabel and Kaelble method (Owens and Wendt 1969).

Scanning electron microscopy: energy-dispersive X-ray spectroscopy

An ESEM Quanta 600 FEG (FEI, Eindhoven, NL) scanning electron microscope was utilized to examine the surface structure during different steps of film preparation. To gain electrical conductivity a 15 nm thick carbon layer was vaporized on the film surface before. Images were recorded in the high vacuum mode either with secondary electrons (ETD Everhart–Thornley detector, giving topographic contrast) or with backscattered electrons (SSD: Solid State Detector, delivering compositional contrast).

Multi parameter surface plasmon resonance spectroscopy

MP-SPR spectroscopy was accomplished with a SPR Navi 200 from Bionavis Ltd., Tampere, Finland, equipped with two different lasers (670 and 785 nm, respectively) in both measurement channels, using gold-coated glass slides as substrate (gold layer 50 nm). All measurements were performed using a full angular scan (39°–78°, scan speed: 8° s^{-1}). Protein adsorption was investigated with Bovine Serum Albumin (BSA) (1 mg ml^{-1}) and fibrinogen (FIB) (1 mg ml^{-1}) both in a 100 mM NaCl solution containing 10 mM PBS at pH 7.4. Flow was adjusted to 50 µl min^{-1} for 5 min at 25 °C. Each measurement was repeated 3 times at least. BioNavis Dataviewer software was used for processing all two wavelength SPR experiments (Scheme 1).

Results and discussion

In a first step, the film formation properties of CX solutions by spin coating were investigated as a function of the CX concentration. It turned out that the CX concentration must be in a range between 0.75 and 4.0 wt% to obtain homogenous films on the different substrates (i.e. Si-wafer, glass slides, gold coated glass slides). Below concentrations of 0.75 wt% CX incompletely covered films were obtained, whereas above 4.0 wt% CX fully covered but inhomogeneous films having a wide range of defects were observed (data not shown). After deposition by spin coating, the solid CX films were regenerated using HCl. When the films were immersed in aqueous 3 M HCl, the films peeled off the substrate; therefore this method was not investigated in further detail. In contrast, the exposure to HCl vapors created from concentrated hydrochloric acid led to the regeneration of the CX to cellulose. The regeneration of the CX can be observed by naked eye, particularly when glass slides were employed as substrates. On these films, the yellow CX film steadily decolorizes with time concomitant with the formation of a white particle like coverage on the surface. This white material corresponds to the formation of salt crystals composed of NaCl (obtained as side product by reaction of the sodium xanthate and HCl) and can be easily removed by rinsing the films with water after regeneration (see AFM section). As expected, the higher the concentration of the CX solution used for film preparation was, the more pronounced the formation of this residue was.

The layer thickness of the CX films gradually increased with increasing CX concentration from 31 ± 3 (0.75 wt%) to 688 ± 10 nm (4.0 wt%). One would expect that the films significantly shrink during regeneration since the xanthate group is rather bulky and hydrogen bond formation would lead additionally to densification of the films as known for related cases involving other cellulose derivatives such as TMSC (Kontturi et al. 2011; Mohan et al. 2012). However, directly after exposure of the films to HCl vapors, the opposite phenomenon was observed. Some films showed an increase in film thickness or did not change significantly which relates to the formation of NaCl, which certainly does not only form on the surface but also in the interior of the film. After removal of NaCl from the films by rinsing with water, the film thickness reduced significantly. Finally, pure cellulose films with film thicknesses between 21 ± 2 and 413 ± 11 nm were manufactured. It is of interest that the film with the smallest layer thickness showed just 23% of shrinking whereas for all the other films shrinkage was between 40 and 44% (Fig. 1). Similar observations have been made when studying the film thickness reduction during regeneration of TMSC; obviously the substrate limits the shrinking and densification of the films to some extent (Ehmann et al. 2015). Afterwards, the films were subjected to a drying procedure at 105 °C over a period of 1 h. The films showed a slight shrinkage whereas here the thinnest films were affected to a larger extent (17% layer thickness decrease) than the thicker ones (few

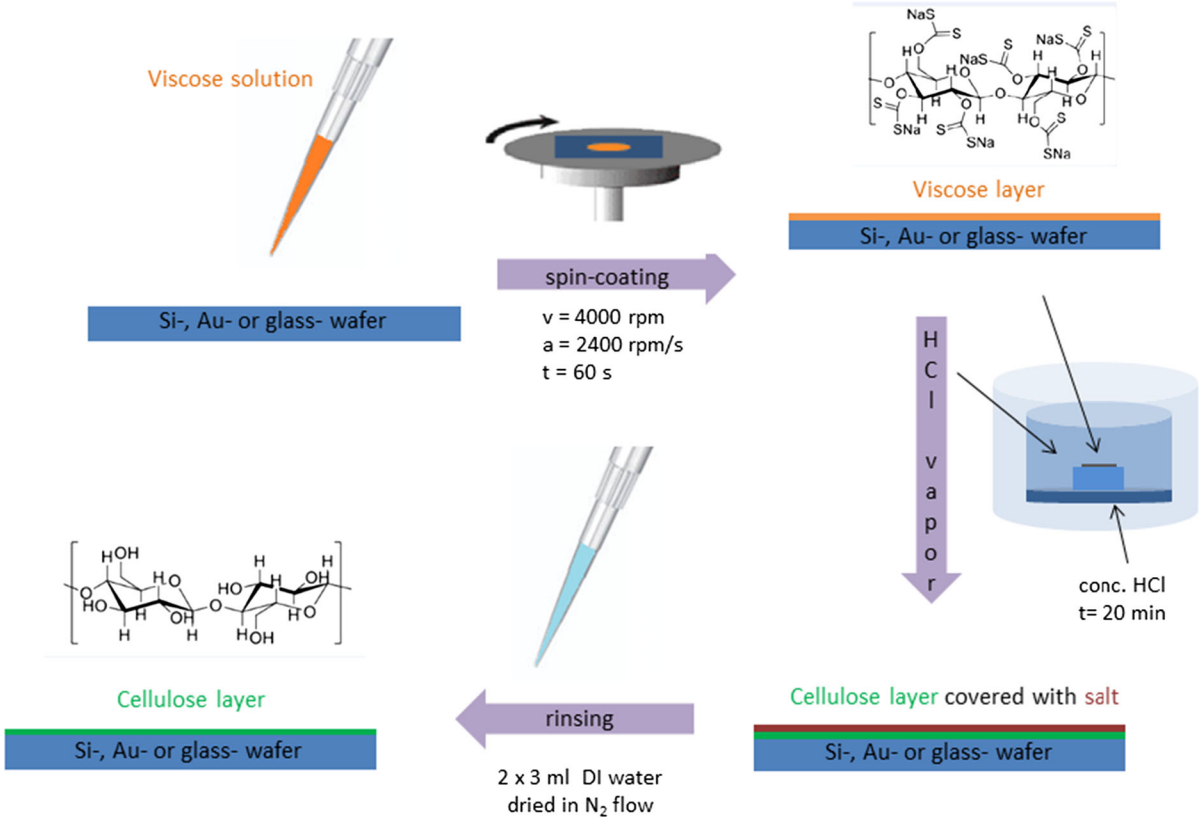

Scheme 1 Cellulose thin film production based on aqueous cellulose xanthate ('Viscose') solutions

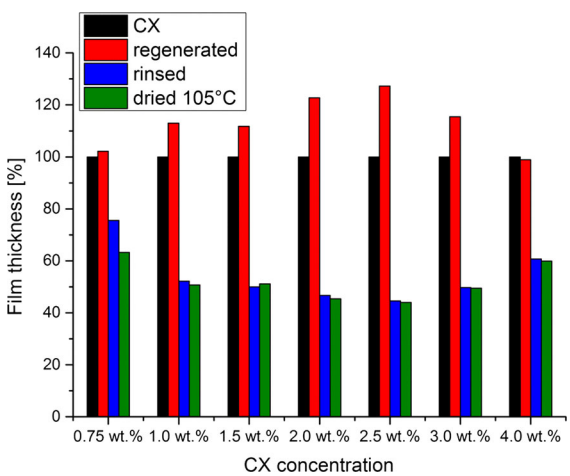

Fig. 1 Film thickness changes [%] in dependence of process parameters

percent decrease). An overview on the layer thickness data is provided in Table 1.

A commonly used method to monitor chemical reactions of cellulose derivatives is IR spectroscopy. A complication in the IR spectroscopic analysis of the CX films arises from the tendency of CX to decompose at ambient conditions. In the case of CX thin films, the IR spectra indicated that significant amounts of CX decomposition products had been formed after spin coating. The decomposition products can be identified as CS_2 ($\nu_{C=S}$ at 1520 cm^{-1}), sodium sulfide (1420, 920 cm^{-1}) and sodium trithiocarbonate (1670, 1427, 925 and 885 cm^{-1}) and, in traces, H_2S (ν_{S-H} at 2630 cm^{-1}, Fig. S7, Supporting Information). The remaining bands at 1452 and 1382 cm^{-1} as well as a weak band at 2725 cm^{-1} can be assigned to NaOH, which is present in the films stemming from the dissolution of CX (Andrews et al. 1960; Dautzenberg and Philipp 1970; Ogura and Sobue 1968). Since NaOH is highly hygroscopic, the water peak at 1640 cm^{-1} is pronounced as well. The C–S and C=S vibrations for the CX have been reported in the range between 1050 and 1250 cm^{-1} and interfere with the decomposition products as well as with vibrations at the pyranose ring, which also show absorption bands

Table 1 Comparison of the layer thickness d [nm] of the films depending on initial CX concentration by stylus force profilometry

	CX	After 20 min HCl	Rinsed	Dried 105 °C
0.75 wt%	31 ± 3	31 ± 3	24 ± 2	20 ± 2
1.0 wt%	51 ± 3	58 ± 2	30 ± 3	29 ± 1
1.5 wt%	103 ± 2	115 ± 3	58 ± 1	59 ± 1
2.0 wt%	167 ± 2	205 ± 6	96 ± 3	93 ± 2
2.5 wt%	243 ± 5	309 ± 6	138 ± 3	136 ± 2
3.0 wt%	401 ± 4	463 ± 7	230 ± 3	229 ± 2
4.0 wt%	688 ± 10	680 ± 8	413 ± 11	407 ± 10

in this range. Therefore, an unambiguous assignment is not possible (Fig. 2).

During ongoing regeneration, all bands related to C=S and C–S vibrations as well as the NaOH disappear and a cellulose II like spectrum is obtained. It seems that the HCl treatment leads to partial oxidation of the film surface since a weak band at 1762 cm^{-1} characteristic for C=O vibrations in COOH of oxidized cellulose is observed. Washing the films with water removes the water soluble oxidized cellulose fragments and pure cellulose II films are obtained. This is featured by broad bands from 3600 to 3100 cm^{-1}(ν_{OH}) and from 3000 to 2850 cm^{-1} (C–H stretching vibrations), a series of small weak bands in the region of 1430–1150 cm^{-1} (C–O–H bending at 1430 cm^{-1}, C–H deformation at 1372 cm^{-1}, OH in plane deformation at 1330 and at 1200 cm^{-1}), a strong and overlapping bands from 1160 to 950 cm^{-1} (asym. C–O–C vibration at 1155 cm^{-1}, sym. C–O vibration at 1060 cm^{-1} and C–O stretching at 1035 cm^{-1}) and a small band at 899 cm^{-1} (C–O–C valence vibration) (Široký et al. 2010). Additionally, the spectra of the regenerated CX films show a band at 1640 cm^{-1} indicating adsorbed water.

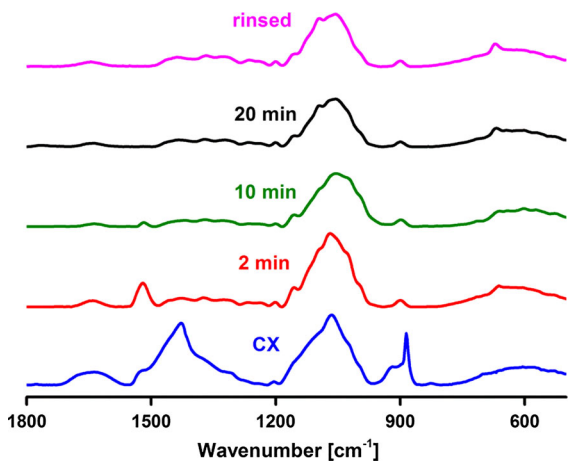

Fig. 2 Smoothed ATR-IR spectra of the 600–2000 cm^{-1} region of cellulose xanthate films (prepared from a 3 wt% solution of CX) during the exposure to HCl vapors. The original spectra for the individual exposure times showing the full range can be found in the Supporting Information (Figs. S7–S10)

When the CX thin films are stored over a period of 14 days, hydrolysis reactions take place. The intensity of the IR bands at 885, 920, 1427 and 1670 cm^{-1} (corresponding to the sodium trithiocarbonate) decrease, while the intensity of the bands corresponding to the major decomposition products of sodium sulfide and trithiocarbonate, namely sodium carbonate and sodium hydroxide become more intense (1770, 1458, 1378 cm^{-1}: Na_2CO_3, 1452, 1382: NaOH, Fig. S11, Supporting Information) (Ingram and Toms 1957). In addition, the CX partially hydrolyzes as well since the intensity of the bands in the 1000–1250 cm^{-1} changed as well.

The morphology of the films shows a rather homogeneous surface structure, which is altered by the concentration used for film preparation. In general, an increase of the concentration of CX solutions used for the preparation of the films leads to surfaces with higher RMS roughness (R_q) values. Figures 3 (10 × 10 μm^2) and 4 (2 × 2 μm^2) depict two different types of films, one prepared from 2.5 wt% (Figs. 3a–d, 4a–d) and the other from 1.5 wt% (Figs. 3e–h, 4e–h) CX solutions. It can be clearly seen that the surfaces feature much higher R_q values for the 2.5 wt% films (6.9 nm) than for the 1.5 wt% ones (3.0 nm). The exposure of the films to HCl vapors leads to a significant increase in roughness to 24 and 28 nm, respectively. However, this increase in roughness is not related to rough cellulose surfaces but to the formation of NaCl particles on the surfaces. As already indicated for the profilometry results, more particles

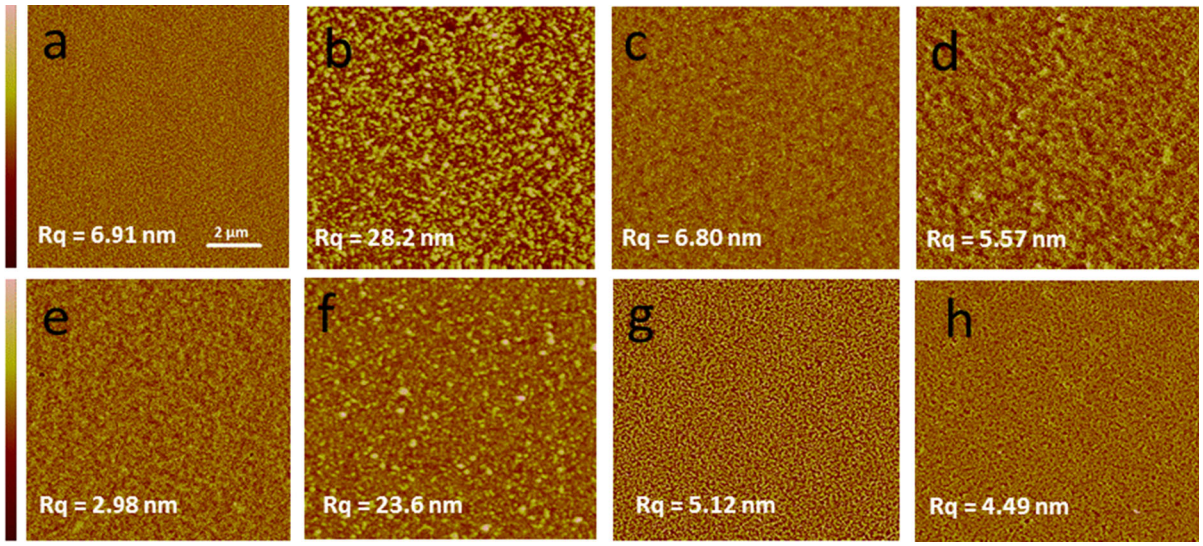

Fig. 3 AFM images (10 × 10 µm^2) and corresponding RMS roughness of different steps in cellulose thin film processing with a 2.5 wt% (upper row) and a 1.5 wt% (lower row) CX solution. The images show the films directly after spin coating (**a**, **e**), after 20 min lasting exposure to HCl atmosphere (**b**, **f**), after rinsing with de-ionized water (**c**, **g**) and after drying for 1 h at 105 °C (**d**, **h**). Z-scale is 100/200/50/50 nm for (**a**–**d**) and 30/300/30/50 nm for (**e**–**h**)

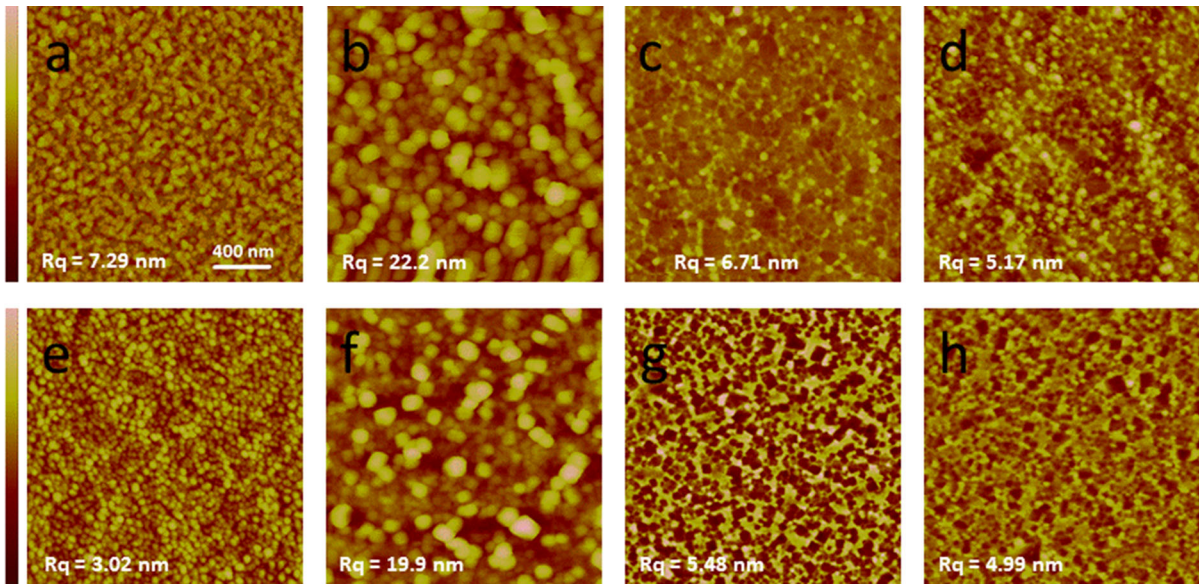

Fig. 4 AFM images (2 × 2 µm^2) and corresponding RMS roughness of different steps in cellulose thin film processing with a 2.5 wt% (upper row) and a 1.5 wt% (lower row) CX solution. The images show the films directly after spin coating (**a**, **e**), after 20 min lasting exposure to HCl atmosphere (**b**, **f**), after rinsing with de-ionized water (**c**, **g**) and after drying for 1 h at 105 °C (**d**, **h**). Z-scale is 100/200/50/50 nm for (**a**–**d**) and 30/150/100/50 nm for (**e**–**h**)

are present on surfaces with increasing CX concentration in solutions prepared for film manufacturing and indeed this can also be observed in the AFM images. When the particles are removed by simply rinsing them with water, R_q values are reduced to their initial values (6.8 and 5.1 nm), a phenomenon which has been observed for cellulose thin films derived from TMSC as well. The films exhibit homogeneous surface morphology and a subsequent drying step slightly alters the structure, thereby further reducing

the roughness values. Compared to cellophane, the macroscopic congener, the films do not exhibit a preferred orientation (see Fig. S6 for an AFM image of a cellophane film). This orientation is induced by the drawing of the films in machine direction. As a consequence, the cellophane films show different mechanical properties in machine and cross direction as well as a different hydroexpansion behavior in both directions.

To validate the chemical reactions and the changes in surface morphology appearing in the different steps of cellulose thin film processing, SEM–EDX measurements were performed. The SEM images reveal flower like structures on the surface of CX films directly after the spin coating step (Fig. 5a), which probably originate from sodium hydroxide. These structures are visible in the AFM images as well but since a smaller area was chosen, they could not be identified as separate phase. Further, the growth of crystallites during CX regeneration (Fig. 5b) is visible, which disappear after rinsing with water (Fig. 5c). EDX spectra clearly show that the crystals in Fig. 5b consist of sodium chloride. For the crystals present on the surface of untreated CX films, EDX spectra (Fig. S3–S5, Supporting Information) show a small sulfur peak in addition to the common sodium and chloride peaks. The additional sulfur peak and the different crystalline structure indicate the presence of two different crystals (sodium hydroxide and probably sodium sulfide).

An important parameter for the investigation of the surface properties of cellulose thin films is wettability. However, the determination of water contact angles on CX films could not be performed since the films were partially dissolved by water thereby giving no meaningful results while with CH_2I_2 contact angles ranging from 38° to 60° were obtained. After regeneration, the presence of NaCl particles on the surfaces prevented the measurement of the contact angles for both liquids. After rinsing the films with water, static water contact angles between 27° and 38° were determined. The drying of the films did not change the wettability with both liquids significantly. In general, these cellulose surfaces are a bit more hydrophobic than those prepared from TMSC where usually static water contact angles between 24° and 33° have been reported.

Based on this data, the surface free energies (SFE) of the surfaces were determined according to the Owens–Wendt–Rabel and Kaelble method (Kaelble 1970; Owens and Wendt 1969; Rabel 1971). This method exploits the wettability behavior of two different liquids in order to calculate the total surface free energy as well as the dispersive and polar components. In this paper, water and diiodomethane were chosen as test liquids. Figure 6 illustrates that the surface free energy decreases significantly after rinsing the films with de-ionized water. However, the following heat treatment did not have any substantial impact on the surface free energy. Taking a closer look at the decrease in SFE after the washing step reveals that the polar part of SFE energy stays constant over all process steps and only the disperse part of SFE is slightly changing (Table 2).

SPR spectroscopy is one of the methods of choice to investigate protein adsorption on thin films allowing for the evaluation of the dry adsorbed mass (adsorbed mass without coupled water) as well as the adsorption

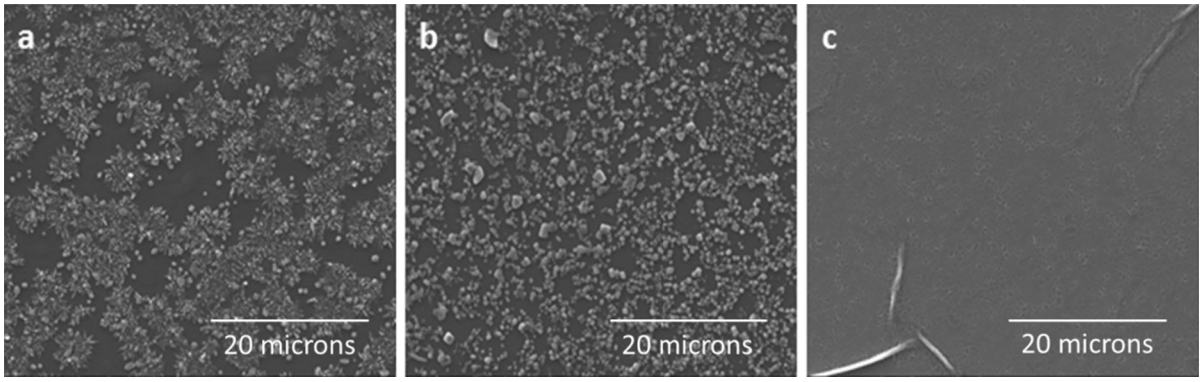

Fig. 5 SEM images displaying the film surface after **a** spin coating of 2.5 wt% CX solution, **b** regeneration of CX in HCl vapor and **c** after rinsing the film with water

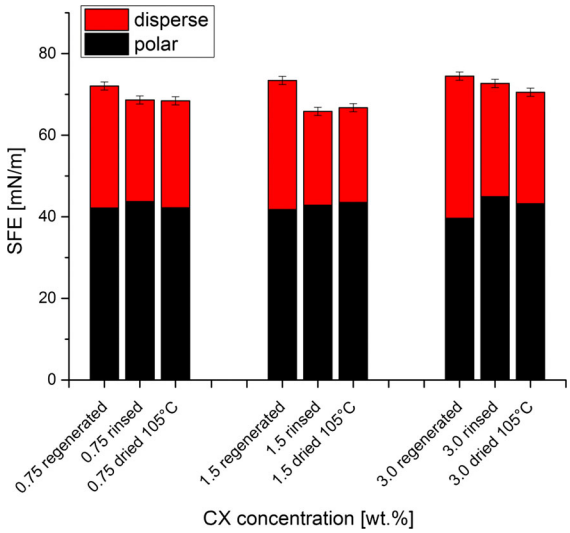

Fig. 6 Surface free energy of cellulose layers prepared from different concentrations, determined directly after film regeneration, rinsing and heat treatment

kinetics. Protein adsorption was tested using bovine serum albumin (BSA), a widely accepted marker for nonspecific protein interaction, and fibrinogen (FIB), a serum protein which plays an important role in the blood coagulation cascade (Pallister and Watson 2010). Since the herein investigated cellulose thin films are potential materials for the usage in life science applications, SPR experiments were accomplished at a pH value of 7.4 which corresponds to the pH value of human blood. The adsorption experiments were designed in a way that the films were first equilibrated for 45 min using buffer, followed by injection of the protein solutions over a period of 5 min and finalized by a subsequent rinsing step. At these conditions, the protein amount deposited (Fig. 7) on regenerated and washed films was determined to be 1.11 ± 0.18 and 0.22 ± 0.08 mg m^{-2} for FIB and BSA, respectively (Mohan et al. 2017). The preferred adsorption behavior for FIB in contrast to BSA is observed for other surfaces as well and can be attributed to the size of FIB. FIB (340 kDa) is a larger protein than BSA (66.5 kDa) and displays a larger contact area hereby increasing the extent of adsorption. Heat treatment of the cellulose films led to a decrease in the change of the SPR angle by the half which corresponds to lower protein adsorption (0.55 ± 0.07 mg m^{-2} for FIB and 0.11 ± 0.04 mg m^{-2} for BSA). The reduction in the adsorbed protein amount is accompanied with a change in surface morphology of the thin films since the wettability, another factor potentially playing a role, remains nearly constant after drying. A decrease in roughness minimizes the available surface area therefore leading to reduced interaction. There is not any noteworthy difference in adsorption kinetics (see sensograms, Fig. 7b) for all of the experiments, however it seems that proteins start to desorb even before the rinsing step is initiated (after 10 min) at the heat treated surfaces, whereas on the washed films non-bound material is only removed upon rinsing. This could be also related to the overshooting effect as described recently (Rabe et al. 2011). Different phenomena have been described in literature to explain this effect such as the Vroman effect (competition of high affinity species with low adsorption speed vs low affinity species with high adsorption rate), and the Daly and Wertz effect (change of protein conformation after adsorption). In our case it is obvious that reorientation takes place on the surfaces since both proteins under investigation can adsorb in different conformations.

Compared to other cellulosic surfaces, for instance cellulose thin films prepared from TMSC, cellulose films made from viscose offer similar protein adsorption behavior. Depending on the adsorption parameters, e.g. adsorption time, flow rate, ionic strength and others, values in the range of 0.3–0.6 mg BSA·m^{-2} determined by SPR are reported in literature.

Table 2 Static contact angle for viscose thin films in different concentrations and various steps of film production

	0.75 wt%		1.50 wt%		3.0 wt%	
	H_2O	CH_2I_2	H_2O	CH_2I_2	H_2O	CH_2I_2
CX	n. d	38 ± 1	n. d.	60 ± 2	n. d.	48 ± 2
Regenerated	25 ± 1	34 ± 1	21 ± 1	36 ± 1	15 ± 1	40 ± 2
Rinsed	34 ± 1	31 ± 1	38 ± 1	33 ± 1	27 ± 1	28 ± 1
Dried 105 °C	33 ± 1	34 ± 1	37 ± 1	32 ± 1	30 ± 1	32 ± 1

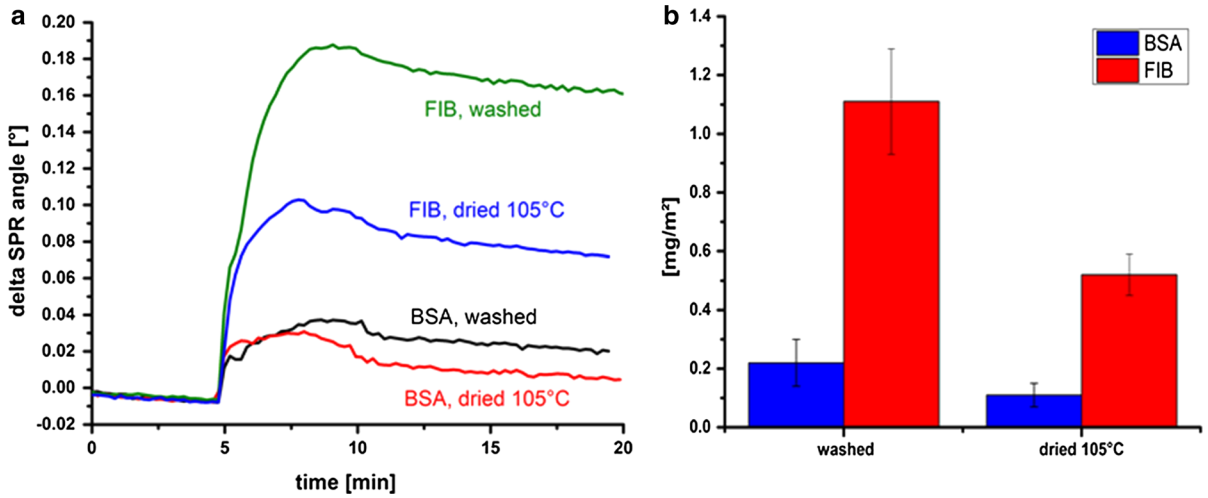

Fig. 7 670 nm sensogram recorded during the adsorption of FIB and BSA on washed and heat treated films (**a** prepared from 1 wt% CX solutions). **b** The amount of protein adsorbed on differently treated films, calculated through the change in the SPR angle via the de Feijter equation (De Feijter et al. 1978)

Conclusion

In summary, the manufacturing and properties of cellulose thin films derived from CX have been presented. These films, which may be best described as two-dimensional model systems for viscose based materials, display similar properties as other cellulosic materials in terms of wettability/surface free energy and protein interaction behavior. The use of CX as starting material offers the possibility to prepare thin films in the nanometer range from aqueous solutions in large scale whereas regeneration can be performed via the gas phase. During this reaction, volatile side products are generated and NaCl particles are formed which are easily removed by simply rinsing the films with water. Afterwards, homogenous films are obtained which show a regular but rougher and more porous surface compared to those derived from TMSC for instance. The films show similar behavior towards proteins as other cellulose matrices. In future work, we will focus how these films perform in other areas compared to those derived from other sources such as TMSC.

Acknowledgments Open access funding provided by Graz University of Technology.

References

Andrews DA, Hurtubise FG, Krassig H (1960) The presence of monothiocarbonate substituents in cellulose xanthates. Can J Chem 38:1381–1394

Blomstedt M, Kontturi E, Vuorinen T (2007) Optimising CMC sorption in order to improve tensile stiffness of hardwood pulp sheets. Nord Pulp Paper Res J 22:336–342

Dautzenberg H, Philipp B (1970) Über Bildungsweise und Verhalten des Natriumdithiocarbonats. Z Anorg Allg Chem 375:113–123

De Feijter JA, Benjamins J, Veer FA (1978) Ellipsometry as a tool to study the adsorption behavior of synthetic and biopolymers at the air–water interface. Biopolymers 17:1759–1772

Ehmann HMA, Werzer O, Pachmajer S et al (2015) Surface-sensitive approach to interpreting supramolecular rearrangements in cellulose by synchrotron grazing incidence small-angle X-ray scattering. ACS Macro Lett 4:713–716

Filpponen I, Kontturi E, Nummelin S et al (2012) Generic method for modular surface modification of cellulosic materials in aqueous medium by sequential "click" reaction and adsorption. Biomacromolecules 13:736–742

Götze K (1951) Chemiefasern nach dem Viskoseverfahren. Springer Verlag, Heidelberg

Hämmerle FM (2011) The cellulose gap. Lenz Ber 89:12–21

Ingram G, Toms BA (1957) 868. The hydrolysis of sodium trithiocarbonate and its reaction with ethanol. J Chem Soc 4328–4344

Kaelble DH (1970) Dispersion-polar surface tension properties of organic solids. J Adhes 2:66–81

Kargl R, Mohan T, Ribitsch V et al (2015) Cellulose thin films from ionic liquid solutions. Nord Pulp Paper Res J 30:6–13

Kontturi E, Thüne PC, Niemantsverdriet JW (2003) Cellulose model surfaces simplified preparation by spin coating and characterization by X-ray photoelectron spectroscopy, infrared spectroscopy, and atomic force microscopy. Langmuir 19:5735–5741

Kontturi E, Tammelin T, Österberg M (2006) Cellulose model films and the fundamental approach. Chem Soc Rev 35:1287–1304

Kontturi E, Suchy M, Penttila P et al (2011) Amorphous characteristics of an ultrathin cellulose film. Biomacromolecules 12:770–777

Kontturi KS, Kontturi E, Laine J (2013) Specific water uptake of thin films from nanofibrillar cellulose. J Mater Chem A 1:13655–13663

Mohan T, Spirk S, Kargl R et al (2012) Exploring the rearrangement of amorphous cellulose model thin films upon heat treatment. Soft Matter 8:9807–9815

Mohan T, Niegelhell K, Nagaraj C et al (2017) Interaction of tissue engineering substrates with serum proteins and its influence on human primary endothelial cells. Biomacromolecules 18:413–421

Niegelhell K, Süßenbacher M, Jammernegg K et al (2016) Enzymes as biodevelopers for nano- and micropatterned bicomponent biopolymer thin films. Biomacromolecules 17:3743–3749

Niinivaara E, Faustini M, Tanunelin T, Kontturi E (2015) Water vapor uptake of ultrathin films of biologically derived nanocrystals: quantitative assessment with quartz crystal microbalance and spectroscopic ellipsometry. Langmuir 31:12170–12176

Niinivaara E, Faustini M, Tammelin T, Kontturi E (2016) Mimicking the humidity response of the plant cell wall by using two-dimensional systems: the critical role of amorphous and crystalline polysaccharides. Langmuir 32: 2032–2040

Ogura K, Sobue H (1968) Studies on the derivatives of sodium cellulose xanthate. Part I. Infrared absorption spectra and characteristic frequencies of C–S and C=S groups in sodium cellulose xanthate and its stable derivatives. J Polym Sci Part B Polym Lett 6:63–67

Orelma H, Filpponen I, Johansson L-S et al (2011) Modification of cellulose films by adsorption of CMC and chitosan for controlled attachment of biomolecules. Biomacromolecules 12:4311–4318

Orelma H, Johansson L-S, Filpponen I et al (2012) Generic method for attaching biomolecules via avidin–biotin complexes immobilized on films of regenerated and nanofibrillar cellulose. Biomacromolecules 13:2802–2810

Owens DK, Wendt RC (1969) Estimation of the surface free energy of polymers. J Appl Polym Sci 13:1741–1747

Pallister CJ, Watson MS (2010) Haematology. Scion Publishing, Bloxham

Rabe M, Verdes D, Seeger S (2011) Understanding protein adsorption phenomena at solid surfaces. Adv Colloid Interface Sci 162:87–106

Rabel W (1971) Einige Aspekte der Benetzungstheorie und ihre Anwendung auf die Untersuchung und Veränderung der Oberflächeneigenschaften von Polymeren. Farbe Lack 77:997–1005

Reishofer D, Rath T, Ehmann HM et al (2017) Biobased cellulosic–$CuInS_2$ nanocomposites for optoelectronic applications. ACS Sustain Chem Eng 5:3115–3122

Schaub M, Wenz G, Wegner G et al (1993) Ultrathin films of cellulose on silicon wafers. Adv Mater 5:919–922

Široký J, Blackburn RS, Bechtold T et al (2010) Attenuated total reflectance Fourier-transform Infrared spectroscopy analysis of crystallinity changes in lyocell following continuous treatment with sodium hydroxide. Cellulose 17:103–115

Taajamaa L, Rojas OJ, Laine J et al (2013) Protein-assisted 2D assembly of gold nanoparticles on a polysaccharide surface. Chem Commun 49:1318–1320

Wolfberger A, Kargl R, Griesser T, Spirk S (2014) Photoregeneration of trimethylsilyl cellulose as a tool for microstructuring ultrathin cellulose supports. Molecules 19:16266–16273

Wolfberger A, Petritz A, Fian A et al (2015) Photolithographic patterning of cellulose: a versatile dual-tone photoresist for advanced applications. Cellulose 22:717–727

Supporting Information

Homogeneous cellulose thin films by regeneration of cellulose xanthate – properties and characterization

Michael Weißl[1,2], Katrin Niegelhell[2], David Reishofer[2], Armin Zankel[3], Josef Innerlohinger[4], and Stefan Spirk[2]

1) Graz University of Technology, Institute for Chemistry and Technology of Materials, Stremayrgasse 9 8020 Graz

2) Graz University of Technology, Institute for Paper, Pulp and Fibre Technology, Inffeldgasse 23A 8010 Graz

3) Institute for Electron Microscopy and Nanoanalysis, NAWI Graz, Graz University of Technology and Centre for Electron Microscopy, Steyrergasse 17, 8010 Graz, Austria

4) Lenzing AG, Werkstrasse 2, 4860 Lenzing, Austria.

Correspondence:

Stefan Spirk

stefan.spirk@tugraz.at

+43 (316) 873 – 30763

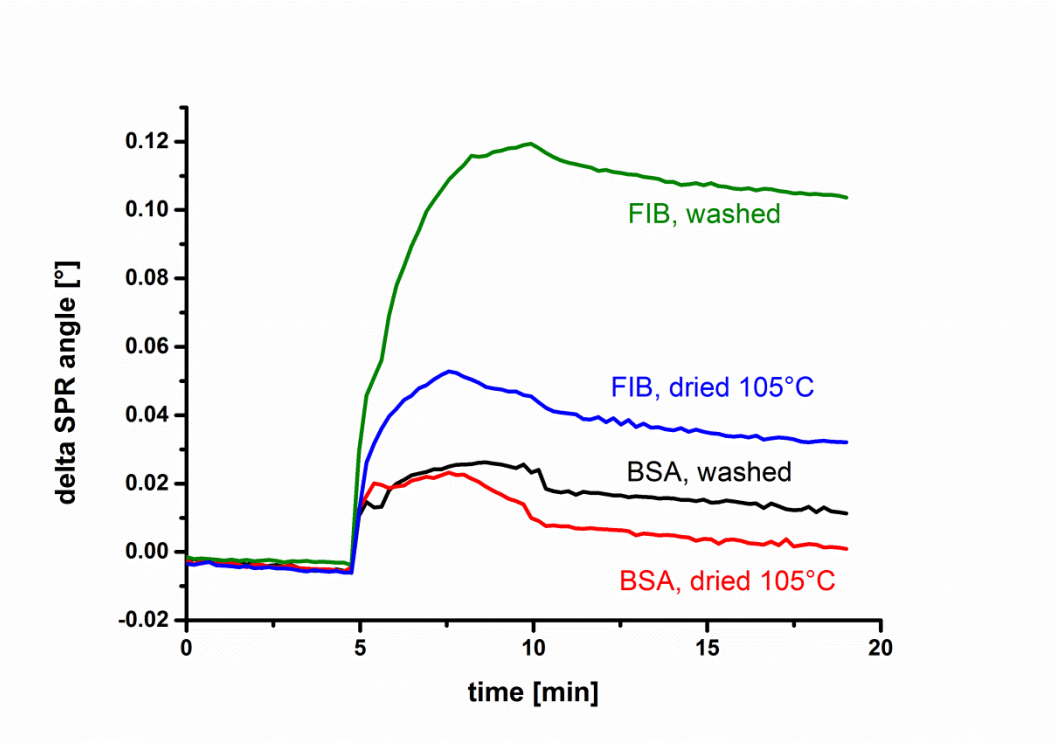

Figure S1. 785 nm sensogram recorded during the adsorption of FIB and BSA on washed and heat treated films.

Table S1. Surface roughness of cellulose thin films in different stages of processing and with variation in CX concentration during spin coating, calculated via AFM images.

	10x10 µm² images			2x2 µm² images		
	0.75 wt.%	1.50 wt.%	2.50 wt.%	0.75 wt.%	1.50 wt.%	2.50 wt.%
CX	1.5	3.0	6.9	2.0	3.0	7.3
regenerated	16.0	23.6	28.2	14.9	19.9	22.2
washed	3.8	5.1	6.8	4.1	6.9	6.7
dried at 105°C	2.9	4.5	5.6	3.0	5.0	5.2

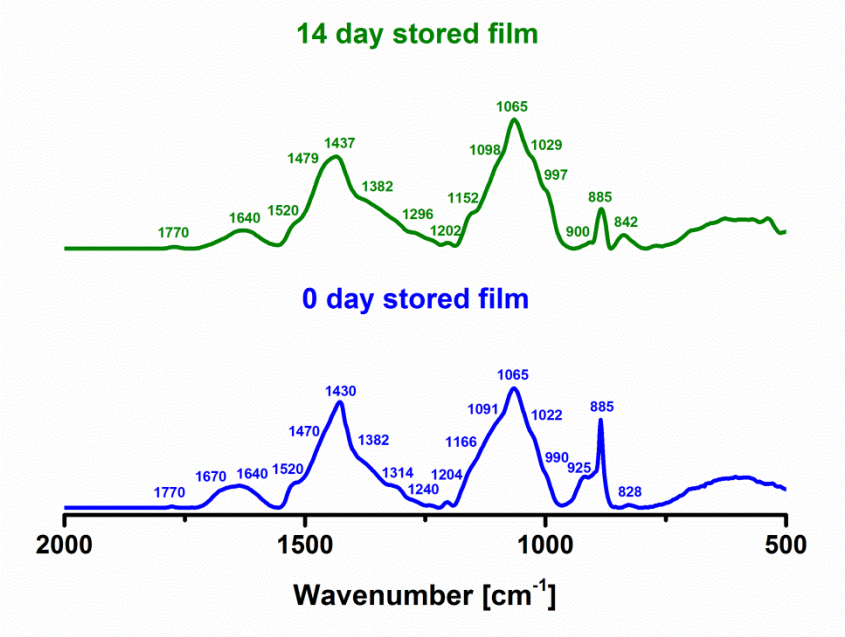

Figure S2. ATR-IR spectra of CX films after preparation and storage for 14 days under ambient conditions.

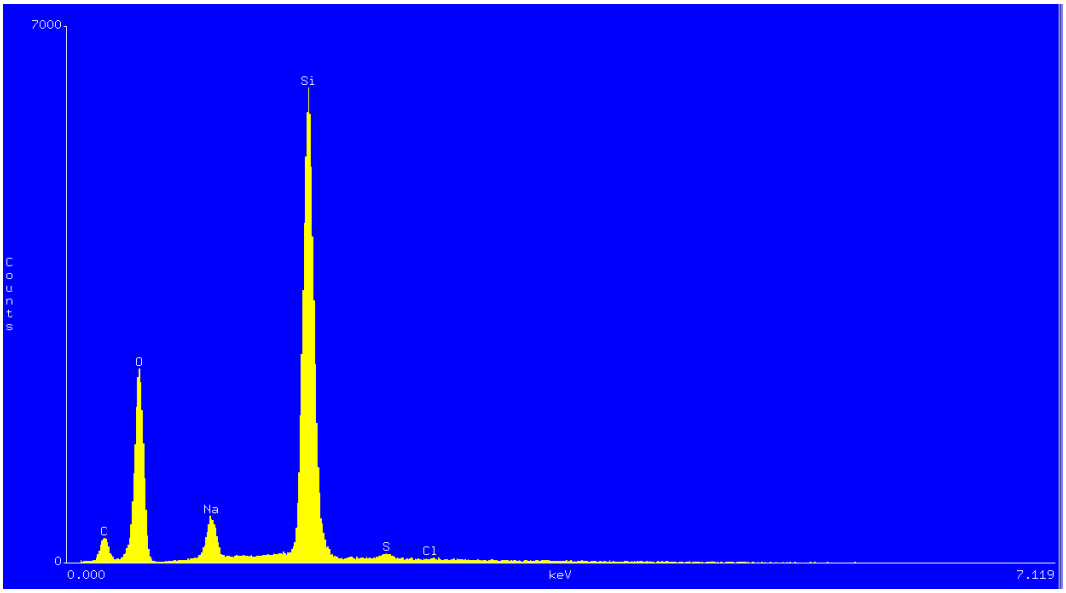

Figure S3. SEM-EDX spectrum of the salt crystals present on the films after spin coating of the CX solutions.

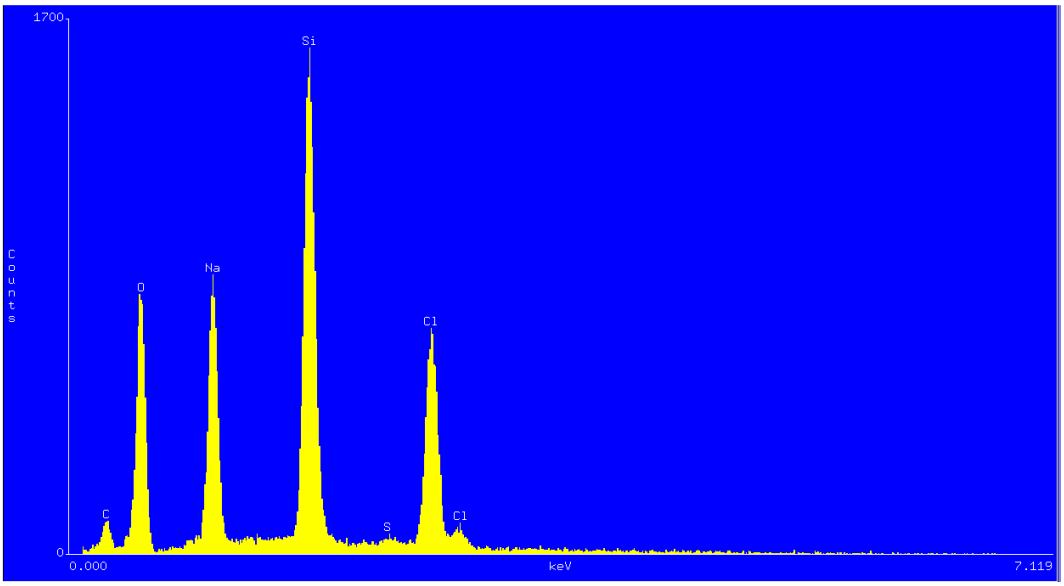

Figure S4. SEM-EDX spectrum of the salt crystals present in the films after regerneration with HCl vapors.

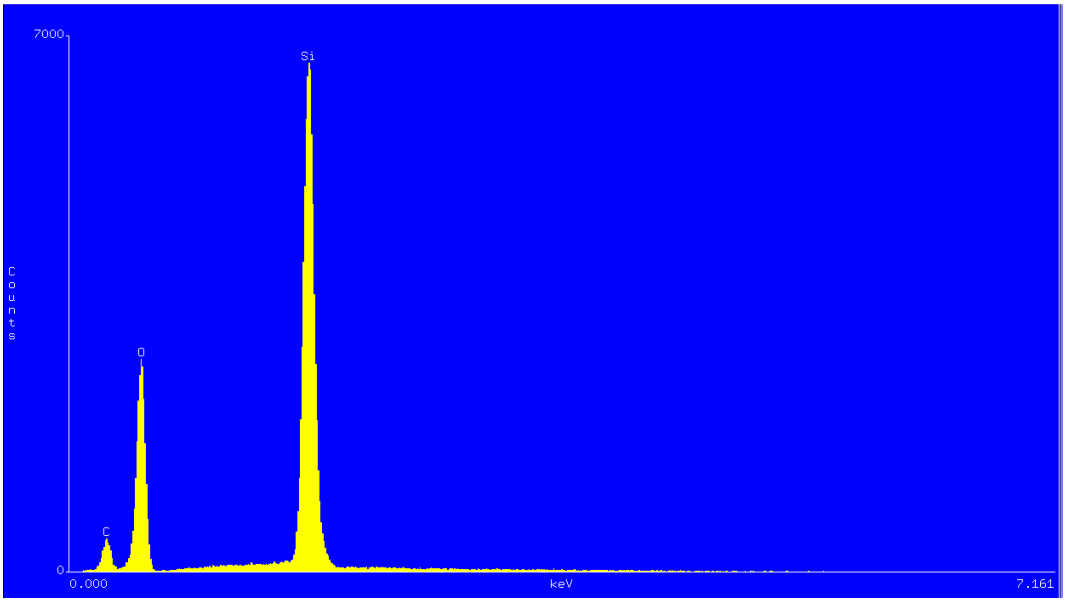

Figure S5. SEM-EDX spectrum of the films after rinsing with water.

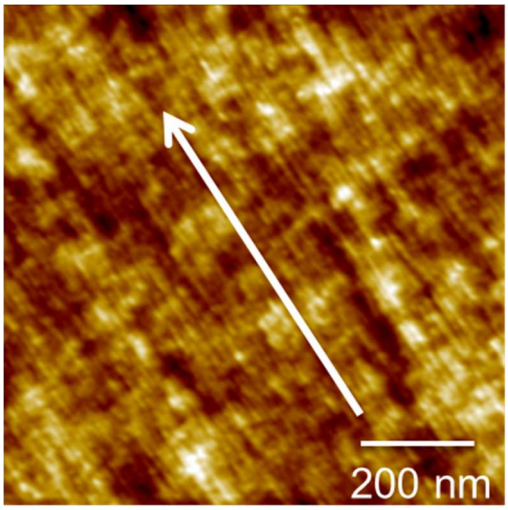

Figure S6. AFM topography image (1 x 1 μm^2) of native cellophane (no top coating) film (thickness 80 microns, from Innovia). The white arrow indicates the machine direction.

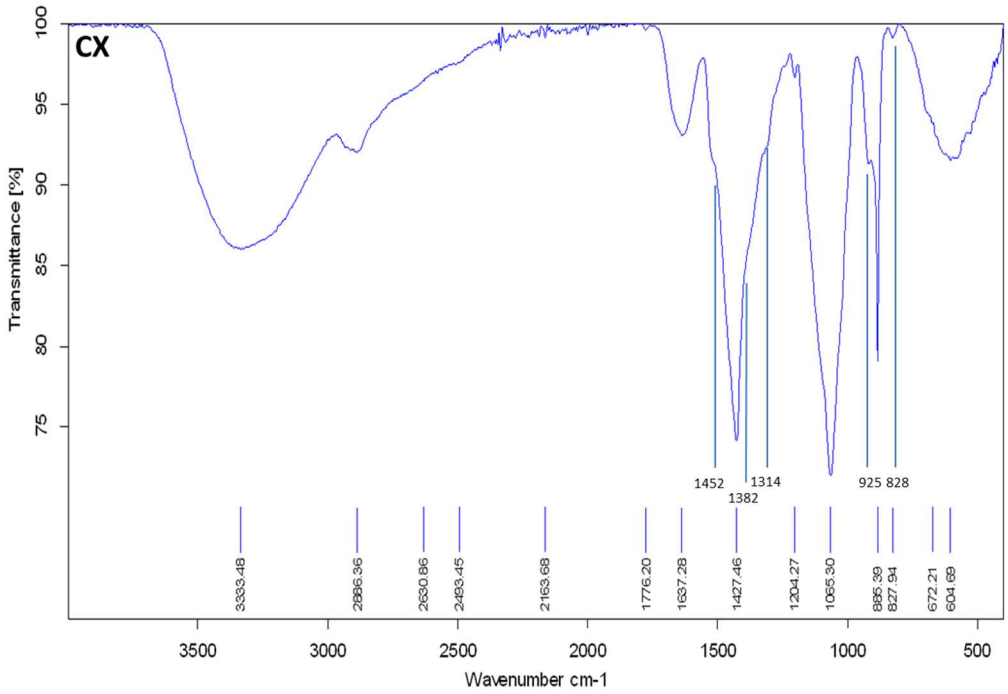

Figure S7. ATR-IR spectrum of CX films

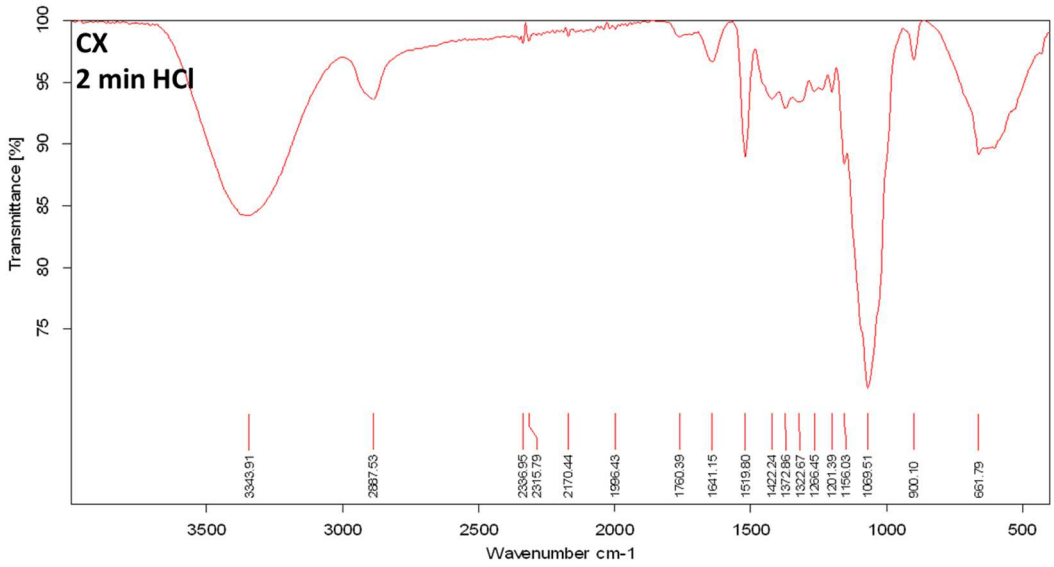

Figure S8. ATR-IR spectrum of CX films exposed for 2 minutes to HCl vapors.

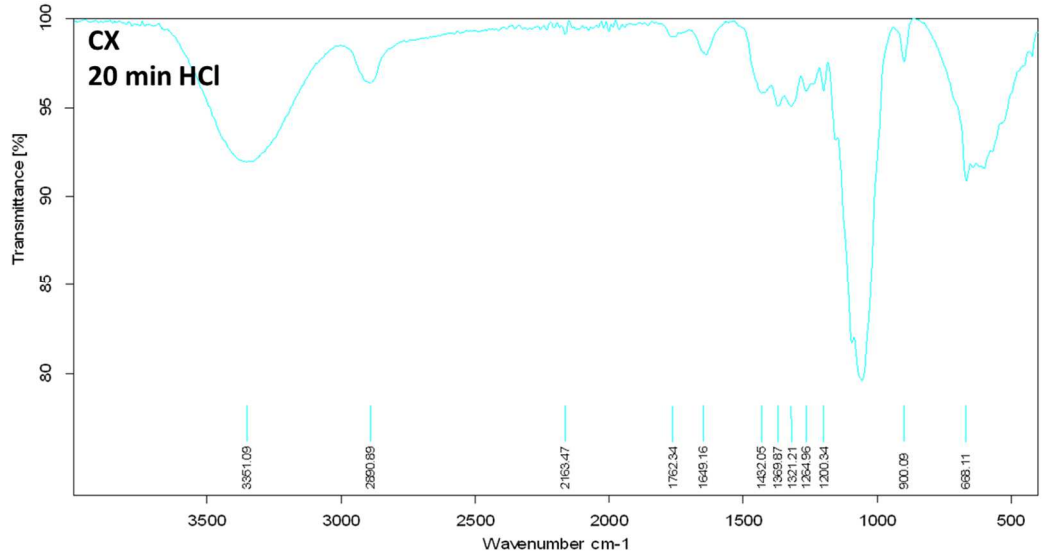

Figure S9. ATR-IR spectrum of CX films exposed for 20 minutes to HCl vapors.

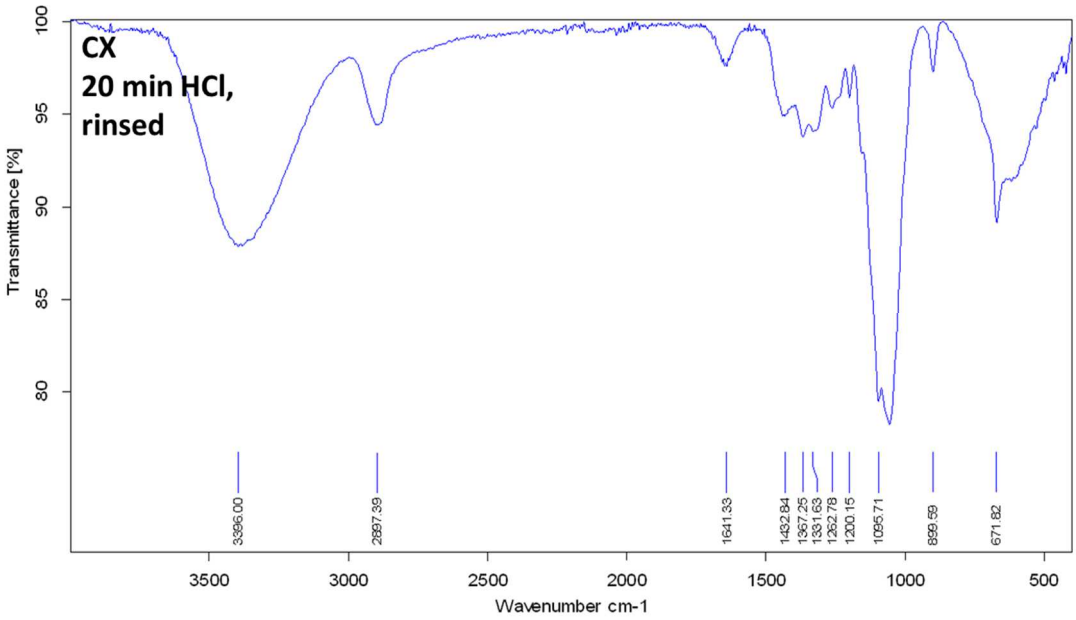

Figure S10. ATR-IR spectrum of CX films exposed for 20 minutes to HCl vapors.

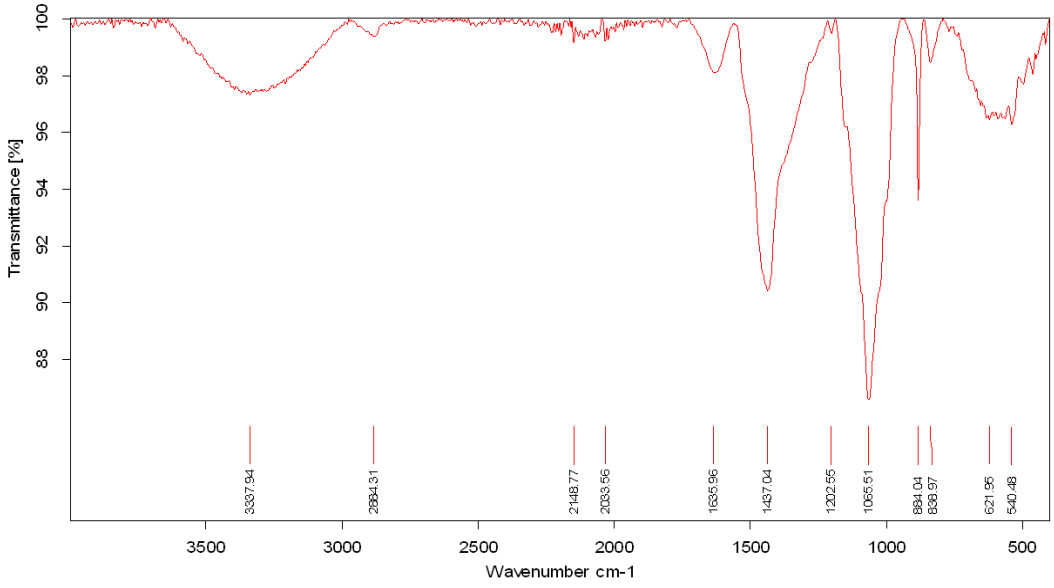

Figure S11. ATR-IR spectrum of CX films exposed for 14 days to ambient atmosphere

Paper #5

Multi-layered nanoscale cellulose/$CuInS_2$ sandwich type thin films

Published in Carbohydrate Polymers

For this paper, I conducted most of the experiments, interpreted the data and wrote a significant part of the manuscript.

Carbohydrate Polymers 203 (2019) 219–227

Contents lists available at ScienceDirect

Carbohydrate Polymers

journal homepage: www.elsevier.com/locate/carbpol

Multi-layered nanoscale cellulose/$CuInS_2$ sandwich type thin films

Michael Weißl[a], Thomas Rath[b,*], Jürgen Sattelkow[c], Harald Plank[c], Samuel Eyley[d], Wim Thielemans[d], Gregor Trimmel[b], Stefan Spirk[a,*]

[a] Graz University of Technology, Institute of Paper, Pulp and Fibre Technology, Inffeldgasse 23A, 8010, Graz, Austria
[b] Graz University of Technology, Institute for Chemistry and Technology of Materials, NAWI Graz, Stremayrgasse 9, 8020, Graz, Austria
[c] Graz University of Technology and Centre for Electron Microscopy, Institute for Electron Microscopy and Nanoanalysis, Steyrergasse 17, 8010, Graz, Austria
[d] Renewable Materials and Nanotechnology Research Group, Department of Chemical Engineering, KU Leuven Campus Kulak Kortrijk, Etienne Sabbelaan 53, 8500, Kortrijk, Belgium

ARTICLE INFO

Keywords:
Cellulose xanthate
Cellulose thin films
Copper indium sulfide
Metal xanthates
Multilayer systems

ABSTRACT

A generic procedure for the manufacturing of cellulose-metal sulfide multilayered sandwich type thin films is demonstrated at the example of copper indium sulfide. These multilayers were created by alternate spin coating steps of precursors, followed by their conversion using either acidic vapors, or heat treatment. As precursors, cellulose xanthate, a widely available cellulose derivative employed in viscose fiber manufacturing and commercial copper and indium xanthates were used. After conversion of the single layers into cellulose and copper indium sulfide, the film properties (structure, thickness, photoelectric activity) of the single and multilayer systems consisting of alternate layers of cellulose and copper indium sulfide were studied. For the proof of concept, up to five layers were built up, showing a clear separation of the cellulose and the metal sulfide layers as demonstrated using cross sectional analysis using ion slope beam cutting and SEM imaging. Finally, the conversion of xanthates was performed using UV light and a mask, allowing for the creation of 2D patterns.

1. Introduction

Amorphous nanometric thin films of cellulose consist of randomly oriented chains with hardly any long range order (Kontturi, Tammelin, & Österberg, 2006). Such materials offer a wide range of opportunities in understanding cellulose interaction with a variety of biomolecules (Filpponen et al., 2012; Kargl et al., 2013; Kontturi, Tammelin, Johansson, & Stenius, 2008; Mohan et al., 2013; Niegelhell et al., 2016; Orelma, Johansson, Filpponen, Rojas, & Laine, 2012) as well as water (Mohan et al., 2012) and they represent versatile substrates for functional layers in advanced materials such as optoelectronic devices (Reishofer, Rath et al., 2017; Wolfberger et al., 2015). Although one might expect that direct dissolution of cellulose and subsequent processing e.g. by spin coating can be used to produce such homogeneous nanometric films, problems associated with complete removal of solvents, homogeneous surface morphology and adhesion of the films on the substrate during regeneration impedes investigations of thin films manufactured via this route for such advanced applications. A different approach employs cellulose derivatives as starting materials which are converted back to cellulose after the processing step. In this context, the major material that has been used for the preparation of nanometric cellulose films is trimethylsilyl cellulose (TMSC) (Kontturi, Thüne, & Niemantsverdriet, 2003; Schaub, Wenz, Wegner, Stein, & Klemm, 1993). TMSC can be dissolved in various organic solvents (depending on its degree of substitution with silyl groups) and converted back to cellulose after the processing step, e.g. by exposure to acidic vapors. Featureless surface morphologies are obtained via this route with high reproducibility. However, a major challenge of TMSC is, though commercially available in kg scale, that it is still rather expensive (several thousands of Euros/kg) and its production is difficult to upscale. Further, the use of water based systems for the creation of cellulose thin films would be desired. A potential solution to this challenge is the use of water soluble cellulose derivatives, which in addition should be already produced in large scale. Cellulose xanthate (CX) is such a large scale, low cost commodity which is used in the viscose process for fiber/film formation. It is produced by alkali treatment of pulps (to remove low molecular weight components and homogenize molar mass distribution), followed by reaction with CS_2 to form CX. This solution is then subjected to ripening, where the xanthation pattern along the cellulose chains is significantly altered, leading to preferred substitution at C6. Afterwards, the material can be further processed to fibers and films. CX can be easily dissolved in aqueous NaOH in high concentrations and its properties in thin film formation can be tuned by variation of viscosity as shown recently (Weißl et al., 2018). A potential

* Corresponding authors.
E-mail addresses: thomas.rath@tugraz.at (T. Rath), stefan.spirk@tugraz.at (S. Spirk).

https://doi.org/10.1016/j.carbpol.2018.09.063
Received 2 July 2018; Received in revised form 18 September 2018; Accepted 23 September 2018
Available online 26 September 2018
0144-8617/

limitation is that the regeneration of the xanthate to cellulose leads to the formation of sulfur containing products. However, in modern viscose manufacturing sites, the recycling rate of these products is larger than 99%, thereby not causing any significant negative impact for the environment. In addition, there are many processes in industry where sulfur containing compounds are released anyhow during the creation of new materials or compounds such as metal sulfides. Metal sulfides provide a wealth of properties whereas those with low band gap are particularly interesting for the creation of photoactive systems for optoelectronics (Lai, Lu, & Chen, 2012). One potential route to manufacture such metal sulfides is the so called xanthate route, where a metal xanthate precursor is processed and by simple thermal treatment, decomposition of the xanthate followed by the formation of the metal sulfides occurs (MacLachlan et al., 2015; Macreadie Lauren, Maynard-Casely Helen, Batten Stuart, Turner David, & Chesman Anthony, 2014; Vagvala, Pandey, Ogomi, Ma, & Hayase, 2015). The side products of the xanthate decomposition are volatile and leave the metal sulfide matrix during the annealing step. This route does not only work for simple binary metal sulfides but also for more complex ones such as $CuInS_2$, a widely studied material with low band gap and high photoactivity. For the formation of $CuInS_2$, a mixture of a copper and an indium xanthate needs to be heated to temperatures between 160 and 200 °C (Rath et al., 2011). This method is very convenient for the fabrication of $CuInS_2$ nanocrystals, thin films or the formation of $CuInS_2$ nanocrystals directly in polymer thin films or other organic matrices (Al-Shakban et al., 2018; Dunst et al., 2014; MacLachlan et al., 2015; Rath, Kaltenhauser et al., 2013; Rath, Padeste et al., 2013). However, only a few reports aim at replacing synthetic polymers used in this context by renewable ones such as cellulose (Reishofer, Ehmann et al., 2017; Reishofer, Rath et al., 2017). In addition, the creation of multilayers involving cellulose and $CuInS_2$ requires the development of a technology that is capable of reproducibly manufacturing a subsequent layer system with basically no defects. In this paper, we address this challenge by using xanthates as the precursors for the creation of sandwich type structures featuring alternate cellulose and $CuInS_2$ layers. We study their formation and characterize the multilayered systems using FIB – SEM for any defects. Finally, we study the (photo-) conductivity properties of the layers in sandwich type structures involving up to 5 layers and correlate the layer thickness and the type of deposition with the obtained electrical response.

2. Experimental

2.1. Materials

Cellulose xanthate (CX) solution (10 wt.%, gamma: 52, NaOH: 6%, degree of polymerization: 550) was kindly provided by Lenzing AG (Lenzing, Austria).

Copper and indium xanthates (copper *O*-2,2-dimethylpentan-3-yl dithiocarbonate, indium O-2,2-dimethylpentan-3-yl dithiocarbonate) (Fig. S1, Supporting information) were purchased from Aglycon GmbH where it was synthesized based on a published protocol (Rath et al., 2011). Sulfuric acid (95 wt.%) and chloroform were purchased from VWR Chemicals, trifluoroacetic acid (TFA), chlorobenzene and hydrogen peroxide (30 wt.%) from Sigma-Aldrich.

Silicon wafers from Siegert Wafers (Aachen, Germany, wafer thickness: 675 ± 25 µm, 1 cm × 2 cm), glass slides from Roth (Karlsruhe, Germany, thickness: 1000 µm, 1.5 cm × 1.5 cm), Au-coated glass slides from BioNavis (Tampere, Finland, gold layer thickness: 50 nm, 1 cm × 2 cm, SPR102-AU), Filter Chromafil Xtra PVDF-45/25 0.45 µm as well as a two-component conductive epoxy glue from Chemtronics (Kennesaw, USA) were used as obtained.

2.2. Multilayer preparation

As substrates for the multilayer films, single side polished silicon wafers, gold coated glass slides and glass slides were used. The slides were cleaned by dipping them into piranha acid (H_2SO_4:H_2O_2 = 3:1 (v/v)) for 30 min (10 min for gold slides) and intensely washed with MilliQ water ($\geq 18\,M\Omega\,cm^{-1}$) afterwards.

For layers 1, 3 and 5 of the thin film stack, cellulose xanthate (80 µl per square centimeter of substrate) was deposited onto the surfaces and subjected to spin coating (a = 2500 rpm s^{-1}, v = 4000 rpm, t = 60 s). Spin coating was followed by regeneration of the deposited CX layers in vaporous TFA atmosphere. For the regeneration procedure, the TFA was diluted (1:1, with deion. water), placed into a watchglass (2 mL), and the substrates were positioned above the liquid TFA phase with help of a petri dish. A crystalizing dish was used as a lid to close the system. After 20 min exposure to the gaseous TFA atmosphere, regeneration of the cellulose xanthates to cellulose is accomplished as proven by ATR-IR spectroscopy (Fig. S2, Supporting information). Afterwards, the films were rinsed twice with water (8 mL) followed by drying in a stream of dry nitrogen. This process has to be repeated for every single cellulose layer.

For the preparation of the nanocrystalline $CuInS_2$ layers, (Layer 2 and 4), a precursor solution (CuInX, in chlorobenzene) containing copper xanthate (32.2 mg mL^{-1}, 1 equiv., 0.126 mmol L^{-1}) and indium xanthate (147.8 mg mL^{-1}, 1.7 equiv., 0.215 mmol L^{-1}) was prepared. This CuInX solution (20 µL per square centimeter of substrate) was transferred onto the substrate and subjected to spin coating (a = 1000 rpm s^{-1}, v = 1000 rpm, t = 60 s). After spin coating, the CuInX was exposed to 170 °C for 15 min to generate the nanocrystalline $CuInS_2$ thin film by thermal decomposition of the metal xanthates (Pradhan, Katz, & Efrima, 2003). The process steps have to be repeated for every $CuInS_2$ layer in the multilayer system.

For electrical characterization, the single $CuInS_2$ layers of the multilayer system were contacted with copper electrodes. For this, conductive two component epoxy glue was employed. After mixing the two components, a little spot was placed on the $CuInS_2$ surface and small copper stripes (15 mm × 3 mm) were fixed on the $CuInS_2$ layers via the small glue spots. To accelerate the solidification of the epoxy glue, the substrates were placed in a drying oven at 60 °C for two hours. After fixing the electrodes on the $CuInS_2$ layers, the step wise multilayer development could be continued.

2.3. Optical microscopy

Light microscopy investigations were carried out on an Olympus BX60 microscope fitted with an Olympus E-520 camera.

2.4. Profilometry

The layer thickness was determined with a Bruker DekTak XT surface profiler. The scan length was set to 1000 µm over the time duration of 3 s with the hills and valleys scanning profile. The diamond stylus had a radius of 12.5 µm and the employed force was 3 mg. The measured profile was then used to determine the thickness. Each layer thickness has been determined by averaging 10 measurements on three different slides.

2.5. Attenuated total reflection – infrared spectroscopy

The infrared spectra were recorded with an ALPHA FT-IR spectrometer (Bruker; Billerica, MA, U.S.A.). For the measurements, an attenuated total reflection (ATR) attachment was used with 64 scans at a resolution of 4 cm^{-1} and a scan range between 4000 and 400 cm^{-1}. The samples were prepared on Au-coated glass slides (SPR102-AU). The data were analyzed with OPUS 4.0 software.

2.6. XPS

Spectra were recorded on a Kratos Axis Supra X-ray Photoelectron

Spectrometer employing a monochromatic Al Kα ($h\nu$ = 1486.7 eV, 10 mA emission) X-ray source, hybrid (magnetic/electrostatic) optics with a slot aperture, hemispherical analyzer, multichannel plate and delay line detector (DLD) with a take-off angle of 90°. The analyzer was operated in fixed analyzer transmission (FAT) mode with survey scans taken with a pass energy of 80 eV and high resolution scans with a pass energy of 20 eV. Samples were electrically isolated from the instrument. All scans were acquired under charge neutralization conditions using a low energy electron gun within the field of the magnetic lens. The resulting spectra were processed using CasaXPS software. Binding energy was referenced to aliphatic carbon at 285.0 eV.

2.7. Atomic force microscopy

The multilayer system was characterized with a FastScanBio AFM operated by a Nanoscope V controller (Bruker NANO, Santa Barbara, CA). All studies were performed in tapping mode with a Fast Scan A (Bruker AFM Probes, Camarillo, CA) cantilever with spring constants of 18 N/m, resonance frequencies around 1.4 MHz and a nominal tip end radius of 5 nm. Sample roughness for each layer was measured at least at 3 different areas. At each region, 10 × 10 µm overview and 1 × 1 µm detail scans for high resolution were conducted. Concomitantly, to establish soft-repulsive conditions throughout the AFM investigation scan rates, amplitude set points, and feedback gains were monitored steadily for artifact free imaging conditions and lowest possible energy dissipation. Data analysis was conducted in NanoScope Analysis 1.5 (Bruker, Santa Barbara, CA).

2.8. Ion beam slope cutting and scanning electron microscopy

Ion beam slope cutting and scanning electron microscopy (SEM) were performed in a NOVA 200 dual beam instrument (Thermo Fischer). SEM imaging has been performed at 10 keV and 540 pA with shortest possible image acquisition times to minimize e-beam damage for the cellulose layers. Broad ion beam processing was performed with an ILION instrumentation (GATAN) using 4 keV and cooled sample stages.

For the cutting, the sample was fixed on a metal blade and exposed to a perpendicular oriented broad ion beam using Ar ions. The metal blade does not protect the sample itself (Fig. S3, Supporting information) but also ensures a flat cross cut after processing. To further minimize heating effects, the entire sample was cooled by liquid nitrogen to −160 °C. The resulting cross section was flat and thus well suited for SEM based imaging and elemental analysis.

2.9. Contact angle and surface free energy determination

For the calculation of the surface free energy (SFE) Milli-Q water ($\geq$18 MΩ cm^{-1}) and diiodomethane were employed as test liquids. The drop shape analysis was done in the sessile drop modus at 25 °C with a DSA100 system (Krüss GmbH, Hamburg, Germany) equipped with a T1E CCD video camera (25 fps). The dispense rate of the 3 µL droplets was adjusted to 166 µL/min and the time before the image was captured was set to 2 s. Each sample was measured at least three times. The contact angle (CA) calculations (software: DSA1 v 1.90) were performed with the Young-Laplace equation and the surface free energy calculation with the Owens-Wendt-Rabel & Kaelble method (Owens & Wendt, 1969).

2.10. UV-VIS spectroscopy

Transmission and reflection spectra were recorded on a Perkin Elmer LAMBDA 35 spectrophotometer equipped with a 50 mm integrating sphere attachment. Absorption spectra were calculated from the transmission and reflection spectra.

2.11. Electrical characterization

JV characteristics of the $CuInS_2$ thin films were recorded in a glovebox using a Keithley 2400 source measure unit and a custom made LabView software. The samples were illuminated by a Dedolight xenon lamp with a spectrum similar to the AM 1.5 G spectrum at 100 mW cm^{-2}. The current was measured between −1000 mV and 1000 mV for both illuminated and non-illuminated samples. The distance between the two electrodes was set to 10 mm.

2.12. Micropatterning

Micro patterning of the $CuInS_2$ films by selective conversion of the precursor layers by UV light.

CuInX was selectively converted to $CuInS_2$ by patterned exposure of the layers to UV light emitted from an Efos Novacure UV spot curing system N2001 (Ontario, Canada). The lamp was equipped with a radiometer to regulate light intensity. The samples were placed in a silica glass tube with their back side up, the UV source was placed directly below the samples on the outer side of the tube. Before starting illumination, with a power of 5000 mW for 20 min, the glass tube was evacuated. To get a defined micro structuring, thin photomasks with varying structures (1 cm × 1 cm) were placed above the CuInX layers. After UV treatment, the non-exposed areas of the CuInX precursor film were removed by rinsing with chloroform and the sample with the remaining $CuInS_2$ structures were placed on a heating plate to obtain full conversion to $CuInS_2$.

3. Results and discussion

The general strategy for the solution-based manufacturing of multilayered cellulose-$CuInS_2$ systems was to use xanthates as precursors for both the cellulose, and the $CuInS_2$ thin films. The idea is to alternatively spin coat the respective xanthates and to convert the precursor layers into cellulose or the metal sulfide by exposure to acid vapors (CX) or exposure to elevated temperatures (CuInX). By variation of the concentration of either the CX or the CuInX variations in film thickness can be obtained.

3.1. Regeneration

Since HCl vapors are prone to attacking the $CuInS_2$ layers, trifluoroacetic acid (TFA) vapor was found to be the most promising alternative. A useful means to investigate the regeneration of cellulose xanthate is to employ ATR-IR spectroscopy and to follow the appearance and disappearance of functional groups as a function of exposure to TFA vapors. TFA itself features characteristic bands at 1775 ($\nu_{C=O}$), 1624 (ν_{C-O}), 1460 cm^{-1} ($\nu_{C-O;}$ ν_{sC-O-C}) and two series of strong, overlapping bands from 1250 to 1100 cm^{-1} ($\nu_{CF3;}$ $\nu_{F-CF2;}$ $\nu_{F-C-F;}$ ν_{C-C}) and from 891 to 785 cm^{-1} ($\nu_{C-C;}$ ν_{C-O-O}) as well as strong bands at lower wave numbers, namely 660 cm^{-1} (δ_{CF3}); 600 cm^{-1} (δ_{F-CF2}), and 520 cm^{-1} (δ_{F-C-F}) corresponding to vibrations of the fluorinated carbon and carbon - carbon vibrations (Redington & Lin, 1971; Spirk, Belaj, Kahr, & Pietschnig, 2009).

The spectra of the pure CX thin films indicate the partial regeneration of the films during the spin coating step as well as the presence of by-products in the CX solution. C=S and C–S vibrations have been reported in a range of 1250–1050 cm^{-1} for the CX and these bands interfere with decomposition products like sodium sulfide (1420, 920 cm^{-1}) or sodium trithiocarbonate (1670, 1427, 925 and 885 cm^{-1}). The remaining bands are caused by additional decomposition products such as CS_2 ($\nu_{C=S}$ at 1520 cm^{-1}) and, in traces, H_2S (ν_{S-H} at 2630 cm^{-1}) as well as NaOH (2725, 1452 and 1382 cm^{-1}) (Andrews, Hurtubise, & Krassig, 1960; Dautzenberg & Philipp, 1970; Ogura & Sobue, 1968). After exposure of the CX layers to acidic vapors of TFA, the spectrum changes significantly, and the bands

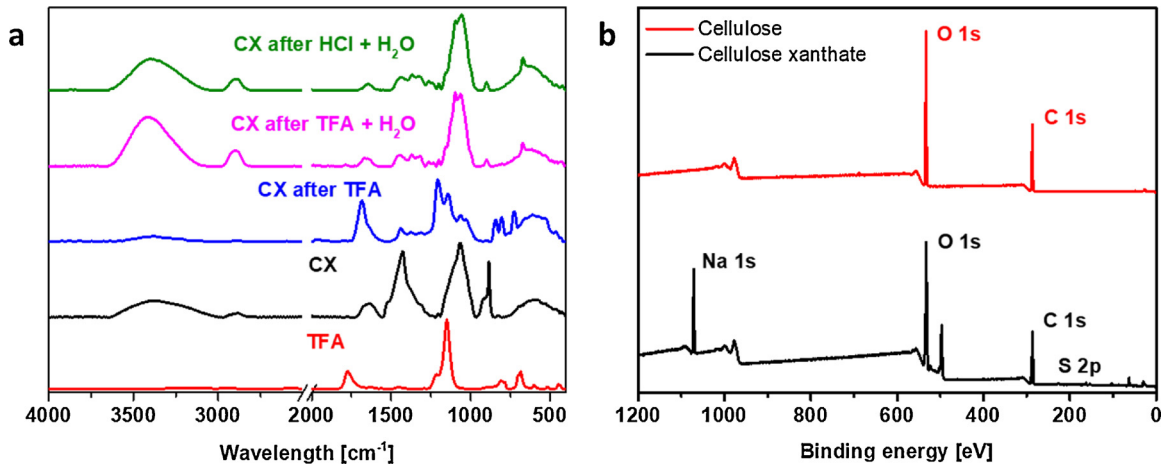

Fig. 1. a) ATR-IR spectra of TFA, a CX film after spin coating and CX films after exposure of CX to HCl or TFA acidic atmosphere for 20 min followed by washing with deionized H_2O. b) XPS survey spectra of a CX film after spin coating and after the regeneration procedure.

corresponding to C═S, C–S or NaOH vibrations disappear. Instead, IR bands of two different species became visible, namely cellulose II bands and those ascribed for TFA-related compounds which are partially overlapping with the cellulose II bands. We have reported in a former study (Weißl et al., 2018) that sodium chloride is developed by deposition of CX layers in HCl vapor phase and in accordance to this, sodium trifluoroacetate (NaTFAA) is formed after TFA treatment. The bands related to vibrations of C═O, C–O, C−C and C–O−O (1684, 843, 725), are slightly shifted to lower wavenumbers compared to the TFA bands. In addition to the described NaTFAA bands, the bands at 3500 cm^{-1}–3200 cm^{-1} (ν_{OH}), and from 1450 to 1310 cm^{-1} (C–O−H bending at 1430 cm^{-1}, C–H deformation at 1372 $cm^{-1}$and OH in plane deformation at 1330 cm^{-1}) as well as a weak band at 900 cm^{-1} (C–O−C valence vibration) indicate the presence of cellulose II. After washing the samples with water, the bands associated to NaTFAA vanish and a characteristic cellulose II type spectrum (Fig. 1a) is observed (Široký, Blackburn, Bechtold, Taylor, & White, 2010). Finally, it should be noted here that immersion of the films in diluted solutions of TFA (which would eliminate the washing step to remove the salts) led to the peeling off the film from the substrate.

In addition to ATR-IR spectroscopy XPS was employed to validate the regeneration of the precursors (CX and CuInX) to cellulose and $CuInS_2$.

The cellulose xanthate film showed several sulfur environments. Based on the $S2p_{3/2}$ binding energy, the environment at 161.9 eV corresponds well to the two equivalent sulfur atoms of organic xanthates in the literature (Mikhlin, Karacharov, & Likhatski, 2015). The second sulfur environment at 163.6 eV could be assigned to the extra sulfur atom present in trithiocarbonates, while the higher binding energy environments at 166.2 eV and 168.1 eV are typical of oxygen containing sulfur environments such as sulfoxides and sulfonates/sulfates (respectively). In the O1s spectrum, the lower binding energy environment at 531.3 eV corresponds well with metal salts of oxygen species and sulfates, while the higher binding energy environment at 533.0 eV corresponds with organic oxygen environments. Finally, the C1s spectrum contains four environments. Besides the usual aliphatic carbon (contamination) at 285.0 eV, there is C–O at 286.7 eV and O−C–O at 288.2 eV typical of cellulosic materials. The fourth environment with a binding energy of 289.4 eV is ascribed to xanthate due to the similarity in binding energy to urethanes, carbonates or ureas. After exposure to TFAA and rinsing with water, the sulfur containing bands disappear and a typical XPS spectrum of pure cellulose is obtained, with C1s and O1s contributions matching previously published data on cellulose thin films (Fig. S4a, Supporting information) (Mohan et al., 2012).

High resolution spectra of the $CuInS_2$ layers showed that the binding energies of the $Cu2p_{3/2}$ and $In3d_{5/2}$ (932.3 and 445.0 eV) are in very good agreement with literature values (932.2 vs 444.7 eV) for $CuInS_2$ (Fig. S4b, Supporting information) (Rath, Kaltenhauser et al., 2013; Rath, Padeste et al., 2013; Scheer & Lewerenz, 1994). The sulfur 2p spectrum confirmed the results from the Cu2p and In3d spectra, with binding energies for $S2p_{3/2}$ of 161.9 eV and $S2p_{1/2}$ of 163.0 eV characteristic for $CuInS_2$. The C1s spectrum of the $CuInS_2$ sample revealed a large amount of aliphatic carbon contamination (285.0 eV) with very small contributions due to C–X (O,S) species at 286.6 eV and O−C═O at 288.9 eV. These species correlate well with the O1s spectrum which shows three environments at 530 eV, 531.9 eV and 533.3 eV corresponding to metal oxides, and various carbon-oxygen species. The predominance of these latter two environments points to a relatively small amount of oxidation of the $CuInS_2$ layer with oxygen being confined to the organic contamination overlayer.

3.2. Multilayer architecture

After optimization of the regeneration of the CX, multilayer formation was studied. CX always was the very first layer deposited by spin coating onto the substrate. After conversion to cellulose by TFA vapor treatment, rinsing with water to remove NaTFAA, and drying in a stream of nitrogen, the CuInX solution was deposited by spin coating as well. The $CuInS_2$ film was created by heating the films on a heating plate at 170° for 15 min (Fradler et al., 2014; Rath et al., 2011). After cooling, the procedure was repeated until five layers (cellulose – $CuInS_2$ – cellulose – $CuInS_2$ – cellulose) had been deposited onto the substrate. The development of the multilayer as well as the conversion of the CX into cellulose and the CuInX into $CuInS_2$ can be followed by ATR-IR spectroscopy since also the copper and indium xanthates feature characteristic bands. In Fig. 2 the IR spectra of a three-layered system (cellulose – $CuInS_2$ – cellulose) are shown.

The deposition of the CuInX onto the cellulose layer results in the appearance of new bands assignable to the bulky branched alkyl group of the CuInX in the region of 3000–2850 cm^{-1} (ν_{CH3}, ν_{CH2}, ν_{CH}) and strong bands at 1240 ($\nu_{C=S}$) and 1214 cm^{-1} (ν_{C-O-C}). After heat treatment, these bands disappear since the volatile side products leave the film while $CuInS_2$.was formed. The remaining two spectra in Fig. 2 describe the deposition of another CX layer on the $CuInS_2$ and its conversion to the cellulose by exposure to TFA vapors.

For the 5 layered system, layer thicknesses of 154, 150 and 168 nm have been determined for the cellulose layers (L1, L3, L5), while for the $CuInS_2$ layers thicknesses of 30 (L2) and 32 nm (L4) were determined (Fig. 1) An overview on the layer thicknesses can be found in the SI

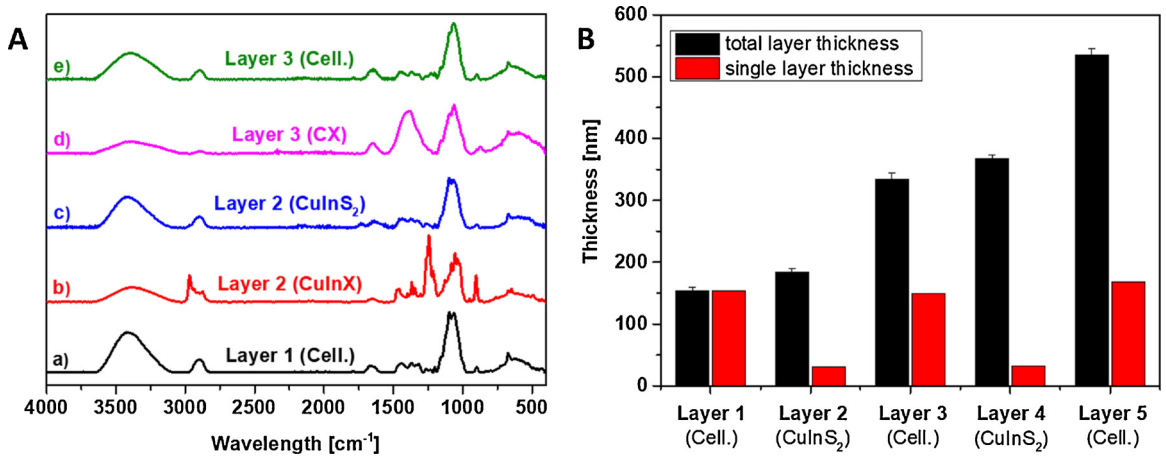

Fig. 2. Left: ATR-IR spectra showing the development of a three-layered (cellulose – $CuInS_2$ – cellulose) multilayer system, starting with a fully processed cellulose layer(a), followed by the deposition and corresponding conversion of CuInX to $CuInS_2$ (b,c). The last two steps shown in the figure belong to the development of the third layer of the system, namely the deposition of CX and its regeneration to cellulose in TFA acidic atmosphere (d,e). Right: Development of the total film thicknesses and the individual layer thicknesses in a five layered cellulose $CuInS_2$ system.

(Table S1). The height profiles used for determination of the layer thickness revealed smooth surfaces without any major irregularities as shown in profilometry investigations.

3.3. Surface morphology and cross section analysis

To gain a more detailed topological information on the different layers in the cellulose $CuInS_2$ multilayer device, atomic force microscopy was employed (Fig. 3). When taking into consideration that there are already two more layers below, layer 3 (a cellulose layer) showed a rather flat surface, with a RMS roughness below 3 nm. The structure is regular and smooth over a large area and just a few agglomerates (height ca 10 nm) are visible. The surface after deposition of layer 4 ($CuInS_2$) changes, although the RMS roughness is in the same range. However, there is a certain influence of the layer 3; particularly the few aggregates can be clearly seen. A closer look onto the $CuInS_2$ layer illustrates that the $CuInS_2$ layer consists of spherical grains with the larger ones having diameters ranging from 20 to 30 nm (Fig. S5, Supporting information). After deposition of the 5th layer and subsequent regeneration, a similar topography as for layer 3 was observed. Although the surface structure and roughness is a little smoother, compared to L3.

Although profilometry and AFM images suggest that the single layers are homogeneous and hence do not intermingle, only cross section images are capable to prove a full picture of the multilayer structure. However, a major problem in such investigations is the preparation of cross sections due to the following reasons. Cellulose is a sensitive material prone to decomposition in an ion/electron beam and, in addition, the multilayer consists of hard (Si-Wafer, $CuInS_2$) and soft (cellulose) layers making polishing, microtomy or FIB sectioning extremely challenging. For such samples, the favored option is probably to employ ion beam slope cutting. Here, a protective metal stripe is deposited on the surface of the layer and an Ar-beam is used to cut a slice of the layer, which can then be moved using micromanipulators to SEM imaging at the same time. Further, the sample needs to be cooled (−160 °C) in order to avoid any degradation of cellulose by the ion beam. Using this approach, we obtained high quality cross sectional images with hardly any beam damage of our samples. The cross sections (Fig. 4) images confirmed the results of the other analyses and a clear multilayer structure is observed. The layers feature a high degree of conformity, they show a constant thickness over a large area (i.e. 40 microns) and the different layers are clearly separated. These cross sections were employed for a more precise determination of the $CuInS_2$ layer thicknesses and more accurate data than with profilometry was obtained. The cellulose layers feature a layer thickness between 140 and 150 nm, while the $CuInS_2$ layers feature layer thicknesses of 45–50 nm. These layer thicknesses are a bit smaller than those determined by profilometry which is probably due to the slight shrinkage of the cellulose layers during heating as reported earlier (Mohan et al., 2012). The thickness of the $CuInS_2$ layer can be easily tuned, for instance an increase in the CuInX concentration by a factor of 2 in the solution yielded final $CuInS_2$ layer thicknesses ranging from 90 to 100 nm (i.e. layer thickness doubled).

It should be also mentioned that the cellulose and $CuInS_2$ layers exhibit good compatibility when it comes to the surface free energy (SFE, Fig. 5). The cellulose layers derived from CX exhibit a SFE of ca. 70 mN m^{-1} with a major disperse contribution to the total SFE, and a similar behavior is observed for the $CuInS_2$ surfaces (60 mN m^{-1}, with major disperse contributions). Only slight deviations for the different layers of each material are observed, which are probably caused by

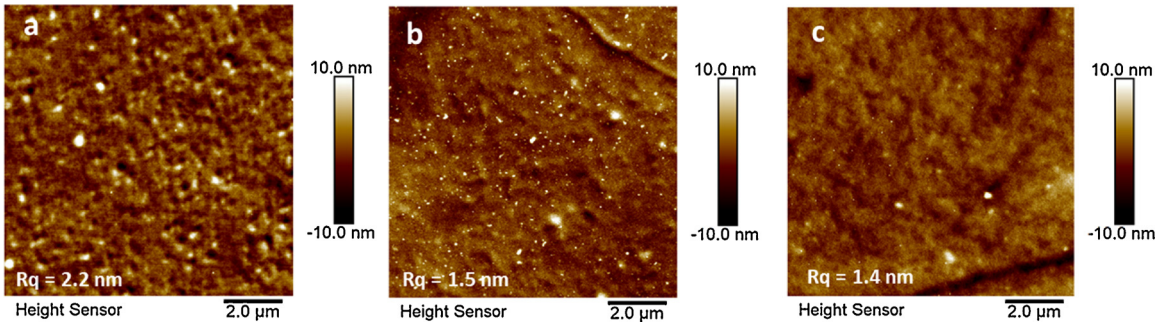

Fig. 3. AFM topography images (10 × 10 μm^2) after the final processing of Layer 3 (a), Layer 4 (b) and Layer 5 (c).

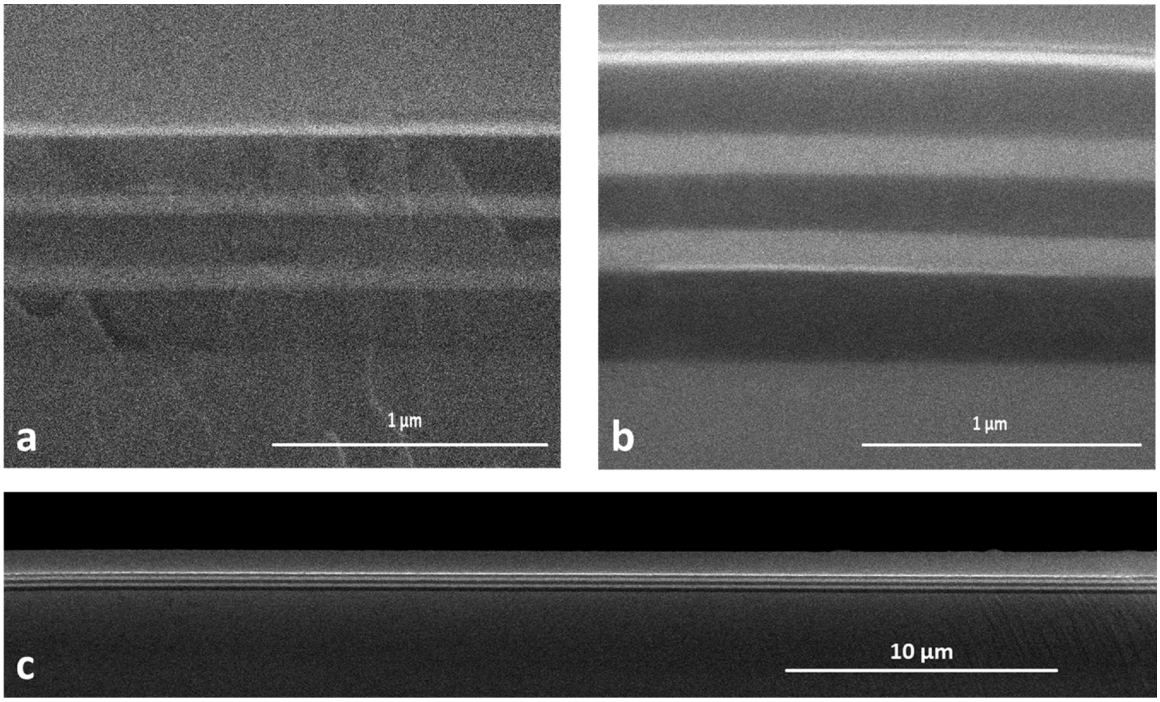

Fig. 4. SEM images of cross sections of a five layered system, spin coated with 32.2 CuInX (a) and 64.4 mg ml^{-1} CuInX (b,c) deposited on a silicon wafer. The layer sequence in all images is (from bottom to top): silicon-cellulose-CIS-cellulose-CIS-cellulose-metal stripe.

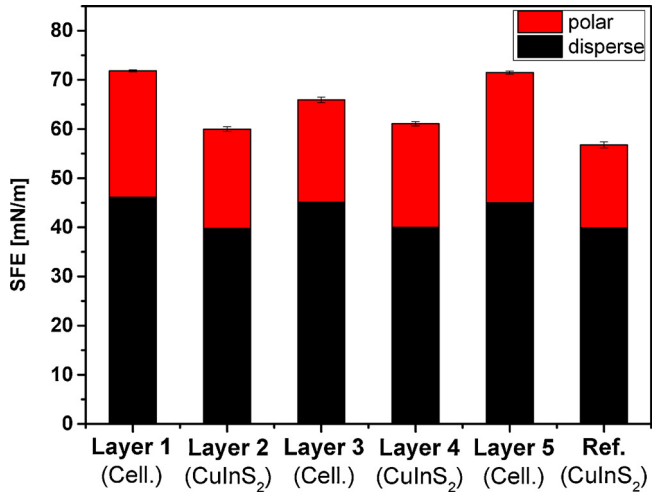

Fig. 5. SFE values for every layer in the 5 layered system and a $CuInS_2$ reference thin film prepared on a silicon substrate. The CuInX concentration used for spin coating was 32.2 mg ml^{-1}.

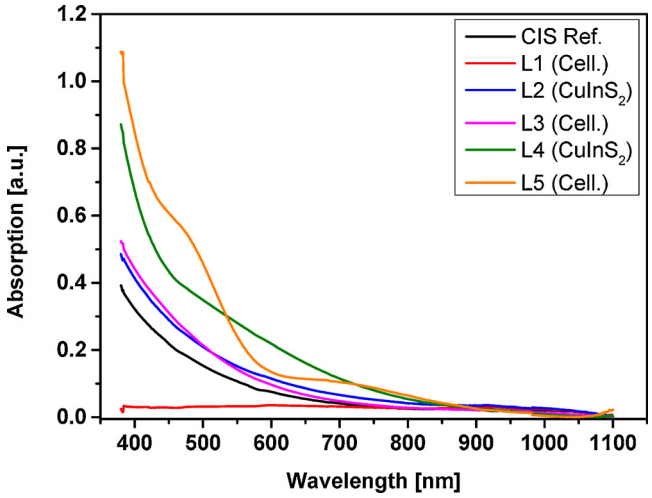

Fig. 6. VIS absorption spectra of a cellulose $CuInS_2$ multilayer device with an increasing number of layers in the system having a final layer thickness of 560 nm and comparison to a $CuInS_2$ reference layer (40 nm). Thicknesses for the single layers are around 160 nm for cellulose and 40 nm for $CuInS_2$.

roughness contributions.

3.4. Photo(electric) characterization

It is well known that $CuInS_2$ is an excellent semiconductor with a bandgap of 1.5 eV, absorbing in the visible (VIS) range of the electromagnetic spectrum. Fig. 6 compares UV–vis absorbance spectra in dependence of the number of deposited layers. These spectra have been obtained from the transmission and reflection spectra as described in the experimental section. The absorption onset for $CuInS_2$ nanoparticles is reported between 800 and 900 nm in literature, which fits well to the onset points visible in Fig. 6 (Rath et al., 2011; Reishofer, Rath et al., 2017).

The cellulose layers are VIS transparent and did not absorb light in this wavelength region. Any absorption in the multilayer is therefore due to absorption of the $CuInS_2$ layers. According to the Lambert-Beer law, the intensity of the absorption is proportional to the layer thickness of the films. Hence, a doubling of the layer thickness (when going from L2 to L4) results in a doubling of the absorption of the films. The significantly changed shape of the absorption spectrum of the multilayer stack after deposition of layer 5 originates from interference phenomena, which are also clearly observed in the reflection spectra of these films (Fig. S8, Supporting information).

Semiconducting layers separated by thin insulating films might find various technologically relevant applications. To electrically characterize the $CuInS_2$ thin films sandwiched between the cellulose layers, current/voltage curves of the $CuInS_2$ layers in different stages are shown in Fig. 7. The current/voltage curves show a linear characteristic due to the Ohmic nature of the contacts to the $CuInS_2$ films. It can be

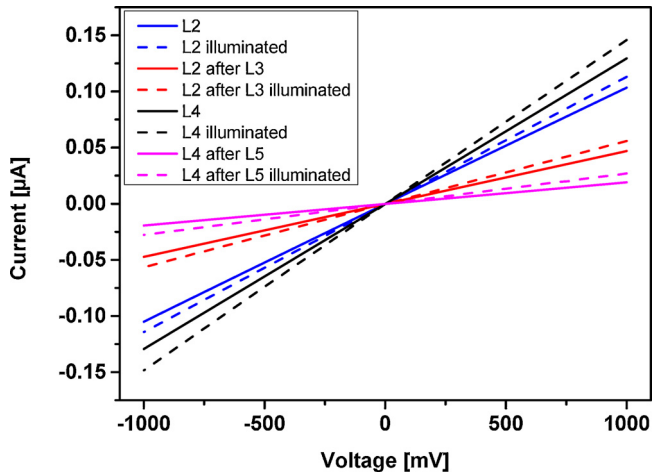

Fig. 7. Current/voltage characteristics of the $CuInS_2$ layers after every layer spin coated on the system (CuInX concentration: 64.4 mg ml^{-1}).

clearly seen that the $CuInS_2$ layers are conductive and they also exhibited photoconductivity upon illumination. The two different layers consisting of $CuInS_2$ (i.e. L2 and L4) feature nearly the same current flow at a given potential and also the induced photocurrents are very similar. However, obviously the deposition of a top coating of cellulose onto these layers causes a drop in conductivity, which is observed for most of the samples. A possible reason for this could be the presence of microcracks, which could form due to the swelling of the cellulose film on top of the $CuInS_2$ film during the rinsing step to remove the NaTFAA salt formed during the regeneration of the cellulose xanthate. However, as the SEM images of the cross-sections revealed, the multilayer structure is intact and no indications of cracks throughout the whole layers were observed. Another issue in the determination of the currents is in the contacts to the $CuInS_2$ films. If the contact is exposed to the regeneration procedure, the electrode surface or the interface may be passivated leading to higher contact resistance. Moreover, the thicknesses of the $CuInS_2$ films are very low (only about 40–50 nm), which also explains the relatively low currents at a 10 mm distance between the electrodes.

To explore this further, the layer thickness of the $CuInS_2$ layers was increased by increasing the CuInX concentration in the precursor solution. Additionally, these layers have then been compared to layers of similar thickness but obtained by consecutive spin coating steps of CuInX followed by immediate conversion to $CuInS_2$.

As mentioned above, a single $CuInS_2$ layer spin coated from the standard CuInX concentration (32.2 mg/mL) results in a layer thickness of approximately 40–45 nm. Each additional, subsequent spin coating of CuInX onto this layer leads to an increase of the thickness of another 40–45 nm, i.e. after two and three subsequent deposition and annealing steps, $CuInS_2$ layers with 90 and 140 nm thickness are obtained. When the CuInX concentration was increased (64.4 mg/mL), the $CuInS_2$ layer thickness was ca. 100, 200 and 300 nm, respectively. As can be seen in Fig. S10a/b (Supporting information), the deposition of a single $CuInS_2$ layer (100 nm) results in lower (photo-)conductivity than for a layer with the same thickness but deposited in several spin coating steps. Based on this observation it can be speculated that the $CuInS_2$ layers manufactured in several incremental steps are more capable to absorb the strain caused by the swelling of cellulose during the rinsing, thereby resulting in better electrical performance than the single deposited layers with the same thickness.

3.5. Preparation of microstructured $CuInS_2$ thin films by UV-light illumination

In addition to hybrid and inorganic thin film solar cells, $CuInS_2$ layers are also applied in waveguides, sensors, photodetectors, electroluminescent devices or photo catalysts. In most of these applications microstructured films are required, which contain spatially confined patterns of the semiconductor. It has been reported that microstructures of $CuInS_2$ can be realized by exposure of the copper and indium xanthate film to UV light (Rath, Kaltenhauser et al., 2013; Rath, Padeste et al., 2013). During this process, the metal xanthate film acts as a negative resist, the CuInX film becomes insoluble by conversion to $CuInS_2$ in the UV exposed areas.

In the case of our multilayer system, metal masks have been positioned onto the CuInX films after spin coating followed by exposure to UV-light. After the UV treatment, the films were washed in chloroform, to remove the non-exposed areas. For the patterning, masks with varying geometry have been used, each having a diameter of ca. 500 µm in diameter (see Fig. S11). To prevent excessive exposure of the cellulose films to UV light, we chose a short exposure time with relatively low UV light intensity. This mild UV exposure enabled the patterning of the film, however, to improve the conductivity of the patterned $CuInS_2$ thin films, they were annealed after the development procedure in a second step. By the heating step at 170 °C, the step height of the patterns decreased to values comparable to those observed for the conventionally heat treated films and also the obtained conductivities were comparable (see Fig. 8).

4. Conclusion

We demonstrated a proof of concept for the scalable manufacturing of cellulose-metal sulfide multilayered sandwich type films using cellulose xanthate precursors for the formation of cellulose and metal

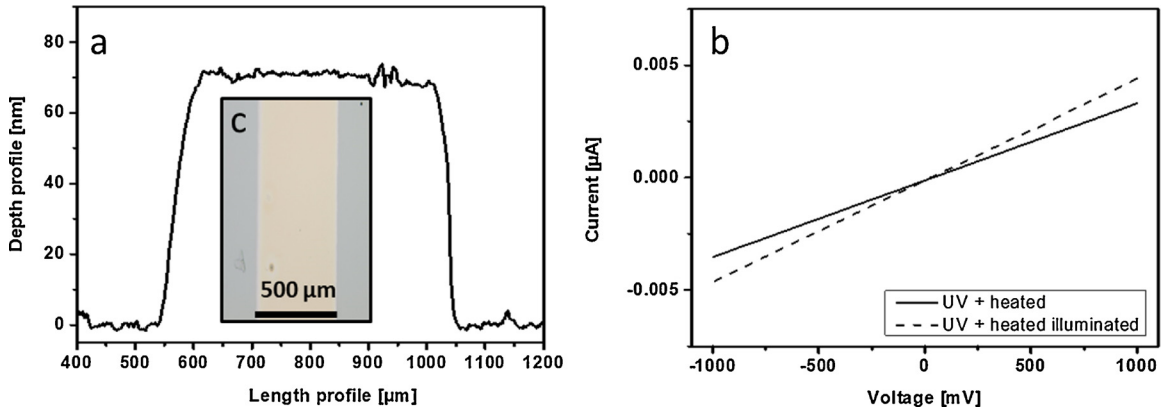

Fig. 8. Microscopy image of a $CuInS_2$ stripe generated by UV exposure Step height of a $CuInS_2$ stripe generated by UV exposure determined by profilometry (a) and its current/voltage profile (b). Microscopy image of the $CuInS_2$ stripe on a silicon wafer (c).

xanthate precursors for the formation of $CuInS_2$ layers. The approach uses subsequent spin coating steps to deposit the precursors onto a substrate (e.g., a silicon wafer) accompanied by a conversion in either cellulose (by TFA) or $CuInS_2$ (by heat). By variation of the concentration of the precursors, the film thickness can be easily varied for both of the components and homogeneous layers were obtained as shown by cross sectional analysis using SEM. The CuInX layers could also be converted to $CuInS_2$ using UV light, whereas the usage of masks allowed for the creation of $CuInS_2$ micropatterns with well-defined edges on the cellulose thin films. In principle, patterning at smaller scale is possible if masks with smaller feature sizes would be employed. The metal sulfide layers were conductive and photoconductivity was observed upon illumination. A 5 layered device could yield up to 0.05 µA at 1000 mV when the layer thickness of the $CuInS_2$ was set to 50 nm and the distance between the electrodes to 10 mm.

The combination of CX as starting material for the development of cellulose thin films and CuInX as source for the inorganic $CuInS_2$ layers enables a fully solvent based process, in which every single layer could be produced via spin coating and the corresponding development of the layer. Cellulose as bottom, intermediate and top layer is a green, biodegradable, highly available and lightweight matrix while being an insulator for a conductive system. In addition, the presented approach is generic allowing for the generation of any metal sulfide from metal xanthate thereby opening many opportunities in different fields such as catalysis, thin film membranes and battery systems to mention just a few. Since CX, a major industrial product for viscose fibers and film manufacturing is used, the scalability of the approach into industrial dimension is in principle possible. Although the subsequent spin-coating of different layers seems laborious, all the involved steps could be automatized in industry and the involved solution-based processing steps can be adapted to roll-to-roll compatible coating techniques. This includes the regeneration of CX to cellulose, rinsing as well as the heat treatment to convert the CuInX precursor to $CuInS_2$. It should be mentioned, that the recycling of the gaseous side products during the conversion of the xanthates is a well optimized process and does not pose major problems in industrial scale as already demonstrated for viscose manufacturing sites. However, the process still requires further optimization before upscaling can be taken into account. This involves a better understanding of the whole process involving probably *in situ* studies during the formation of the $CuInS_2$ layers at the cellulose-$CuInS_2$ interface as well as thorough investigations on the influence of the cellulose xanthate regeneration on the $CuInS_2$ layers underneath by grazing incidence small and wide angle scattering.

Acknowledgments

We kindly thank Martina Dienstleder (Graz Center for Electron Microscopy) for providing the schematic description of the ion beam slope cut technique and the Lenzing AG (Dr. Josef Innerlohinger) for supporting us with cellulose xanthate. WT and SE acknowledge financial support through the Accelerate3 project from the Interreg Vlaanderen-Nederland program and Flanders Innovation & Entrepreneurship for XPS. W.T. also thanks the Provincie West-Vlaanderen (Belgium) for financial support through his Provincial Chair in Advanced Materials.

Appendix A. Supplementary data

Supplementary material related to this article can be found, in the online version, at doi:https://doi.org/10.1016/j.carbpol.2018.09.063.

References

Al-Shakban, M., Matthews, P. D., Zhong, X. L., Vitorica-Yrezabal, I., Raftery, J., Lewis, D. J., et al. (2018). On the phase control of CuInS2 nanoparticles from Cu-/In-xanthates. *Dalton Transactions, 47*(15), 5304–5309.

Andrews, D. A., Hurtubise, F. G., & Krassig, H. (1960). The presence of monothiocarbonate substituents in cellulose xanthates. *Canadian Journal of Chemistry, 38*(8), 1381–1394.

Dautzenberg, H., & Philipp, B. (1970). Über Bildungsweise und Verhalten des Natriumdithiocarbonats. *Zeitschrift fur Anorganische und Allgemeine Chemie, 375*(2), 113–123.

Dunst, S., Rath, T., Radivo, A., Sovernigo, E., Tormen, M., Amenitsch, H., et al. (2014). Nanoimprinted comb structures in a low bandgap polymer: Thermal processing and their application in hybrid solar cells. *ACS Applied Materials & Interfaces, 6*, 7633–7642.

Filpponen, I., Kontturi, E., Nummelin, S., Rosilo, H., Kolehmainen, E., Ikkala, O., et al. (2012). Generic method for modular surface modification of cellulosic materials in aqueous medium by sequential "click" reaction and adsorption. *Biomacromolecules, 13*, 736–742.

Fradler, C., Rath, T., Dunst, S., Letofsky-Papst, I., Saf, R., Kunert, B., et al. (2014). Flexible polymer/copper indium sulfide hybrid solar cells and modules based on the metal xanthate route and low temperature annealing. *Solar Energy Materials and Solar Cells, 124*, 117–125.

Kargl, R., Mohan, T., Koestler, S., Spirk, S., Doliska, A., Stana-Kleinschek, K., et al. (2013). Functional patterning of biopolymer thin films using enzymes and lithographic methods. *Advanced Functional Materials, 23*(3), 308–315.

Kontturi, E., Tammelin, T., & Österberg, M. (2006). Cellulose model films and the fundamental approach. *Chemical Society Reviews, 35*, 1287–1304.

Kontturi, E., Thüne, P. C., & Niemantsverdriet, J. W. (2003). Cellulose model surfaces simplified preparation by spin coating and characterization by X-ray photoelectron spectroscopy, infrared spectroscopy, and atomic force microscopy. *Langmuir, 19*(14), 5735–5741.

Kontturi, K. S., Tammelin, T., Johansson, L.-S., & Stenius, P. (2008). Adsorption of cationic starch on cellulose studied by QCM-D. *Langmuir, 24*(9), 4743–4749.

Lai, C.-H., Lu, M.-Y., & Chen, L.-J. (2012). Metal sulfide nanostructures: Synthesis, properties and applications in energy conversion and storage. *Journal of Materials Chemistry, 22*(1), 19–30.

MacLachlan, A. J., Rath, T., Cappel, U. B., Dowland, S. A., Amenitsch, H., Knall, A. C., et al. (2015). Polymer/nanocrystal hybrid solar cells: Influence of molecular precursor design on film nanomorphology, charge generation and device performance. *Advanced Functional Materials, 25*, 409–420.

Macreadie Lauren, K., Maynard-Casely Helen, E., Batten Stuart, R., Turner David, R., & Chesman Anthony, S. R. (2014). Soluble xanthate compounds for the solution deposition of metal sulfide thin films. *ChemPlusChem, 80*(1), 107–118.

Mikhlin, Y. L., Karacharov, A. A., & Likhatski, M. N. (2015). Effect of adsorption of butyl xanthate on galena, PbS, and HOPG surfaces as studied by atomic force microscopy and spectroscopy and XPS. *International Journal of Mineral Processing, 144*, 81–89.

Mohan, T., Spirk, S., Kargl, R., Doliska, A., Vesel, A., Salzmann, I., et al. (2012). Exploring the rearrangement of amorphous cellulose model thin films upon heat treatment. *Soft Matter, 8*, 9807–9815.

Mohan, T., Zarth, C., Doliska, A., Kargl, R., Grießer, T., Spirk, S., et al. (2013). Interactions of a cationic cellulose derivative with an ultrathin cellulose support. *Carbohydrate Polymers, 92*, 1046–1053.

Niegelhell, K., Süßenbacher, M., Jammernegg, K., Ganner, T., Schwendenwein, D., Schwab, H., et al. (2016). Enzymes as biodevelopers for nano- and micropatterned bicomponent biopolymer thin films. *Biomacromolecules, 17*(11), 3743–3749.

Ogura, K., & Sobue, H. (1968). Studies on the derivatives of sodium cellulose xanthate. Part I. Infrared absorption spectra and characteristic frequencies of C—S and C═S groups in sodium cellulose xanthate and its stable derivatives. *Journal of Polymer Science Part B: Polymer Letters, 6*(1), 63–67.

Orelma, H., Johansson, L.-S., Filpponen, I., Rojas, O. J., & Laine, J. (2012). Generic method for attaching biomolecules via avidin-biotin complexes immobilized on films of regenerated and nanofibrillar cellulose. *Biomacromolecules, 13*, 2802–2810.

Owens, D. K., & Wendt, R. C. (1969). Estimation of the surface free energy of polymers. *Journal of Applied Polymer Science, 13*(8), 1741–1747.

Pradhan, N., Katz, B., & Efrima, S. (2003). Synthesis of high-quality metal sulfide nanoparticles from alkyl xanthate single precursors in alkylamine solvents. *The Journal of Physical Chemistry B, 107*(50), 13843–13854.

Rath, T., Edler, M., Haas, W., Fischereder, A., Moscher, S., Schenk, A., et al. (2011). A direct route towards polymer/copper indium sulfide nanocomposite solar cells. *Advanced Energy Materials, 1*(6), 1046–1050.

Rath, T., Kaltenhauser, V., Haas, W., Reichmann, A., Hofer, F., & Trimmel, G. (2013). Solution-processed small molecule/copper indium sulfide hybrid solar cells. *Solar Energy Materials and Solar Cells, 114*, 38–42.

Rath, T., Padeste, C., Vockenhuber, M., Fradler, C., Edler, M., Reichmann, A., et al. (2013). Direct extreme UV-lithographic conversion of metal xanthates into nanostructured metal sulfide layers for hybrid photovoltaics. *Journal of Materials Chemistry A, 1*, 11135–11140.

Redington, R. L., & Lin, K. C. (1971). Infrared spectra of trifluoroacetic acid and trifluoroacetic anhydride. *Spectrochimica Acta, Part A, 27*(12), 2445–2460.

Reishofer, D., Ehmann, H. M., Amenitsch, H., Gspan, C., Fischer, R., Plank, H., et al. (2017). On the formation of Bi2S3-cellulose nanocomposite films from bismuth xanthates and trimethylsilyl-cellulose. *Carbohydrate Polymers, 164*, 294–300.

Reishofer, D., Rath, T., Ehmann, H. M., Gspan, C., Dunst, S., Amenitsch, H., et al. (2017). Biobased cellulosic–CuInS2 nanocomposites for optoelectronic applications. *ACS Sustainable Chemistry & Engineering, 5*, 3115–3122.

Schaub, M., Wenz, G., Wegner, G., Stein, A., & Klemm, D. (1993). Ultrathin films of cellulose on silicon wafers. *Advanced Materials, 5*(12), 919–922.

Scheer, R., & Lewerenz, H. J. (1994). Photoemission study of evaporated CuInS2 thin films. II. Electronic surface structure. *Journal of Vacuum Science & Technology A, 12*(1), 56–60.

Široký, J., Blackburn, R. S., Bechtold, T., Taylor, J., & White, P. (2010). Attenuated total reflectance Fourier-transform infrared spectroscopy analysis of crystallinity changes in lyocell following continuous treatment with sodium hydroxide. *Cellulose, 17*(1), 103–115.

Spirk, S., Belaj, F., Kahr, J., & Pietschnig, R. (2009). A one-dimensional coordination polymer formed by a 2:1 adduct of trifluoroacetic acid and its sodium salt. *Journal of Fluorine Chemistry, 130*(3), 365–367.

Vagvala, T. C., Pandey, S. S., Ogomi, Y., Ma, T., & Hayase, S. (2015). Investigation of metal xanthates as latent curing catalysts for epoxy resin via formation of in-situ metal sulfides. *Inorganica Chimica Acta, 435*, 292–298.

Weißl, M., Niegelhell, K., Reishofer, D., Zankel, A., Innerlohinger, J., & Spirk, S. (2018). Homogeneous cellulose thin films by regeneration of cellulose xanthate: Properties and characterization. *Cellulose, 25*(1), 711–721.

Wolfberger, A., Petritz, A., Fian, A., Herka, J., Schmidt, V., Stadlober, B., et al. (2015). Photolithographic patterning of cellulose: A versatile dual-tone photoresist for advanced applications. *Cellulose, 22*, 717–727.

Supporting Information

Multi-layered nanoscale cellulose/$CuInS_2$ sandwich type thin films

Michael Weißl[1], Thomas Rath*[2], Jürgen Sattelkow[3], Harald Plank[3], Samuel Eyley[4], Wim Thielemans[4], Gregor Trimmel[2] and Stefan Spirk*[1]

1) Graz University of Technology, Institute of Paper, Pulp and Fibre Technology, Inffeldgasse 23A 8010 Graz

2) Graz University of Technology, Institute for Chemistry and Technology of Materials, NAWI Graz, Stremayrgasse 9 8020 Graz

3) Graz University of Technology and Centre for Electron Microscopy; Institute for Electron Microscopy and Nanoanalysis, Steyrergasse 17, 8010 Graz, Austria

4) Renewable Materials and Nanotechnology Research Group, Department of Chemical Engineering, KU Leuven Campus Kulak Kortrijk, Etienne Sabbelaan 53, 8500 Kortrijk, Belgium.

Correspondence:

Stefan Spirk

Email: stefan.spirk@tugraz.at

+43 (316) 873 – 30763

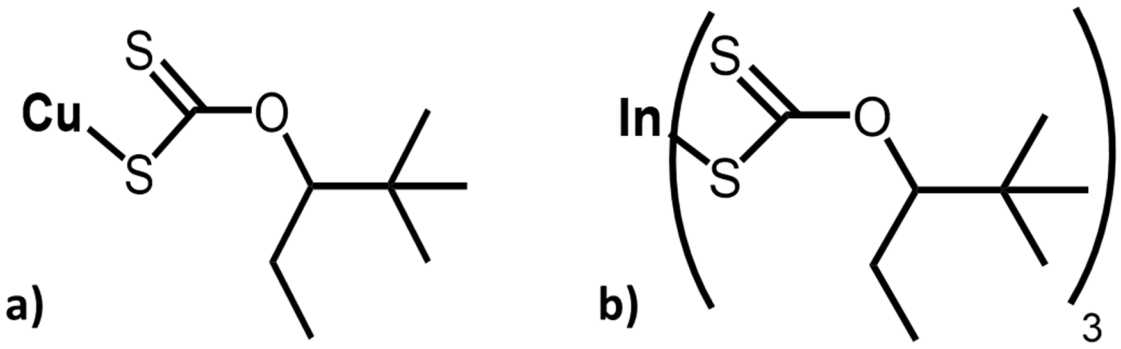

Figure S1. Chemical structures of a) CuX (copper O-2,2-dimethylpentan-3-yl dithiocarbonate) and b) InX (indium O-2,2-dimethylpentan-3-yl dithiocarbonate)

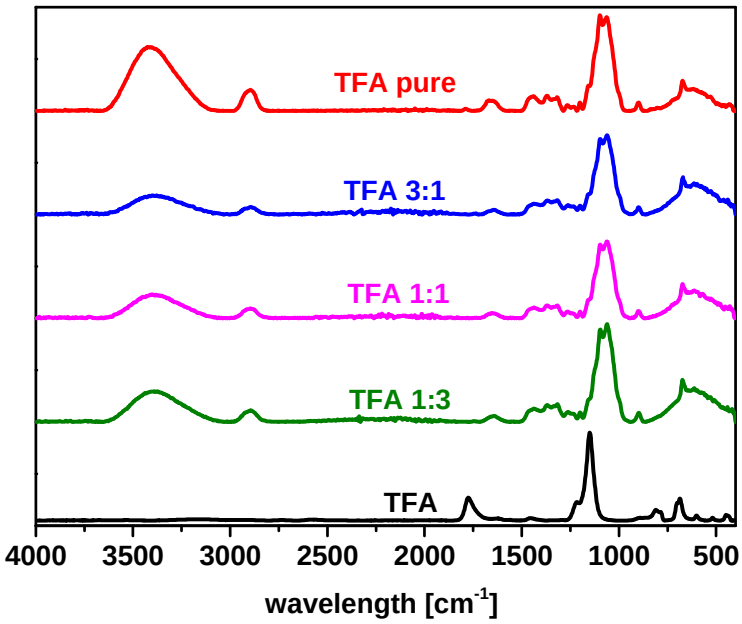

Figure S2. Comparison of ATR-IR spectra after regeneration of CX films with vapors created from different TFA aqueous solutions.(pure, 3:1, 1:1, 1:3) for 20 minutes.

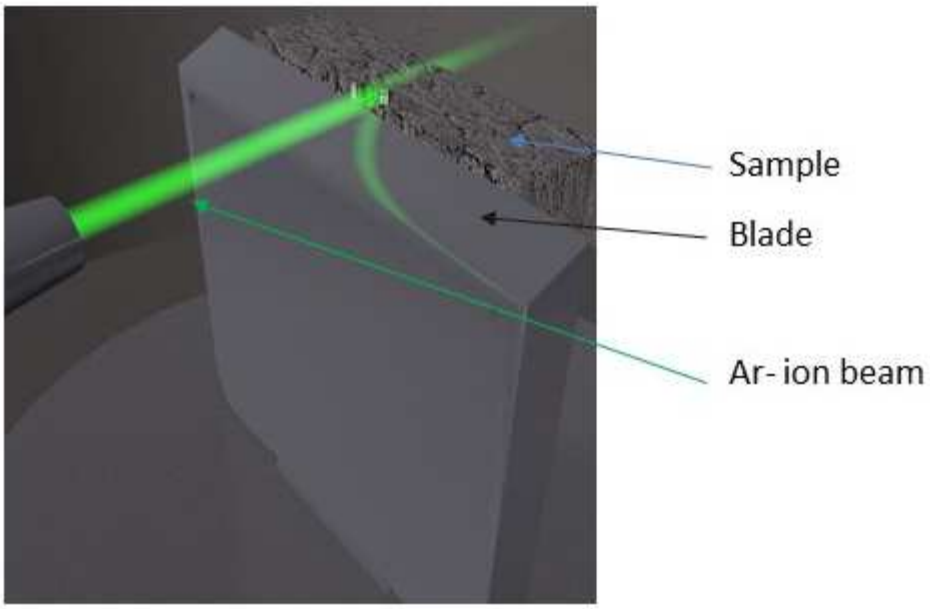

Figure S3. Schematic description of the sample preparation in the low energy ion beam slope cutting process as preliminary treatment for the scanning electron microscopy.

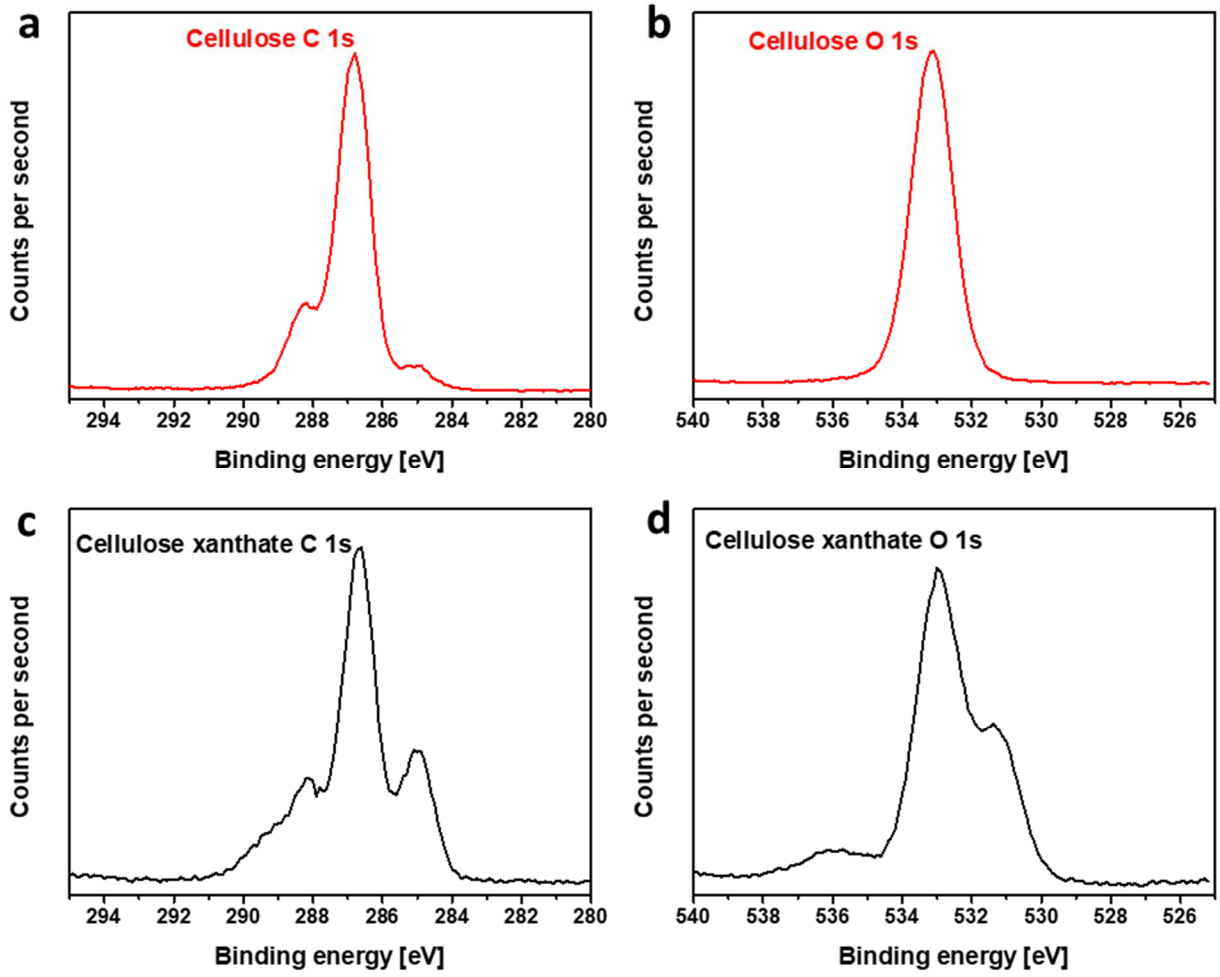

Figure S4a. XPS high resolution spectra of carbon 1s and oxygen 1s from a TFA vapor regenerated and washed Cellulose film (a, b) and carbon 1s and oxygen 1s spectra of a CX precursor film (c, d).

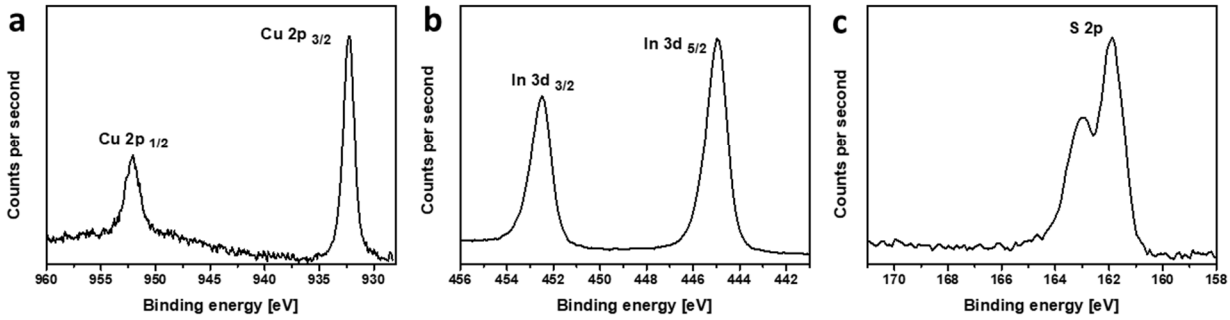

Figure S4b. XPS high resolution spectra of Cu 2p (a), In 3d (b) and S 2p (c) in a $CuInS_2$ layer with 30 nm thickness.

Table S1. Layer thicknesses [nm] of the multilayered thin films in dependence of the number of layers.

	Average total layer thickness	Standard deviation	Average single layer thickness
Layer 1	153.9	6.1	153.9
Layer 2	184.5	4.8	30.6
Layer 3	334.0	10.9	149.5
Layer 4	366.8	5.9	32.8
Layer 5	535.0	11.4	168.2

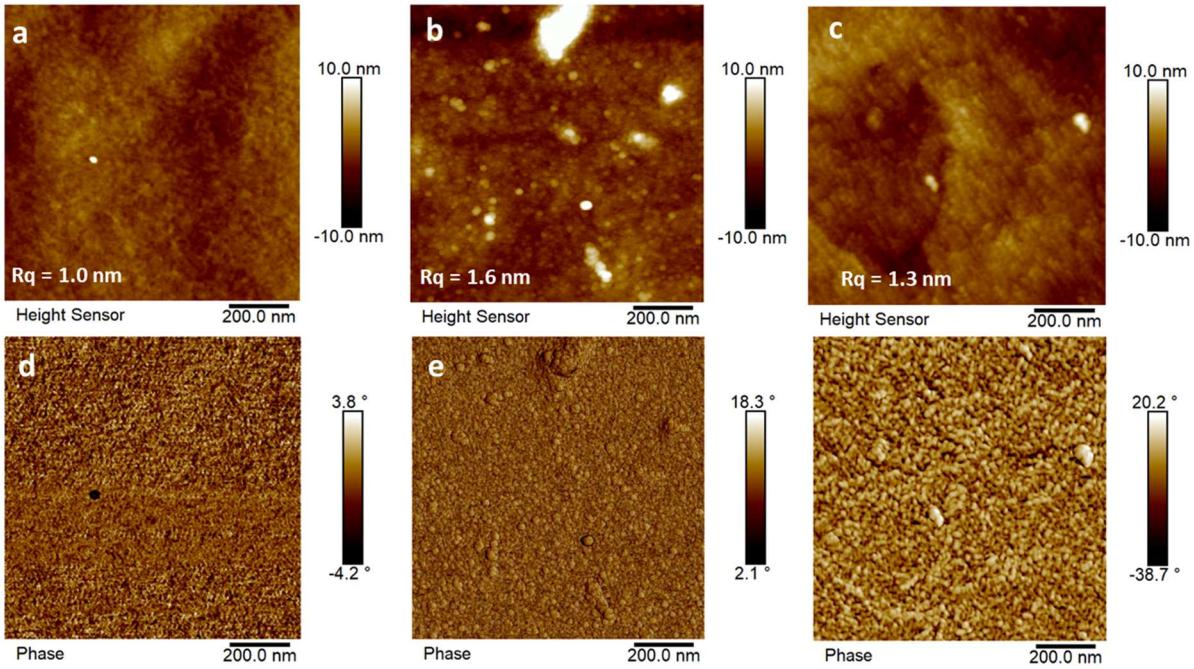

Figure S5. AFM topography images (1 x 1 µm²) in the upper row, AFM phase images (1 x 1 µm²) in the lower row after the final processing of Layer 3 (a, d), Layer 4 (b, e) and Layer 5 (c, f).

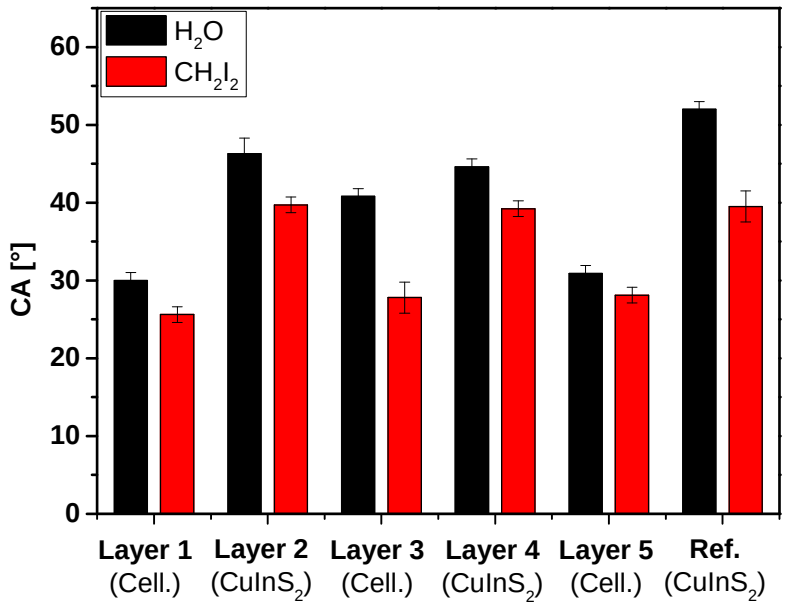

Figure S6. Static contact angles (H_2O, CH_2I_2) in dependence of the number of applied layers in the multilayer stack and a $CuInS_2$ reference thin film prepared on a silicon substrate.

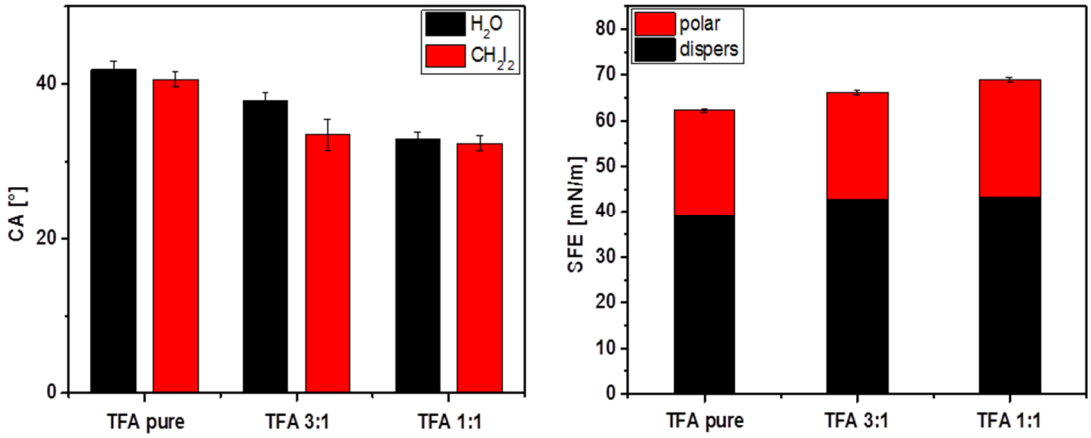

Figure S7. Static contact angles (H2O, CH2I2) of cellulose layers regenerated in TFA vapors from different TFA dilution (left) and the corresponding SFE values (right)

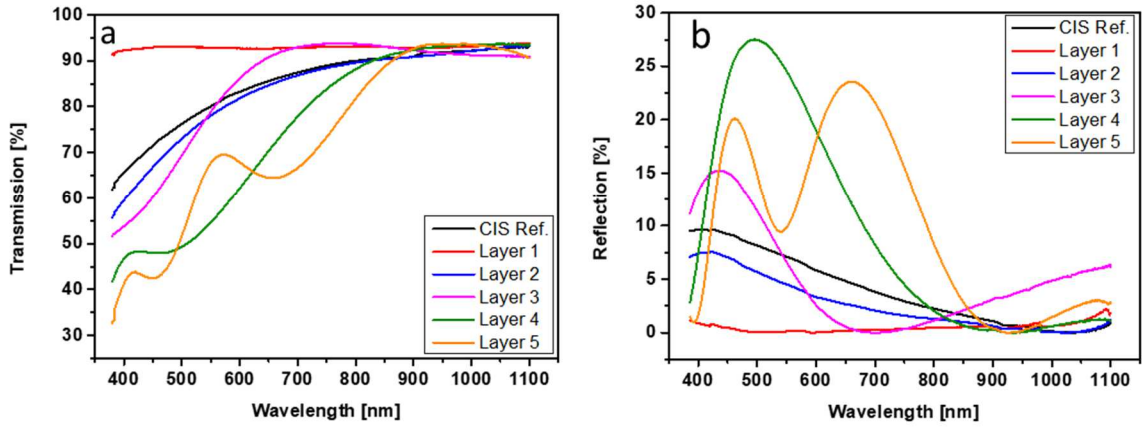

Figure S8. UV-Vis transmission (a) and reflection (b) spectra of a cellulose $CuInS_2$ multilayer device with an increasing number of layers in the system

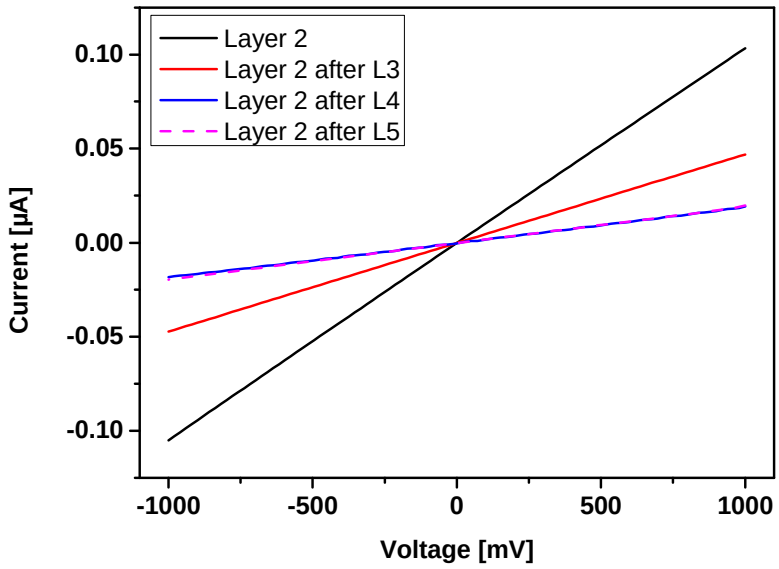

Figure S9. Current/voltage curves of L2 ($CuInS_2$, thickness 100 nm) during development of a five layered system

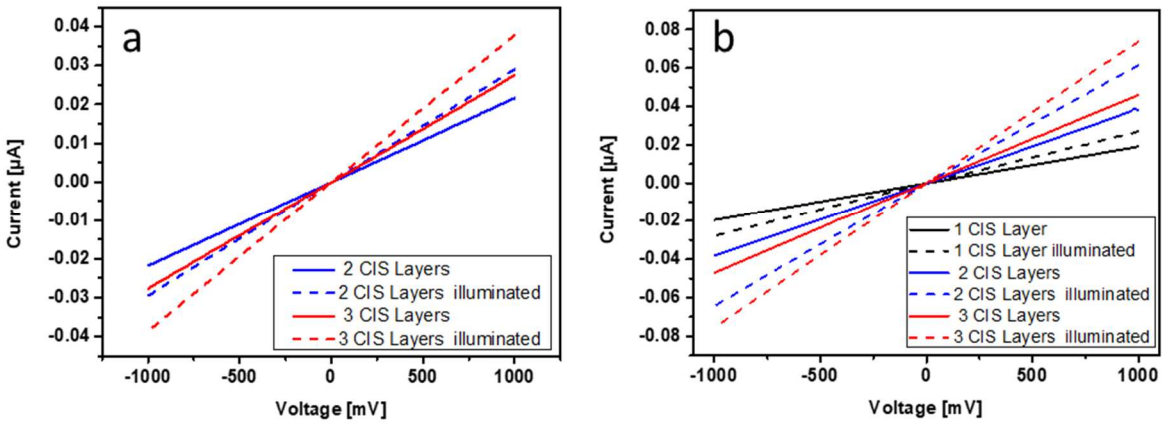

Figure S10. (a) Current/voltage curves of a $CuInS_2$ layer consisting of up to three single $CuInS_2$ layers spin coated with the standard concentration (layer thickness 40 - 45 nm per sublayer and (b) 100 nm per sublayer. In all two/three samples, the $CuInS_2$ film is embedded between two cellulose layers.

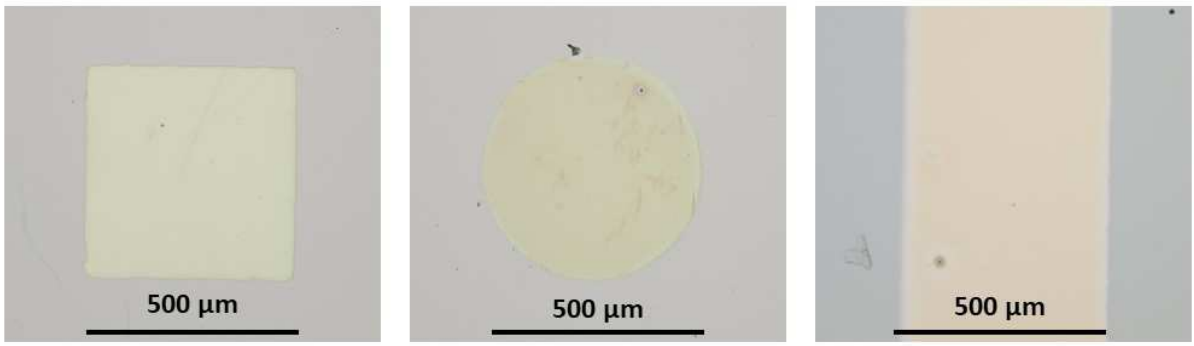

Figure S11. Photographic images of CuInX films on Si Wafers exposed to UV irradiation using differently shaped masks.

Paper #6

Cellulose carbamate derived cellulose thin films – Preparation, characterization and blending with cellulose xanthate

Submitted to Cellulose

For this paper, I conducted most of the experiments, interpreted the data and wrote a significant part of the manuscript.

Cellulose carbamate derived cellulose thin films – Preparation, characterization and blending with cellulose xanthate

Michael Weißl[1], Mathias Andreas Hobisch[1], Leena Sisko Johansson[2], Kay Hettrich[3], Eero Kontturi[2], Bert Volkert[3], Stefan Spirk[1]

1) Institute for Paper, Pulp and Fibre Technology, Graz University of Technology, Inffeldgasse 23, 8010 Graz, Austria

2) Department of Bioproducts and Biosystems (BIO2), Aalto University, P.O.Box 16300, 00076 Aalto, Finland

3) Fraunhofer Institute for Applied Polymer Research IAP ,Geiselbergstrasse 69, 14167 Potsdam-Golm, Germany

Correspondence:

Stefan Spirk

stefan.spirk@tugraz.at

+43 (316) 873 – 30763

Abstract:

Cellulose carbamate (CC) was employed as a water-soluble precursor in the manufacturing of cellulose based thin films using the spin coating technique. An intriguing observation was that during spin coating of CC from alkaline aqueous solutions, regeneration to cellulose was accomplished without the addition of any further chemicals. After rinsing, homogeneous thin films with tunable layer thickness in a range between 20 and 80 nm were obtained. Further, CC was blended with cellulose xanthate (CX) in different ratios (3:1, 1:1, 1:3) and after regeneration the properties of the resulting *all*-cellulose blend thin films were investigated. We could not observe any phase separation by means of atomic force microscopy, indicating good compatibility of the two different cellulose domains. The layer thickness of the blend thin films is nearly independent of the ratio of the components, with values between 50 and 60 nm for the chosen conditions. The water uptake capability (80-90% relative to the film mass) determined by H_2O/D_2O exchange in a quartz crystal microbalance is independent of the blend ratio.

Keywords

Cellulose carbamate; Cellulose xanthate; all cellulose blend films; Cellulose thin film; Cellulose swelling

1. Introduction:

Despite being rather old, the Viscose process still is the most important and frequently used technology for the production of regenerated wood based fibers with annual production volumes exceeding 3.5 million tons, mainly for the textile industry.(Wang et al. 2016) (Hämmerle 2011) However, there are several environmental drawbacks of this technology. For instance, the necessity to use CS_2 to form the cellulose precursor material (cellulose xanthate, CX), as well as the development of volatile sulfur containing compounds (e.g. H_2S, COS) during the regeneration procedure requires complex recovery technologies, which manifest into higher prices of the final fiber products. These disadvantages have led to the development of new fiber spinning technologies such as the Lyocell and the Ioncell processes that both avoid the use of cellulose derivatives by direct dissolution into NMMO/water and ionic liquids.(Rosenau et al. 2001; Sixta et al. 2015) However, costs are still higher for fibers derived from these processes since also here the recovery of the solvents requires substantial energy input. Another technology that has raised attention in recent years is the Carbacell process. The Carbacell process relies on cellulose carbamate (CC), which is easily obtained by reacting cellulose with urea. CC is soluble in cold alkali and can be subjected to wet spinning processes similar to those in viscose plants.(Fink et al. 2014) As regeneration bath, a diluted acid or a sodium carbonate solution can be used.(Wendler et al. 2012) The similarities in the solvent, the spinning process and the regeneration bath also allows for fiber spinning of solutions containing CX and CC, with the goal to reduce the usage of CS_2 in the fiber manufacturing process.

In recent literature, the processing of regenerate cellulose fibers from spinning dopes, blended with CC and CX was described and mechanical properties of the obtained fibers were studied. But fundamental questions concerning the miscibility of the two cellulose derivatives or possibly occurring phase separation during various process steps, could not be answered in these macroscopic studies. In addition, development of dense core shell structured fibers during wet spinning and subsequent fiber stretching prohibits a detailed study of the cellulose interfaces in those blend materials.(Protz et al. 2018)

Thus the processing of cellulose thin films based on CC, CX and blends of these solutions delivers promising possibilities to study the influence of the CC on the CX. Cellulose thin films provide a confined two-dimensional network with a well-defined surface morphology and chemistry. (Kontturi et al. 2006) Literature gives many examples, where thin films have been employed to study the influence of certain conditions on the behavior of cellulose and its derivatives, or to observe the interaction of cellulose with biopolymers or proteins.(Ehmann et al. 2015; Mohan et al. 2017; Niegelhell et al. 2016; Niinivaara et al. 2016) In a previous work, some of us published a method for the processing of cellulose thin films based on the spin coating and following HCl vapor exposure of CX films.(Weißl et al. 2018) This made us interested in the fundamental suitability of CC solutions to form thin film structures. As the processing of the CC can be assigned as green and sustainable, the solubility in diluted sodium hydroxide allows to avoid organic solvents and the regeneration in acidic media should also be possible in an acidic vapor phase. Further, CX and CC are soluble in the same solvent, offering opportunities to blend the solutions and spin coat cellulose thin films from two different sources, thereby creating *all*-cellulose blend thin films.(Protz et al. 2018) The blending of these two promising and well known cellulose derivatives does not only allow to study cellulose - cellulose interfaces in a well-defined environment, but can be used to explore the influence of CC on CX during the formation and regeneration to cellulose. Through the confined two-dimensional structure, this blend film processing could show interactions and effects which are not visible in the wet spinning of blended solutions from CC and CX.

2. Experimental:

2.1 Materials

Cellulose carbamate (CC) with a DS of 0.3 (N content 2.51% according to elemental analysis), a DP of 450 and a dry mass of 92% was provided from Fraunhofer Institute for Applied Polymer Research (Potsdam-Golm, Germany) and used without any further treatment. Cellulose xanthate (CX) stock solution with a cellulose content of 10 wt.%, a DS of 0.5 and a DP of 550 was provided from Lenzing AG (Lenzing, Austria). Sodium hydroxide, hydrochloric acid (37%), sulfuric acid (95%) and hydrogen peroxide (30%) were purchased from VWR chemicals. De-ionized (DI) water was produced in house with an Elga PURELAB Prima (Bucks, United Kingdom) water treatment system. Chromafil Filters Xtra PVDF-45/25 0.45 µm were used as obtained. Single side polished silicon wafers from Siegert Wafers (Aachen, Germany, wafer thickness: 675 ± 25 µm, 1 cm × 2 cm) and gold coated glass slides from BioNavis (Tampere, Finland, gold layer thickness: 50 nm, 1 cm × 2 cm) were used as substrates for the cellulose thin films. QCMD sensors (QSX301) were purchased from nanoscience Instruments (phoenix, USA)

2.2 Cellulose Carbamate film processing

For the spin coating process, CC (1.0, 1.5, 2.0, 2.5 wt.%) was dissolved in 8% NaOH solution at -10 °C under vigorous stirring for 24 h. The solutions were filtered through a 0.45 µm filter and subjected to spin coating (v = 4000 rpm, a = 2500 rpm/s, t = 60 s). The slides used as substrates for the films were cleaned by dipping them into piranha acid (H_2SO_4:H_2O_2 = 3:1 (v/v)) for 30 min (10 min for gold slides) followed by intense rinsing with MilliQ water. After spin coating, the films were stored for at least 1 h under ambient conditions before they were rinsed with 10 ml DI water and dried under nitrogen flow. Additionally, the films were treated in acid vapor atmosphere (37% HCl) for a period of 20 min (Figure S1, SI) with subsequent rinsing (10 ml DI water) and a final drying process at 105°C for 60 min.

2.3 CC/CX Blend film processing

A 2.0 wt.% CX solution was prepared by diluting the provided stock solution with 8% NaOH under adequate shaking and subsequent filtration through a 0.45 µm filter. This CX solution was mixed with a 2.0 wt.% CC solution in different ratios (1:0, 3:1, 1:1, 1:3, 0:1) for a period of 10 min under sonication. This solution was deposited on a substrate and subjected to spin coating (v = 4000 rpm, a = 2500 rpm/s, t = 60 s), followed by HCl vapor exposure (20 min) with subsequent rinsing (10 ml DI water) and drying in a stream of nitrogen.

2.4 Optical Microscopy

Light microscopy images were taken by an Olympus BX60 equipped with an Olympus E-520 camera. Prior to investigating the samples, carrier substrates were fixed on a glass layer.

2.5 Elemental Analysis

Elemental analysis was carried out by a vario MICRO analyser from Elementar (Langensebold, Germany), where the samples are burned within a jet injection of oxygen. The gaseous components were purified and separated on a TPD column, before quantification with a thermal conductivity detector. Helium was used as a carrier gas.

2.6 XPS

Surface chemistry was evaluated with XPS, using a Kratos AXIS Ultra photoelectron sprctrometer with monochromated Al Kα irradiation at low power (100W) and under neutralization. Prior to the experiment samples were pre-evacuated overnight, in order to stabilize experimental conditions. Samples were measured together with the lab-defined of in-situ reference of 100% cellulose (Whatman). Both wide energy resolution scans, with 1 eV step and 80 eV CAE, and high resolution scans of C1s and O1s regions with 0.1 eV step and 20 eV CAE were recorded on 2-3 locations. Nominal analysis spot size is 400 x 800 µm. All binding energies were charge-corrected using the cellulose C1s main component of C-O at 286.7 eV, after fitting the high resolution carbon data into four Gaussian components with equal half widths, using CasaXPS software.(Johansson and Campbell 2004)

2.7 Profilometry

The layer thickness was determined with a Bruker DekTak XT surface profiler. The scan length was set to 1000 µm over the duration of 3 s with the hills and valleys scanning profile. The diamond stylus had a radius of 12.5 µm and the employed force was 3 mg. The sample was samples were scraped before measuring and the obtained profile was then used to determine the thickness. Each layer thickness has been determined by averaging 9 measurements on three different slides.

2.8 Attenuated total reflection – infrared spectroscopy

The infrared spectra were recorded with an ALPHA FT-IR spectrometer (Bruker; Billerica, MA, U.S.A.). For the measurement, an attenuated total reflection (ATR) attachment was used with 48 scans at a resolution of 4 cm^{-1} and a scan range between 4000 and 400 cm^{-1}. The samples were prepared on Au-coated glass slides (SPR102-AU). The data were analyzed with OPUS 6.0 software.

2.9 Atomic force microscopy

The surface was investigated with a Tosca™ 400 atomic force microscope (AFM, Anton Paar, Austria) in tapping mode using Al-coated cantilevers (ARROW-NCR, NanoWorld AG, Switzerland) with a resonance frequency of 285 kHz and a force constant of 42 N m^{-1}. All measurements were acquired at room temperature under ambient conditions. All calculations and image processing was performed with Tosca™ analysis (V7.4.8341, Anton Paar, Austria).

2.10 Contact angle and surface free energy determination

For the calculation of the surface free energy (SFE) Milli-Q water (≥18 $M\Omega cm^{-1}$) and diiodomethane were employed as test liquids. The drop shape analysis was done in the sessile drop modus at 25 °C with a DSA100 system (Krüss GmbH, Hamburg, Germany) equipped with a T1E CCD video camera (25 fps). The dispense rate of the three µL droplets was adjusted to 256 µL/min and the time before the image was captured was set to 1 s. Each sample was measured at least six times on at least two samples. The contact angle (CA) calculations (software: DSA1 v 1.90) were performed with Young-Laplace equation and the surface free energy calculation according to the Owens-Wendt-Rabel & Kaelble method.(Owens and Wendt 1969)

2.11 Quartz crystal microbalance with dissipation monitoring

A QCM-D from Q-Sense (Gothenburg, Sweden) with simultaneous detection of the resonance frequency (Δf) and energy dissipation (ΔD) of an oscillating piezoelectric crystal was employed. Dissipation describes the frictional losses which cause a damping of the oscillation in correlation to the

viscoelastic properties to the materials absorbed on the crystals. Rigid layers are assumed to fully couple to the oscillation of the crystal, where the change in frequency Δf is given by the Sauerbrey equation

$$\Delta m = C\frac{\Delta f_n}{n} \quad (1)$$

C is the Sauerbrey constant (-17.7 ng Hz^{-1} cm^{-2} for a 5 MHz crystal), Δ*m* is the changing mass of the crystal due to the adsorbed layer and *n* is the overtone number.(Sauerbrey 1959) The baseline resonance frequencies for the crystals were determined before depositing the cellulose layers and subsequent determination of the water content in the layers was done with a H_2O/D_2O exchange experiment, as described by Kittle et al.(Kittle et al. 2011; Mohan et al. 2012)

Determination of the water equilibrium content

By exploiting differences in viscosity and density of H_2O/D_2O, the amount of water uptake by the accessible parts of the thin films can be determined. Based on the Kanazawa(Keiji and Gordon 1985) equation it follows:

$$\frac{\Delta f_{H_2O}}{n} = \frac{\frac{\Delta f_{film}}{n} - \frac{\Delta f_{bare}}{n}}{\frac{\rho_{D_2O}}{\rho_{H_2O}} - 1} \quad (2)$$

where Δ*f*(film) and Δ*f*(bare) describe the frequency shifts caused by an exchange of H_2O by D_2O on a bare substrate and on substrates coated with a blend film respectively. The density ρ is 0.9982 g/cm^3 for H_2O and 1.1050 g/cm^3 for D_2O, *n* is the overtone number and Δf(H_2O) is the frequency shift, induced by the water absorbed in the cellulose films. With the Sauerbrey equation, Δf(H_2O) can directly be transferred in a total water content.

$$\Gamma_{water} = C * \frac{\Delta f_{H_2O}}{n} \quad (3)$$

After recording the resonance frequencies before and after coating, the QCM-D flow cell was flushed with MilliQ water (0.1 ml/min) for 30 minutes. After equilibration, the water was exchanged with D_2O and the cells were flushed for another 30 minutes with D_2O. Finally, the system was changed back to water again. The H_2O/D_2O exchange was also done with uncoated crystals, as reference. For each experiment, at least three parallel measurements have been performed. The determined mass of the exchanged water was then correlated to the film mass to adjust the results to the thickness of the films.

3. Results and discussion:

Formation and characterization of pure CC thin films

The microscopic studies of the layers during the ongoing process steps in the film formation (spin coating, rinsing, acid vapor deposition, drying) delivered interesting observations. The spin coating of CC solutions with concentrations between 1.0 and 2.5 wt.% provided fully and regularly covered slides with a smooth surface. Below a concentration of 1.0 wt.% the coverage of the slide was incomplete and inhomogeneous above 2.5 wt.% the solution could not be filtered anymore and the resulting films showed a high surface roughness and irregularities caused by aggregates (data not shown).

After spin coating was finished, a crystalline, needle-shaped top layer formed covering the whole substrate within seconds (Figure S2, SI). After rinsing the films with de-ionized water, the crystalline top layer was washed away and a smooth cellulose layer with a defined morphology remained on the substrate. The following acid vapor deposition as well as the drying process did not cause a visible change in the surface morphology of the films.

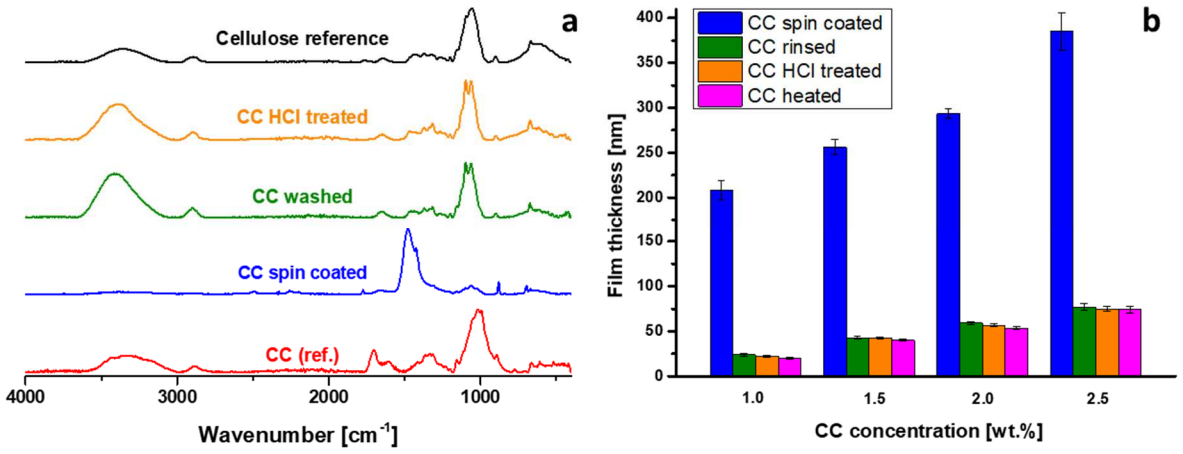

Figure 1 a) ATR-IR spectra of the CC source (ref.) and the CC during the processing to cellulose thin films. b) Film thickness of CC thin films during processing of different CC concentrations

Figure 1a summarizes the IR spectra of the thin films during processing and the corresponding reference materials. The CC used as starting material features characteristic broad bands in a region of 3600 to 3100 cm^{-1} (OH vibration) and around 2900 cm^{-1} (CH stretching) followed by a series of small bands between 1430 to 1150 cm^{-1} (C-O-H bending at 1430 cm^{-1}, C-H deformation at 1372 cm^{-1}, OH in plane deformation at 1330 and at 1200 cm^{-1}) and strong overlapping bands between 1160 and 890 cm^{-1} (asym. C-O-C vibration at 1155 cm^{-1}, sym. C-O vibration at 1060 cm^{-1}, C-O stretching at 1035 cm^{-1} and C-O-C valence vibration at 899 cm^{-1}). (Široký et al. 2010) In addition to the cellulose induced bands, two significant bands at 1620 and 1700 cm^{-1} indicate the presence of carbamates.(Nada et al. 2000; Xiong et al. 2017)

After spin coating, the spectrum of the precipitated CC shows interesting differences in comparison to the CC source material. Strong overlapping bands at 1480, 1420 and 880 cm^{-1} are characteristic for sodium carbonate and clearly dominate the spectrum, whereas bands caused by cellulose and sodium hydroxide are much less pronounced.(Neufeld et al. 2002) The intensive sodium carbonate band and the described growth of a crystalline structures after spin coating suggest the expected formation of a sodium

salt top layer.(Weißl et al. 2018) After rinsing the substrates, a spectrum matching all the cellulose bands as described by Siroky et al is obtained (Široký et al. 2010). Further treatment in an HCl vapor phase or drying at 105°C does not affect the cellulose structure according data from infrared spectroscopy. The detailed spectra are shown in Figure S3 to S6, SI. The feature at 1647 to 1650 cm^{-1} can be assigned to adsorbed water on cellulose as described in literature. This band occurs in all the spectra even in those that do not contain any cellulose carbamate (i.e. cellulose from CX).

To further confirm that regeneration of the CC already occurs during spin coating, XPS spectroscopy was employed. The XPS survey spectra did not reveal the presence of nitrogen and sodium in the films after rinsing (Figure S7, SI). Figure 2 summarizes carbon and oxygen high resolution spectra of spin coated CC after rinsing the films with DI water and after additional HCl vapor treatment.

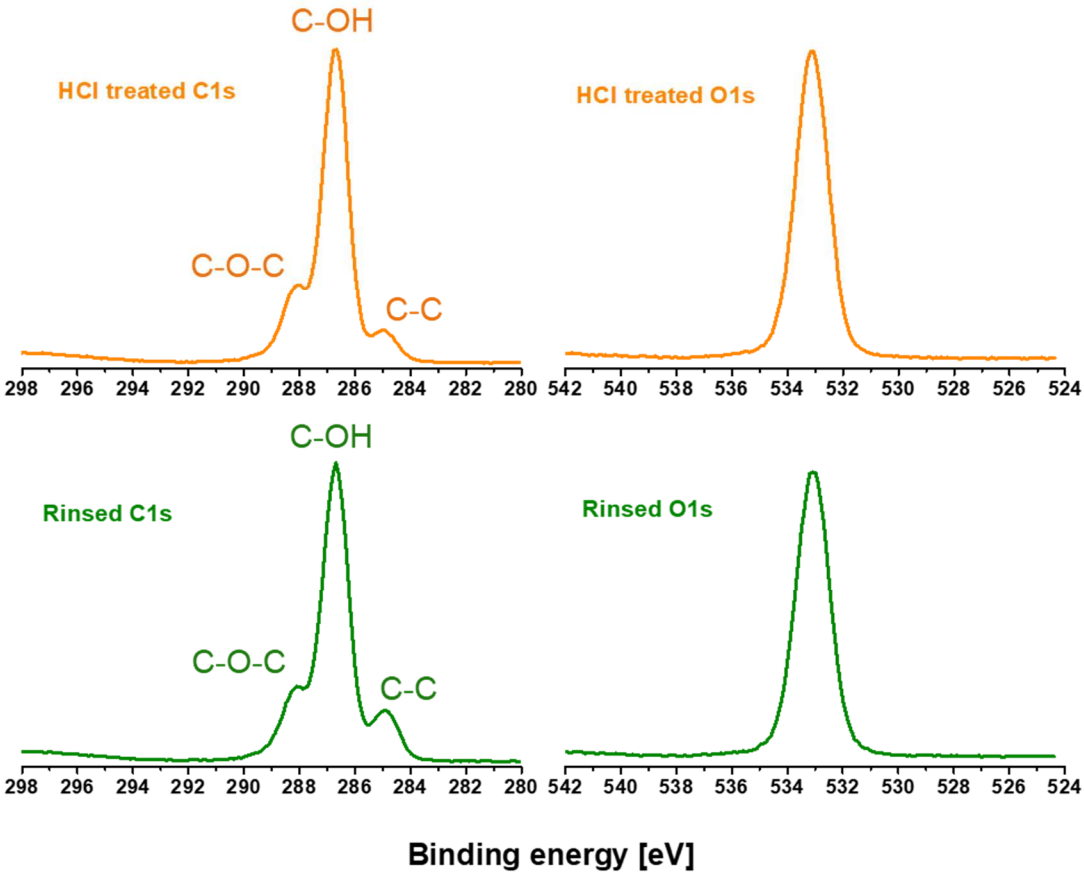

Figure 2 XPS high-resolution spectra of C and O environment after rinsing and HCl vapor treatment.

Both, the C1s and the O1s environments match the bonding energies previously described for cellulose materials. The C1s peaks showed three single environments namely C-C (H) at 284.5, C-OH at 286.5 and C-O-C at 288 eV, respectively, whereas the O1s peak features only one environment at 533.5 eV. A shift in the described binding energies or new bands suggesting changes in the cellulose structure, could not be detected within all post spin coating treatments.(Shchukarev et al. 2002)

The conversion to cellulose by spin coating is an intriguing observation. To the best of our knowledge, there are not any reactions that are induced by spin coating in literature. In our case, we have a case where the basicity of the system is strongly increasing during spin coating due to water evaporation leaving hydrated sodium hydroxide inside the film. It is known that primary carbamates in general may be subject to decomposition under alkaline conditions via an addition-elimination mechanism. In such

reactions, the nucleophile (OH-) attacks the carbon at the carbamate group under elimination of NH_3.(Moidoveanu and David 2002) These reactions are very often kinetically driven, i.e. steric hindrance plays a role and determines under which conditions these reactions take place. In case of cellulose, the carbamate group is sterically protected and anchored on a polymer, thereby slowing down the reaction.(Fu et al. 2014; Nada et al. 2000) There are reports to regenerate cellulose carbamate fibers in diluted hot alkaline solutions, corroborating the kinetic nature of the decomposition reaction.(Klemm et al. 2005; Kunze and Fink 2005) In our case, the conversion to cellulose probably involves the diffusion of the labile carbamic acid to the cellulose-air interface, where there it is decomposed to form sodium carbonate under elimination of ammonia. This would also explain the formation of the crystalline layer shortly after spin coating has been accomplished and is supported by the ATR IR spectra that show all the typical bands associated with sodium carbonate.

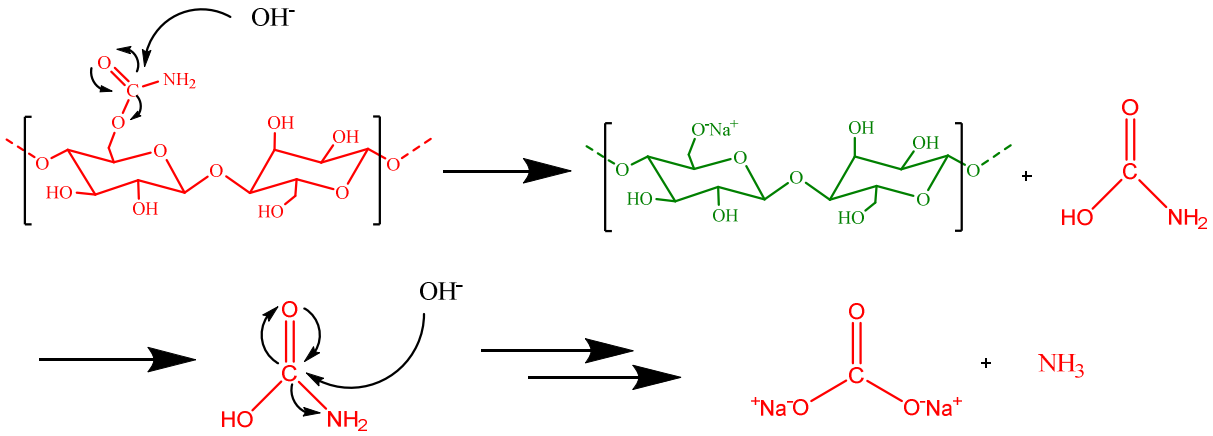

Scheme 1 Carbamate decomposition induced by the increasing basicity of the system during ongoing spin coating

The layer thickness for films prepared from different CC solutions is depicted in Figure 1b. It is noticeable that the evolution of the layer thickness during the processing is similar for the different concentrations. Prior to rinsing the films with DI water, a thickness of 200 to 400 nm is measured; after rinsing the thickness decreases significantly and remains nearly unchanged after the HCl vapor treatment and the drying step at 105°C. The cellulose layer thickness after removing the NaOH crystals is 22, 42, 56 and 75 nm for concentrations of 1.0, 1.5, 2.0 and 2.5 wt.% respectively.

AFM was employed to gain further information about the surface morphology and structure of the CC films. Compared to cellulose thin films from different sources like trimethylsilyl cellulose (TMSC)(Niegelhell et al. 2016; Schaub et al. 1993) or cellulose xanthate (CX) (Weißl et al. 2018), the surface of CC thin films features more aggregates (10 - 13 nm) concomitant with slightly higher roughness. The AFM images (Figure 3) suggest that already concentrations of 1.0 wt.% are suitable to completely cover the substrates. The morphology of films from all concentrations tested is regular and smooth with a RMS roughness between 5 nm (lowest concentration) and 12 nm (highest concentration). Compared to the increase in the root mean square (RMS) roughness with increasing CC concentration, no trend of increasing or decreasing surface roughness or any other change in surface morphology could be identified within the single processing steps (Figure S8, SI).

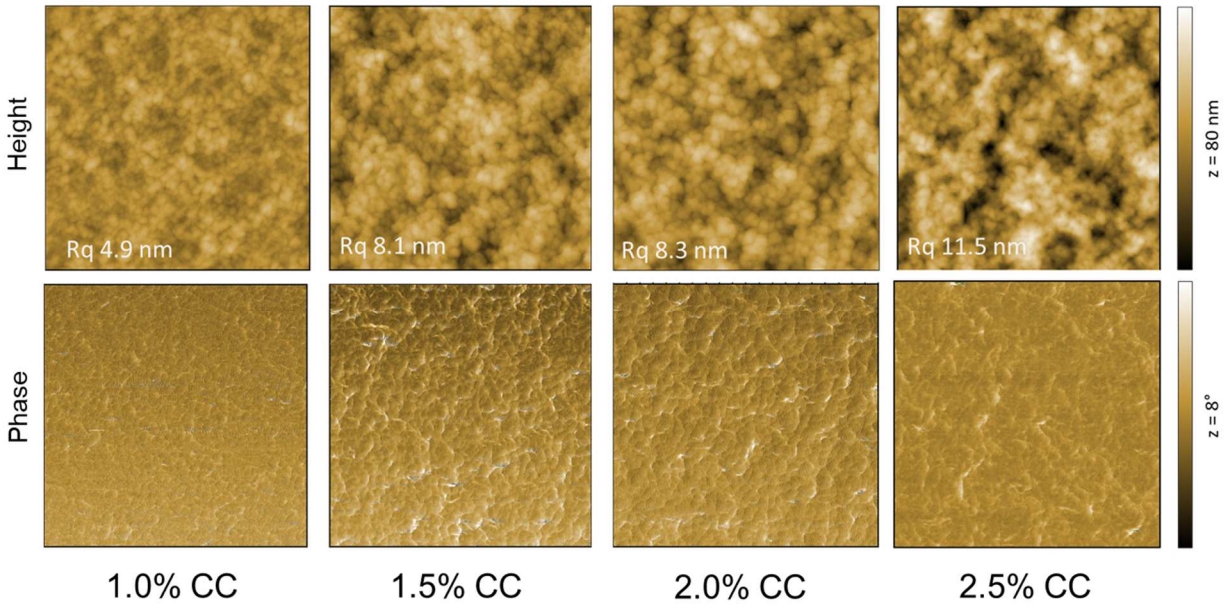

Figure 3 2x2 µm² AFM height (upper row) and phase (lower row) images of CC based thin films after spin coating and rinsing with DI water; starting with concentrations from 1.0 to 1.5, 2.0 and 2.5 wt. %

CC films spin coated from a 1.5 wt.% solution displayed static water contact angles between 12 and 27 degrees, depending on the post treatment. At higher CC concentrations used for spin coating, the development of the contact angle followed the same direction but the range between the different treatments was much smaller (from 19 to 26 degrees for 2.0 wt.% CC, and from 29 to 32 degrees for 2.5 wt. %).

The SFE of films spin coated from different concentrations was calculated from the H_2O and diiodmethane contact angles following the Owens, Wendt, Reynolds and Kaeble method(Owens and Wendt 1969). The obtained SFE (66-77 mN/m) are in the range reported for cellulose thin films.(Mohan et al. 2011; Weißl et al. 2018; Weißl et al. 2019)

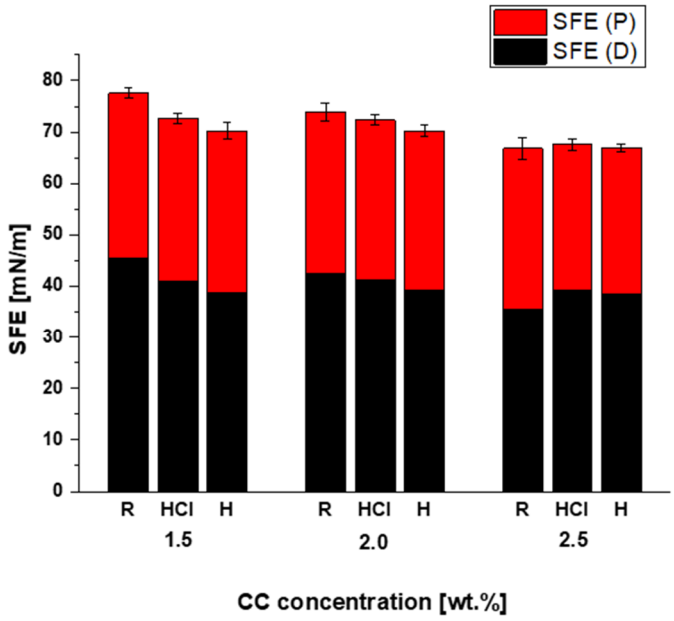

291

292 *Figure 4 SFE values calculated with the H_2O and diiodomethane contact angles, whereby D describes the disperse*
293 *contribution and P describes the polar contribution to the overall surface free energy. (R is rinsed, HCl is HCl*
294 *treated and H is heated)*

295

Formation and characterization of CC/CX blend films

CC and CX are both soluble in 8% NaOH solutions which was exploited to blend solutions in 1:3, 1:1 and 3:1 ratios. After spin coating the blend solutions, and subsequent regeneration to all-cellulose blend thin films, their properties were determined and correlated to cellulose thin films derived from CX and CC, respectively. CX does not regenerate during spin coating; therefore an HCl vapor treatment was performed to ensure conversion of the CX domains to cellulose. The domains consisting of CC are not affected by this procedure as discussed above.

Taking a closer look into the ATR-IR spectra of the blend films and reference materials, the region between 850 and 950 cm^{-1} attracts attention. For the pure CX, the bands there can be assigned to vibrations related to sodium sulfide (1420, 920 cm^{-1}) and sodium trithiocarbonate (1670, 1427, 925 and 885 cm^{-1}). After HCl vapor exposure and rinsing with water, the blend films and the source materials are both fully regenerated and infrared spectroscopy only reveals bands related to cellulose (Figure S9, SI). The IR spectra in combination with XPS of the pure CC and the CX shown in a previous publication confirm the full regeneration of the different cellulose derivatives to yield *all*-cellulose blend films.(Weißl et al. 2019)

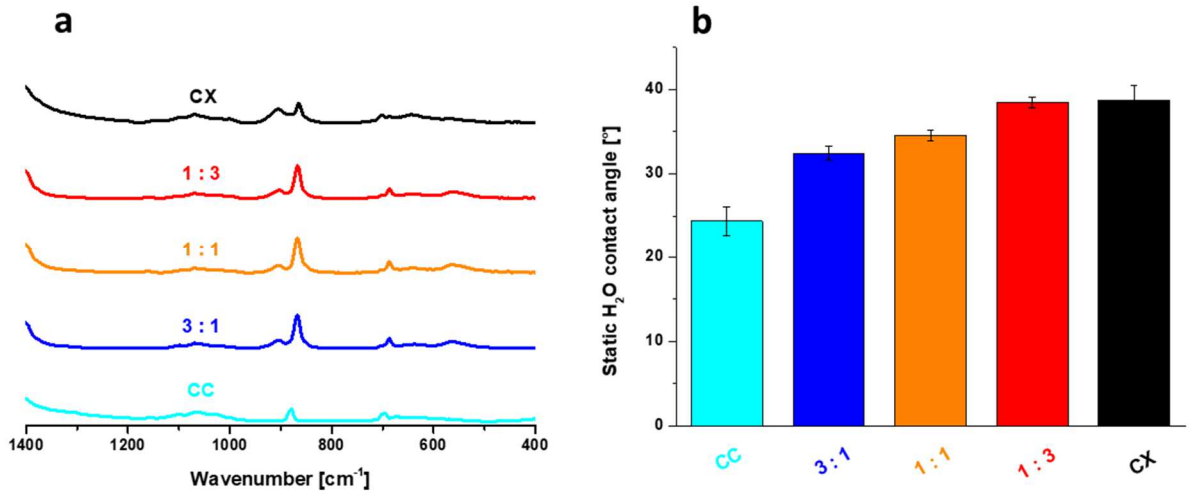

Figure 5 a) ATR-IR spectra of 2% CX, 2% CC and blends (1:3, 1:1, 3:1) after spin coating b) H2O contact angles of 2% CX, 2% CC and blend (1:3, 1:1, 3:1) films after HCl vapor treatment and rinsing with DI water.

The estimation of the layer thickness was executed with stylus profilometry. The reference materials had a thickness of 57 and 59 nm for CC and CX respectively. The blend films were all in the range of 52 nm after regeneration and rinsing independent of the blend ratio. (Figure S10, SI)

Determination of the static H_2O contact angles is documented in Figure 5b. The pure CC film had a contact angle of 24° after HCl vapor deposition and with increasing CX content in the blend films, the contact angle is continuously increasing, until a value of 37° - similar to the pure CX based film - is reached. The increase in the contact angle is unlikely caused by any chemical difference in the films but connected to a change in the surface morphology between the CC and the CX based layers. If the Wenzel equation is used for correcting the contact angles for the roughness of the films, differences between the films are rather small (33-38° for water; Figure S11a, SI). The surface free energy followed the linear behavior, shown in the contact angle measurements, ranging from 72 mN/m for pure CC to 64 mN/m for pure CX based films (Figure S11b, SI).

AFM is employed to check the miscibility of CC and CX on a microscale. The evaluation of the surface morphology is summarized in Figure 6 and indeed, differences in surface structure and in the roughness are observable. The detailed mechanism on the formation of the structures visible in the phase images remains unclear. One option is that the two cellulose derivatives undergo vertical phase separation during spin coating, followed by spinodal decomposition.

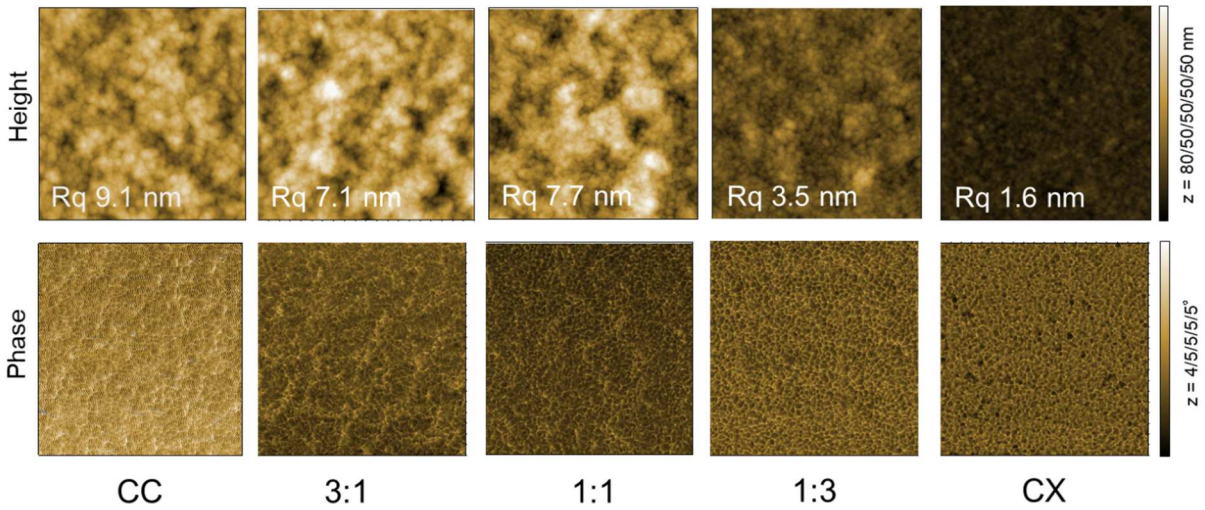

Figure 6 2x2 µm² AFM height (upper raw) and phase (lower raw) images of 2% CC, blend (3:1, 1:1, 1:3) and 2% CX films after HCl vapor treatment and rinsing with DI water.

The CC based films show large bulky substructures, causing pronounced hills and valleys. These structures are further reflected in the RMS roughness of the thin films, where pure CC films have R_q values of around 10 nm. With increasing CX content in the blend films, the substructures become smaller and the surface shows a more regular shape. The RMS roughness decreases to 3.5 nm for the blend films consisting of 75% of CX. The CX reference material has the smallest RMS roughness, of all samples analyzed.

Finally, the water uptake and the swelling behavior of the blend films were investigated by a H_20/D_2O exchange monitored in a QCM-D device.(Kittle et al. 2011; Mohan et al. 2012)

Figure 7a shows the frequency shifts of a bare substrate and the cellulose covered substrates during the H_2O/D_2O exchange, recorded by QCM-D. The black dashed line represents the bare substrate and shows a Δf_3 shift of ca. 71 Hz between H_2O and D_2O. If a cellulose layer is present on the substrates, the Δf_3 are significantly higher and in the range of 115 up to 120 Hz, where the blend films (1:3, 1:1; 3:1) and the pure CC based films all have comparable shifts. Only the pure CX based show a more intensive shift of around 130 Hz, which correlates to the slightly higher layer thickness.

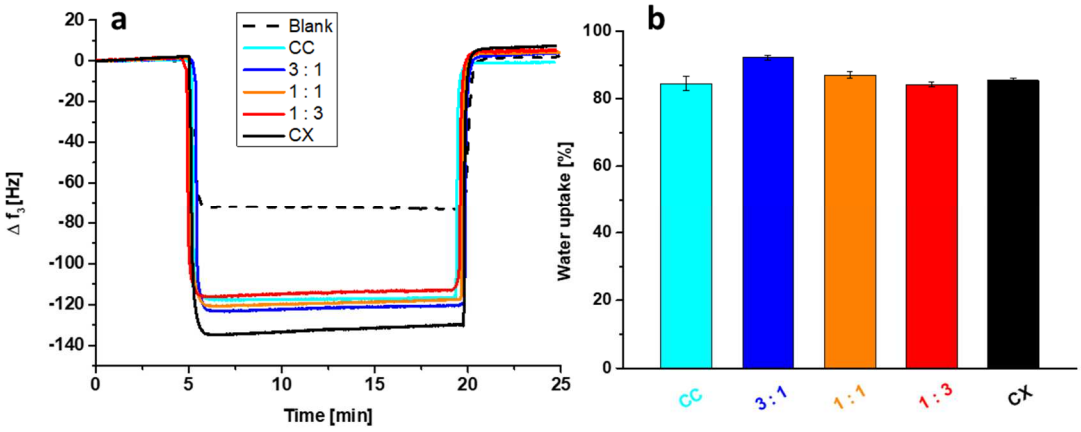

Figure 7 a) QCM-D monitored frequency shifts (Δf3) of 2% CX, 2% CC and blend (1:3, 1:1, 3:1) films in a H_2O/D_2O exchange experiment. b) Water uptake of the reference materials and the blend films during the H_2O/D_2O exchange experiment.

According to the frequency shifts, the total amount of water Γ_{water} is calculated and yields 6.3 ± 0.2 µg/cm² for the CC based cellulose films. The blend films systems exchanged 6.7 ± 0.2 (3:1), 6.7 ± 0.1 (1:1) and 6.7 ± 0.2 µg water /cm² (1:3). With 7.4 ± 0.1 µg/cm² the total water uptake is obviously higher in the CX based regenerated cellulose film. These values correlate with the mass of the cellulose films, therefore the film thickness needs to be taken into account for determining the degree of water uptake. The thickness was 50 nm for CC based layers, around 52 nm for the blend films and 57 nm for the CX based films. With the layer thickness and the density of cellulose (1.5 g/cm³) (Holbery and Houston 2006), the dry mass of the cellulose films is calculated. The dry mass is 7.5 ± 0.2 µg/cm² for the CC based cellulose films, 7.3 ± 0.2 (3:1), 7.7 ± 0.1 (1:1) and 7.9 ± 0.1 µg/cm² (1:3) for the blend films and 8.7 ± 0.2 µg/cm² for the CX based films. The swelling behavior is presented in Figure 7b and it can be concluded that there is no trend observable within the thin films derived from different cellulose sources. Only the 3:1 blend (CC:CX) shows a slightly higher water uptake (92%), all the other films feature a water uptake capacity between 84 and 87%.

Table 1 Summary of QCM-D H_2O/D_2O exchange experiment

	Dry mass [µg/cm²]	Γ_{water} [µg/cm²]	Water uptake [%]
CC	7.5 ± 0.2	6.3 ± 0.2	85 ± 2
3:1	7.3 ± 0.2	6.7 ± 0.2	92 ± 1
1:1	7.7 ± 0.1	6.7 ± 0.1	87 ± 1
1:3	7.9 ± 0.1	6.7 ± 0.2	84 ± 1
CX	8.7 ± 0.1	7.4 ± 0.1	85 ± 1

4. Conclusion:

Here, we introduced a new system for manufacturing cellulose thin films, which is based on ecofriendly CC. Since CC is water soluble the use of organic solvents is omitted compared to the other often employed cellulose derivative, TMSC. In addition, CC can be synthesized via environmentally friendly procedures in significant amounts at competitive prices. The regeneration process itself does not require any additional treatment but is induced by increasing the NaOH concentration during the spin-coating via evaporation of the water, as confirmed by IR and XPS spectroscopy. Such an *in situ* reaction in a polymer film during spin coating has no precedent in literature. Exposure to acid vapors or elevated temperature does not cause changes in the film morphology or chemistry of the films. Further, the film thickness can be easily adjusted within a range of 20 to 80 nm by varying the CC concentration. Only the increased surface roughness, caused by the high sodium hydroxide content in the solvent, could be a drawback for the processing of thin and well-defined cellulose layers based on CC, depending on their purpose.

Blending of CX with CC is a promising method to partly substitute the frequently employed CX as source for regenerated cellulose products. Further, these all cellulose blend films deliver an interesting possibility to investigate cellulose interfaces. Within this study, it could be shown that the blending and the regeneration of the cellulose derivatives do not lead to phase separation regardless of the mixing ratio.

Acknowledgements:

Lenzing AG and Fraunhofer Institute for Applied Polymer Research IAP are gratefully thanked for providing the cellulose xanthate stoke solution and cellulose carbamate powder. Professor Gregor Trimmel and the PCCL are thanked for experimental support. EK is grateful for the support by the FinnCERES Materials Bioeconomy Ecosystem

Literature:

Ehmann HMA, Werzer O, Pachmajer S, Mohan T, Amenitsch H, Resel R, Kornherr A, Stana-Kleinschek K, Kontturi E, Spirk S. (2015) Surface-Sensitive Approach to Interpreting Supramolecular Rearrangements in Cellulose by Synchrotron Grazing Incidence Small-Angle X-ray Scattering. ACS Macro Letters 4: 713-716

Fink H-P, Ganster J, Lehmann A. (2014) Progress in cellulose shaping: 20 years industrial case studies at Fraunhofer IAP. Cellulose 21: 31-51

Fu F, Guo Y, Wang Y, Tan Q, Zhou J, Zhang L. (2014) Structure and properties of the regenerated cellulose membranes prepared from cellulose carbamate in NaOH/ZnO aqueous solution. Cellulose 21: 2819-2830

Hämmerle FM. (2011) The cellulose gap. Lenz Ber 89: 12-21

Holbery J, Houston D. (2006) Natural-fiber-reinforced polymer composites in automotive applications. JOM 58: 80-86

Johansson L-S, Campbell JM. (2004) Reproducible XPS on biopolymers: cellulose studies. Surf Interface Anal 36: 1018-1022

Keiji KK, Gordon JG. (1985) The oscillation frequency of a quartz resonator in contact with liquid. Anal Chim Acta 175: 99-105

Kittle JD, Du X, Jiang F, Qian C, Heinze T, Roman M, Esker AR. (2011) Equilibrium Water Contents of Cellulose Films Determined via Solvent Exchange and Quartz Crystal Microbalance with Dissipation Monitoring. Biomacromolecules 12: 2881-2887

Klemm D, Heublein B, Fink HP, Bohn A. (2005) Cellulose: Fascinating Biopolymer and Sustainable Raw Material. Angew Chem Int Ed 44: 3358-3393

Kontturi E, Tammelin T, Österberg M. (2006) Cellulose model films and the fundamental approach. Chem Soc Rev 35: 1287-1304

Kunze J, Fink H-P. (2005) Structural Changes and Activation of Cellulose by Caustic Soda Solution with Urea. Macromolecular Symposia 223: 175-188

Mohan T, Kargl R, Doliška A, Vesel A, Köstler S, Ribitsch V, Stana-Kleinschek K. (2011) Wettability and surface composition of partly and fully regenerated cellulose thin films from trimethylsilyl cellulose. J Colloid Interface Sci 358: 604-610

Mohan T, Niegelhell K, Nagaraj C, Reishofer D, Spirk S, Olschewski A, Stana Kleinschek K, Kargl R. (2017) Interaction of Tissue Engineering Substrates with Serum Proteins and Its Influence on Human Primary Endothelial Cells. Biomacromolecules 18: 413-421

Mohan T, Spirk S, Kargl R, Doliška A, Vesel A, Salzmann I, Resel R, Ribitsch V, Stana-Kleinschek K. (2012) Exploring the rearrangement of amorphous cellulose model thin films upon heat treatment. Soft Matter 8: 9807-9815

Moidoveanu SC, David V. (2002) Derivatization Reactions for Analytes with Various Functional Groups. Journal of Chromatography Library 65: 639-845

Nada A-A, Kamel S, El-Sakhawy M. (2000) Thermal behaviour and infrared spectroscopy of cellulose carbamates. Polym Degrad Stab 70: 347-355

Neufeld AK, Cole IS, Bond AM, Furman SA. (2002) The initiation mechanism of corrosion of zinc by sodium chloride particle deposition. Corros Sci 44: 555-572

Niegelhell K, Süßenbacher M, Jammernegg K, Ganner T, Schwendenwein D, Schwab H, Stelzer F, Plank H, Spirk S. (2016) Enzymes as Biodevelopers for Nano- And Micropatterned Bicomponent Biopolymer Thin Films. Biomacromolecules 17: 3743-3749

Niinivaara E, Faustini M, Tammelin T, Kontturi E. (2016) Mimicking the Humidity Response of the Plant Cell Wall by Using Two-Dimensional Systems: The Critical Role of Amorphous and Crystalline Polysaccharides. Langmuir 32: 2032-2040

Owens DK, Wendt RC. (1969) Estimation of the surface free energy of polymers. J Appl Polym Sci 13: 1741-1747

Protz R, Weidel G, Lehmann A. (2018) Man-made cellulosic fibers via the viscose process - new opportunities by cellulose carbamate. Lenz Ber 94: 77-84

Rosenau T, Potthast A, Sixta H, Kosma P. (2001) The chemistry of side reactions and byproduct formation in the system NMMO/cellulose (Lyocell process). Prog Polym Sci 26: 1763-1837
Sauerbrey G. (1959) Verwendung von Schwingquarzen zur Wägung dünner Schichten und zur Mikrowägung. Zeitschrift für Physik 155: 206-222
Schaub M, Wenz G, Wegner G, Stein A, Klemm D. (1993) Ultrathin films of cellulose on silicon wafers. Adv Mater 5: 919-922
Shchukarev A, Sundberg B, Mellerowicz E, Persson P. (2002) XPS study of living tree. Surf Interface Anal 34: 284-288
Široký J, Blackburn RS, Bechtold T, Taylor J, White P. (2010) Attenuated total reflectance Fourier-transform Infrared spectroscopy analysis of crystallinity changes in lyocell following continuous treatment with sodium hydroxide. Cellulose 17: 103-115
Sixta H, Michud A, Hauru L, Asaadi S, Ma Y, King Alistair WT, Kilpeläinen I, Hummel M. (2015) Ioncell-F: A High-strength regenerated cellulose fibre. Nord Pulp Pap Res J 30: 43-57
Wang S, Lu A, Zhang L. (2016) Recent advances in regenerated cellulose materials. Prog Polym Sci 53: 169-206
Weißl M, Niegelhell K, Reishofer D, Zankel A, Innerlohinger J, Spirk S. (2018) Homogeneous cellulose thin films by regeneration of cellulose xanthate: properties and characterization. Cellulose 25: 711-721
Weißl M, Rath T, Sattelkow J, Plank H, Eyley S, Thielemans W, Trimmel G, Spirk S. (2019) Multi-layered nanoscale cellulose/CuInS2 sandwich type thin films. Carbohydr Polym 203: 219-227
Wendler F, Schulze T, Ciechanska D, Wesolowska E, Wawro D, Meister F, Budtova T, Liebner F (2012) Cellulose Products from Solutions: Film, Fibres and Aerogels. The European Polysaccharide Network of Excellence (EPNOE): Research Initiatives and Results. Springer Vienna, Vienna
Xiong L-K, Yu G-M, Yin C-Y. (2017) Synthesis and characterization of cellulose carbamate by liquid-solid phase method. Fibers Polym 18: 88-94

SI Cellulose carbamate derived cellulose thin films – Preparation, characterization and blending with cellulose xanthate

Michael Weißl[1], Mathias Andreas Hobisch[1], Leena Sisko Johansson[2], Kay Hettrich[3], Eero Kontturi[2], Bert Volkert[3], Stefan Spirk[1]

1) Institute for Paper, Pulp and Fibre Technology, Graz University of Technology, Inffeldgasse 23, 8010 Graz, Austria

2) Department of Bioproducts and Biosystems (BIO2), Aalto University, P.O.Box 16300, 00076 Aalto, Finland

3) Fraunhofer Institute for Applied Polymer Research IAP, Geiselbergstrasse 69, 14167 Potsdam-Golm, Germany

Correspondence:

Stefan Spirk

stefan.spirk@tugraz.at

+43 (316) 873 – 30763

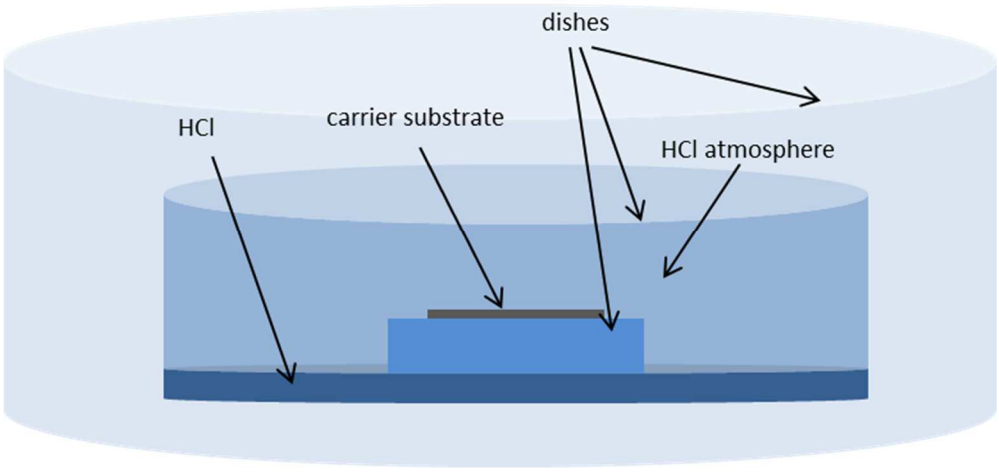

Figure S1 Describing the HCL vapor treatment of CC and CC/CX blend thin films.

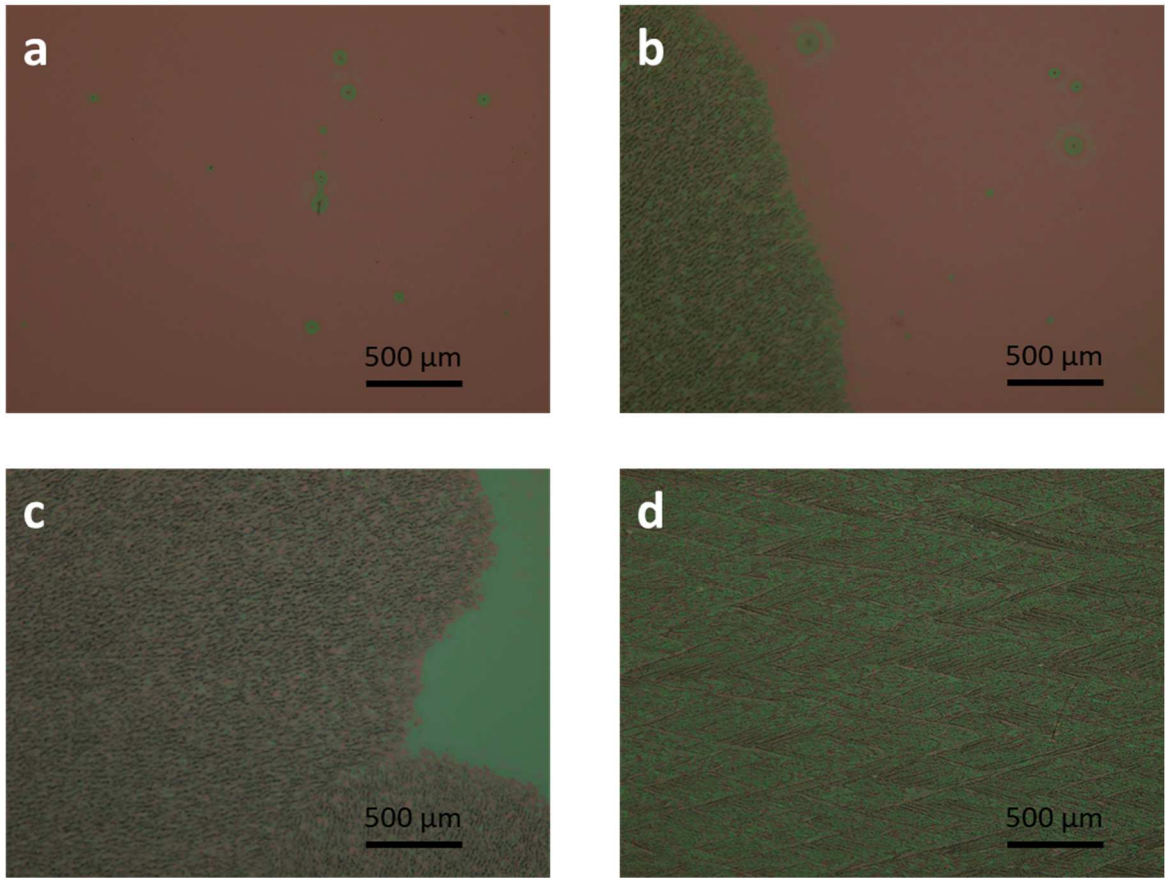

Figure S2 Microscopic observation (magnification 1:50) of the crystal growth during the post drying period after the spin coating of the CC solutions. a) directly after spin coating of a 1.5 wt.% CC solution b) few minutes after spin coating the spontaneous and rapid crystal growth is initiated c) image taken only seconds after image b d) the final crystalline layer, covering the whole substrate

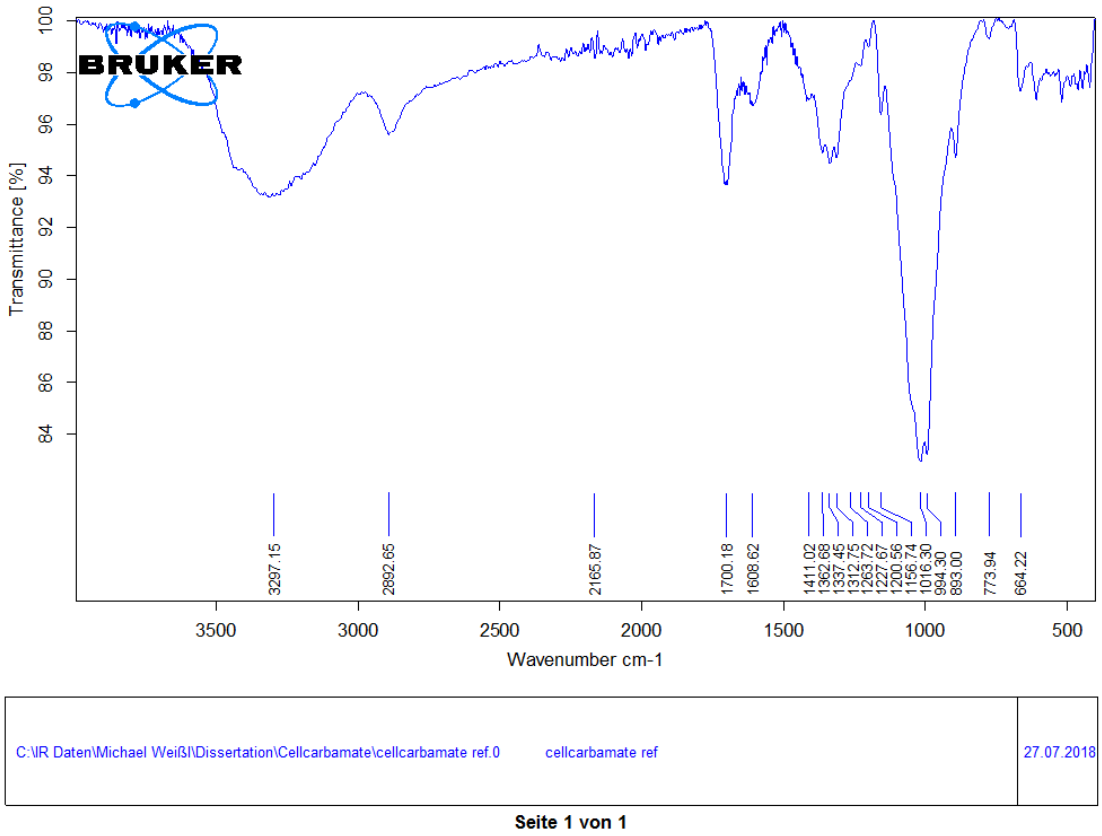

Figure S3 ATR-IR spectrum of cellulose carbamate reference material

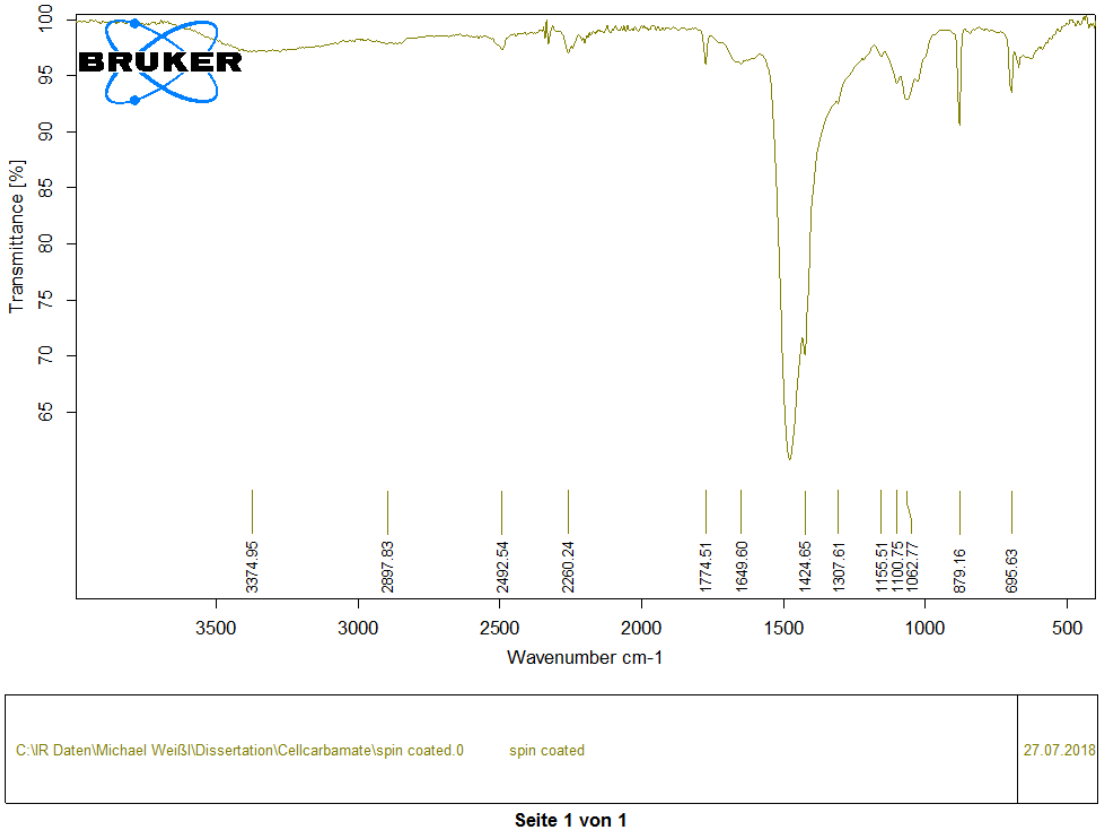

Figure S4 ATR-IR spectrum of a cellulose carbamate based thin film after the spin coating, before rinsing with DI water

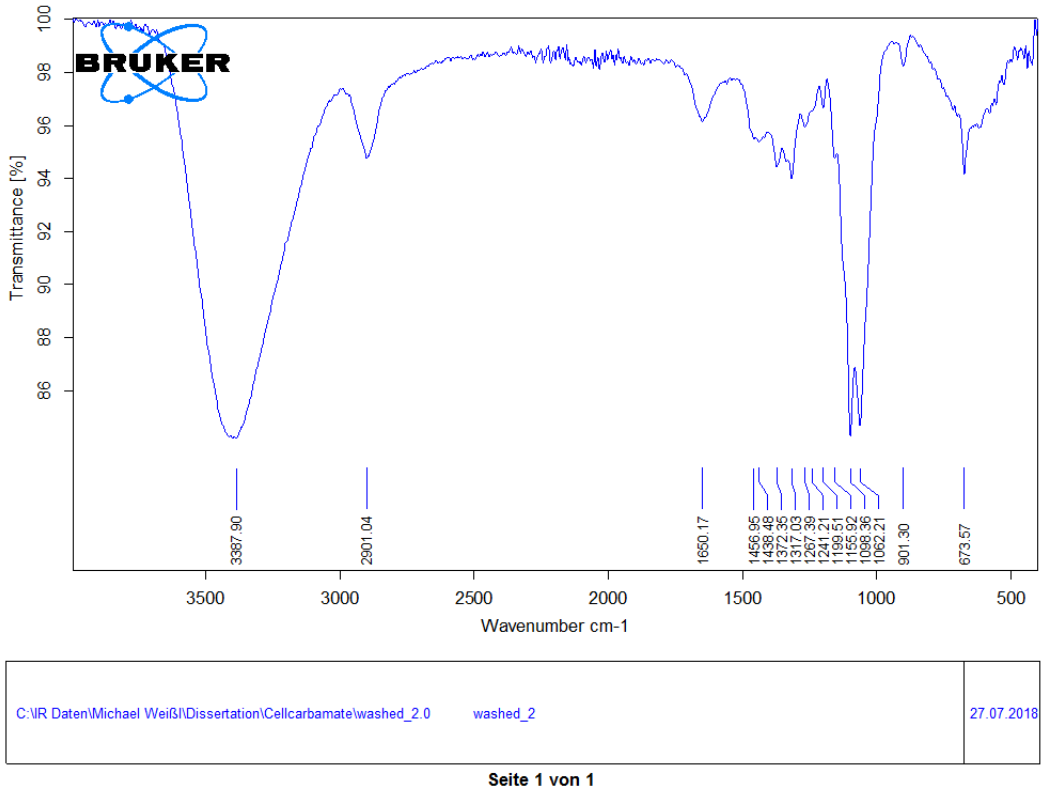

Figure S5 ATR-IR spectrum of a cellulose carbamate based thin film after the spin coating and rinsing with DI water

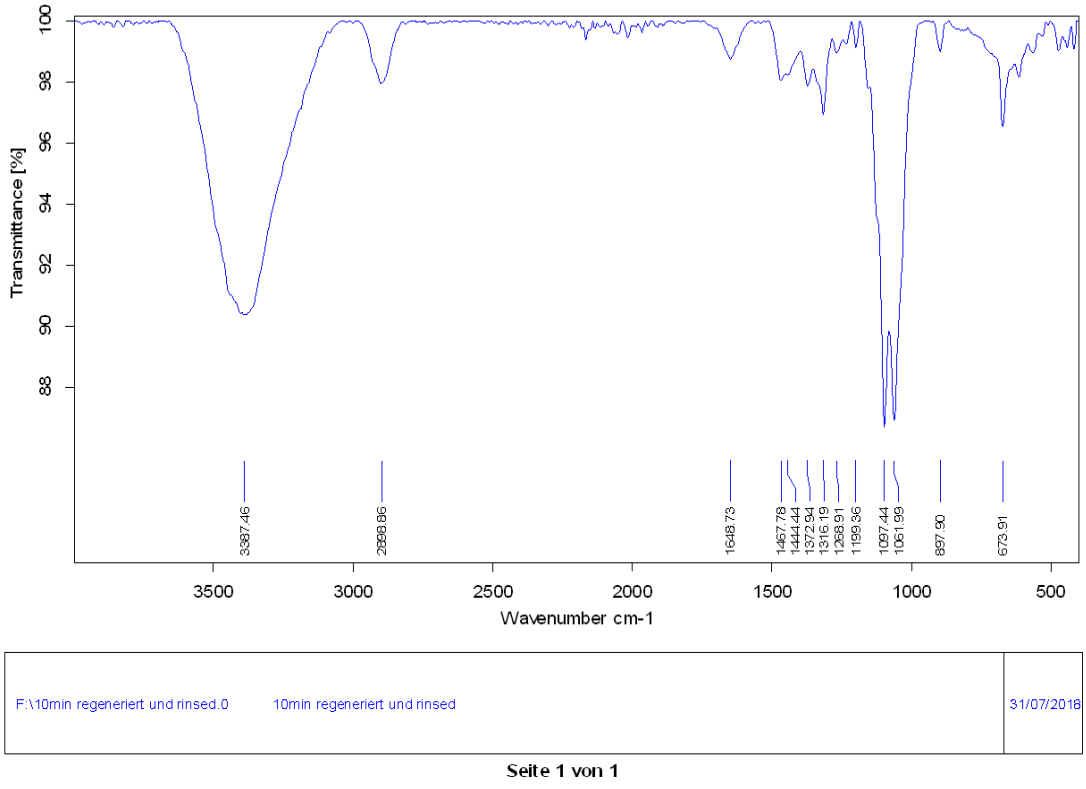

Figure S6 ATR-IR spectrum of a cellulose carbamate based thin film after the HCl treatment and rinsing with DI water

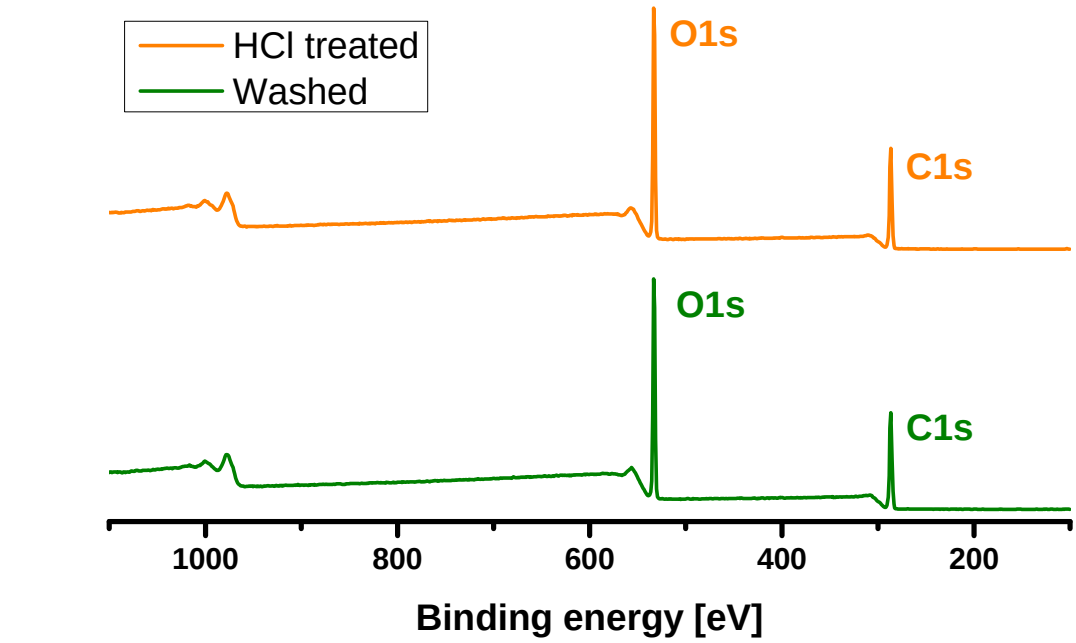

Figure S 7 XPS survey spectra of CC based thin films after rinsing and HCl vapor treatment

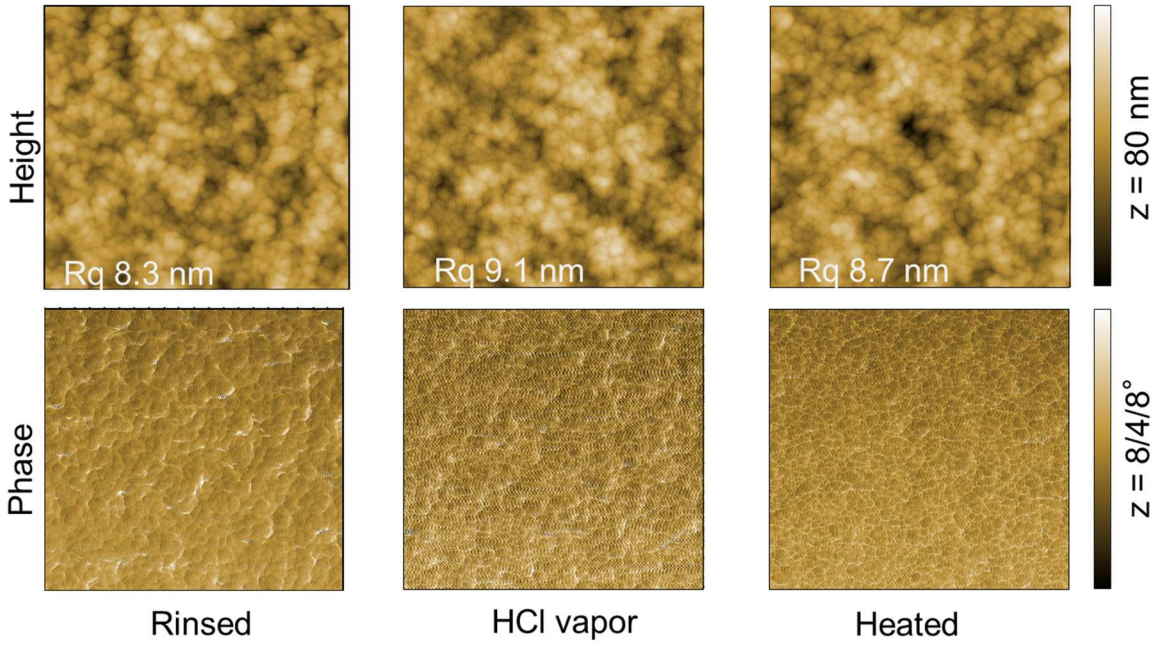

Figure S8 2x2 µm² AFM images height (upper row) and phase (lower row) images of 1.5 wt. % CC based thin films after spin coating and rinsing, HCl vapor deposition and heat treatment at 105°C for 1 hour

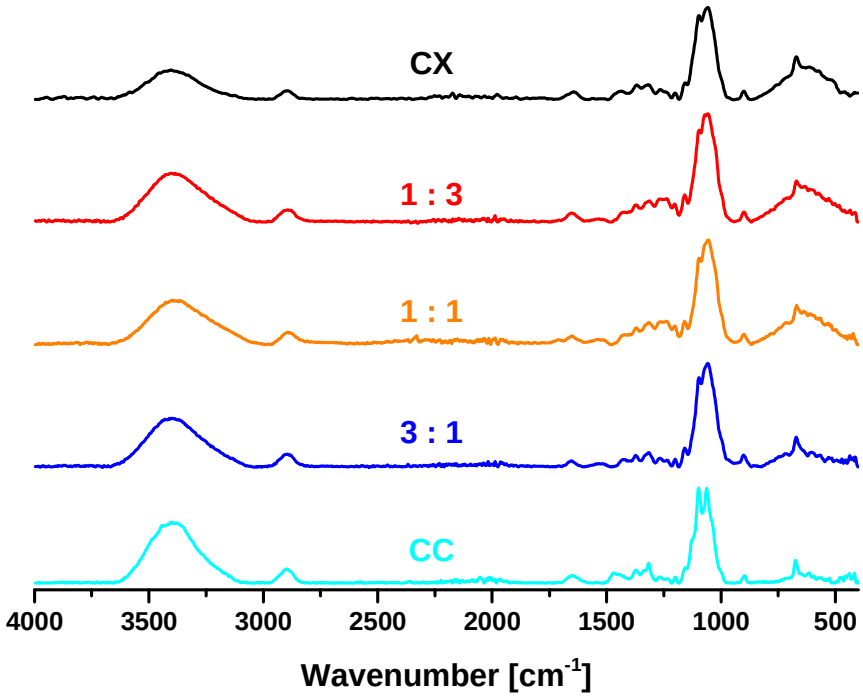

Figure S9 ATR-IR spectra of CC, CX and blend films after HCl vapor deposition and subsequent rinsing with DI water

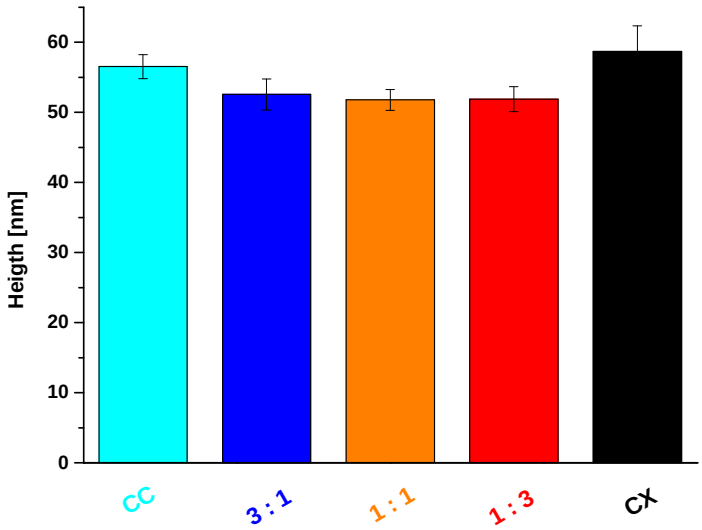

Figure S10 Layer thickness of CC, blend and CX based thin films determined by stylus force profilometry

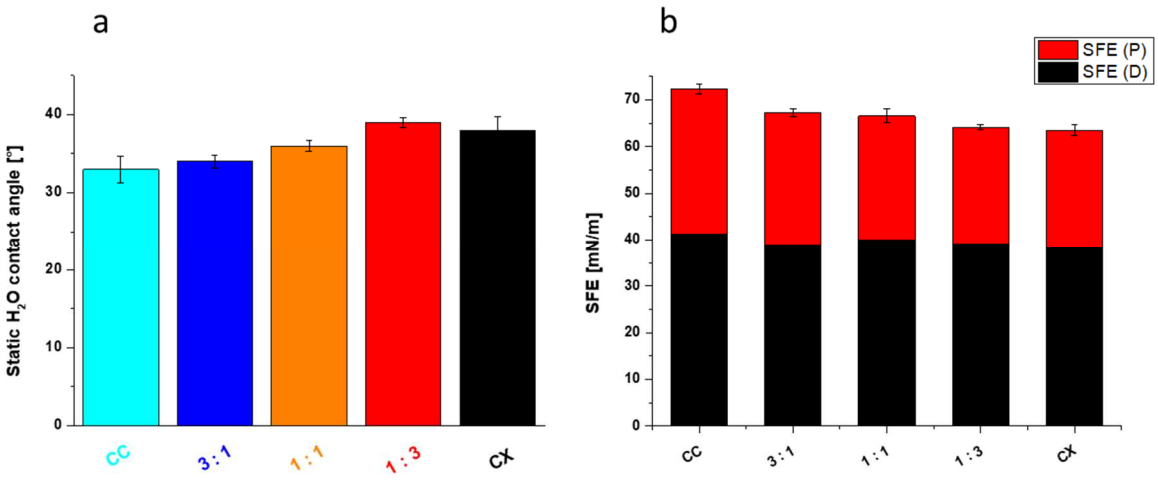

Figure S11 a) Wenzel corrected static H_2O contact angles b)SFE values of CC, blend and CX based thin films, calculated from H_2O and diiodomethane contact angles